Comparative analyses of dopaminergic signalling in the mouse brain



Freya Marijatta

Lincoln College

University of Oxford

A thesis presented for the degree of

Doctor of Philosophy

Hilary Term 2023

ABSTRACT

Despite dopamine being one of the most extensively studied neurotransmitters in the mammalian brain, there remains a great deal of debate as to the dynamics and function of dopaminergic signalling in the midbrain and striatum. Here, I report on a series of *in vivo* experiments in both anaesthetised and awake mice that were designed to explore the nature of dopaminergic signalling, both within and across midbrain-striatal circuits.

Simultaneous use of single-unit electrophysiology in concert with fast-scan cyclic voltammetry (FCV) would be a powerful approach to addressing questions about the nature of the relationship between midbrain dopaminergic neuron firing and striatal dopamine release. I developed and demonstrated a method of achieving this in anaesthetised mice. The data reported a positive linear relationship between optogenetically evoked dopaminergic neuron firing and striatal dopamine release, which suggests a close relationship between these two modes of dopaminergic signalling. However, the combination of electrophysiology and FCV presented unique challenges that might be avoided with the use of optical (photometric) approaches for recording striatal dopamine release.

To compare the signalling dynamics of the novel genetically encoded fluorescent dopamine sensor dLight with FCV, I recorded electrically evoked striatal dopamine transients with both dLight photometry and FCV, across a broad range of midbrain stimulation parameters, in anaesthetised mice. Furthermore, to investigate whether dLight might be a useful tool for investigating striatal heterogeneity in dopaminergic signalling, transients were recorded from both dorsolateral striatum (DLS) and ventral striatum (VS). My findings revealed that: (1) dLight and FCV transients both reflected the intensity of midbrain stimulation; (2) photometric dLight transients were consistently faster than dopamine transients recorded with FCV; and (3) dopaminergic signalling in DLS occurred at faster timescales than in VS. This faster timescale in DLS dopamine signals may reflect differences in the local modulation of striatal dopamine release and uptake. As FCV and dLight displayed similar dynamics in response to midbrain stimulation, I concluded that dLight photometry would be a suitable tool for reading out dopaminergic signalling accompanying behaviour.

To explore the functional heterogeneity of dopamine release in the dorsal and ventral striatum, I recorded photometric dLight transients from the DLS and VS of mice performing treadmill-based locomotion, with and without reward contingency, and in response to instrumental cues. Dopaminergic signalling around locomotion, reward

collection and cue presentation were broadly similar in both striatal regions. Dopamine signals decreased around the initiation of locomotive bouts ('peri-initiation trough') but increased after bout termination ('post-termination') and reward delivery. Furthermore, instrumental cues were represented in both striatal regions, but the valence of the cue response in the dopamine signal was dependent on the mouse's behavioural performance. However, dopamine signals from each striatal region had dissociable dynamics in some cases, with more phasic fluctuations in the DLS and delayed transients in VS. Overall, these findings suggest that both DLS and VS dopamine encode movement and reward, and thus that a binary functional distinction between dorsal and ventral striatum is oversimplistic.

In conclusion, there is considerable heterogeneity in the dynamics of dopaminergic signalling in different striatal regions. I have made some important steps towards characterising the dynamics of the dLight fluorescent sensor *in vivo*, including in relation to behaviour. Furthermore, I have demonstrated a novel approach for exploring diversity in different modes of dopaminergic signalling, namely midbrain neuronal firing and striatal release. This thesis lays groundwork for future explorations of the nature and heterogeneity of dopamine signalling in the brain.

ACKNOWLEDGEMENTS

It has been a long journey from the start of this DPhil until this point. In my first year, Britain was still in Europe, our government had not yet entirely imploded, and the possibility of a global pandemic turning the whole world upside down seemed like something out of a disaster film rather than a plausible eventuality. Despite the unpredictability of the past few years, I am thrilled and relieved that I have indeed achieved my goal of writing up my doctoral thesis.

None of this would have been achievable without the help and support of my fellow scientists. Principal thanks go to Peter Magill and Mark Walton for their feedback and supervision. I would also like to thank the members of their respective labs for providing a wonderful and welcoming environment in which to study. Particular thanks are due to Guy Yona, Julien Carponcy, Yangfan Peng, Lauren Burgeno & Camille Loiseau, without whom I would no doubt be staring miserably at a blank Word document rather than the veritable behemoth I have before me.

Through the challenges of writing this thesis, several people have made life that much more worth living. I would like to thank George, my fellow student of the dopamine arts, for invaluable advice and support over thesis-writing coffee breaks, and for letting me complain about having to write this thesis. I would also like to thank JJ for also letting me complain about having to write this thesis, as well as for the moral support cookies. Finally, I would like to thank my mother, without whom none of me would be possible.

Finally, in the immortal (paraphrased) words of Snoop Dogg, I would like to thank myself. Good job!

TABLE OF CONTENTS

Abstract ..... **i**

Acknowledgements ..... **iii**

Table of Contents ..... **iv**

List of Figures ..... **xiii**

List of Tables ..... **xvi**

Glossary of terms ..... **xvii**

Chapter 1. General Introduction **1**

1.1. The anatomy of dopaminergic circuits in the mammalian brain 1

1.1.1. Dopaminergic neurons of the midbrain *1*

1.1.2. Dopaminergic neuronal projections to striatum *2*

1.1.3. Morphology of striatum-projecting dopamine neurons *4*

1.1.4. Tonic and phasic modes of dopaminergic signalling *5*

1.1.5. Methodological approaches to measuring phasic dopamine release *6*

1.1.6. Dynamics and function of striatal dopamine release *7*

1.1.7. Short-term plasticity of striatal dopamine release *9*

1.2. Functions of striatal dopaminergic modulation 11

1.2.1. Reward and motivation *11*

1.2.2. Dopamine and Parkinson's disease: A role in action initiation? *14*

1.3. Heterogeneity among dopamine circuits 17

1.3.1. Dopaminergic neuronal heterogeneity 17

1.3.2. Striatal heterogeneity 20

1.3.3. Heterogeneity in local striatal microcircuitry 22

1.4. Research aims 25

Chapter 2. Materials and Methods 26

2.1. Animals 26

2.2. Stereotaxic cranial surgery 27

2.2.1. General procedure for recovery surgeries 27

2.2.2. General procedure for non-recovery surgeries 27

2.2.3. Intracranial injection of viral vectors 28

2.2.4. Headplate fixation 30

2.2.5. Fibre-optic cannula implantation 31

2.3. Fast-scan cyclic voltammetric recordings of dopamine transients 31

2.3.1. Acquisition of voltammetric data 31

2.3.2. Recording FCV in vivo 32

2.3.3. Electrically evoked FCV 33

2.3.4. Analysis of voltammetric data 34

2.4. Recording optically evoked dopaminergic neuronal activity and striatal dopaminergic release 35

2.4.1. Single-unit electrophysiology: Preparation of experimental animals *35*

2.4.2. Single-unit electrophysiology: Data acquisition and processing *36*

2.4.3. Single-unit electrophysiology: Optogenetic stimulation *37*

2.4.4. Single-unit electrophysiology: Labelling of single neurons *38*

2.4.5. Simultaneous FCV and single-unit electrophysiology *38*

2.5. dLight photometry 39

2.5.1. dLight as an optical sensor for dopamine *39*

2.5.2. Measuring dLight with pyPhotometry *39*

2.5.3. Photometric assessment of electrically evoked dopamine release *40*

2.5.4. Pre-processing of photometric data *42*

2.5.5. Motion correction of photometric data *43*

2.6. Head-fixed behavioural training 45

2.6.1. Behavioural apparatus: Treadmill *45*

2.6.2. Behavioural apparatus: Training environment and video recording *46*

2.6.3. Behavioural apparatus: pyControl *47*

2.6.4. Behavioural apparatus: Synchronisation *49*

2.7. Immunohistochemistry 50

2.7.1. Perfusion fixation and tissue processing *50*

2.7.2. Immunohistochemistry: Juxtacellularly recorded neurons *51*

2.7.3. Immunohistochemistry: dLight *52*

Chapter 3. Results I: combining optically evoked single-unit electrophysiology with fast-scan cyclic voltammetry 54

3.1. Introduction 54

3.2. Aims 57

3.3. Methods 58

3.3.1. A note on methodological approaches to measuring striatal dopamine in vivo 58

3.3.2. Recording optically evoked firing of dopaminergic neurons and striatal dopaminergic release 59

3.3.3. Difficulties inherent in pairing electrophysiology and voltammetry 62

3.3.4. Removing FCV artifact from electrophysiological data 63

3.3.5. Pre-processing single-unit and FCV data 68

3.4. Results 69

3.5. Discussion 75

3.5.1. Similar modulation of dopaminergic neuron firing and striatal dopamine release 75

3.5.2. Evaluation of methods in addressing research questions 79

3.5.3. Combining FCV and single-unit recordings 81

3.5.4. Novel approaches 83

3.5.5. Future work and conclusions 85

Chapter 4. Results II: Measuring electrically evoked dopamine transients with FCV and dLight photometry 88

4.1. Introduction 88

4.2. Aims 92

4.3. Methods 92

4.3.1. Recording electrically evoked dopamine transients 92

4.3.2. Data processing 96

4.3.3. Defining parameters of interest 97

4.3.4. Linear mixed-effects modelling 99

4.4. Results: Electrically evoked FCV transients 101

4.4.1. LMM for frequency, number of pulses and region on peak height 104

4.4.2. LMM for frequency, NP and region on FCV FWHH 107

4.4.3. LMM frequency, NP and region on FCV T50 108

4.5. Results: Electrically evoked dLight transients 111

4.5.1. LMM for frequency, NP and region on dLight peak 113

4.5.2. LMM for frequency, NP and region on dLight FWHH 116

4.5.3. LMM for frequency, NP and region on dLight T50 118

4.5.4. LMM for frequency, NP and region on dLight τ 122

4.6. Results: Comparing dopamine transients measured with FCV and dLight photometry 123

4.7. Discussion 126

4.7.1. Increasing frequency and NP resulted in larger dopamine transients.... 126

4.7.2. Evaluating the timescale of FCV transients with different stimulation parameters..... 129

4.7.3. Evaluating the timescale of dLight transients with different stimulation parameters..... 130

4.7.4. Regional differences in evoked transients in both modalities..... 131

4.7.5. Comparing dLight photometry with FCV..... 133

4.7.6. Limitations of the present study..... 135

4.7.7. Conclusions and future work..... 137

Chapter 5. Results III: Locomotion- and reward-related dopamine signalling in dorsolateral and ventral striatum..... 141

5.1. Introduction 141

5.2. Aims..... 144

5.3. Methods..... 145

5.3.1. Surgery..... 145

5.3.2. Water restriction..... 146

5.3.3. Behavioural training: Apparatus..... 146

5.3.4. Behavioural training: Habituation..... 147

5.3.5. Behavioural training: Run-for-reward (RFR) task..... 147

5.3.6. Behavioural training: Go/No-go (GNG) task..... 148

5.3.7. Behaviour training: Training progression for the GNG task..... 151

5.3.8. Isolating locomotive bouts..... 152

5.3.9. Isolating rewarded and non-rewarded locomotive bouts during RFR.... 154

5.3.10. Processing dLight data..... 155

5.3.11. Time-based linear regression..... 156

5.3.12. Using time-based linear regression across data from different tasks... 156

5.3.13. Identifying cue-learning in mice trained in the GNG task..... 157

5.3.14. Exclusion criteria for analyses..... 158

5.4. Results: dLight activity in DLS and VS during spontaneous movement.....160

5.4.1. Treadmill and dLight data during initiation and termination of spontaneous locomotion..... 160

5.4.2. The effect of bout speed and duration on striatal dopamine signals around the initiation of spontaneous locomotion..... 165

5.4.3. The effect of bout speed and duration on striatal dopamine signals around termination of spontaneous locomotion..... 170

5.5. Results: dLight activity in DLS and VS during reward contingent movement 173

5.5.1. dLight transients during initiation and termination of non-rewarded bouts during RFR..... 174

5.5.2. dLight transients during initiation and termination of rewarded bouts during RFR..... 177

5.5.3. Regional differences in the latencies of peri-initiation troughs during RFR 179

5.5.4. The effect of reward contingency on dLight signals in DLS and VS around initiation and termination of running bouts *181*

5.5.5. Representation of reward in DLS and VS dLight signals *184*

5.6. Results: Response to instrumental cues in DLS and VS 188

5.7. Discussion 194

5.7.1. Encoding of self-paced movement initiation and termination in both DLS and VS *195*

5.7.2. Dopaminergic encoding of movement vigour in DLS and VS *197*

5.7.3. Dopaminergic encoding of reward contingency in DLS and VS *198*

5.7.4. Cue and reward responses in DLS and VS dopamine signals *200*

5.7.5. VS signals occur with different timing *201*

5.7.6. Strengths and limitations of the present study *202*

5.7.7. Future work *204*

Chapter 6. General Discussion 207

6.1. Summary 207

6.1.1. Chapter 3 - Combining optically evoked single-unit electrophysiology with fast-scan cyclic voltammetry *208*

6.1.2. Chapter 4 - Measuring electrically evoked dopamine transients with FCV and dLight photometry *210*

6.1.3. Chapter 5: Locomotion- and reward-related dopamine signalling in dorsolateral and ventral striatum *211*

6.2. Theoretical and technical considerations 214

6.2.1. Measurement of evoked potentials in anaesthetised preparations 214

6.2.2. Characterising the neural correlates of movement and reward 215

6.3. Future directions 216

6.3.1. The (potentially separable) dopaminergic signalling accompanying movement and reward 216

6.3.2. FCV and dLight: What do they measure? 216

6.3.3. Closing the loop: What is the relationship between dopamine neuron firing and striatal release? 217

6.4. Concluding statement 218

References 220

LIST OF FIGURES

2.1: A demonstration of motion correction on dLight data collected in a head-fixed behavioural mouse. 45

2.2: A diagram of the behavioural apparatus used for training within the sound-attenuating chamber. 48

3.1: Graphical illustration of the process of data collection and the pre-processing of optically evoked FCV signal. 61

3.2: A demonstration of template subtraction to remove FCV scan artifacts from electrophysiological data. 64

3.3: Schematic of the creation of artificial test data and subsequent artifact removal. 67

3.4 Simultaneously recorded spike and FCV data for a single neuron. 70

3.5: Histological verification of neuron identity and location and of FCV lesion location for a single animal. 71

3.6: Data from all neurons responsive to optical stimulation, recorded simultaneously with FCV. 73

4.1: Experimental configuration for measuring electrically evoked FCV and dLight transients. 95

4.2: A, Electrically evoked dopamine transients measured with FCV. 103

4.3: Plots showing the effect of frequency, NP and region on the peak amplitude of electrically evoked FCV transients in arbitrary units (A.U.). 104

4.4: The mean (SEM) FWHH of electrically evoked FCV transients at all frequencies and numbers of pulses, separated by striatal region. 107

4.5: The T50 of electrically evoked FCV transients at all frequencies and numbers of pulses, separated by striatal region and interaction plot. 109

4.6: Electrically evoked dopamine transients measured with dLight photometry. 112

4.7: Plots showing the effect of frequency, NP and region on the peak amplitude of electrically evoked dLight transients in arbitrary units (A.U.). 114

4.8: The FWHH of electrically evoked dLight transients at all frequencies and numbers of pulses, separated by striatal region and interaction plot. 117

4.9: The T50 of electrically evoked dLight transients at all frequencies and numbers of pulses (separated by striatal region) and interaction plots. 119

4.10: The mean (SEM) τ of electrically evoked dLight transients at all frequencies and numbers of pulses, separated by striatal region. 122

4.11: Interaction plot showing the FWHH of electrically evoked dLight and FCV transients in each region. 125

5.1: Schematic of the surgical protocol for behavioural animals represented on coronal sections. 145

5.2: Structure of the full GNG task. 150

5.3: Transformation of raw treadmill data into discrete bouts of locomotion. 154

5.4: Mean (SEM) treadmill and dLight data across all locomotive bouts 161

5.5: Comparisons and trial-by-trial correlations of peri-initiation troughs and post-termination peaks in DLS and VS. 163

5.6: Histograms of the parameters for each spontaneous running bout across all animals. 165

5.7: Breakdown of the timepoint-based regression by each of the four predictors (bout speed, bout duration, pre-bout interval and bout number) around bout initiation. 167

5.8: Breakdown of the timepoint-based regression by each of the four predictors (bout speed, bout duration, pre-bout interval and bout number) around bout termination. 171

5.9: Mean (SEM) treadmill and dLight data across all non-rewarded locomotive bouts in the run-for-reward (RFR) task. 175

5.10: Histograms showing the distribution of locomotive bout parameters (speed, duration, inter-bout interval and time to reward) for non-rewarded and rewarded bouts during RFR. 176

5.11: Mean (SEM) treadmill and dLight data across all rewarded locomotive bouts in the run-for-reward (RFR) task. 178

5.12: Comparisons of the latencies of peri-initiation troughs between DLS and VS. 181

5.13: The effect of reward contingency on dLight signals recorded from the DLS and VS around the initiation and termination of locomotion. 182

5.14: Evaluating reward peaks after delivery of rewards in the RFR task. 187

5.15: Mean (SD) treadmill and dLight data from rewarded GO trials of individual animals performing the GNG task. 189

5.16: Mean (SEM) treadmill and dLight data from rewarded GO trials of weak and strong learners performing the GNG task. 191

5.17: Cue response across cue-learner animals in rewarded GNG trials. 192

5.18: Reward peak of cue-learner animals in rewarded GNG trials. 193

LIST OF TABLES

2.1: All primary antibodies used for immunohistochemistry. 53

2.2: All secondary antibodies used for immunohistochemistry. 53

4.1: Fixed effects, estimates and statistics for peak amplitude of electrically evoked FCV transients. 105

4.2: Fixed effects, estimates and statistics for FWHH of electrically evoked FCV transients. 108

4.3: Fixed effects, estimates and statistics for T50 of electrically evoked FCV transients. 110

4.4: Fixed effects, estimates and statistics for peak amplitude of electrically evoked dLight transients. 115

4.5: Fixed effects, estimates and statistics for FWHH of electrically evoked dLight transients. 118

4.6: Fixed effects, estimates and statistics for T50 of electrically evoked dLight transients. 120

4.7: Fixed effects, estimates and statistics for τ for electrically evoked dLight transients. 123

4.8: Fixed effects, estimates and statistics on FWHH of combined FCV and dLight data. 124

5.1: Quantiles for each predictor of dLight signal. 166

GLOSSARY OF TERMS

ΔF/F	change in fluorescence relative to baseline
AAV	adeno-associated virus
Ag/AgCl	silver/silver chloride
AMCA	aminomethylcoumarin acetate
AP	anterior-posterior
ATP	adenosine triphosphate
AUC	area under the curve
ChI	cholinergic interneurons
ChR2	channel-rhodopsin 2
cpGFP	circularly-permuted green fluorescent protein
D1R	D1 receptor
D2R	D2 receptor
DAT	dopamine transporter
DC	direct current
dH_2O	distilled water
DLS	dorsolateral striatum
DMS	dorsomedial striatum
DS	dorsal striatum
DV	dorsal-ventral
FCV	fast-scan cyclic voltammetry
FWHH	full-width at half-height
GFP	green fluorescent protein
GFAP	glial fibrillary acidic protein
GNG	Go/No-Go (task)
iEEG	intracranial encephalogram
ICC	intra-class correlation
ISI	inter-stimulus interval
IR	infrared
L-DOPA	L-dihydroxyphenylalanine
LED	light-emitting diode
LMM	linear mixed-effects model

M	mean
ML	medial-lateral
MSN	medium spiny (projection) neuron
NA	numerical aperture
NAc	nucleus accumbens
NAcc	core of the nucleus accumbens
NaCl	sodium chloride
NAcsh	shell of the nucleus accumbens
NB	Neurobiotin
NDS	normal donkey serum
NP	number of pulses
O_2	oxygen
PBS	phosphate-buffered saline
PD	Parkinson's disease
PFA	paraformaldehyde
RFP	red fluorescent protein
RFR	run-for-reward (task)
RPE	reward prediction error
SD	standard deviation
SE	standard error
SEM	standard error of the mean
SSD	sum of squared deviations
SNc	substantia nigra *pars compacta*
SNL	substantia nigra *pars lateralis*
T50	decay time from peak to half peak
TD	temporal difference
TH	tyrosine hydroxylase
TTL	transistor-transistor logic
VGCC	voltage-gated calcium channel
VS	ventral striatum
VTA	ventral tegmental area
WT	wild-type

Chapter 1. GENERAL INTRODUCTION

1.1. The anatomy of dopaminergic circuits in the mammalian brain

1.1.1. Dopaminergic neurons of the midbrain

Dopamine is a monoaminergic neurotransmitter in the catecholamine family, neurotransmitters endogenously synthesised from the amino acid L-tyrosine. Dopaminergic neurons typically contain tyrosine hydroxylase (TH), the enzyme responsible for the conversion of L-tyrosine to L-dihydroxyphenylalanine (L-DOPA), and DOPA decarboxylase, which converts L-DOPA to dopamine (Molinoff & Axelrod, 1971).

The first attempt at describing the anatomical arrangement of dopaminergic neurons in the mesencephalon was conducted in rats (Dahlström & Fuxe, 1964). These neurons were divided into three nuclei: A8, A9 and A10. Today, these are commonly referred to as the retrorubral field, the substantia nigra *pars compacta* (SNc) and the ventral tegmental area (VTA), respectively, and make up the dopaminergic midbrain. Of these, the VTA and SNc are most commonly studied, in part because of their putative roles in reward processing and Parkinson's disease, respectively. The majority of VTA and SNc neurons are dopaminergic, but they also contain a proportion of GABAergic and glutamatergic neurons (Fields, Hjelmstad, Margolis, & Nicola, 2007; Morales & Margolis, 2017; Swanson, 1982; Wise, 2004).

There is considerable heterogeneity in the connectivity of midbrain dopaminergic neurons. The dopaminergic neurons in the VTA receive inputs from hypothalamus, dorsal raphe, prefrontal cortex, ventral pallidum, lateral habenula and striatum (Barrot et al.,

2012; Beier et al., 2015; Comoli et al., 2003; Herkenham & Nauta, 1979; Ikemoto, 2007; Lammel et al., 2012; Watabe-Uchida, Zhu, Ogawa, Vamanrao, & Uchida, 2012; Xiao, Priest, Nasenbeny, Lu, & Kozorovitskiy, 2017). On the other hand, the SNc preferentially receive excitatory inputs from somatosensory and motor cortices as well as subthalamic nucleus, and inhibitory inputs from the striatum and neighbouring substantia nigra *pars reticulata* (Comoli et al., 2003; Haber & Knutson, 2010; Lerner et al., 2015; Mailly, Charpier, Menetrey, & Deniau, 2003; Rizzi & Tan, 2019; Watabe-Uchida et al., 2012). This heterogeneity across midbrain dopaminergic neurons also extends to their projection targets, especially to the striatum. The striatum and its relationship to dopamine is discussed in the section below.

1.1.2. Dopaminergic neuronal projections to striatum

Midbrain dopaminergic neurons are known to heavily innervate the striatum, the major input nucleus of the basal ganglia. The striatum has historically been divided into dorsal and ventral compartments, which are commonly further subdivided: dorsal striatum (DS; also known as the caudate putamen) into dorsomedial striatum (DMS) and dorsolateral striatum (DLS); ventral striatum (VS; also known as the nucleus accumbens, or NAc) into NAc core (NAcc) and shell (NAcsh). The primary output neuron of the striatum is the GABAergic medium spiny projection neuron (MSN), although it also contains populations of GABAergic and cholinergic interneurons (Bolam, Wainer, & Smith, 1984; Figueredo-Cardenas, Morello, Sancesario, Bernardi, & Reiner, 1996; Kawaguchi, Wilson, Augood, & Emson, 1995; Tepper et al., 2018).

The projections of midbrain dopaminergic neurons to the striatum have historically been divided into two distinct pathways. The nigrostriatal pathway consists of dopaminergic neurons in the SNc projecting to the DS. The mesolimbic pathway instead consists of dopaminergic neurons in the VTA projecting to the VS, but also to the olfactory tubercule, amygdala, and other limbic regions (Björklund & Dunnett, 2007; Ungerstedt, 1971). However, recent advances in genetic labelling have shown that striatal dopaminergic projections are far more diverse than was previously thought. Within each region of the dopaminergic midbrain are a number of molecularly distinct subtypes of dopaminergic neurons, each of which commonly projects to different subregions within the striatum (Poulin et al., 2018). Rather than a crude binary classification, striatal projections from midbrain dopaminergic neurons are better described as a gradient, with more medial dopaminergic neurons (VTA) projecting to more ventral aspects of the striatum and more lateral dopaminergic neurons (SNc) projecting to more dorsal aspects. However, the organisation of these projections is not quite as clear cut as this, as dopamine neurons across both VTA and SNc project to ventromedial regions of dorsal striatum.

Midbrain-striatal connectivity is not purely unidirectional. While most striatal MSNs innervate basal ganglia targets such as globus pallidus (internal and external), subthalamic nucleus and substantia nigra *pars reticulata*, a subset also innervate dopaminergic cell groups of the midbrain. The pattern of this connectivity is conceptualised as a series of loops going back and forth between midbrain and striatum, moving from medial to lateral aspects of midbrain, and correspondingly from ventral to dorsal aspects of striatum (Aoki et al., 2019; Haber, Fudge, & McFarland, 2000; Ikemoto, 2007). However, there is also evidence that this can occur in reverse, as some of the MSNs

targeted by of more lateral SNc neurons can themselves project back to more medial SNc neurons (Lerner et al., 2015).

1.1.3. Morphology of striatum-projecting dopamine neurons

Striatum-projecting midbrain dopaminergic neurons have varied morphology. Dopaminergic neurons of the SNc have uniquely dense and complex unmyelinated arborisation, typically covering ~3% of the neostriatal volume. These neurons usually project to DS and have very little collateral arborisation outside of striatum (Matsuda et al., 2009). By contrast, those VTA neurons that preferentially innervate the striatum (as opposed to other brain regions) typically consist of a single main axon, and exhibit an order of magnitude less branching than is observed in their SNc neighbours (Aransay, Rodríguez-López, García-Amado, Clascá, & Prensa, 2015).

The size and complexity of the axonal arborisation of a cell is important as it affects action potential propagation. In an unmyelinated axon, action potential propagation requires ATP (Attwell & Laughlin, 2001). The energy cost of propagation increases exponentially with larger and more complex axonal arbor. As such, propagating action potentials across the extensive and frequently branching arborisation of unmyelinated SNc dopaminergic neurons is highly energetically demanding (Pissadaki & Bolam, 2013). This has been suggested as an explanation for the selective vulnerability of SNc dopaminergic neurons in Parkinson's disease: these cells may exist on a precarious energy balance even in the healthy brain, one which may turn negative with the introduction of stress (e.g. mitochondrial dysfunction). This would naturally result in further stress to the cell, subsequent malfunction, and eventual death (Pissadaki & Bolam, 2013).

1.1.4. Tonic and phasic modes of dopaminergic signalling

Within the midbrain, the dopaminergic neurons of anaesthetised animals, or of animals awake but at rest, typically exhibit tonic activity, firing single action potentials (or 'spikes') at a rate of 1-10 spikes per second (Dai & Tepper, 1998; Grace & Bunney, 1983; Starkweather, Babayan, Uchida, & Gershman, 2017). However, in awake animals that are moving or engaged in a task, dopaminergic neurons have also been extensively reported to exhibit transient increases in their firing rates, typically 15-50 spikes/s for 200-500 ms. This phasic or 'burst' firing typically occurs in response to salient stimuli, either internal or external (Dodson et al., 2016; Eshel, Tian, Bukwich, & Uchida, 2016; Montague, Dayan, & Sejnowski, 1996; Schultz, Dayan, & Montague, 1997; Starkweather et al., 2017; Watabe-Uchida, Eshel, & Uchida, 2017).

Due to the dopaminergic innervation of the striatum, action potentials in dopaminergic neurons result in striatal dopamine release, but this release is dependent on the mode of firing. Bursting events in the soma of midbrain dopaminergic neurons trigger phasic dopamine release, significantly greater than that triggered from tonic firing (Floresco, West, Ash, Moore, & Grace, 2003; Garris, Ciolkowski, Pastore, & Wightman, 1994; Gonon, 1988; Grace, 1991, 1993). Alongside these phasic increases in striatal dopamine release, phasic decreases in both striatal dopamine release and neuronal firing rates have also been reported, in response to certain types of movement and aversive stimuli (Brown et al., 2009; Dodson et al., 2016; Joshua et al., 2009; Roitman et al., 2008; Sulzer et al., 2016; Ungless et al., 2004).

However, recent evidence has demonstrated that phasic changes in dopaminergic neuronal firing rates do not always precede or correlate with striatal dopamine release

(Cachope & Cheer, 2014; Mohebi et al., 2019; Sulzer et al., 2016). For example, Mohebi et al. (2019) found that, while both the firing of VTA dopaminergic neurons and dopamine release in the NAc encoded a cue predicting a reward, NAc release alone encoded the expectation of reward. As yet, the relationship between neuronal firing and striatal dopamine release has not been fully characterised.

1.1.5. Methodological approaches to measuring phasic dopamine release

The most commonly applied technique for measuring phasic dopamine levels in striatum is fast-scan cyclic voltammetry (FCV). FCV is an electrochemical technique which can read out levels of extracellular dopamine at sub-second rates. Application of a range of voltages to a carbon-fibre microelectrode triggers a redox reaction in dopamine molecules, and the resulting movement of electrons can be read out with a potentiostat (Clark & España, 2023). As a result, changes in current can be used to approximate changes in the levels of dopamine at the carbon-fibre surface of the microelectrode.

However, recent advances in genetically-encoded fluorescent sensors have provided an alternative technique for the measurement of dopamine at sub-second timescales (Patriarchi et al., 2018; Sun et al., 2020). These fluorescent sensors comprise a dopamine receptor bound to circularly permuted green fluorescent protein (cpGFP). When dopamine binds to this modified receptor, the resulting conformational change increases the fluorescence of the conjugated cpGFP, thereby allowing for optical readout of dopamine release.

But while fluorescent sensors are an exciting new methodology, their novelty means that their dynamics have yet to be comprehensively characterised *in vivo*. As yet, no

published work has directly compared optically measured transients to those measured with FCV, which is often considered a 'gold-standard' measure of dopamine release (although there is some unpublished work investigating this relationship, c.f. Salinas et al., 2022). Such a comparison is important as both techniques assess fundamentally different aspects of dopamine signalling: FCV measures the concentration of extracellular dopamine, while fluorescent sensors are tied to the kinetics of their conjugated modified dopamine receptor – which, unlike FCV, has a non-linear dynamic range.

1.1.6. Dynamics of striatal dopamine release

The release of dopamine has a powerful modulatory effect on striatal circuits. Dopamine exerts its neurochemical influence on striatal cells through two main families of G-protein coupled receptors: The D1 receptor (D1R) and D2 receptor (D2R) families, primarily expressed on MSNs (Gerfen, 1992; Neve, Seamans, & Trantham-Davidson, 2004; Surmeier, Ding, Day, Wang, & Shen, 2007; Surmeier, Song, & Yan, 1996). Most dopaminergic intercellular communication is by volume transmission, with released dopamine diffusing beyond the synaptic cleft (Rice & Cragg, 2008). The majority of dopamine release occurs not at synaptic boutons but instead from sparse 'active-zone' axonal release sites (Liu, Kershberg, Wang, Schneeberger, & Kaeser, 2018; Trudeau et al., 2014) and there is a lack of postsynaptic specialisation at a majority of these (Descarries, Watkins, Garcia, Bosler, & Doucet, 1996), with most dopamine receptors located extrasynaptically (Hersch et al., 1995; Khan, Mrzljak, Gutierrez, de la Calle, & Goldman-Rakic, 1998; Sesack, Aoki, & Pickel, 1994; Yung et al., 1995). Due to the dense and wide-spanning dopaminergic axonal arborisation, particularly in DS (Matsuda et al., 2009),

dopamine released from the firing of a single dopaminergic neuron can in theory modulate activity across a broad area of striatum. This architecture means that dopamine neurons are well-placed to modulate the activity of the basal ganglia circuit on a broad scale.

The primary mechanism for the clearance of dopamine is the dopamine transporter (DAT). However, DAT is only expressed by dopamine neurons, which means that the diffused dopamine molecules are only reuptaken when they encounter dopamine cell membranes or processes (Rice, Patel, & Cragg, 2011). Due to the relative slowness of the DAT transport cycle (Povlock & Schenk, 1997; Prasad & Amara, 2001), the decrease in dopamine concentration at the site of release resulting from diffusion is in fact faster than clearance by DAT (Cragg & Rice, 2004; Rice & Cragg, 2008). Larger, longer-lasting dopamine transients are more strongly regulated by uptake as there is more time available for DAT-mediated clearance (Rice & Cragg, 2008).

While much of the research into striatal dopaminergic dynamics has examined transients evoked by stimulation of the midbrain or medial forebrain bundle, mimicking the release triggered by endogenous "burst-like" firing in midbrain dopaminergic neurons, spontaneous transients *in vivo* have also been reported in many recording sites, including the NAc (Phillips, Stuber, Heien, Wightman, & Carelli, 2003; Roitman, Stuber, Phillips, Wightman, & Carelli, 2004; Sombers, Beyene, Carelli, & Wightman, 2009; Stuber, Roitman, Phillips, Carelli, & Wightman, 2005; Wightman et al., 2007). Sites without these spontaneous transients still show stimulation-evoked increases in striatal dopamine concentration (Wightman et al., 2007).

1.1.7. Short-term plasticity of striatal dopamine release

A number of factors affect the release probability and short-term plasticity of dopaminergic signalling in the striatum. Activation of D2 autoreceptors present on dopamine axons results in short-term depression of striatal dopamine release: after release consequent from an initial stimulation pulse, further release is inhibited (Rice et al., 2011; Santiago & Westerink, 1991). Condon et al. (2019) also argues that DAT itself is an important facilitator of short-term plasticity. As well as enabling the clearance of extrasynaptic dopamine, DATs have been argued to promote short-term facilitation of striatal dopamine release, as inhibition of DAT increases the peak amplitudes of evoked dopamine transients. This effect is also frequency-dependent, but in a region-dependent manner: in both the DS and VS, this effect occurs in response to low-frequency stimulation; in the DS alone, DATs clamp release following high-frequency stimulation, leading to release-insensitive short-term depression (Condon et al., 2019).

Perhaps one of the most studied modulators of this short-term plasticity is acetylcholine. Cholinergic interneurons (ChI) make up only 2-5% of striatal neurons (Descarries & Mechawar, 2000; Oorschot, 1996) but, similar to SNc dopaminergic neurons, produce extensive axonal arbor within the striatum (Exley & Cragg, 2008; Zhou, Wilson, & Dani, 2002). Also similar to dopaminergic neurons, they are tonically active and change their firing in response to learning-related stimuli (Calabresi, Centonze, Gubellini, Pisani, & Bernardi, 2000; Morris, Arkadir, Nevet, Vaadia, & Bergman, 2004; Pisani, Bernardi, Ding, & Surmeier, 2007; Pisani, Centonze, Bernardi, & Calabresi, 2005).

ChIs have been extensively reported to modulate dopamine release via nicotinic cholinergic receptors expressed on dopaminergic axons, (Kramer et al., 2022; Threlfell &

Cragg, 2011). This modulation occurs bidirectionally in a frequency-dependent manner, such that a decrease in cholinergic tone enhances the contrast in the concentration of striatal dopamine release resulting from tonic vs phasic firing (Rice & Cragg, 2004; Threlfell & Cragg, 2011; Zhang & Sulzer, 2004). Activation of these nicotinic receptors on dopamine axons keeps the initial release probability of dopamine high but depresses subsequent release resulting from high frequency firing. However, acetylcholine does not have a role merely in modulating ongoing dopamine release, as synchronised firing of ChIs can directly trigger striatal dopamine release (Threlfell et al., 2012) and generate action potentials in dopaminergic axonal projections, even in the absence of somatic dopaminergic firing (Liu et al., 2022).

Other neurotransmitters also indirectly affect the short-term plasticity of striatal dopamine release via this nicotinic mechanism. Activation of muscarinic receptors located on ChIs indirectly modulates striatal dopamine release, but this effect requires the action of these nicotinic receptors (Threlfell et al., 2010; Threlfell & Cragg, 2011). Nitric oxide is also thought to have a similar effect. Produced by nitrous oxide-containing GABA interneurons (Hidaka & Totterdell, 2001; Kraus & Prast, 2001), it can enhance the frequency dependence of striatal dopamine release, again via these nicotinic receptors (Hartung, Threlfell, & Cragg, 2011).

Glutamate and GABA also have modulatory effects on striatal dopamine release. Glutamate normally inhibits striatal dopamine release resulting from pulse train stimulation (but not single pulses) while GABA instead promotes it (Avshalumov & Rice, 2003), both acting via the effects of hydrogen peroxide on dopaminergic axons. Glutamate promotes (and conversely, GABA suppresses) the generation of endogenous hydrogen

peroxide in striatal MSNs (Bao et al., 2009) expressing glutamatergic and GABAergic receptors (Bernard & Bolam, 1998; Q. Chen et al., 1998; Fujiyama, Fritschy, Stephenson, & Bolam, 2000). The hydrogen peroxide then diffuses and binds to ATP-sensitive potassium channels located on dopaminergic axons (Avshalumov & Rice, 2003; Rice et al., 2011), resulting in short-term depression of striatal dopamine release. This mechanism underlies the opposing effects of glutamate and GABA on pulse-train-evoked striatal dopamine release. These effects are to an extent modulated by endogenous striatal cannabinoid signalling, as cannabinoid receptors cause presynaptic inhibition of striatal GABA release, thereby affecting GABA's indirect modulation of striatal dopamine release. (Szabo et al., 1999; Sidló et al., 2008).

1.2. Functions of striatal dopaminergic modulation

1.2.1. Reward and motivation

For decades, dopamine has been strongly associated with reward and reinforcement. Animals implanted with intracranial stimulation electrodes in dopamine-rich regions will continually self-stimulate (Corbett & Wise, 1980). Additionally, addiction to many drugs of abuse, such as cocaine (Weiss, Paulus, Lorang, & Koob, 1992) or heroin (Kiyatkin, 1994), is thought to be driven by their excitatory effects on dopaminergic systems. Given the above, dopamine is often considered a substrate for reinforcement and motivation (Di Chiara, 1995; Koob, 1992; Schultz, Apicella, & Ljungberg, 1993).

Perhaps the most influential and well-studied theory of dopaminergic function is the reward prediction error (RPE) hypothesis originally developed by Read Montague and

Peter Dayan, working with Wolfram Schultz, which has dominated the field for the better part of 25 years. The RPE hypothesis posits that phasic dopamine acts as a learning signal. Unexpected rewards represent a positive prediction error and are accompanied by a phasic increase in dopamine. After learning a stimulus that strongly predicts a reward, the classical RPE hypothesis suggests that this positive prediction error shifts to the stimulus itself rather than occurring at reward delivery; meanwhile, omission of an expected reward would result in a negative prediction error at the time of expected reward delivery (Montague et al., 1996; Schultz et al., 1997). Through electrophysiological recordings of midbrain dopaminergic neurons in behaving monkeys prior to the origin of this hypothesis, Schultz and colleagues (1993) found that these neurons showed a phasic increase in firing in response to delivery of unexpected rewards. However, these reward-related responses disappeared over the course of training. Instead, these neurons responded to conditioned cues signalling task-relevant information: a cue signalling which lever to press to obtain a reward, and another being a 'go' cue to make the lever press. A few years later, Schultz and colleagues (Montague et al., 1996; Schultz et al., 1997) posited the RPE hypothesis to explain these findings, arguing that the role of phasic dopamine was as a Hebbian learning signal. Within the framework of RPE, unexpected rewards result in a phasic increase in dopaminergic activity. When rewards are expected, for example following the presentation of a conditioned stimulus predicting delivery of a reward, this phasic increase will occur in response to the conditioned stimulus but not to the reward itself. However, if the same conditioned stimulus does *not* result in the predicted reward, dopamine activity will instead transiently decrease at the expected timepoint of reward delivery. The RPE-like characteristics of dopamine signalling have

been reported across a wide range of paradigms (Chang et al., 2016; Keiflin, Pribut, Shah, & Janak, 2019; Lak, Stauffer, & Schultz, 2014; Stauffer et al., 2016; Steinberg et al., 2013; Watabe-Uchida et al., 2017; Witten et al., 2011).

This pattern of firing was argued to represent a temporal difference (TD) error signal, a class of reinforcement learning model (Sutton, 1988; Sutton & Barto, 2018). The model proposes that the RPE term conveys the difference between the expectation of future reward and present information, such as a reward-predicting cue or unexpected reward. TD error is calculated by summing the weighted average of recently experienced reward with the degree of violation of that expectation and multiplying the result by a learning rate. In this way, the RPE hypothesis posits that dopamine represents TD error, and thus can act as a learning signal.

Indeed, the RPE-like firing of dopaminergic neurons has been observed, studied and manipulated in midbrain dopaminergic neurons across many studies, not only by Schultz and colleagues (Schultz et al., 1997) but also by many others in the field (Chang et al., 2016; Keiflin et al., 2019; Lak et al., 2014; Stauffer et al., 2016; Steinberg et al., 2013; Watabe-Uchida et al., 2017; Witten et al., 2011). However, dopaminergic activity does not always follow the expectations of RPE. Coddington and Dudman (2018) demonstrated that in their paradigm, the extinction of the reward signal only occurs at the latest stages of training. The authors argue that the classic RPE dopamine dynamics found by Schultz and colleagues in fact reflect overtraining rather than the 'normal' dopamine learning signal. The cue-related response will increase with training, but this will not necessarily result in extinction of the reward response. Despite the longevity and popularity of RPE, there are

still several aspects regarding how these signals are represented in the brain that are not yet fully understood.

1.2.2. Dopamine and Parkinson's disease: A role in action initiation?

Although dopamine has been widely studied for its role in reward and reinforcement, a dopamine deficit has also long been associated with movement-related pathology. The progressive neuropathy of Parkinson's disease (PD) is characterised by the dysfunction and eventual death of dopaminergic neurons in the SNc, resulting in an array of movement impairments (Kalia & Lang, 2015).

The Direct/Indirect pathway model, proposed by Albin et al. (1989) and DeLong (1990), is the classical explanation as to how the malfunction of dopaminergic striatal modulation results in parkinsonian motor deficiencies. The nominal direct and indirect pathways represent two parallel circuits through the basal ganglia network. Ultimately, the direct pathway has a net excitatory effect on motor-critical cortical targets, while the indirect pathway has a net inhibitory effect. Crucially, these two pathways arise from discrete populations of MSNs in the striatum, differentiated primarily by the expression of D1Rs on direct-pathway MSNs and D2Rs on indirect-pathway MSNs. D1Rs and D2Rs have opposing intracellular effects, and therefore dopamine has opposing effects on direct pathway and indirect pathway MSNs (Neve et al., 2004). Dopamine binding to D1Rs activates adenylyl cyclase within direct pathway MSNs, which enhances their activity. Dopamine binding to D2Rs instead inactivates adenylyl cyclase, and therefore dopamine suppresses the activity of indirect pathway MSNs. Additionally, due to differences in the affinities of these receptors, the D2Rs are occupied at lower concentrations of dopamine

(e.g. during tonic firing) while phasic dopamine release would mostly recruit the lower affinity D1Rs (Gerfen et al., 1990; Gerfen & Surmeier, 2011; Surmeier et al., 2007). The loss of dopamine tone as PD progresses would result in over-activity in the indirect pathway and thereby shift the balance of dopaminergic excitation and inhibition towards inhibition, resulting in depressed activity in motor cortex. Indeed, stimulation of the direct pathway in the DS promotes locomotion, while stimulating the indirect pathway reduces movement (Cazorla et al., 2014; Kravitz et al., 2010).

From this model, one would expect to see increased activity in the direct pathway and decreased activity in the indirect pathway during movement. Correspondingly, immobility would be accompanied by a decrease in direct pathway activity and an increase in indirect pathway activity. However, recording D1R- and D2R-expressing MSNs during movement found that both subtypes show increased activity during movement and display minimal activity during immobility (Barbera et al., 2016; Cui et al., 2013; Isomura et al., 2013; Jin, Tecuapetla, & Costa, 2014; Klaus et al., 2017; Markowitz et al., 2018; Parker et al., 2018; Tecuapetla, Matias, Dugue, Mainen, & Costa, 2014), leading some researchers to posit a more nuanced view of these circuits. Some have argued that this dual pathway architecture would allow for a role of nigrostriatal dopamine in action selection, which then becomes disordered in Parkinson's disease, resulting in the dysfunction of voluntary movement (Costa, 2007; Howard, Li, Geddes, & Jin, 2017; Stopper, Tse, Montes, Wiedman, & Floresco, 2014; Surmeier, Plotkin, & Shen, 2009). These circuits have also been posited to modulate ongoing movements: Yttri and Dudman (2016) found that stimulation of either pathway can bolster or reduce movement, but the direction of effect is dependent on whether the stimulation occurred during fast- or slow-

movement trials: stimulation of direct pathway neurons increased movement velocity during the former, but stimulation of indirect pathway neurons increased the velocity of the latter. The balance of activity between direct and indirect pathway neurons might thus reflect some aspect of movement vigour (c.f. review: Klaus et al., 2019).

In the dopaminergic system, encoding of movement vigour has been reported in neurons that also encode action initiation. da Silva et al. (2018) found a subpopulation of dopaminergic neurons which increased their firing before the initiation of self-paced actions. Furthermore, this relationship is causal, as optogenetic activation increased the likelihood of action initiation while inactivation decreased this likelihood. Indeed, several authors have similarly reported encoding of action initiation in the phasic firing and axonal activity of dopaminergic neurons (Coddington & Dudman, 2018; Dodson et al., 2016; Howe & Dombeck, 2016; Jin & Costa, 2010). The evidence supporting a role for dopamine in the initiation of actions dovetails with the parkinsonian literature: PD patients specifically struggle with the initiation of movements, but movement *can* be triggered with strong, external cues (Rubinstein, Giladi, & Hausdorff, 2002; Snijders, Kesteren, & Bloem, 2012).

These findings challenge the notion that phasic dopaminergic activity only reflects RPE, but there is compelling evidence for a multiplexing of function. Hamid et al. (2016) trained rats in a two-arm bandit task and optogenetically activated dopaminergic neurons at different timepoints within each trial. When rats were idle, stimulation promoted trial initiation but did not act as a learning signal, as this stimulation had no effect on subsequent left/right choice. However, stimulation after the left/right choice had been made *did* impact on subsequent choice, in line with the predictions of the RPE hypothesis.

Furthermore, dopamine concentrations in NAc are shaped by both action initiation and reward, as RPE-like signals in response to a 'go' cue are only in evidence when movement is required to obtain reward. Furthermore, Syed et al. (2016) found an RPE-like phasic increase in NAc dopamine release to an instrumental cue only when reward delivery was contingent on movement, suggesting that RPE is action- rather than simply value-dependent. These findings provide compelling evidence that phasic dopaminergic activity functions as both a learning and a movement signal. Indeed, these concepts are not entirely separable: it has long been argued that dopamine has a specific role in motor and skill learning, in particular for the learning of sequences of actions (Bailey & Mair, 2006; Graybiel, 1998; Hikosaka, Miyashita, Miyachi, Sakai, & Lu, 1998; Hikosaka et al., 1999; Yin et al., 2009).

That these are relatively novel findings in a literature spanning decades perhaps reflects a common theme in behavioural paradigms used to measure RPE, namely that collection of reward often necessitates some form of movement. As such, isolating separable dopaminergic correlates for reward and movement respectively would require careful experimental design to avoid this confound. As yet, the exact nature of this multiplexing of function has not yet been fully explored.

1.3. Heterogeneity among dopamine circuits

1.3.1. Dopaminergic neuronal heterogeneity

Dopamine signalling is complex, not only in the heterogeneity of the anatomical circuits but also in understanding its function. But while the association of dopaminergic

signalling with such a broad range of behaviours may seem contradictory, this functional heterogeneity may at least partially be explained by anatomical heterogeneity. The broad division of nigrostriatal versus mesolimbic function has historically posited separable roles for both circuits. SNc neurons are selectively dysfunctional in PD and the direct/indirect pathway model is associated with the nigrostriatal pathway. By contrast, much of the literature focusing on reward-associated dopamine signalling has focused on the mesolimbic pathway. And indeed, the phasic firing of dopaminergic neurons of the VTA and SNc have been associated with different aspects of behaviour. While movement correlates have been recorded in VTA dopamine neurons (Hughes et al., 2020), neurons displaying RPE-like firing activity are commonly found in the VTA, more so than the SNc (Schultz et al., 1993), suggesting that VTA dopamine might be more strongly associated with reward and learning. Optogenetic activation of both VTA and SNc neurons in the absence of external reward can turn a neutral stimulus into a conditioned stimulus, but only for cues associated with VTA stimulation does this conditioned stimulus reinforce instrumental actions; SNc cues instead resulted in more vigorous, undirected movement (Saunders, Richard, Margolis, & Janak, 2018).

In contrast, SNc neurons are associated more closely with action initiation and vigour. Dodson et al. (2016) found that most dopaminergic neurons recorded in substantia nigra *pars lateralis* (SNL) *increased* their firing prior to movement onset, while neurons in the SNc typically phasically *decreased* their firing; meanwhile, some VTA neurons showed an SNL-like increase in phasic firing at movement onset but most recorded did not encode movement at all. In a similar vein, Howe and Dombeck (2016) found with photometric recordings of calcium transients that the axons of SNc dopaminergic neurons tended to

display movement-related activity, while those of VTA neurons typically encoded reward. Based on the targets of these axonal projections, this translates to a gradient of function across the dorsal-ventral striatal axis from movement to reward. Additionally, action initiation-encoding neurons which change their firing based on the vigour of ensuing movements were also reported specifically in the SNc (da Silva et al., 2018). The dopaminergic encoding of reward vs. action initiation describes dissociable regions of the circuits.

Aside from their associated behavioural correlates, there is diversity in the electrical and molecular properties of midbrain dopaminergic neurons. Different subtypes are associated with distinct projections, broadly following a medial-lateral gradient in rodent midbrain. Among subtypes of midbrain dopaminergic neurons, differences in bursting, pausing and even mean firing frequencies have been reported. For instance, low *in vivo* burstiness has been reported in medial compared to lateral DLS-projecting SNc neurons (Farassat et al., 2019).

There are also molecular differences between these dopaminergic neuronal subtypes (Anderegg, Poulin, & Awatramani, 2015; Poulin et al., 2018). Of particular interest in this thesis are those molecular differences which might shape the resulting dopamine release. SNc dopaminergic neurons have been consistently reported to contain more DAT than those in VTA (Afonso-Oramas et al., 2009; Bannon & Whitty, 1997; Freed et al., 1995; González-Hernández, Barroso-Chinea, de la Cruz Muros, del Mar Pérez-Delgado, & Rodríguez, 2004; Reyes, Cottam, Kirik, Double, & Halliday, 2013; Sanghera et al., 1994). There is also meaningful variation among VTA subpopulations in this regard, with the highest levels of DAT typically found in dorsolateral VTA (Lammel et al., 2008; Reyes et

al., 2013). Differences in the expression of the vesicular monoamine transporter have also been reported between subtypes of midbrain dopaminergic neurons, but these findings have been mixed: one study found higher levels in dorsal, ventral and medial SNc compared to VTA (Reyes et al., 2013); however, another reported in higher levels in VTA compared to SNc (Liang, Nelson, Yazdani, Pasbakhsh, & German, 2004). Some SNc dopaminergic neurons can also co-release GABA, which may affect GABA-mediated modulation of dopamine release (Tritsch, Ding, & Sabatini, 2012; Tritsch, Oh, Gu, & Sabatini, 2014).

1.3.2. Striatal heterogeneity

The striatum itself also shows considerable heterogeneity beyond the diversity of its dopaminergic efferents. The direct/indirect pathway model for PD (Albin et al., 1989) is studied in dorsostriatal circuits; conversely, much of the RPE literature has focused on VS, specifically NAcc, as the projection target of VTA dopamine neurons. But additionally, dorsal and ventral striatum have dissociable roles in learning, with DS associated with instrumental learning (Balleine, Liljeholm, & Ostlund, 2009) while VS is more strongly associated with Pavlovian learning (Day & Carelli, 2007). In a conditioned avoidance response task, in which both Pavlovian and instrumental learning are required, striatal lesions in either DS or VS (specifically, the NAcc) resulted in impaired learning of the instrumental component, but only VS lesions affected learning of the Pavlovian component (Wendler et al., 2014).

This functional heterogeneity extends even beyond the binary of dorsal and ventral striatum. Most of the major hypotheses about the role of dopamine in reward learning

arise from studies of NAcc dopamine in particular, and signalling in this subregion is critical for Pavlovian cue-reward learning and cue motivation (Day, Roitman, Wightman, & Carelli, 2007; Hamid et al., 2016; Mohebi et al., 2019; Saunders et al., 2018). Dopamine in the NAcsh is itself more heterogeneous, with 'hotspots' of dopaminergic signalling (Al-Hasani et al., 2015; Castro & Berridge, 2014; Richard & Berridge, 2011). Unlike NAcc, NAcsh dopaminergic signalling is not particularly associated with associative learning, but rather with reward reinforcement and representing motivational drive (Bassareo & Di Chiara, 1999; Kelley & Delfs, 1991; Saddoris, Cacciapaglia, Wightman, & Carelli, 2015; Saunders et al., 2018; Wyvell & Berridge, 2000).

The dorsal striatum is also heterogeneous in function, with a number of studies finding dissociable roles for the DMS and DLS in learning. Sometimes referred to as the 'associative' striatum, the DMS is most often associated with action-outcome learning critical for 'goal-directed' behaviours, which are sensitive to changes in the value of outcomes (Gremel & Costa, 2013; Hilario, Holloway, Jin, & Costa, 2012; Yin, Ostlund, Knowlton, & Balleine, 2005). On the hand, the DLS, or 'sensorimotor' striatum, is thought to be responsible for stimulus-response learning that is critical for 'habit-like' behaviours, insensitive to changes in outcome value (Balleine, Delgado, & Hikosaka, 2007; Dickinson, 1994). This distinction has reached a broad consensus in the literature (c.f. reviews: Corbit, 2018; Schreiner et al., 2020; Yin & Knowlton, 2006), although some have argued against a strict DLS/DMS dichotomy of function (Malvaez & Wassum, 2018; Vandaele & Janak, 2018).

The dynamics of dopamine release are also heterogeneous across the striatum. In the DS, dopamine release is maximal < 500 ms after the onset of stimulation and decays during

continued stimulation; in NAcsh, dopamine instead increases progressively throughout the stimulation train (Rice et al., 2011). The frequency dependence of dopamine release also varies by striatal region. The ratio of dopamine release evoked by single pulse stimulation as opposed to high-frequency stimulation trains is highest in VS and lowest in DLS (Davidson & Stamford, 1993; Patel, Trout, & Kruk, 1992; Trout & Kruk, 1992). Some studies have reported VS dopamine release as overall more frequency- and pulse number-dependent than in DS (Cragg, 2003; Cragg, Hille, & Greenfield, 2000; Cragg et al., 2000; Davidson & Stamford, 1993; Exley, Clements, Hartung, McIntosh, & Cragg, 2008; Patel et al., 1992; Rice & Cragg, 2004). Within the DS in particular, there is considerable site-to-site variation in the magnitude and characteristics of evoked dopamine transients measured with FCV even across very short distances within the striatum, possibly due to interference from myelinated fibres in the striatum or small-scale differences in local dopaminergic regulation (May & Wightman, 1989).

1.3.3. Heterogeneity in local striatal microcircuitry

The kinetics, volume and duration of dopamine signals are markedly distinct across striatal subregions (Brown, McCutcheon, Cone, Ragozzino, & Roitman, 2011; Cragg et al., 2000; Howe & Dombeck, 2016; Jones, Garris, Kilts, & Wightman, 1995; Sulzer et al., 2016; van Elzelingen et al., 2022), which may be due to differences in local modulation of dopamine release and/or uptake. One candidate underlying variable signalling across the striatum is DAT, which is the primary mechanism of dopamine clearance from the extracellular space (Giros, Jaber, Jones, Wightman, & Caron, 1996; Jones et al., 1999, 1998; Rice & Cragg, 2008). DAT exists in higher concentration in the DS than VS, and in NAcc

than in NAcsh (Ciliax et al., 1995; Cragg et al., 2000; Jones et al., 1995; Jones, O'Dell, Marshall, & Wightman, 1996; Marshall, O'Dell, Navarrete, & Rosenstein, 1990; Nirenberg et al., 1997; Stamford, Kruk, Palij, & Millar, 1988). As a result, DS dopamine is cleared more quickly relative to VS, which naturally affects the dynamics of the signal (Calipari, Huggins, Mathews, & Jones, 2012; Cragg & Rice, 2004; Garris & Wightman, 1994; Jones et al., 1995). Accordingly, DAT-mediated modulation of short-term plasticity of striatal dopamine release is also more powerful in DS than VS (Condon et al., 2019). Aside from DAT, there is also greater regulation of striatal dopamine release by D2 autoreceptors in the VS relative to the DS (Davidson & Stamford, 1993; Patel et al., 1992; Trout & Kruk, 1992; Wieczorek & Kruk, 1995), as well as differences in the initial release probability, which is lower in VS relative to DS (Cragg, 2003; Davidson & Stamford, 1993; Patel et al., 1992; Trout & Kruk, 1992).

Another candidate is ChIs, which are major modulators of axonal dopamine release (Kramer et al., 2022; Rice & Cragg, 2004; Threlfell & Cragg, 2011; Threlfell et al., 2012; Zhang & Sulzer, 2004; Zhou, Liang, & Dani, 2001). The role of cholinergic receptors in this modulation also differs across DS and VS. Nicotinic acetycholine receptors containing α6 and β2 subunits are expressed throughout the striatum, but they play a significantly larger role in regulating VS dopamine release relative to DS (Exley et al., 2008). Similarly, M2 and M4 muscarinic acetylcholine receptors are required for cholinergic regulation of dopamine release within the DS, but only M4 receptors are necessary for this regulation in VS (Threlfell et al., 2010), consistent with the differential expression of these receptor subtypes in ChIs across the striatum (Alcantara et al., 2001; Yan & Surmeier, 1996). Additionally, fewer subtypes of voltage-gated calcium channels present on VS axons

impact dopamine regulation relative to those present on DS axons (Brimblecombe, Gracie, Platt, & Cragg, 2015). But although there is considerable evidence to suggest heterogeneity in dopamine modulation across the striatum, the dynamics of dopamine signalling in different striatal subregions (and their functional relevance) remain unclear.

1.4. Research aims

Dopaminergic activity is dissociable across several axes: anatomically, functionally, and dynamically. Despite being one of the most well-studied neurotransmitters in the mammalian brain, the complexity and heterogeneity of dopaminergic circuitry and function means there is still considerable room to investigate the dynamics of its signalling. While the phasic activity of dopaminergic neurons is associated with the release of dopamine in striatum, there remain unanswered questions about the exact nature of this relationship. Additionally, much is unknown about the dynamical and functional heterogeneity of dopaminergic signalling in different subregions of the striatum. Furthermore, despite the enormous potential of these fluorescent sensors, their relative novelty means that their dynamics *in vivo* have not yet been fully characterised.

The work in this thesis was carried out to gain insight into the heterogeneity of different modes of dopamine signalling *in vivo*, by recording dopaminergic neuronal firing and dopamine release in different striatal subregions in both awake and anaesthetised mice. My specific aims were to:

- Develop a method to examine the relationship between evoked dopaminergic neuronal firing and striatal dopamine release (Chapter 3).
- Compare the dynamics of dopamine signalling read out by FCV and a novel fluorescent sensor for dopamine (Chapter 4)
- Investigate regional differences in striatal dopamine release dynamics (Chapter 4).
- Evaluate the dynamics and behavioural correlates of striatal dopamine release from DLS and VS in reward and movement (Chapter 5).

Chapter 2. MATERIALS AND METHODS

2.1. Animals

All experimental procedures in this thesis were carried out on mice and conducted in accordance with the Animals (Scientific Procedures) Act, 1986 (United Kingdom).

For experiments requiring selective expression of channel-rhodopsin (ChR2) in dopaminergic neurons for optogenetic stimulation (see the experiment described in section 2.4), adult mice expressing Cre recombinase under the control of the promoter of the DAT gene ($DAT^{IREScre}$, The Jackson Laboratory, 006660; Bäckman et al., 2006) were used. These mice, henceforth referred to as DAT-Cre mice, were heterozygous for the Slc6a3-internal ribosome entry site (IRES)-Cre transgene and were maintained on a C57BL/6J background. Adult C57Bl/6J mice, henceforth referred to as wild-type (WT) mice, were used for all other experiments.

Both male and female mice were used and group-housed with their littermates whenever possible: animals were only single-housed when there was evidence of significant infighting between cage mates or when no littermates were available. Mice were 8-16 weeks at date of first procedure and were maintained in ventilated cages on a 12/12-hour light/dark cycle (lights on 7:00 – 19:00). Mice were provided with ad libitum access to food and water, except for those on a water restriction protocol (see section 5.3.2). Details regarding the specific age and sex of animals for each experiment can be found in the associated results chapter.

2.2. Stereotaxic cranial surgery

2.2.1. General procedure for recovery surgeries

Mice underwent recovery surgery to express viral constructs in the brain (see section 2.2.3) and for the chronic implantation of headplates (section 2.2.4) and optic fibre cannulae (section 2.2.5). Mice were anaesthetised using 3% (v/v) isoflurane (Abbott; delivered in O_2 at 2 L/min) for induction and 1–2% isoflurane for maintenance. Depth of anaesthesia was regularly assessed by checking for the absence of a hindlimb withdrawal reflex in response to a firm pinch of the hindpaw. The head was then shaved and the mouse was placed in a stereotaxic frame (David Kopf Instruments) on a homeothermic heating mat (Harvard Apparatus). Prior to surgery, perioperative analgesia was administered systemically (buprenorphine, 0.08 mg/kg, s.c.; Ceva) and local anaesthetic (0.5% bupivacaine hydrochloride, 0.02 ml, s.c.; Aspen) was delivered to the incision site. Corneal dehydration was prevented using a carbomer eye gel (Optixcare). Post-surgery, animals were returned to their home cage once they had regained full ambulatory capabilities and monitored in the following days to assess their recovery.

2.2.2. General procedure for non-recovery surgeries

Non-recovery procedures were employed for mice undergoing anaesthetised recordings of neural activity. General anaesthesia in mice was induced with 3-4% isofluorane (Abbott; delivered in O_2 at 2L/min) and maintained with urethane (ethyl carbamate dissolved in distilled water (dH_2O), 10% (w/v); initial dose 1.55 mg/kg i.p.; Sigma Aldrich). Mice were considered sufficiently anaesthetised when they no longer had

a hindlimb withdrawal reflex. Their heads were shaved and they were placed in the stereotaxic frame (David Kopf Instruments). To counter respiratory depression caused by urethane administration, air enriched with O_2 was delivered throughout the procedure. If the hindlimb withdrawal reflex was present, the animal was topped up with additional urethane (0.15 mg/kg, i.p.). A carbomer eye gel (Optixcare) was used to prevent dehydration. Body temperature was maintained at 36.5 ± 0.5°C using a homeothermic heating mat (Harvard Apparatus). After recordings were completed, mice were perfused as outlined in section 2.7.1.

2.2.3. Intracranial injection of viral vectors

Expression of florescent proteins and ChR2 in the brain was achieved by intracranial injection of adeno-associated viral constructs (AAVs). The mouse's skull was exposed, and injection coordinates were marked relative to Bregma. Small craniotomies (~2mm^2) were drilled above the site of each intracranial injection. Before surgery, a calibrated glass micropipette (7087-07, Blaubrand® intraMark, Brand) was made using a vertical puller (PE-2, Narishige) to create a long tip (manually broken to make a flat tip with an inner diameter of 15-20 μm). All viruses were stored at -80°C, thawed and loaded into the micropipette via suction by a 25 mL syringe on the day of surgery. The filled micropipette was lowered into the craniotomy to the appropriate depth from brain surface and pressure-injected into the brain using the syringe. Pipettes remained in the brain for 5 minutes after each injection to allow for diffusion of the virus and minimise reflux along the pipette track.

Mice subjected to optogenetic stimulation (section 2.4.3) were injected with an opsin prior to recording. The opsin chosen for these experiments was a Cre-dependent viral vector expressing a 'double-floxed' mutant of ChR2 (AAV2-Ef1a-DIO-hChR2(E123T/T159C)-EYFP at ~1x10^{13} genome copies/ml; University of North Carolina Vector Core). The hChR2(E123T/T159C) double mutation combines the larger photocurrents from the T159C mutation with the faster kinetics from the E123T mutation, chosen so that the opsin would be sensitive to stimulation frequencies encompassing the physiological range of dopaminergic firing. In these mice, 500 nl of the AAV construct was pressure-injected into the ventral tegmental area (VTA; *AP* = -3.2, *ML* = ±0.5, *DV* = 3.8) and another 500 nl into substantia nigra *pars compacta* (SNc; *AP* = -3.2, *ML* = ±1.6, *DV* = 3.6) at a rate of ~100nl/min. Recordings from mice injected with this opsin were carried out 4-8 weeks after the initial injection to allow time for viral expression.

The dLight viral construct (see section 2.5.1) was injected into the striatum of mice for optical recording of dopamine transients. For non-recovery anaesthetised experiments, (section 2.5.3) 200 nl of undiluted dLight 1.1 AAV (AAV5-CAG-dLight1.1 at ~7×10^{12} genome copies/ml; Addgene) was pressure-injected into the striatum in the dorsolateral striatum (DS; *AP* = 0.5, *ML* = ±2.3, *DV* = 2.5) and a further 200 nl into the ventral striatum (VS; *AP* = 1.4, *ML* = ±0.8, *DV* = 3.8) at 50-100nl/min, one injection per hemisphere. For these mice, subsequent photometric recordings were conducted at least 3 weeks after the initial injection.

For mice undergoing behavioural training, tdTomato (ssAAV-5-hSyn1-chI-tdTomato-WPRE-SV40p(A) at 4.9 x 10^{12} genome copies; ETH Zurich Viral Vector Facility) was also expressed alongside dLight as a control fluorophore to allow for two-channel motion

correction (section 2.5.5). In these mice, 500 nl of a viral mixture was pressure-injected each striatal site (DLS and VS, at the same co- ordinates as above striatum at a rate of ~66 nl/min. The mixture consisted of sterile saline and AAVs expressing dLight 1.1 and tdTomato in a ratio of 4:5:1, prepared on the day of each surgery. Animals under this behavioural experimental protocol were photometrically recorded from only after full recovery from surgery, 1-2 weeks after intracranial injection.

2.2.4. Headplate fixation

Mice used for head-fixed behavioural training underwent headplate fixation surgery at least one week prior to habituation. Custom-designed headplates (0.82 g; width = 2.3 cm, length = 1.2 cm) were machine printed in titanium (Protolabs) and sterilised in 70% ethanol. The skull was exposed in the shape of the headplate, such that the back bar sat just behind lambda and the remainder of the frame made good contact with the anterior skull. The skull surface was first prepared with Red Activator solution (Super-Bond C&B, Sun Medical) to make the skull surface more porous and thereby increase later adhesion of the cement. The skull was washed thoroughly with sterile saline 30 s after application. The edges of the skin were then affixed to the skull with Vetbond Tissue Adhesive (3M) just outside the bounds of the headplated area. Superglue (Loctite) was used to keep the headplate in place on the skull prior to cementing. An additional EEG screw was affixed to the skull behind lambda through the headplate. This screw was attached to a stripped wire for optional grounding of the animal during behaviour. Once all components were in place, cement (Super-Bond C&B, Sun Medical) was applied, keeping within the bounds of the headplate. The combined weight of the cement and headplate was ~1.2g.

2.2.5. Fibre-optic cannula implantation

Mice which underwent head-fixed behavioural training were also implanted with fibre-optic cannulae for dLight recordings. After the skull was prepared for headplate fixation, mice were pressure-injected with a diluted mixture of dLight 1.1 and tdTomato (section 2.2.3) in the DLS (*AP* = +0.5, *ML* = ±2.3, *DV* = 2.5) and ipsilateral VS (*AP* = +1.4, *ML* = ±0.8, *DV* = 3.8). Following injection, steel ferrule-coupled fibre-optic cannulae (200μm, 0.39 NA, 5mm long; ThorLabs) was stereotaxically lowered into the striatum to the same coordinates as each injection and cemented in place (Super-Bond C&B, Sun Medical). Each cannula was affixed separately.

2.3. Fast-scan cyclic voltammetric recordings of dopamine transients

2.3.1. Acquisition of voltammetric data

All fast-scan cyclic voltammetry (FCV) data were recorded from urethane-anaesthetised mice (see section 2.2.2). FCV data were acquired using a potentiostat (EI-400, Cypress Systems). Waveform application and data acquisition were carried out through Tarheel CV (LabVIEW, National Instruments) via a multifunction input/output card (PCI-6052E, National Instruments). A silver/silver chloride (Ag/AgCl) reference electrode was used to maintain an absolute potential relative to the working electrode, a carbon-fibre microelectrode. When the system was active but not scanning, the working electrode was held at -0.4 V. During a voltammetric scan, potential was applied to the working electrode in a triangular waveform, such that it ramped linearly to a maximum

potential of 1.3 V and returned to the holding potential at a rate of 400 V/s (8.5 ms total scan time).

All electrodes used for these recordings were made in-house. Working electrodes were made by threading a carbon fibre (7 μm tip diameter) through a borosilicate tube such that fibre was exposed on both sides. The recording side was insulted with epoxy resin while the other was attached to a silver pin with conductive silver epoxy. The pin and silver epoxy were then insulated with epoxy resin and the carbon fibre tip was trimmed to 150-200 μm. Reference electrodes were constructed by attaching silver wire (cut to ~6 mm) to a silver pin using silver epoxy and insulating the point of connection with epoxy resin. To create the silver chloride layer, the silver wire portion of the electrode was soaked overnight in sodium hypochlorite.

2.3.2. Recording FCV in vivo

To voltammetrically record evoked dopamine release, both the reference and working electrodes were lowered into the brain and interfaced with the potentiostat. Reference electrodes were cemented in place either far anterior (experiments described in section 2.3.3 or Chapter 4) or far posterior in the brain (experiments described in section 2.4.5 or chapter 3), to minimise damage to critical brain tissue. Prior to data acquisition, the working electrode was cycled in the striatum at 60Hz for at least 20 minutes, until the recorded signal was stable and without drift. The depth of both the stimulation and the working electrode were adjusted incrementally to determine the optimal recording location. During data acquisition, the sampling frequency of the potentiostat was set to 10 Hz (one scan every 100 ms).

Just prior to terminal anaesthesia and perfusion, a current (50 μA for 30 s, delivered by a constant current isolator: A360D or A365R, World Precision Instruments) was applied to the working electrode to create a microlesion wherever the carbon fibre was located. This allowed for *post-hoc* histological identification of the FCV recording location.

2.3.3. Electrically evoked FCV

Urethane-anaesthetised WT mice were used to record electrically evoked FCV transients (section 2.2.2). Small craniotomies were made ipsilaterally above the DLS (*AP* = +0.5, *ML* = ±2.3, *DV* = +2.5) and/or the VS (*AP* = +1.4, *ML* = ±0.8, *DV* = +3.8). A larger window was removed over the ipsilateral midbrain, starting from just lateral to the superior sagittal sinus (at least 1mm^2). An additional craniotomy was drilled in the far anterior contralateral hemisphere for placement of the FCV reference electrode. The FCV reference and working electrodes were positioned in the brain as described in section 2.3.2, with the reference in the hemisphere contralateral to the recording site.

A parallel bipolar stimulation electrode (MS303/2-A/SPC, Plastics One, Bilaney) coupled to a constant current stimulus isolator (DS3, Digitimer) was lowered incrementally into the midbrain craniotomy (*AP* = ∼-3.2, *ML* = ∼±1.0, *DV* = 4.7-5.2). Electrical stimulation was driven by TTL pulses to the stimulus isolator via Tarheel to avoid stimulation artifacts in the FCV data: the software times stimulation so that it does not co-occur with FCV scans.

The effect of stimulation was recorded at each depth of the stimulation electrode until a positive evoked dopamine response could be observed. A negative transient or an initial dip in prior to a positive transient indicated that the stimulating electrode was above the

optimal recording site. The location of both the stimulation electrode and working electrode were adjusted incrementally until an optimal recording site had been located.

Data were collected by manually inputting stimulation parameters according to pre-randomised blocks consisting of one of each stimulation parameter, at an ISI of 55-65 s. This target ISI was occasionally exceeded to check errors in the parameter definitions and file names, but care was taken to ensure that each ISI was not below this range. Between 4 and 6 blocks were recorded for each stimulation type. In cases where time constraints or poor signal to noise ratio prohibited collection of the full set of parameters, lowest priority was given to collecting 3 pulse stimulation and second lowest to 5 Hz stimulation. Animals in which only a subset of parameters were collected were still included in the final dataset.

After collection from the initial recording site, the process was repeated for the second site in the ipsilateral hemisphere. The position of the stimulating electrode was not changed for the second recording unless the signal to noise ratio of the evoked dopaminergic response was too low for meaningful data to be collected. The region initially recorded was counter-balanced between animals to avoid order effects.

2.3.4. Analysis of voltammetric data

FCV data were imported into MATLAB for further processing. Raw data were background-subtracted using a background 1 second prior to stimulation and low-pass filtered with a 4^{th}-order Butterworth filter at 0.0340 Hz. Chemometric analysis was used to extract dopamine traces from the processed data using an open-access toolbox for FCV chemometrics in Tarheel (https://github.com/TJP-code/fcv_data_processing; as used in

Panayi et al., 2023). A principal components regression was performed using a previously acquired training set of other analytes. The first component from this regression was extracted as the dopamine trace for each trial. Data were mean normalised to the pre-stimulation baseline. Electrical artifacts were removed by thresholding and replacing the artifact epoch with a linear interpolation.

2.4. Recording optically evoked dopaminergic neuronal activity and striatal dopaminergic release

2.4.1. Single-unit electrophysiology: Preparation of experimental animals

For these experiments, DAT-Cre mice underwent recovery surgery 3-6 weeks prior to recording (section 2.2.1). This surgery involved the injection of an Cre-dependent opsin into the midbrain for the selective expression of ChR2 in dopaminergic neurons (section 2.2.3). All recordings were conducted under urethane anaesthesia (section 2.2.2).

To ground the animal, a silver wire was inserted through the mouse's neck muscle and connected to the electrophysiology amplifier. An intracranial electroencephalogram (iEEG) was recorded to aid in monitoring of depth of anaesthesia by inserting a stainless screw over left secondary motor cortex (*AP* = +2.5, *ML* = -2.5) referenced to an identical screw over ipsilateral cerebellum. A rectangular craniotomy was drilled over the intended recording site. This craniotomy was regularly supplied with physiological saline (0.9% w/v) to avoid drying of the cortical surface. Following each experiment, mice were injected with pentobarbitone and transcardially perfused with fixative (section 2.7.1).

2.4.2. Single-unit electrophysiology: Data acquisition and processing

Action potentials of single neurons were juxtacellularly recorded with glass electrodes (manually broken to give a tip diameter of 1.5 ± 0.2 μm; 7-27 MΩ impedance in situ; GC120F-10, Harvard Apparatus; made using vertical puller, PE-2, Narishige). Electrodes were filled with 0.5 M NaCl containing Neurobiotin (1.5% w/v, Vector Laboratories). The juxtacellular electrode was stereotaxically positioned above the midbrain craniotomy at a 15° angle from anterior to posterior. The insertion coordinates for the electrode were calculated using Pythagorean theorem, such that the original injection track was the adjacent (0°) and the new juxtacellular electrode track was the hypotenuse (θ = 10°). At the correct depth, the tip of the electrode would be positioned within the midbrain. The electrode was then lowered into the brain at these coordinates using a computer-controlled micro-manipulator (IVM-1000; Scientifica).

Single unit activity was recorded and amplified (10x) through the active bridge circuitry of an ELX-01MX amplifier (NPI Electronic Instruments). These signals were filtered at 0.3-5 kHz and subject to a further 100x amplification (DPA-2FS filter/amplifier; NPI Electronic instruments). Raw iEEG signals were band-pass filtered at 0.3-1500 Hz (-3 dB limits) and subject to 2000x amplification (DPA-2FS filter amplifier; NPI Electronic Instruments) prior to acquisition. Both signals were sampled at 20 kHz using a Power 1401 analogue-digital converter and Spike2 acquisition and analysis software (Version 8.14; Cambridge Electronic Design). A Humbug (Quest Scientific) was used to eliminate mains noise at 50 Hz.

To minimise bias when searching for neurons, pre-defined criteria were used for identification. Putative dopaminergic neurons had a biphasic action potential with a

duration of ≥ 0.9 ms (interval between the point the upward slope is > 15% and the minimum of the trough) and a baseline firing rate of ≤ 11 spikes/s (Ungless & Grace, 2012).

2.4.3. Single-unit electrophysiology: Optogenetic stimulation

Optogenetic stimulation was driven by a 100 mW 473 nm diode-pumped solid-state laser (CL473-100-O, CrystaLaser). Laser pulses were driven by TTL pulses from the Power1401 analogue-digital convertor via the output sequencer in Spike2. Before each session, the power of the laser was calibrated to ~10 mW output at the tip as measured by an optical sensor coupled to an optical power meter (S121C (sensor), PM100D (power meter), Thor Labs).

To identify virally transduced dopaminergic neurons, a naked 100 µm optic fibre (Multimode Fibre, 0.22 NA, Glass Cut Silica Core; ThorLabs) coupled to the laser was inserted into the juxtacellular micropipette alongside the Ag/AgCl wire. This in-glass fibre was used to locally stimulate the juxtacellular recording site as the electrode moved through the brain.

Once the correct midbrain location had been discerned, the juxtacellular electrode was raised. The laser was recoupled with a 200 µm optic fibre (Multimode Fibre, 0.22 NA, Glass Cut Silica Core; ThorLabs) which was then inserted at a 0˚ angle above the midbrain. This fibre could stimulate a wider field of midbrain dopaminergic neurons to evoke robust dopamine release in striatum.

With the 200 µm optic fibre in position, the glass pipette was lowered back into the midbrain, still at a 15° angle. Once a suitable neuron had been identified (putatively

dopaminergic and responsive to optogenetic stimulation), a 5-minute baseline recording of action potential firing was taken before recording the neuron's response to the optogenetic stimulation protocol.

2.4.4. Single-unit electrophysiology: Labelling of single neurons

When possible, cells were juxtacellularly labelled with Neurobiotin after the completion of the recording protocol using the juxtacellular method (Brown et al., 2009; Dodson et al., 2016; Pinault, 1996). The depth of the electrode was carefully adjusted until the amplitude of the action potential was at least 1 mV and an iontotrophic current was applied (1-10 nA anodal current, 200 ms duration, 50% duty cycle). The amplitude of the applied current was manually tuned such that the neuron's firing was entrained to the current pulse, which facilitates selective uptake of neurobiotin in the neuron of interest. Neurons were entrained for 2-5 minutes, which is sufficient to label the somata and often also the proximal dendrites. This allows for the post-hoc localisation and neurochemical identification of the recorded neuron.

2.4.5. Simultaneous FCV and single-unit electrophysiology

For experiments requiring simultaneous acquisition of optically evoked single unit activity and striatal dopamine release, a rectangular craniotomy was drilled above the ipsilateral striatum (approx. AP = +1.5 to +0.5, ML = +0.5 to +2.0) in addition to the midbrain craniotomy for the placement of the FCV working electrode. Another small craniotomy was made behind lambda ipsilaterally for the placement of the FCV reference electrode (section 2.3.2). The FCV working electrode was stereotaxically lowered into the

striatum (*AP* = +1.2, *ML* = +1.3, *DV* = 3.0-3.7). After the 200 µm optic fibre was positioned in the brain, the depth of the working electrode was adjusted until an optically evoked dopamine response could be measured. To synchronise both recordings, stimulation was triggered in Spike2 via a TTL out from Tarheel.

2.5. dLight photometry

2.5.1. dLight as an optical sensor for dopamine

dLight is a genetically encoded dopamine indicator which can be used in combination with an optical sensor to give an online readout of dopaminergic activity in the brain (Patriarchi et al., 2018). dLight 1.1, the construct used for these experiments, consists of circularly permuted green fluorescent protein (cpGFP) module replacing the third intracellular loop of a human dopamine D1 receptor (D1R). Dopamine-binding-induced conformational changes in the dLight receptor result in increased fluorescence in the cpGFP in response to blue light (~465 nm; peak emission = 516 nm). The dLight receptor is packaged in an adeno-associated viral construct (see the description of dLight in section 2.2.3). When injected into the striatum of WT mice, the dLight receptor is expressed locally in the tissue pan neuronally, not restricted to any particular cell type.

2.5.2. Measuring dLight with pyPhotometry

All photometry data were collected using the open-source python-based pyPhotometry acquisition system and software (Akam & Walton, 2019). All light is sent through a 5-port fluorescence mini cube (iFMC5, Doric), a system of filters and optical

collimators which combines both excitation lights toward the sample port and separates fluorescence coming from the sample port. LEDs were used to excite fluorophores in the tissue: a 465 nm blue LED (CLED_465, Doric) for the excitation of 'GFP-like' proteins (e.g. dLight) and a 560 nm green LED (CLED_560, Doric) for 'RFP-like' proteins (e.g. tdTomato), connected to the mini cube with mono fibre optic patch cords (200 μm diameter, NA = 0.48, Doric). Fluorescence was sent and sampled via another patch cord (200 μm diameter, NA = 0.57, Doric) sleeve-coupled to an optic fibre cannula in the brain (200 μm, NA = 0.39, Thor Labs). Received light was sent (via mono fibre patch cords; 600 μm, NA = 0.48, Doric) to two photoreceivers (Newport Visible Femtowatt Photoreceiver Module, 2151, Newport), which convert the photometric signal into an analogue voltage and sends this to the pyPhotometry acquisition board.

With two fluorophores, data can either be acquired in continuous mode, with constant illumination in both channels (sampling rate = 1 kHz) or in 2-colour time-division mode (sampling rate = 130 Hz). In this latter mode, the red and green channels are sampled alternately, which drastically reduces crosstalk between the two channels, and baseline-subtracted. The separate red and green channels in this set up allow for motion correction by co-expressing a separate fluorophore that is independent of neuronal activity, in my case tdTomato in the red channel. When motion-correction was required (e.g. in non-anaesthetised preparations), signals were acquired in 2-colour time division mode.

2.5.3. Photometric assessment of electrically evoked dopamine release

dLight-injected mice were used to photometrically record electrically evoked dopamine release. For these experiments, WT mice underwent recovery surgery 3-8

weeks prior to recording (section 2.2.1). This surgery involved the injection of dLight 1.1 AAV into the DLS (*AP* = +0.5, *ML* = ±2.3, *DV* = 2.5) and contralateral VS (*AP* = +1.4, *ML* = ±0.8, *DV* = 3.8) to express the dLight receptor at these sites, with the target hemispheres counter-balanced across animals (section 2.2.3). All photometric recordings for these experiments were conducted under urethane anaesthesia (section 2.2.2). Small craniotomies were made for the striatal recording sites contralaterally (matching the location of the injections for each mouse) and for the stimulation sites bilaterally above the midbrain (*AP* = -3.3, *ML* = ±1.0, *DV* = 4.7-5.2).

Photometric recordings were carried out with an acutely implanted ceramic ferrule-coupled fibre optic cannula (200μm diameter, 0.37 NA, manually cleaved fibre; Doric Lenses) sleeve-coupled to the photometry kit. dLight data were acquired with pyPhotometry in continuous mode (section 2.5.2). The LED intensity was adjusted such that the acquired signal was in the middle of the dynamic range of the measurement apparatus, or to maximum output when this was not possible (60-100mA).

To avoid clashing between the midbrain stimulation electrode and striatal optic fibre, optic fibres were inserted at a 10° angle from anterior to posterior. Therefore, the appropriate coordinates for the recording craniotomies were calculated for each animal using Pythagorean theorem, such that the original injection track was the adjacent (0°) and the new optic fibre track the hypotenuse (θ = 10°). A new DV was calculated based on the injection coordinates, taking the difference in the height of the skull anterior to the injection site into account. An increase in the baseline fluorescence closer to the target site was taken as a sign that the fibre was in an area of dLight expression.

A concentric stimulation electrode (Rhodes Medical Instruments) coupled to a constant current stimulus isolator (A365R, World Precision Instruments) was lowered incrementally towards the midbrain or MFB stimulation site ipsilateral to the striatal recording site. Electrical stimulation was driven by TTL pulses to the stimulus isolator via the output sequencer in Spike2. The effect of midbrain stimulation was recorded at each depth of the stimulation electrode until a measurable evoked dLight response could be observed in striatum. The locations of both the stimulation electrode and optic fibre were adjusted incrementally until an optimal recording site had been located.

A custom script was created in Spike2 to trigger a train of electrical stimuli every 30 s in a fully randomised order for a given number of trials for each stimulation parameter. A 30-minute baseline recording was acquired prior to data acquisition consisting of 3 trials (3 x 18 = 54 total trials), with the actual dataset consisting of 10 trials (10 x 18 = 180 trials).

After collection from the initial striatal recording site, the process was repeated for the second striatal site in the contralateral hemisphere. The region initially recorded was counter-balanced between animals to avoid order effects. Animals were perfused after these recordings had concluded (section 2.7.1).

2.5.4. Pre-processing of photometric data

All pre-processing was carried out in Python (Anaconda version 4.10.3) using functions from the *scipy* and *numpy* modules. Imported signals were first median-filtered (kernel size = 5) then low-pass filtered at 5Hz using a 2nd-order zero-phase Butterworth filter to reduce noise and electrical artifacts. When photobleaching occurs it causes a

negative drift in the signal baseline over the course of the recording, which was corrected by subtracting a 4th-degree polynomial fitted to the whole signal.

In experiments involving behaving mice (section 2.6), signals were motion-corrected at this stage. Motion was estimated by regressing the dLight signal onto the tdTomato signal. Estimated motion was subtracted from the dLight signal.

ΔF/F, the change in fluorescence relative to baseline, was then calculated as,

$$\frac{\Delta F}{F} = \frac{filtered\ signal - F0}{F0}$$

where F0 is the mean of the filtered signal.

2.5.5. Motion correction of photometric data

Shifting of the fibre in the brain as the animal moves can cause movement artifacts in the dLight data, thus photometric signals in behaving animals are usually motion corrected. One form of motion correction involves recording a comparison signal at the isosbestic point of the target fluorescent protein, which can be simplistically defined as the specific wavelength or frequency at which the absorbance of the sample is the same regardless of its state. When dLight absorbs light at its isosbestic point, the emitted fluorescence will be the same when it is bound to dopamine and when it is not. Therefore, the isosbestic signal should contain the same motion artifacts as the target wavelength but no state-dependent activity and thus can be used to remove motion artifacts.

Another option is to use a separate control fluorophore not tied to any state-dependent activity. Red fluorophores such as tdTomato are commonly used for this purpose, as their excitation and emission spectra only moderately overlap with green

fluorophores (e.g. dLight1.1). This works on the same principle as the isosbestic signal, but has the key advantage of ensuring that the control signal has absolutely no tie to any state-dependent activity; if the 'isosbestic' signal is not truly isosbestic, motion correction may affect readout of state-dependent activity.

All motion-correction in these experiments was performed using tdTomato as a control fluorophore. The tdTomato signal was pre-processed in the same way as the dLight signal, as described above. Motion was estimated by regressing this tdTomato signal onto the pre-processed dLight signal and applying the parameters of this regression to the tdTomato signal. The estimated motion was then subtracted from the dLight signal to give a final estimate of motion-corrected dLight.

While it is well-established that movement artifacts are present in photometric recordings conducted in freely moving animals, this is not necessarily the case for head-fixed animals: the presence or absence of any movement artifacts would be dependent on the security of a particular head-fixed setup. In these experiments, the data were manually inspected for movement artifacts but none were found. A typical example from these data is shown in Figure 2.1. Note that the tdTomato signal is relatively flat and the estimated motion is minimal. Overlaying the mean pre-processed dLight signal and the mean motion-corrected signal around a behaviourally relevant timepoint in the task (cue delivery), as shown in Figure 2.1E, suggests that motion-correction does not meaningfully affect the dLight signal either positively or negatively. However, as the downside of encountering and not correcting for movement artifacts going forward is greater than the benefits of not performing a harmless correction, all photometric data from behaving mice in this thesis were motion-corrected as 'best-practise'

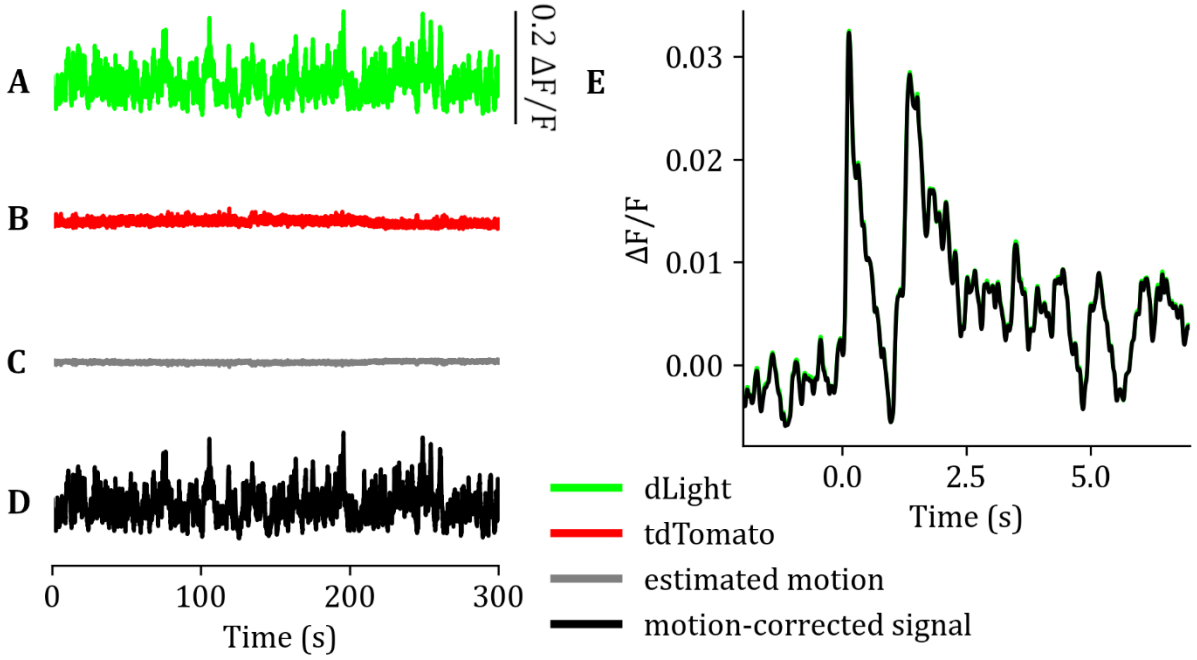


Figure 2.1: ***A demonstration of motion correction on dLight data collected in a head-fixed behavioural mouse.*** *This figure shows a snapshot of photometry data from the behaving mouse, with separate traces are shown for* ***A****, the pre-processed dLight signal;* ***B****, the pre-processed tdTomato signal;* ***C****, estimated motion; and,* ***D****, the motion-corrected signal.* ***E****, Mean dLight and mean motion-corrected signal centred around cue delivery (0 s).*

2.6. Head-fixed behavioural training

2.6.1. Behavioural apparatus: Treadmill

The task required mice to run on a treadmill, which was custom-built for this setup using 3D designs built in Fusion 360 (Autodesk), adapted from the design used by a previous member of the lab (as used in Avvisati et al., 2022). See Figure 2.2 for a picture of the assembled treadmill.

The plastic components for the base of the treadmill were 3D-printed (Ultimaker S3). These consisted of two wheels, a middle support for the treads and four axle supports. A stainless-steel rod was threaded through each wheel and glued in place (Loctite). A

miniature ball bearing (623-2RS, RS PRO), housed within an axle holder, was then glued onto each axle.

A frame was constructed for the treadmill to sit in, constructed using a MakerBeam hardware. Individual beams were trimmed when necessary to ensure that the dimensions of the frame matched the length of the axles. The axle holders were fitted to the frame with a nut and bolt, so that the treadmill could be easily removed from the frame for cleaning. The frame itself was affixed to an optical post on a rail (ThorLabs), so that the position and height of the treadmill could be adjusted when necessary.

The treadmill surface was a series of identical interlocking treads, which were also custom printed. As each tread had to be printed very accurately while also being flexible enough for assembly, the treads were printed on a resin printer (Form 2 or Form 3L, FormLabs, using Black V4 resin). Each tread was trimmed of its supports and inspected to ensure print quality. Treads were washed in isopropyl alcohol and UV cured for 30 minutes. The full track was then manually assembled, with each connection rotated to minimise stiffness in the joints.

2.6.2. Behavioural apparatus: Training environment and video recording

Mice were trained in custom-built behavioural apparatus within an MDF sound attenuating cubicle (ENV018MD-27, Med Associates). All components were attached to an anodized solid aluminium breadboard using optical post assemblies from ThorLabs (see Figure 2.2). Head-fixation was maintained using a machine-printed titanium frame held above the treadmill (Figure 2.2C). The position of the frame was adjusted for each setup to ensure animals were comfortably positioned on the treadmill.

Illumination of the cubicle was in the infrared (IR) range (LED IR Illuminator Lamp, BW; Figure 2.2D), not within the visible spectrum of mice. This meant that the mouse could perform the task in perceived darkness. Two IR cameras (camera: MQ013RG-ON, xiQ range, XIMEA; lenses: MVL4WA, ThorLabs) were used for each setup, one positioned to record the animals' face and the other a full body profile (Figure 2.2E, F). All video data were recorded using Streampix digital video recording software (NorPix; 100 fps) and then compressed to MP4 using H264.

2.6.3. Behavioural apparatus: pyControl

The setup was designed around pyControl, a system of open-source software and hardware designed for behavioural animal experiments. (Akam et al., 2022). All hardware components of the pyControl behavioural setup (audio board, rotary encoder adapter, lickometer board and rotary encoder adapter) were controlled/read out through ethernet connections to the pyControl breakout board (Figure 2.2G). One of the treadmill's axles was long enough to extend outside of the treadmill's frame. This axle was connected to a rotary encoder (HEDM-5500, Digikey) and interfaced with the rotary encoder adapter for online readout of treadmill movement (Figure 2.2B). A custom-printed case was fitted over the rotary encoder and adapter to hold them in place while the treadmill was moving. Sounds in the task were played through a mini-speaker positioned to the left of the animal (ABS-230-RC, MULTICOMP PRO), connected to pyControl audio board (Figure 2.2H). The volume of each speaker was controlled by the task.

Water was delivered to the mouse through a metal spout (Figure 2.2I). This spout was connected to a small reservoir held above the box by a system of tubes (Versilon™, ABX6FB004, Saint Gobain) and a solenoid valve (LHDA1231215H, Lee Products). The solenoid was connected to a pyControl lickometer (Figure 2.2J) via a twisted cable to minimise noise. By computationally manipulating the duration that the solenoid valve was open, the size of water droplets could be precisely controlled. The target solenoid duration was estimated by weighing the water released from 50 valve events at different durations of solenoid opening (30, 60 and 90 ms) and performing a linear fit through these points, which allowed for extrapolation to the target droplet size (8 µl). Calibration was performed regularly for each setup.

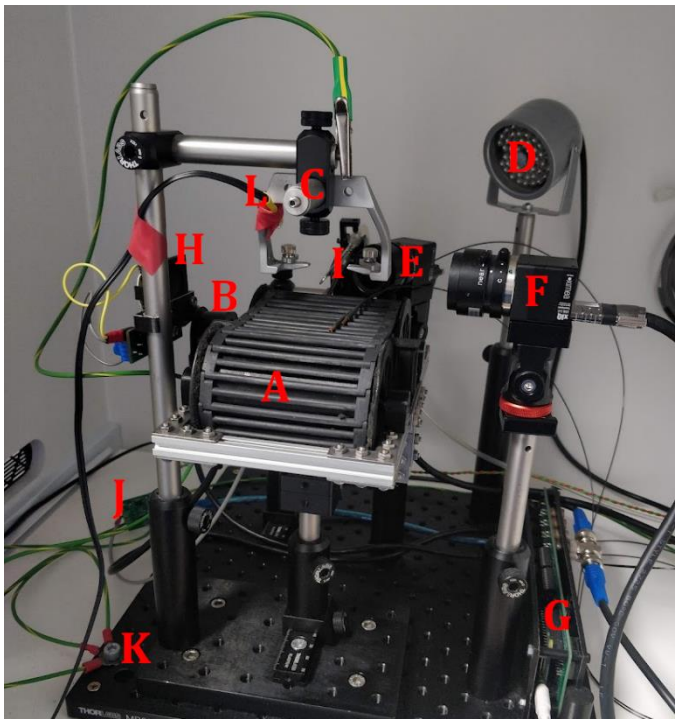


Figure 2.2: ***A diagram of the behavioural apparatus used for training within the sound-attenuating chamber.*** ***A****, treadmill.* ***B****, rotary encoder + adapter.* ***C****, head-fixation.* ***D****, IR lamp.* ***E****, Front camera.* ***F****, Side camera.* ***G****, pyControl breakout board.* ***H****, Speaker + audio board.* ***I****, metal spout for water delivery.* ***J****, lickometer.* ***K****, common ground point.* ***L****, IR LED.*

Aside from controlling the solenoid, the lickometer was also directly connected by cable to the water spout, to record when the animal collected a delivered reward. Lickometers work by recording the change in electrical signal when a grounded animal makes contact with a metal spout held at a different potential, thus completing the circuit. Often this is achieved by the animal standing on a grounded metal surface, but the material of the treadmill in this setup made this impossible. However, the animal was connected via the metal headplate to the rest of the setup. Unfortunately, pyControl's lickometer system was heavily prone to noise, which masked the relevant behavioural signals. Therefore, all metallic components in the setup which might act as an antenna were grounded to an earth bonding plug (298-3890, RS PRO), namely the metallic frame of the shelving on which the boxes sat and the metal components of the behavioural setup. A common ground point on the breadboard (Figure 2.2K) was created by removing the anodized coating from one of the breadboard's holes and fixing all ground wires under a screw. When necessary, an additional cable from the headplate's ground was also connected to the ground point. As a final step to eliminate noise from the lickometer, all in-box hardware were powered through an isolated DC power supply (762-2685, Tenma).

A total of two behavioural boxes were built. The box each mouse was trained in was kept consistent across sessions wherever possible.

2.6.4. Behavioural apparatus: Synchronisation

Photometry was simultaneously recorded throughout training from two separate photometry kits for each behavioural box using the pyPhotometry system (see 2.5.2). pyControl contains a tool called Rsync, which outputs a pulse train with random inter-

pulse intervals. This pulse was sent to both photometry systems as a digital signal via a BNC out from the pyControl board. Each recorded dLight signal was then synchronised to the pyControl output using the Rsync module in the pyControl software.

To synchronise the camera with behavioural timepoints, an IR LED was positioned in view of both cameras (Figure 2.2L). This LED was powered by the Rsync signal by sending the TTL through a resistor. The flashing of the LED in time with the Rsync pulse was recorded by the camera and so that it could be used for *post-hoc* synchronisation with the behavioural and photometric data.

2.7. Immunohistochemistry

2.7.1. Perfusion fixation and tissue processing

At the end of each experiment, the mouse was terminally anaesthetised with sodium pentobarbitone (20% w/v; 200 mg/kg; i.p.) and perfused with ~20-25 ml 0.1 M phosphate-buffered saline (PBS), pH 7.4 followed by ~40-60 ml 4% (w/v) paraformaldehyde (PFA) in 0.1 M phosphate buffer, pH 7.4. The brain was removed and placed in 4% PFA in 0.1 M PFA overnight at 4°C.

Brains were sectioned coronally (50µm thick), either with a vibrating-blade microtome (VT1000S; Leica Microsystems) or with a freezing-stage microtome (HM 450; Epredia). Brains sectioned with the vibrating-blade microtome were embedded in agar (3% w/v dissolved in dH2O) prior to sectioning. Brains sectioned on the freezing stage microtome were cryopreserved in a 30% sucrose solution for 48 hours prior to cutting or until the brain no longer floated in the solution.

Tissue sections were washed 3 times in PBS and blocked for ~2 hours with a solution containing 10% normal donkey serum (NDS; Jackson Immuno Laboratories) in PBS with Triton solution (0.3% (v/v) Triton X-100 and 0.2% w/v sodium azide). Sections were then incubated overnight at room temperature in 1% NDS in Triton PBS containing primary antibodies. After washing 3 times in PBS, sections were incubated in secondary antibodies diluted in PBS-Triton for at least 4 hours at room temperature or overnight at 4°C. See Table 2.1 for all primary antibodies used in this project; see Table 2.2 for all secondary antibodies. After 3 final washes with PBS, the sections were mounted on microscope slides with a glycerol-based aqueous mounting medium (Vectashield, Vector Laboratories; Slowfade™ Diamond, Invitrogen).

Images were taken on an Axio Imager M2 fluorescent microscope (Zeiss) with a Hamamatsu digital camera (C10600) using Stereo Investigator (MBF Bioscience) or Zen Blue (Zeiss) software, or on an Axio Imager Z2 confocal microscope using Zen Black (Zeiss).

2.7.2. Immunohistochemistry: Juxtacellularly recorded neurons

The brains of mice that had undergone single-unit electrophysiology were sectioned in 6 series. For molecular identification of ChR2-expressing dopaminergic neurons, sections were incubated in Anti-TH (Rabbit; Millipore) and anti-GFP primaries (Rat; Nacalai Tesque). Alongside the associated Anti-Rabbit (AMCA; Jackson Immuno Research) and Anti-Rat secondaries (488; Life Technologies), slices were incubated in Cy3 Streptavidin (GE Healthcare) for molecular identification of neurobiotin-labelled cells. To locate the striatal FCV lesion, sections were also incubated in an Anti-GFAP primary

(mouse; Sigma Aldrich) and associated secondary (Anti-Mouse; Cy5, Jackson Immuno Research). All midbrain slices were mounted and inspected to locate the labelled cell, which was imaged separately; all striatal slices were mounted to locate and image the FCV lesion.

2.7.3. Immunohistochemistry: dLight

For all dLight experiments, brains were sectioned in 4 series. Due to the nature of the circularly permuted GFP used in the dLight construct, many Anti-GFP primaries do not bind to dLight. For all experiments using dLight, the primary used was the monoclonal Anti-GFP from Aves Labs (chicken).

For brains in which electrically evoked dLight was recorded, an Anti-GFAP primary (mouse; Sigma Aldrich) was also used for *post-hoc* location of the fibre-optic cannulae and stimulation electrode tracks, alongside an Anti-TH primary (rabbit, Millipore). Three secondaries were used: Anti-Chicken (488; Jackson Immuno Research), Anti-Mouse (Cy5; Jackson Immuno Research) and Anti-Rabbit (AMCA; Jackson Immuno Research). The striatum and midbrain were separately mounted and imaged.

For mice in which dLight was recorded during head-fixed behaviour, tdTomato was co-expressed with dLight. Native tdTomato has the unusual property of photoconverting when exposed to the 405/AMCA range of light under fluorescence microscope, subsequently fluorescing in the 488 channel as well as Cy3 (Kremers, Hazelwood, Murphy, Davidson, & Piston, 2009) which confounds identification of dLight expression under the protocol described above. Therefore, in these cases, the associated secondary for dLight was Cy5-conjugated (Anti-Chicken; Jackson Immuno Research). These sections were also

incubated in Anti-RFP (rat; Chromotek) and Anti-GFAP primaries (mouse; Sigma Aldrich), followed by Anti-Rat (Cy3, Jackson Immuno Research) and Anti-Mouse (AMCA; Jackson Immuno Research). The striatum of the first series was mounted and imaged to confirm the location of the chronically implanted fibre-optic cannulae.

Table 2.1: All primary antibodies used for immunohistochemistry.

Antigen	Species	Company	Product code	Dilution
GFP	Rat	Nacalai Tesque	04404-84	1:1000
TH	Rabbit	Millipore	AB152	1:1000
GFAP	Mouse	Sigma	G3893-2ML	1:1000
dLight	Chicken	Aves Labs	GFP-1020	1:500
RFP	Rat	Chromotek	5f8	1:500

Table 2.2: All secondary antibodies used for immunohistochemistry.

Target	Conjugate	Company	Product code	Dilution
Streptavidin	N/A	GE Healthcare	PA43001	1:1000
Rat	488	Life Technologies	715-545-153	1:1000
Rabbit	AMCA	Jackson Immuno Research	711-155-152	1:250
Mouse	Cy5	Jackson Immuno Research	715-175-151	1:500
Mouse	AMCA	Jackson Immuno Research	715-155-151	1:250
Chicken	488	Jackson Immuno Research	703-545-155	1:1000
Chicken	Cy5	Jackson Immuno Research	703-175-155	1:1000
Rat	Cy3	Jackson Immuno Research	712-165-153	1:1000

Chapter 3. RESULTS I: COMBINING OPTICALLY EVOKED SINGLE-UNIT ELECTROPHYSIOLOGY WITH FAST-SCAN CYCLIC VOLTAMMETRY

3.1. Introduction

Midbrain dopaminergic neurons in the ventral tegmental area (VTA) and substantia nigra *pars compacta* (SNc) project primarily to the striatum, the major input nucleus of the basal ganglia (Björklund & Dunnett, 2007; Ungerstedt, 1971). *In vivo*, these dopaminergic neurons typically fire tonically at 1-10 Hz (Brown et al., 2009; Dai & Tepper, 1998; Dodson et al., 2016; Grace & Bunney, 1983), and often phasically increase their firing rates to 15-50 Hz in response to salient external or internal stimuli, such as rewards or reward-predicting cues (Montague et al., 1996; Schultz et al., 1997; Watabe-Uchida et al., 2017). This phasic modulation of firing rate is presumed to result in greater dopamine release from the axons of these neurons in striatum (Sombers et al., 2009).

However, dopamine release from axons in striatum might not be solely dependent on the (phasic) firing patterns of dopaminergic midbrain neurons. Older studies have proposed a non-linear relationship between dopaminergic firing and release (Gonon, 1988; Gonon & Buda, 1985). There is also compelling evidence that local striatal influences on dopaminergic neuronal axons, such as those arising from the activity of striatal cholinergic interneurons, can 'gate' dopamine release in striatum (Britt & McGehee, 2008; Cachope et al., 2012; Cragg, 2006; Liu et al., 2018; Rice & Cragg, 2004; Threlfell et al., 2012). More recently, Mohebi et al. (2019) found a functional dissociation

between dopaminergic neuron firing in the VTA and subsequent dopamine release in the nucleus accumbens (NAc): separate FCV, dLight and optrode recordings in different groups of rats performing a reward-guided decision-making task suggested that striatal dopamine release related to motivated approach was not always preceded by, or otherwise closely associated with, phasic changes in dopaminergic neuron firing rate. Yet, if there is indeed a non-linear relationship between dopaminergic neuron firing and dopamine release, then it is not yet fully characterised. This issue is fundamental to how we measure and interpret dopaminergic signals *in vivo* in both striatum and midbrain and resolving it should in turn shed light on the functional role of dopamine in the brain.

Studies seeking to examine dopamine levels in striatal regions at high temporal resolution have typically used fast-scan cyclic voltammetry (FCV), an electrochemical technique which can measure levels of extracellular catecholamines at sub-second rates by measuring changes in current resulting from redox reactions at specific voltages (Clark & España, 2023). Microdialysis can be used to measure dopamine *in vivo* but works at a much slower temporal resolution, typically in the scale of minutes, whereas dopamine transients generally last no longer than a few seconds. Additionally, microdialysis electrodes are an order of magnitude larger than the active surface of FCV electrodes (~500 μm vs ~8 μm), so FCV allows for far greater spatial specificity in striatal recording sites. Another alternative to FCV is amperometry, which works on a similar or faster timescale to FCV; however, it measures all changes in current from the application of a fixed potential, which can make it difficult to ensure one is measuring the correct neuroactive substance (Carter & Shieh, 2010). Because of the advantages of FCV, and as a technique that has been used to measure striatal dopamine for decades now, FCV is often

considered a “gold-standard” technique for measuring dopamine over sub-second timescales in the brain.

When recording the action potential firing of individual neurons (i.e. single-unit activity) in the brain, there is often a trade-off between yield and specificity. Intracellular and juxtacellular recordings produce a low yield, especially *in vivo*, but recorded cells can be subsequently labelled with a tracer (e.g. neurobiotin; NB) for *post-hoc* verification of the cell type (Brown et al., 2009; Dodson et al., 2016; Pinault, 1996; Tepper, Sawyer, & Groves, 1987). By contrast, multi-channel extracellular electrodes (probes) can measure a large number of cells simultaneously and are often stable enough to use in chronic preparations, but one can only use firing properties (e.g. firing rate and shape of neuron) to infer the cell type (although this is not always reliable – c.f. Ungless & Grace, 2012). This issue can be partly circumvented by combining electrophysiological recordings with cell-targeted optogenetics and “opto-tagging” of recorded neurons (Lima, Hromádka, Znamenskiy, & Zador, 2009; Tian, Uchida, & Eshel, 2017), e.g. with the use of an optrode and an opsin selectively expressed in dopaminergic neurons, those responsive to light delivery can be assumed to be dopaminergic (Cohen, Haesler, Vong, Lowell, & Uchida, 2012).

However, opto-tagging is not always a useful substitute for the more refined approach of juxtacellular labelling and histological verification, especially with regards to the question at hand. It is by now well established that midbrain dopaminergic neurons are heterogeneous in terms of their molecular profile and projection targets, and thus their function (Howe & Dombeck, 2016; Poulin et al., 2018). In particular, Dodson et al. (2016) juxtacellularly recorded and labelled dopaminergic neurons in behaving mice and found

differential activation of VTA and SNc neurons at the onset of movements. More recent work has shown that the functional variation among dopaminergic neurons is associated with differences between molecularly and anatomically distinct subpopulations of dopaminergic neurons (Avvisati et al., 2022). It is important to take this heterogeneity into account when drawing any conclusions about the relationship between the firing of midbrain dopaminergic neurons and striatal dopaminergic release.

Juxtacellular and FCV recordings have been used extensively to probe the characteristics of midbrain dopamine neuronal firing and striatal dopamine release respectively, but never in combination. Simultaneously recording action potentials and dopamine release would be particularly effective at answering questions concerning their relationship, as it overcomes ambiguities arising from the use of each technique in separate animals. In a behavioural setting, this would be even more powerful, as it would allow for the detection of trial-by-trial correlations between these signals. In this chapter, I shall describe a method I developed to combine juxtacellular recording and labelling of midbrain dopamine neurons with striatal FCV. As proof of principle, I show optically evoked single-unit and FCV data acquired simultaneously from anaesthetised mice and discuss the merits and downsides of combining these two techniques.

3.2. Aims

- To develop a method for simultaneously recording single-unit activity and FCV in the same animal.
- To examine the relationship between optically evoked dopaminergic neuronal firing and striatal dopamine release.

3.3. Methods

3.3.1. A note on methodological approaches to measuring striatal dopamine in vivo

Until very recently, the most popular technique for measuring phasic dopamine levels in striatum was FCV. Under the correct conditions, FCV can report quantal extracellular dopamine release at subsecond timescales, which makes it a powerful tool for examining dopamine release (Clark & España, 2023). However, the changes in current can be very small relative to the size of the background current, especially at physiological levels of dopamine release. This means that the signals are prone to contamination by electrical noise, which can sometimes make it difficult to obtain useful voltammetric data. Nonetheless, FCV has been well-studied for decades, so the dynamics of the signal are by now fairly well characterised. Microdialysis can also report quantal dopamine release but generally at much slower timescales than FCV, rather on the scale of minutes, which makes it an ineffective tool for measuring phasic dopamine transients (Clark & España, 2023).

In the last few years, genetically-encoded fluorescent sensors such as dLight and $GRAB_{DA}$ have emerged as an alternative to FCV for measuring phasic dopamine fluctuations (Patriarchi et al., 2018; Sun et al., 2020). These fluorescent sensors, consisting of dopamine receptors conjugated with GFP, can be virally expressed in a region of interest and optically recorded, for example using photometry or a miniscope. This approach is more straightforward and often easier to implement *in vivo* than FCV and is far less sensitive to electrical noise, but the resulting data can be more difficult to interpret. FCV can be interpreted as a direct measure of quantal extracellular dopamine release, the size of the measured current increasing mostly linearly with extracellular concentration; on the other hand, fluorescent sensors reflect receptor dynamics and

therefore have non-linear dynamics ranges. Quantal dopamine cannot be estimated from the readout of fluorescent sensors.

When considering their use for *in vivo* experiments, however, estimating dopamine concentration is challenging. As such, one of the main advantages FCV has over fluorescent sensors is more relevant to *ex vivo* applications. Indeed, there is a strong argument to be made that the best applications of FCV are for *ex vivo* study, where the signal-to-noise ratios are higher and dopamine concentration can be quantified, allowing for study of circuit and cellular mechanisms. *In vivo* FCV is especially challenging in chronic preparations, as the electrodes are prone to fouling over time. By comparison, measurement approaches using fluorescent sensors are very easy to translate to *in vivo* study, both acute and chronic.

At the time these experiments were conducted, the first of these fluorescent sensors had not yet been made available. FCV was judged the most appropriate tool for measuring evoked phasic dopamine transients *in vivo*.

3.3.2. Recording optically evoked firing of dopaminergic neurons and striatal dopaminergic release

This chapter contains data from 7 DAT-Cre mice (F = 3). In these experiments, electrophysiological recordings of midbrain neuronal firing in response to optical stimulation were recorded concurrently with striatal dopamine release. Prior to recording, mice were injected with opsin in the midbrain (sections 2.2.1 and 2.2.3). On the day of recording, mice were prepared for general anaesthesia and non-recovery surgery (section 2.2.2). Square window craniotomies were opened above the midbrain for single-

unit electrophysiological recordings (sections 2.4.1 and 2.4.2) and above ipsilateral striatum for FCV recordings (sections 2.3.1 and 2.3.2). An additional small craniotomy was made ipsilaterally behind lambda for the FCV reference electrode.

The experimental setup is shown in Figure 3.1A (see also section 2.4.5). The FCV reference electrode was secured in the brain and interfaced with the voltammetric setup. The FCV working electrode was stereotaxically lowered into the dorsal striatum (*AP* = +1.2, *ML* = ±1.3, *DV* = 3.0-3.7). The juxtacellular recording electrode (glass micropipette) was stereotaxically lowered into the midbrain at a 10° angle from anterior to posterior. A stripped optic fibre was lowered into the midbrain above the juxtacellular electrode to stimulate opsin-expressing dopaminergic neurons (section 2.4.3). The depth of the FCV working electrode was adjusted until an optically evoked dopamine response could be measured.

Once a suitable individual neuron had been isolated with the juxtacellular recording electrode (putatively dopaminergic and responsive to optogenetic stimulation), simultaneous electrophysiological recording (section 2.4.2) and FCV recording (section 2.3.2) was carried out in response to the optical stimulation protocol. Each stimulation consisted of 10 pulses (3 ms pulse width, ~10 mW light) at 10, 30 or 50 Hz. 10 trains of each stimulation frequency were delivered in counterbalanced blocks. After recording, the neuron was juxtacellularly labelled with neurobiotin, although in some cases this was not achieved (section 2.4.4).

At the end of each experiment, the striatum of the animal was lesioned at the location of the carbon fibre tip of the FCV working electrode (section 2.3.2). Mice were then terminally anaesthetised with pentobarbitone and perfused (section 2.7.1). Fixed brains

were sectioned and immunohistochemically processed to recover and identify labelled neurons and to locate the FCV lesion (section 2.7.2).

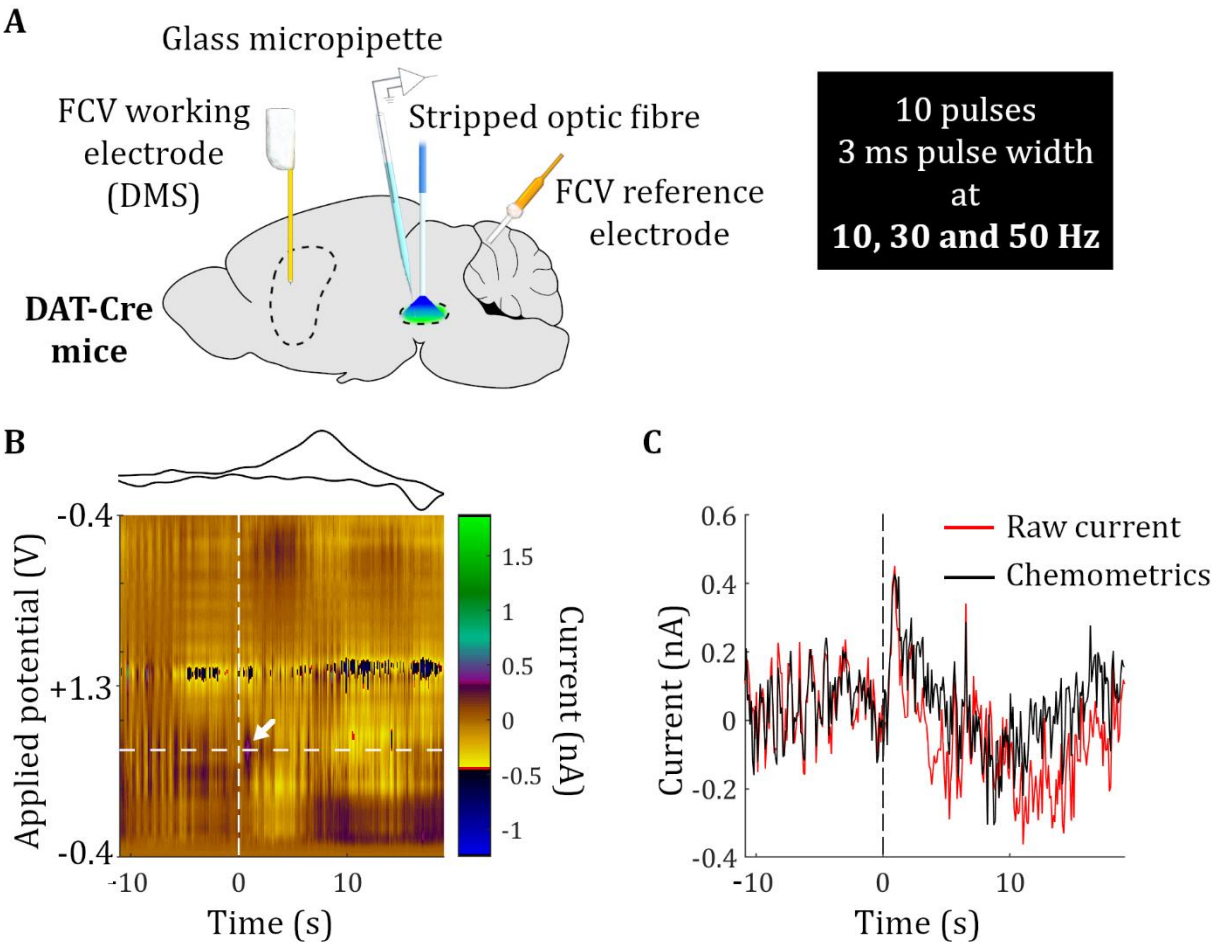


Figure 3.1: ***Graphical illustration of the process of data collection and the pre-processing of optically evoked FCV signal.*** ***A****, Schematic of the experimental setup for simultaneous single-unit and FCV recordings, visualised on a parasagittal section of mouse brain. The black dashed lines demarcate the striatum (left) and the dopaminergic midbrain (right). Optical stimulation parameters for the experiment are given on the right.* ***B****, A single trial from the FCV dataset (30 Hz stimulation) visualised as a colour plot. Peak dopamine after optical stimulation (at timepoint 0, demarcated by the vertical white dashed line) was at 0.664 V (horizontal white dashed line). Data have been low-pass filtered. The cyclic voltammogram 0.8 s after stimulation is shown above the colour plot.* ***C****, The raw and chemometrically extracted dopamine signals from the same trial as B. Optical stimulation occurred at timepoint 0 (black dashed line).*

3.3.3. Difficulties inherent in pairing electrophysiology and voltammetry

Combining two techniques is always technically challenging, as the difficulty of surgery increases with more devices in the brain. However, FCV and electrophysiology have specific incompatibilities that affect the process of data acquisition and the quality of the data recorded.

Application of voltammetric waveforms ('scans') results in large artifacts in the single-unit recording channel. To ensure that these artifacts did not prevent the detection of action potentials fired by dopaminergic neurons recorded with the juxtacellular electrode, the FCV scan waveform was turned off during each track and only applied when cycling or recording. Once a suitable neuron had been isolated, the working electrode was cycled for ~10 minutes until the signal stabilised and the FCV recordings could be conducted, but the presence of a scan artifact in the single-unit recording was unavoidable.

Furthermore, as the voltameter is grounded through the FCV computer, additionally grounding the animal through the electrophysiology rig created a ground loop: noise was reduced in the electrophysiological recordings but was introduced into the FCV recordings. As the resulting signal-to-noise ratio in the FCV was poorer than the signal-to-noise ratio in the electrophysiology recordings without grounding, the animal was left ungrounded for all simultaneous recordings. The additional noise in the single-unit channel added further complications to spike thresholding once data was collected.

3.3.4. Removing FCV artifact from electrophysiological data

The FCV artifact contaminating the electrophysiological data occurs at the same frequency as the FCV scans (10 Hz) and has a similar duration (~10 ms) and a characteristic shape. The amplitude of the artifact varies from recording to recording, but generally peaks between 1 and 2 mV and dips to between 2 and 3 mV (Figure 3.2A).

Action potentials, or 'spikes', were isolated from electrophysiological recordings via spike-sorting (section 2.4.2). The first step of spike-sorting involves identifying a useful threshold to isolate spikes, but as the artifact is generally larger than individual spikes this method will also identify artifacts. While uncontaminated spikes can still be isolated by clustering, the width and prevalence of the scan artifact means that in a not-insignificant portion of cases the spike and artifact co-occur. Figure 3.2B shows an example of a spike 'masked' by the artifact: the shape of the artifact is visibly distorted by the spike, but the peak of the spike (indicated by the black arrowhead) is still clearly identifiable at this resolution. While the spike is still identifiable visually (as the artifact does not saturate the amplifier), it would be difficult to detect via conventional spike-sorting methods.

Given that roughly 10% of each recording consists of artifacts (due to the frequency and duration of FCV scans), ignoring these masked spikes would lead to considerable underestimation of neuronal activity, especially when neurons are firing at higher rates. However, accurately and systematically identifying spikes obscured by the artifact is non-trivial. To address this, I wrote a custom MATLAB script to remove artifacts from electrophysiological recordings. This script works by 1) creating a template of the artifact in each recording; 2) fitting this template to each artifact in turn; and 3) subtracting the fitted template from the electrophysiological data trace (Figure 3.2B). Without a perfect

fit, this final step can result in unnatural peaks and troughs in the clean signal (Figure 3.2C). The resulting signal after artifact removal was therefore checked for errors and manually corrected where necessary.

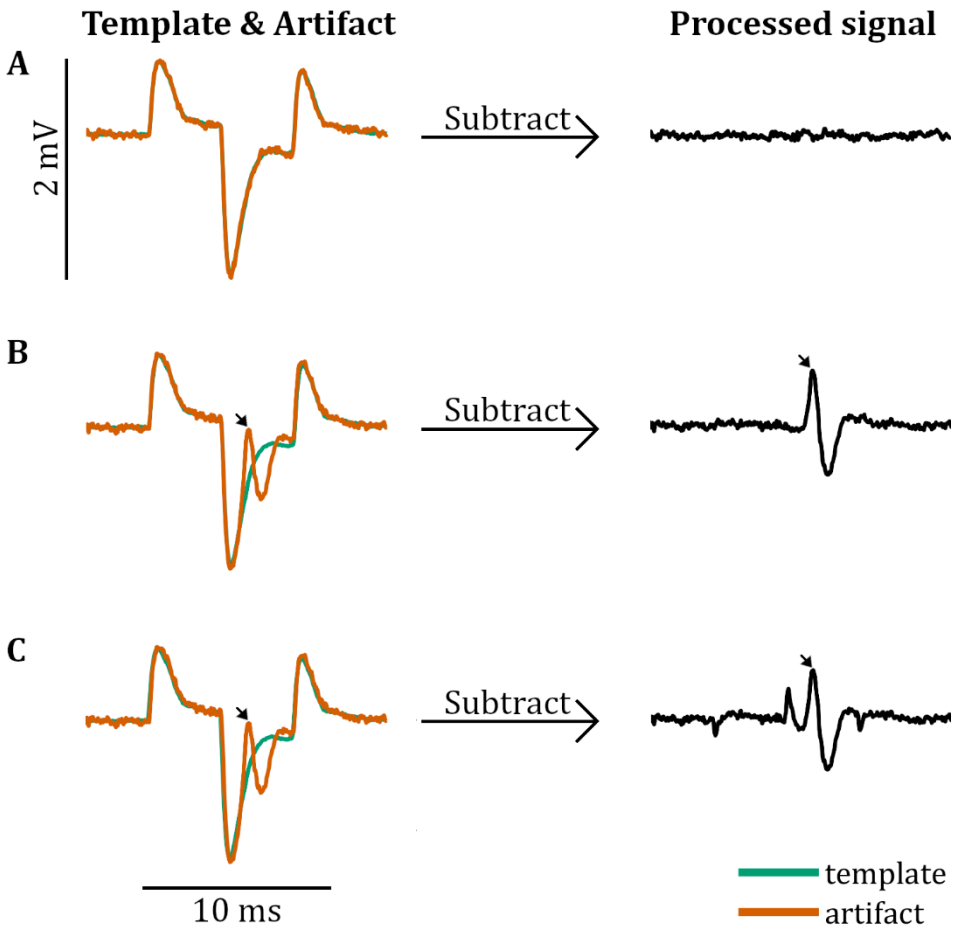


Figure 3.2: ***A demonstration of template subtraction to remove FCV scan artifacts from electrophysiological data****.* ***A****, A phase- and amplitude-matched template is plotted on same axes as an FCV scan artifact extracted from the raw data. Subtracting the template results in the clean signal seen on the right.* ***B****, An example of an artifact removal with a masked spike. Here, subtracting the template results in the recovered spike seen on the right. The peak of the spike is indicated by the black arrows.* ***C****, The same example as B, but the template is improperly fitted. Note that the subtraction errors in C are not present in B.*

First, artifact events were identified by thresholding in Spike2 and then imported to MATLAB. A template artifact was calculated separately for each artifact by finding 200 'local' artifacts (defined as the 100 artifacts preceding and the 100 artifacts following the current artifact). These local artifacts were sorted in order from most consistent in shape (typical artifacts) to least consistent (outliers, e.g. artifacts containing spikes). The template artifact was created by removing the least consistent 50% of artifacts and finding the median of those remaining. This step minimises the effect of minor conformational changes in the artifact across the recording on the artifact-fitting process.

The template was fitted based on two parameters: the phase of the template relative to the current artifact (or the shift across time) and the amplitude. As errors in phase-fitting are more disruptive than those from errors in amplitude-fitting, the phase fitting was calculated first. Both the current and template artifacts were upsampled through interpolation from 20 to 120 kHz to allow for more accurate phase adjustments. As a first pass, the sum of squared deviations (SSD) was calculated between the current artifact and the template at every possible phase-shifted value. The phase-shift that gave the minimum SSD was taken as an initial 'best estimate'.

Following this, the optimal amplitude scalar was calculated. The SSD was calculated between the current artifact and the rescaled template at all values of the scalar between 0.8 and 1.2 at a step-size of 0.0005. As with the phase-estimation, the scalar that provided the minimum SSD was taken as best-estimate.

In several cases, these parameter estimates resulted in an SSD above what would be expected from baseline noise for each recording, which was likely if the artifact co-occurred with a spike. Finding the minimum SSD as described above can provide a poor

readout of template fit, as the spike itself may also be minimised. In such cases, the same phase-fitting procedure was performed instead on the high pass-filtered signals (passband = 0.02 π radians/sample). The sharper angles of the artifact compared to the relatively smooth shape of spikes means that fit adjustment on the filtered signal is less sensitive to conformational changes caused by concurrent spikes. The clean signals for these 'edge case' artifacts were then manually checked and adjusted by eye if necessary to ensure an optimal fit. Once the parameters for best fit were determined for each artifact, the fitted template was subtracted from the raw signal and the resulting signal was downsampled back to 20 kHz, leaving a clean trace. All clean electrophysiological data were spike-sorted by thresholding in Spike2 and imported into MATLAB for further processing.

The key purpose of this script is to recover spikes masked by the artifact, identifiable as a stereotyped distortion in the shape of the artifact. To test whether this script could satisfactorily recover spikes, I created a set of artificial test data by adding 'clean' FCV artifacts from one recording to another artifact-free recording containing 'true' spikes (Figure 3.3). Out of 1215 spikes detected after running the script, only 4 were false positives (identified spikes which were not in the original recording) and 4 were false negatives (spikes from the original recording which could not later be identified; 0.329% false positive and negative respectively; 99.34% true positive). The peak timings of the recovered spikes were identical to those of the true originals.

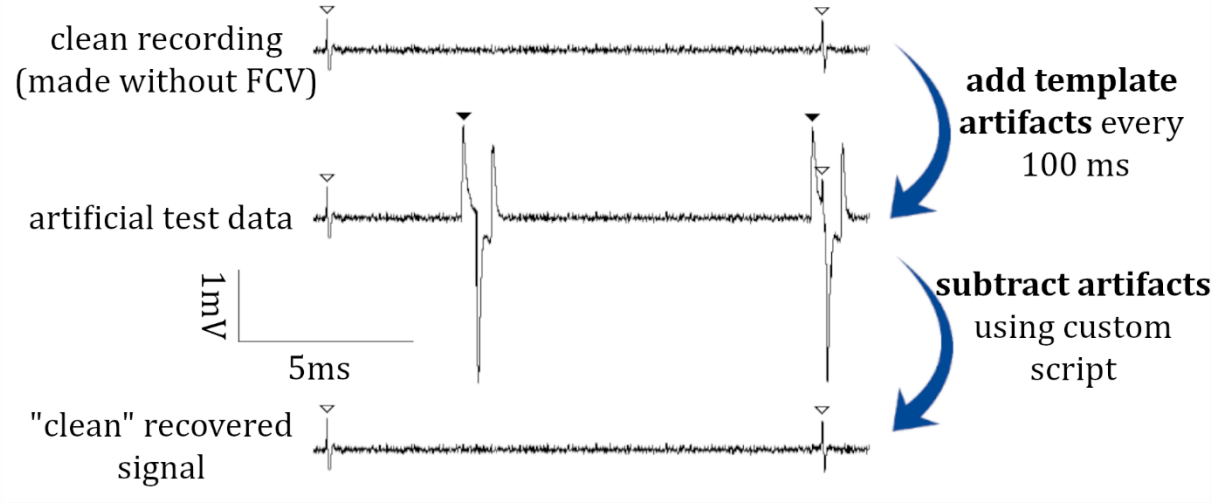


Figure 3.3: ***Schematic of the creation of artificial test data and subsequent artifact removal.*** *Artifacts are added to an electrophysiological recording without artifacts to create the test data. The custom script can remove these FCV artifacts, recovering spikes which would otherwise be missed by standard spike sorting. White arrowheads denote the peaks of spikes; black arrowheads denote the peak of FCV scan artifacts.*

Overall, this demonstrates that this method can be used to remove artifacts from the recorded electrophysiological data with a high degree of accuracy. But under certain conditions, artifact removal becomes far more challenging. This method relies chiefly on two characteristics of the artifact: that it has a consistent shape across recordings and is larger than the recorded spikes. If the artifacts are not consistent, the template will not match well to the artifact and cause subtraction errors. If the spike is a similar size or larger than the artifact, then the script will not be able to fit the template to the artifact. The script is attempting to minimise the overall SSD; with a smaller artifact or a larger spike, subtracting the template from the spike may result in a lower SSD than from the artifact itself. Recordings from three neurons from one of the animals used for this experiment contained small artifacts and large spike amplitudes, and thus were not included in this dataset.

3.3.5. Pre-processing single-unit and FCV data

Juxtacellularly recorded electrophysiological data were put through the artifact removal pipeline described in the previous subsection (section 3.3.4) and the cleaned traces underwent spike sorting (see section 2.4.2). Due to variation in the spontaneous firing rates of neurons, ΔHz was calculated for each stimulation event. This was defined as the difference in firing rate between the stimulation train and a 10 s pre-stimulation baseline to provide a measure of the phasic increase in firing induced by the optical stimulation at each frequency.

Raw FCV data were low-pass filtered (Figure 3.1B) and underwent chemometric analysis (section 2.3.4). The chemometrically extracted dopaminergic transients were then used in all further analyses of FCV data (Figure 3.1C). Data were mean-normalised to a 0.5 s baseline before stimulation (the window was kept small to minimise the effect of signal drift on baselining). The peak of the evoked FCV transient was extracted from the mean trace (averaged across trials) at stimulation frequency.

3.4. Results

Each simultaneous recording can provide electrophysiological, FCV, and anatomical data. Pictured in Figure 3.4 are the full data obtained from a typical simultaneous recording. As shown in Figure 3.4A-C the juxtacellularly recorded neuron was entrained by the optical stimulation, with a clear increase in firing rate at the onset of stimulation. As is fairly typical of neurons in this dataset, the neuron was most strongly entrained to the 10 Hz stimulation (Figure 3.4A) and fired at close to 30 Hz during 30 Hz stimulation (Figure 3.4B) but did not maintain a 50 Hz firing rate for the duration of the 50 Hz pulse train, dramatically decreasing its firing rate after the first few pulses (Figure 3.4C). There is a notable pause in firing of roughly 0.5 s following both 30 and 50 Hz stimulation (Figure 3.4B, C). As shown in the raw trace from the same neuron, the occurrence of optically evoked spikes closely follows the preceding stimulation pulse (Figure 3.4D). The average spike waveform of this particular neuron is shown in Figure 3.4E and displays characteristics typical of an extracellularly recorded action potential from a dopaminergic neuron (Grace & Bunney, 1983; Ungless & Grace, 2012), with a symmetrical peak and trough and a spike width of 1.36 ms. FCV data showed a clear increase in dopamine at the onset of stimulation, with higher frequency stimulation resulting in a higher peak signal. While the increase in neuronal firing rate lasts only for the duration of the stimulation, the FCV signal outlasts it by several seconds (Figure 3.4F). As this neuron was juxtacellularly labelled with NB and the striatum was lesioned following FCV recording, both the cell type and striatal recording location were identified.

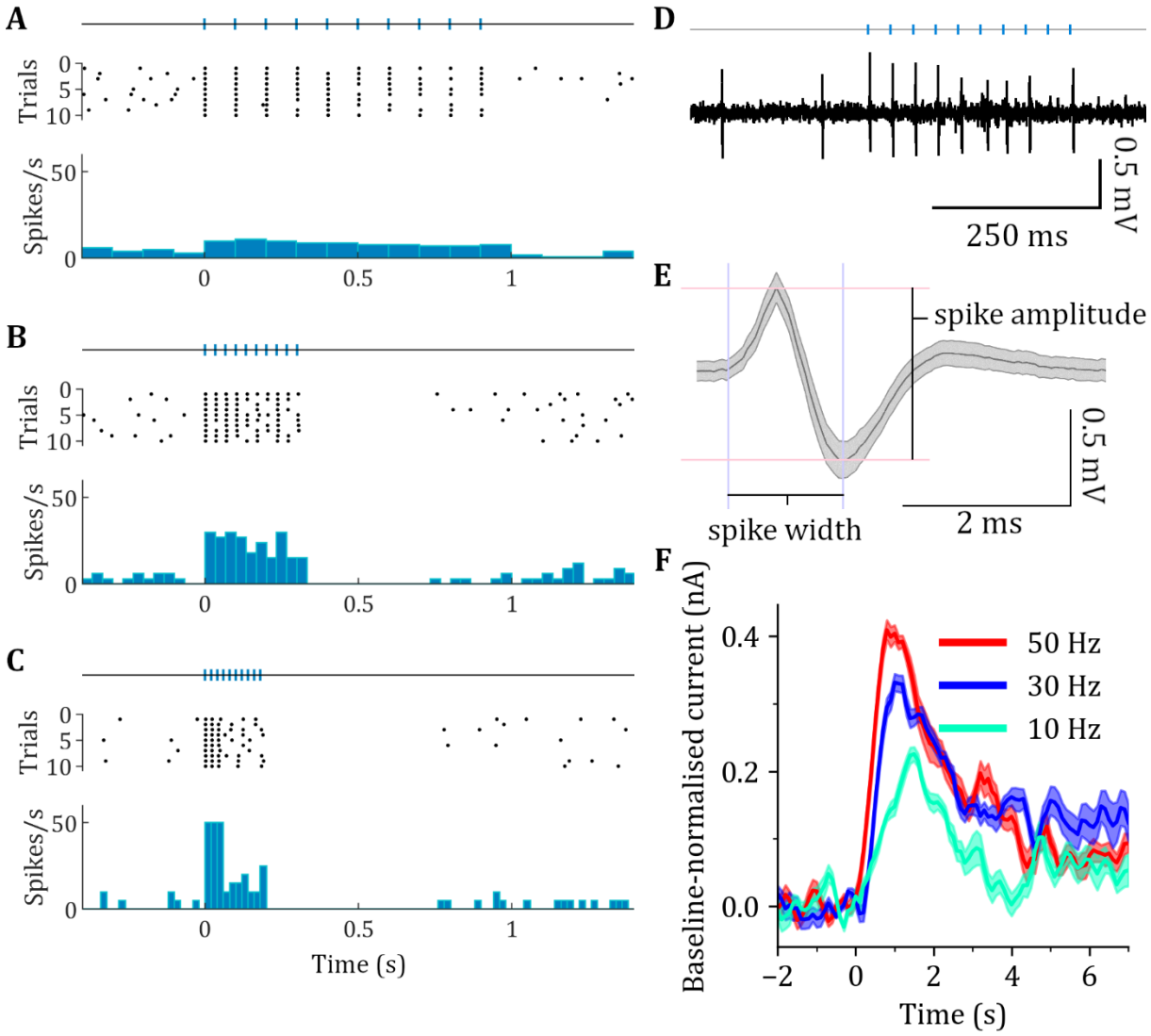


Figure 3.4 ***Simultaneously recorded spike and FCV data for a single neuron.*** *This neuron was histologically verified to be dopaminergic (see Figure 3.5).* ***A-C****, Peristimulus time histograms of single-unit action potentials firing before, during and after optical stimulation at 10 Hz (A), 30 Hz (B) and 50 Hz (C). The optical stimulation train is shown at the top as vertical blue lines. Below is a raster plot of spikes for each trial and then a histogram showing the average spike/s across all 10 trials. Bin size is calibrated such that a single pulse of optical stimulation corresponds to 1 bin.* ***D****, The raw electrophysiological trace from a single 30 Hz stimulation. The stimulation pulses are shown above in blue.* ***E****, The mean (with SD) action potential waveform for the same neuron. Vertical (blue) and horizontal lines (pink) demonstrate respectively how spike width and amplitude were determined.* ***F****, The mean (with SEM) evoked FCV signal collected simultaneously from the dorsal striatum.*

The recorded and labelled neuron was localised to the VTA (Figure 3.5A). It was also verified as dopaminergic by its expression of immunoreactivity for tyrosine hydroxylase (TH), and opsin-expressing due to the presence of GFP immunoreactivity (Figure 3.5B). In Figure 3.5C, the location of the FCV lesion is clear both from the presence of a hole in the tissue just lateral to the ventricle and from the increased GFAP fluorescence surrounding the lesion, indicating that there was increased local tissue response where the lesion was made just prior to the mouse's sacrifice.

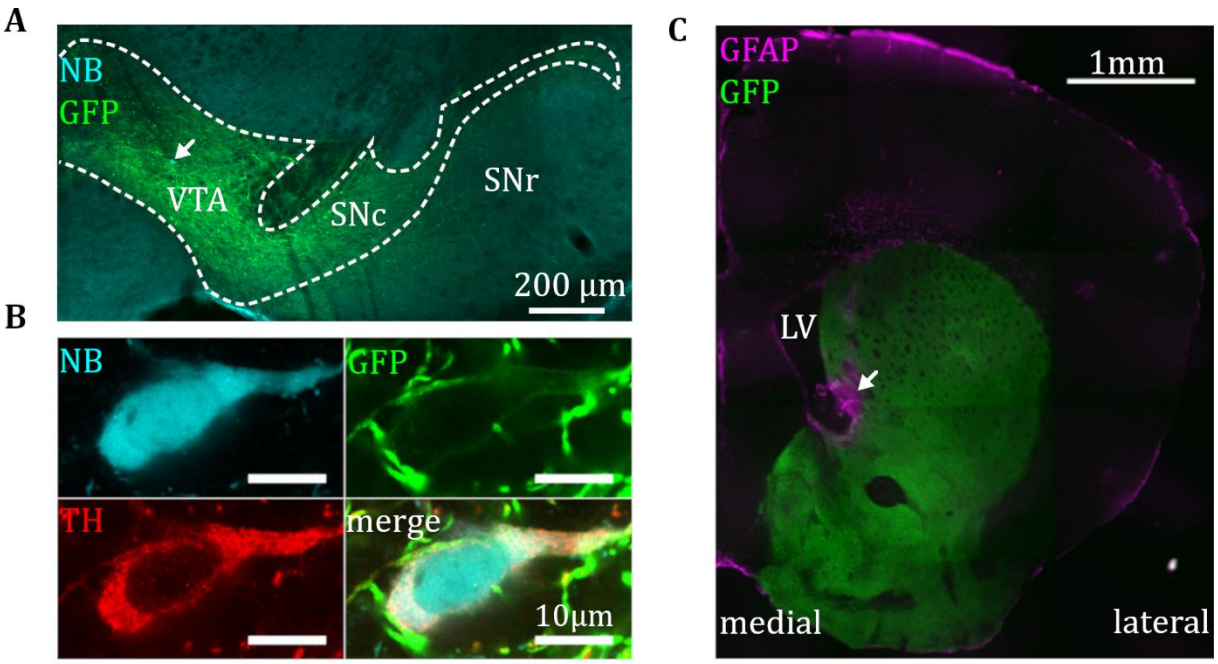


Figure 3.5: ***Histological verification of neuron identity and location and of FCV lesion location for a single animal. A****, The recorded neuron was positive for neurobiotin (NB), GFP and TH, thus verifying that it was a transduced dopaminergic neuron.* ***B,*** *GFP was expressed throughout the midbrain. The neurobiotin-labelled neuron, indicated by a white arrow, was in the VTA.* ***C****, The FCV lesion in the medial aspect of dorsal striatum, demarcated by the white arrow. GFP shows the expression of the opsin, while GFAP shows the local tissue response to lesioning.*

A total of 23 neurons were recorded simultaneously with FCV, 18 of which were responsive to optogenetic stimulation. Of these responsive neurons, 8 were successfully labelled with NB and recovered after anatomical processing; they were located in the VTA (n =5) or SNc (n = 3; Figure 3.6A). These 8 neurons were verified to be dopaminergic (TH-expressing) and opsin-expressing (GFP) and had a mean baseline firing rate of 4.33 spike/s (range = 1.30 – 9.14 spikes/s). The remaining 10 responsive neurons were presumed to be dopaminergic based on the expression of opsin and the characteristics of the waveform matching those typical for dopamine neurons (Dai & Tepper, 1998; Grace & Bunney, 1983). These neurons had a baseline firing rate of 4.23 Hz (range = 0.901 – 7.75 Hz). Non-responsive neurons were not included in further analysis.

The averaged data from all responsive neurons (n = 18) is shown in Figure 3.6. On average, neurons were well entrained to the 10 Hz stimulation, firing one spike consistently for each light pulse with a mean firing rate of 9.32 spikes/s during stimulation (*SD* = 2.43; Figure 3.6B). At 30 Hz stimulation, spike entrainment per pulse was weaker, resulting in a mean firing rate of 20.3 spikes/s (*SD* = 8.12; Figure 3.6C). At 50 Hz stimulation, neuron responses were more varied (*SD* = 14.8) but many failed to fire consistently to each light pulse, firing at an average rate of just 28.1 spikes/s (Figure 3.6D). This is reflected in the peristimulus time histograms (Figure 3.6A-C), wherein neurons recorded during 30 and 50 Hz stimulation, but especially 50 Hz, show a marked decrease in firing frequency over the course of the stimulation train. The average firing rate just after 30 and 50 Hz stimulation is below the average baseline firing rate of all neurons.

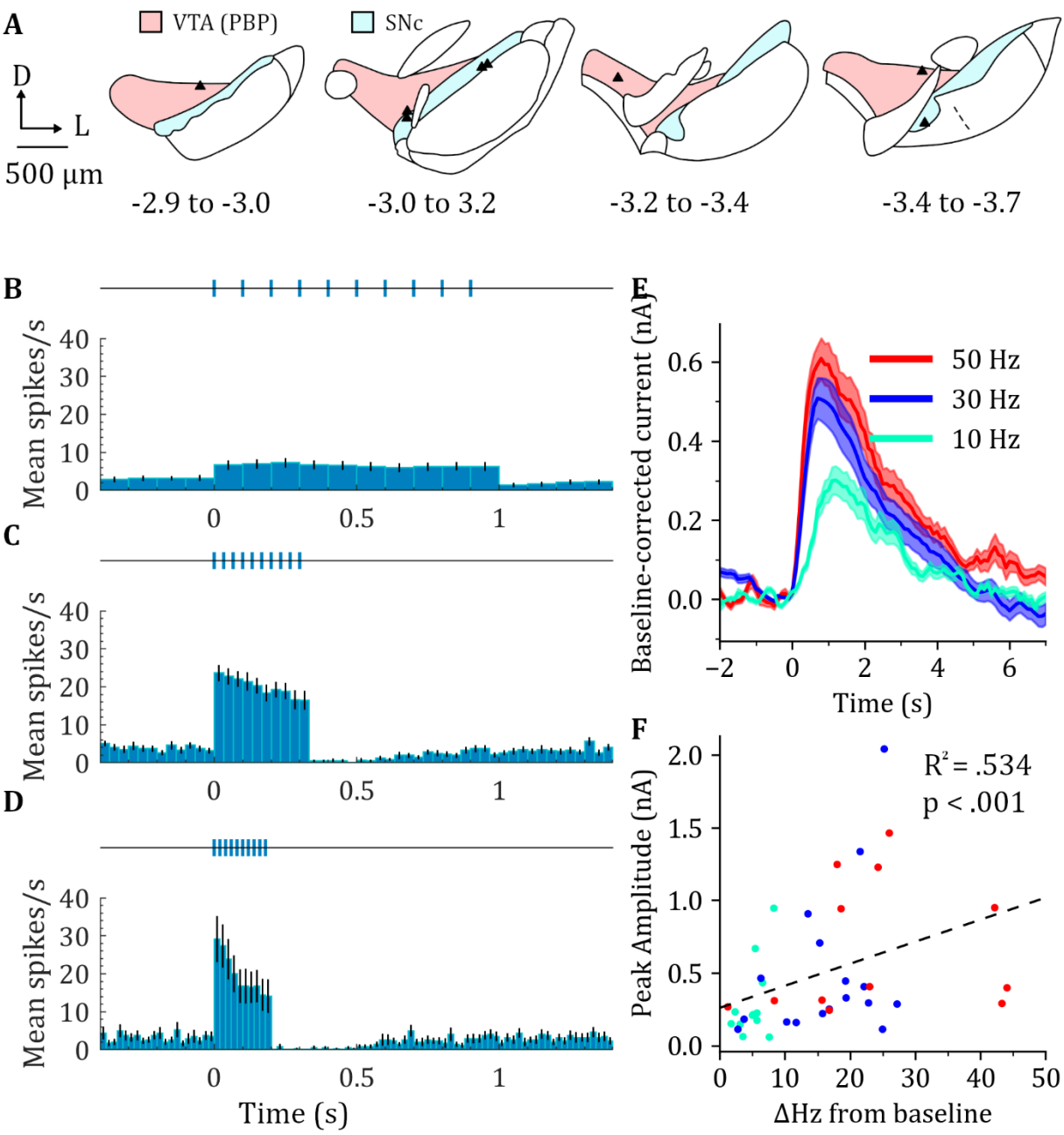


Figure 3.6: ***Data from all neurons responsive to optical stimulation, recorded simultaneously with FCV. A****, The locations of all labelled neurons that were recovered are shown on schematics of midbrain sections at different AP coordinates (in mm, with respect to Bregma). Each neuron is marked with a black triangle.* ***B-D****, Peristimulus time histograms of the mean (with SD error bars) number of action potentials across all neurons before, during and after optical stimulation at 10 Hz (B), 30 Hz (C) and 50 Hz (D). The stimulation train is shown above each histogram.* ***E****, Mean (with SEM) of FCV signal simultaneously recorded with the neurons shown in* ***B-D*** *for each stimulation frequency, averaged across trials.* ***F****, A scatter plot of the ΔHz from baseline for each cell and stimulation type, plotted against the peak amplitude of the simultaneously recorded FCV signal.*

To evaluate whether the firing rate of neurons during stimulation was significantly modulated by the stimulation frequency, the average firing rate during stimulation at each frequency was calculated per animal. These data were entered into a linear random-intercept mixed effects regression with a fixed factor of stimulation frequency predicting firing rate during stimulation and with each neuron as a random factor (SD = 4.68). There was a significant main effect of stimulation frequency, with higher stimulation resulting in higher firing rates (β = 0.486, SE = 0.0832, $t(24.8) = 5.84$, $p < .001$). To explore the nature of this main effect, two *post-hoc* repeated-measures t-tests were performed between 10 and 30 Hz stimulation and between 30 and 50 Hz stimulation. There was a significant difference between the firing rate evoked by 10 and 30 Hz stimulation at the Bonferroni-corrected p-threshold of .025 ($t(11) = 6.35$, $p < .001$), but between 30 and 50 Hz the difference was non-significant ($t(11) = 1.73$, $p = .111$).

The FCV signal appears similarly modulated by frequency, with greater signals evoked by higher frequency stimulation. To evaluate whether the quantity of dopamine release evoked by optical stimulation was significantly modulated by the stimulation frequency, the same analysis described above were performed on the FCV data, with peak signal amplitude as the dependent variable and each neuron as a random factor (SD = 0.361). There was a significant main effect of stimulation frequency, with higher stimulation resulting in higher peak amplitude in the FCV signal (β = 0.00669, SE = 0.00202, $t(34.0) = 3.32$, $p = .00218$). To explore the nature of this main effect, two *post-hoc* repeated-measures t-tests were performed between 10 and 30 Hz stimulation and between 30 and 50 Hz stimulation. There was a significant difference between the peak amplitude of the FCV signal evoked by 10 and 30 Hz stimulation at the Bonferroni-corrected p-threshold of

.025 ($t(16) = 3.72$, $p = .00187$), but between 30 and 50 Hz the difference was non-significant ($t(16) = 0.274$, $p = .787$).

The key advantage of this combined recording approach is that it allows for within-animal comparisons of midbrain neuronal activity and striatal dopamine release. To assess this relationship in my dataset, the ΔHz from baseline firing for each neuron was compared with the peak amplitude of the mean of the simultaneously recorded FCV transient (Figure 3.6E). 10 Hz stimulation has a relatively low ΔHz and peak amplitude. While there is a general tendency for both measures to be greater at higher frequencies of optical stimulation, the data are much more variable beyond 10 Hz. To assess this relationship statistically, the data were entered into a Spearman's correlation and were found to be significantly related ($R = .534$, $p < .001$). Thus, optically evoked phasic firing is positively related to dopamine release.

3.5. Discussion

3.5.1. Similar modulation of dopaminergic neuron firing and striatal dopamine release

Single-unit activity in midbrain and striatal dopamine release were recorded simultaneously in the same animal. The data showed that both neuronal firing and dopamine release were positively modulated by the frequency of optical stimulation. However, this modulation did not increase linearly with frequency. At 10 Hz, all neurons are well entrained, firing at almost the same rate as the stimulation. At 30 Hz, the mean firing rate is greater than at 10 Hz but does not reach the frequency of stimulation; at 50 Hz stimulation, the mean firing rate is not significantly greater than at 30 Hz. The same general pattern was observed in the FCV data, with the peak of the averaged evoked signal

increasing between 10 and 30 Hz but not between 30 and 50 Hz. Higher rates of phasic firing activity were associated with increased peak dopamine release. Taken together, the data suggest a non-linear relationship between stimulation frequency and evoked dopaminergic neuronal activity, which parallels a similar non-linear relationship between stimulation frequency and evoked dopamine release.

The non-linearity in the effect of frequency on both evoked neuronal firing and striatal release may suggest that the highest levels of stimulation in this experiment are beyond the capabilities of the dopaminergic system. The range of stimulation frequencies used in this experiment were chosen to reflect the 15-50 Hz range of phasic dopaminergic activity *in vivo* observed in response to physiologically relevant stimuli (e.g. salient cues or unexpected rewards; Avvisati et al., 2022; Dodson et al., 2016; Eshel et al., 2016; Montague et al., 1996; Schultz et al., 1997; Starkweather et al., 2017), but it may be that some neurons cannot reach this maximum firing frequency as there is a refractory period between successive action potentials. This refractory period arises in part because ion channels controlling the flow of ions into and out of the cell, necessary for both depolarising the membrane to generate an action potential and subsequent repolarisation (and, in the axon, for propagation of the action potential), are inactivated for a short period after opening (Barnett & Larkman, 2007; Debanne, 2004). At the highest frequencies of stimulation, the inter-pulse interval may be shorter than the refractory period in some midbrain dopaminergic neurons. Furthermore, considering that the average dopaminergic burst consists of around five action potentials (Grace & Bunney, 1983), it may also be that in the bursting range (above 10 Hz) neurons struggle to keep pace for the duration of the 10 pulse stimulation train used in this experiment. The fact that there is a

decline in the number of spikes generated across each stimulation train even at 30 Hz, which should be well within the comfortable firing rate of most dopaminergic neurons, further support this interpretation.

Notably, there is a brief pause in single-unit activity lasting on average about a quarter of a second following higher frequency stimulation (30 and 50 Hz). A pause in dopaminergic neuronal firing in response to stimulation has often been observed *in vitro* (Nedergaard, 2004; Shepard & Bunney, 1991), but is not often observed in behaving animals (Dodson et al., 2016; Eshel et al., 2016; Schultz et al., 1997; Starkweather et al., 2017). This could be interpreted as a sign that the dopaminergic system is overtaxed by the stimulation protocol used in this experiment at higher frequencies. It is possible that less intense stimulation (lower frequency, fewer pulses and/or a shorter pulse width) may evoke more physiological patterns of "burst-like" dopaminergic neuronal activity.

There was a significant positive correlation between neuronal firing and dopamine release: both neuronal firing and dopamine release increase with higher frequency (e.g. more intense) stimulation. However, the duration of the evoked response differs markedly between single-unit recordings and dopamine release. In particular, the increase in firing rate in the electrophysiological data lasts only for the duration of the stimulation train, for no longer than 1 second; by contrast, the FCV signal does not return to baseline for several seconds after the onset of stimulation. In addition, while there is a pause in single-unit activity following higher frequency stimulation, there is no corresponding dip in dopamine release. This is not unexpected as, unlike neuronal firing, the duration the evoked striatal release is subject to reuptake dynamics: the frequency of firing may determine the peak, but dopamine will linger in the extracellular space until it

is cleared by either diffusion or uptake. The pause in firing post firing rate increase may be too brief to be read out in the more extended dopamine signal. However, another factor may be the temporal resolution of FCV itself. Measuring dopamine with FCV necessarily means that dopamine molecules in a particular oxidised or reduced state are adsorbed by the carbon fibre tip of the working electrode. However, adsorbed dopamine (or dopamine-o-quinone) will be 'measured' until desorbed from the carbon fibre. The kinetics of this may be slower than the rate of reuptake or diffusion: compared to ascorbate, which does not adsorb to (and thus desorb from) the carbon fibre, the decay of an equivalent dopamine transient measured with FCV can be slower by ~1 second – although it is difficult to extrapolate to the present case, as the exact temporal dynamics of the voltammetric signal are dependent on factors like scan rate and electrode quality (Bath et al., 2000). Without an alternative measure of dopamine release, it is difficult to say whether this influences the timecourse of striatal dopamine release seen in these data. It is also worth noting that the use of heterozygous DAT-Cre mice for these may affect the temporal dynamics of dopamine release and uptake, as they have been reported to have ~17% less DAT than WT mice (Bäckman et al., 2006), which may extend the duration of striatal dopamine transients. This is important to consider when extrapolating these results to other murine phenotypes.

Overall, the data do provide some insight into the relationship between midbrain dopaminergic neuron firing and striatal dopamine release. Both measured signals showed a similar frequency dependence, with maximal responses as the highest stimulation frequencies but also a non-linear relationship between frequency and dopaminergic response. However, there are some distinctions: the voltammetric dopamine response far

outlasts the transient increase in neuronal firing rate, and the pause in neuronal firing following high intensity stimulation cannot be read out with an equivalent dip in the voltammetric signal. It is unclear to what extent these differences reflect real differences in the underlying dynamics of dopaminergic activity in the midbrain and striatum or limitations on the temporal dynamics of FCV.

3.5.2. Evaluation of methods in addressing research questions

One of the aims of this experiment was to assess the relationship between dopaminergic neuronal firing and striatal dopamine release. A single-unit juxtacellular approach was chosen to allow for specificity in the verification of both dopaminergic neuron identity and location. However, to draw conclusions about the relationship between single-unit activity and a population metric such as dopamine release, the individual neurons recorded must be assumed to be representative of the greater population of neurons. While recording with multi-channel probes would reduce specificity, it would allow for the simultaneous recording of a population of midbrain dopaminergic cells, which may be more readily comparable to release dynamics.

Single-unit activity and striatal dopamine release were evoked in anaesthetised animals. Methodologically, this arrangement has several key advantages. Single-unit recording and labelling are both significantly easier in anaesthetised animals than in awake animals, as the brain is much more stable when the animal is not moving. FCV is also easier in this preparation, as recordings can be conducted acutely and thus many of the pitfalls of chronically implanting FCV electrodes are circumvented, such as the necessity of daily cycling and degradation of the measured signal over time. Evoking

dopaminergic firing and release via stimulation under anaesthesia allows for precise experimental control over the phasic activity, where native dopaminergic fluctuations may be more variable and bursting harder to isolate in awake subjects.

Optogenetic stimulation was chosen for this experiment as it has couple of major advantages over electrical stimulation. The opsin can be expressed in a cell type-specific manner, which here allowed for the selective activation of dopaminergic neurons in an orthodromic manner. Electrical stimulation is not selective to any cell type and thus can evoke both orthodromic and antidromic firing. This means that additional circuits may be activated alongside dopamine neurons, which might significantly impact the evoked activity. Additionally, from a practical standpoint, the use of electrical stimulation in concert with electrophysiological recording and FCV may introduce novel stimulation artifacts, drastically complicating the development of the methods described in this chapter.

While measuring evoked signals in anaesthetised animals allows for a high degree of experimental control over the dopamine system, the trade-off is a reduction in the external validity of the data. The dynamics of signals measured in anaesthetised animals cannot necessarily be transposed to activity in awake animals, as the effects of urethane on optically evoked dopamine release are unknown. Additionally, phasic increases in dopaminergic activity evoked by optical stimulation may not reflect native phasic dopaminergic activity patterns evoked by biologically relevant stimuli (e.g. for dopamine, delivery of a reward or movement), for instance the presence of a decrease in firing rate following stimulation. Furthermore, the population of dopamine neurons activated by external stimulation will be hyper-synchronised to an extent that is physiologically

implausible in a native setting. This synchronisation may boost the evoked striatal dopamine release relative to the activity of each individual neuron, which would not be the case with native phasic activity. In this experiment, stimulation at 10 Hz produced a phasic increase in striatal dopamine release which corresponded to a firing rate of roughly 10 Hz. It is as yet unclear whether striatal dopamine release in response to a native burst of equivalent intensity (but less synchronised) could be read out so easily with FCV, especially since 10 Hz is still within the range (albeit the upper limit) of tonic dopaminergic firing *in vivo*.

3.5.3. Combining FCV and single-unit recordings

I have outlined and demonstrated a novel method of performing single-unit recordings and FCV simultaneously in the same mouse. While the FCV dopamine release transients in this study were generally quite small, the frequency of the stimulation could still be read out from the FCV signal. Similarly, I have demonstrated that simultaneously recorded cells can be juxtacellularly recorded and labelled. With the right application, this can be a powerful tool for assessing the online relationship between dopaminergic neuronal firing and dopamine release.

While this experiment was conducted on anaesthetised animals, combining techniques in this way would be especially useful in awake and behaving animals. As several authors have shown, there exists functional heterogeneity among midbrain dopaminergic neurons (e.g. Avvisati et al., 2022; Coddington & Dudman, 2018; Dodson et al., 2016). When recording dopaminergic release in a behaving animal, the ability to label and identify the subtype of dopamine cells in the same animal would allow one to describe

the relationship between firing and release with a much higher degree of precision. Furthermore, recording firing and release in parallel allows one to examine trial-by-trial correlations in a behavioural task, removing the confounds of inter-trial and inter-animal variability from the interpretation of these signals' relationship.

Of course, the principles outlined in this experiment are not necessarily limited to single-unit recordings. With some adjustment, the same method could be used to combined FCV with multi-electrode probe recordings for applications in which having a high yield is more important than specificity in cell types – specifically the artifact removal pipeline, which could be adjusted to remove FCV artifacts from multi-channel recording data. In addition, recording multiple neurons simultaneously allows for exploration of population dynamics and ensemble activity of dopamine neurons, which is a powerful advantage in many applications.

Despite this, combining electrophysiological and voltammetric techniques is undeniably challenging due to their fundamentally limited compatibility. The noise issues introduced by attempting to ground both systems separately, while solvable using a custom voltammetry setup, are likely to arise in many applications using commercially available apparatus. While in this case spikes could still be recovered, this introduces a potential limitation in the quality of the data that can be collected using this combined technique. Furthermore, while I have demonstrated that the FCV artifact can be removed during post-processing via my artifact removal pipeline, the efficiency and accuracy of template-matching relies on the artifact having two primary characteristics: a consistent shape and a larger amplitude than the measured action potentials. When these conditions

are not met, as in some of the data collected for this experiment, spike-sorting remains a challenge.

3.5.4. Novel approaches

Since these data were collected, advancements in the field have provided alternatives to both single-unit electrophysiology and to FCV, each of which have several of the same advantages outlined above. Previously, labelling neurons was the only way to address the issue of midbrain dopaminergic heterogeneity. However, Poulin et al. (2018) demonstrated that specific subtypes of dopamine neurons can be targeted molecularly using specific crossbreeds of mice and INTRSECT viruses, allowing for Cre-/Flp-dependent expression of viral constructs in particular subtypes of dopaminergic neurons. This has already been used to probe the activity of specific subtypes of midbrain dopaminergic cells, identified via opto-tagging (Azcorra et al., 2022). Practically speaking, this would be significantly easier to implement in several cases. The yield of neurons in multi-electrode probe recordings is much higher than for single-electrode recording and labelling techniques, therefore requiring the use of fewer animals and less time to obtain a meaningful sample size. Furthermore, juxtacellular recordings require much greater stability than probe recordings as cells can easily be lost with even small shifts of the electrode's position in the brain, which makes performing single-unit recordings and labelling neurons in behaving animals a particular challenge. While perhaps less refined, opto-tagging molecularly targeted dopaminergic subtypes allows for the exploration of dopaminergic heterogeneity without many of the pitfalls of single-electrode recordings.

While formerly the best way to measure sub-second dopamine release *in vivo*, FCV has new challengers with the advent of dLight (Patriarchi et al., 2018) and $GRAB_{DA}$ (Sun et al., 2020). These genetically encoded fluorescent sensors comprise a dopamine receptor which increases in fluorescence when bound to dopamine. This change in fluorescence can be measured via fibre photometry or a miniscope, allowing for optical rather than voltametric readout of dopamine release. This is an incredibly significant development in the field of dopamine research as FCV on its own presents several challenges. The scientifically meaningful changes in voltammetrically-recorded current are in the scale of nanoamperes, which means that the recordings are highly sensitive to electrical noise. Additionally, the quality of data is highly dependent on the state of the carbon-fibre electrode and the Ag/AgCl reference, which presents particular challenges in chronic applications: both are unstable over time, resulting in shifts in the reference potential (Rodeberg, Sandberg, Johnson, Phillips, & Wightman, 2017). Furthermore, chronically implanted carbon-fibre microelectrodes must be carefully managed, cycled daily and shifted to account for changes in the reference potential over time, none of which is necessary for the chronically implanted optic fibres needed to read out fluorescent sensors. By contrast, the signal-to-noise ratio of optical sensors is primarily dependent on the degree of sensor expression in the brain and the placement of the fibre relative to transduced tissue and the area of interest (e.g., striatum), so photometry can be very reliable over time with an appropriate construct. In many applications, optical measurement of striatal dopamine using fluorescent sensors would be easier to implement than with FCV.

One of the main advantages of FCV over dLight is that it allows for accurate measurement of the actual concentration of dopamine, while the degree of dLight fluorescence can only be interpreted on a relative basis. However, this advantage mostly holds true only for *ex vivo* work where FCV working electrodes can be calibrated outside of the brain slice immediately prior to or after recording; in chronic FCV recordings *in vivo*, it is difficult to make any such claims about dopamine concentration due to the aforementioned shifts in reference current. Nonetheless, FCV does have one key advantage of fluorescent sensors in that that the dynamic range is linear unlike fluorescent sensors (Patriarchi et al., 2018; Sun et al., 2020), which makes it easier to associate the dynamics of FCV signals with the underlying biological signal it is recording.

However, the primary advantage of dLight over FCV regarding the specific questions posed in this chapter are that, unlike FCV, it is not an electrical technique. The primary challenges in combining FCV with juxtacellular recording are the issues in grounding the animal and the presence of an artifact in the electrophysiological recordings, which increases the complexity of data post-processing. As an optical technique, photometry would not interfere in this way with any type of unit recording. Going forward, optical readout through fluorescent sensors for dopamine may prove a powerful tool in addressing my research questions.

3.5.5. Future work and conclusions

Regarding the responsiveness of the dopaminergic system to different intensities of stimulation, the data shown in this chapter is a useful guide to the modulation of dopamine release in response to specific stimulation parameters. Specifically, the non-linearity of

the frequency response in both electrophysiological and FCV data suggests that the parameters used here may have been too intense for the system to keep up with. One may assume that in response to stimulation with parameters closer to the physiological range of burst firing e.g. (~5 pulses), the relationship between stimulation frequency and the dopaminergic response may be closer to linearity. In further stimulation experiments, it would be useful to evaluate a broader range of parameters to explore this relationship.

As discussed in this chapter, several experiments have shown heterogeneity in dopaminergic activity across the midbrain (e.g. Avvisati et al., 2022; Coddington & Dudman, 2018; Dodson et al., 2016). Neurons from both SNc and VTA were recorded here but, due to the difficulty of the methodology employed in this chapter and the low neuronal yield of single-unit recordings, I do not have sufficient data to compare the optically evoked activity in different midbrain regions. Similarly, dopamine release was only recorded in the dorsomedial striatum, which may have different dynamics to dorsolateral striatum or NAc. Regional differences in dopaminergic activity would be very interesting to address in future work.

The advance in genetically encoded fluorescent sensors for dopamine is particularly important to this thesis, as it provides an exciting and potentially simpler alternative methodology for the readout of dopamine release. However, this is a relatively novel technique, first published under five years ago at the time of writing (Patriarchi et al., 2018). It is important to note that these sensors measure something fundamentally different to FCV. Where FCV is a measure of extracellular dopamine, it is more accurate to characterise the dynamics of these sensors, a modified dopamine receptor, as reflecting receptor engagement dynamics rather than dopamine release itself. While FCV has been

used and studied for decades, dLight and $GRAB_{DA}$ may require some verification before one can draw firm conclusions about the physiological relevance of their dynamics, especially as a readout of dopamine release. I address these issues in Chapter 4.

Chapter 4. Results II: Measuring electrically evoked dopamine transients with FCV and dLight photometry

4.1. Introduction

The projections of midbrain dopaminergic neurons to the striatum have commonly been divided into two distinct pathways: the nigrostriatal pathway, originating from neurons in the substantia nigra *pars compacta* (SNc) that project to dorsal aspects of striatum (DS); and the mesolimbic pathway, originating from neurons in the ventral tegmental area (VTA) that project to ventral aspects of the striatum (VS; Björklund & Dunnett, 2007; Ungerstedt, 1971). These pathways are associated with distinct functions. The nigrostriatal pathway has long been associated with movement, as the selective dysfunction of SNc dopaminergic neurons is a hallmark of Parkinson's disease (Kalia & Lang, 2015). Additionally, nigrostriatal activity has been linked to the initiation of locomotion and movement (Avvisati et al., 2022; da Silva et al., 2018; Dodson et al., 2016; Howe & Dombeck, 2016). On the other hand, dopaminergic signalling in the mesolimbic pathway is more closely associated with reward processing (Schultz et al., 1997).

While there is clear heterogeneity across the midbrain-striatal dopaminergic system, this dichotomy is an oversimplification. Rather than a simplistic binary of VTA and SNc neurons, there are a range of molecularly and functionally distinct subtypes of dopaminergic neurons across the midbrain (Avvisati et al., 2022; Dodson et al., 2016; Poulin et al., 2018). Functionally distinct subregions within dorsal and ventral striatum have also been identified. Dorsomedial striatum (DMS) has been implicated in the control

of goal-directed actions, while dorsolateral striatum (DLS) is associated with habit and skill learning (Balleine et al., 2009; Corbit, Nie, & Janak, 2012; Yin, Knowlton, & Balleine, 2005). Meanwhile, VS is divided into nucleus accumbens core, which is associated with Pavlovian learning (Day et al., 2007; Hamid et al., 2016; Mohebi et al., 2019; Saunders et al., 2018), and nucleus accumbens shell, which is instead associated with reward reinforcement and motivation (Bassareo & Di Chiara, 1999; Kelley & Delfs, 1991; Saddoris et al., 2015; Saunders et al., 2018; Wyvell & Berridge, 2000).

Given the functional differences in striatal dopaminergic signalling, one would expect there to be some differences in local modulation of dopamine release across the striatum. Cholinergic signalling is well-established to modulate striatal dopamine release (Cragg, 2006; Rice & Cragg, 2004; Threlfell et al., 2012; Zhang & Sulzer, 2004; Zhou et al., 2001). Nicotinic acetylcholine receptors containing α6 and β2 subunits play a much larger role in regulating dopamine release in the VS (specifically, in the core of the nucleus accumbens) than in the DS (Exley et al., 2008). Additionally, the dopamine release in the DS is more sensitive to regulation from voltage-gated calcium channels (VGCCs) than the VS; fewer subtypes of the VGCCs present on ventrostriatal axons impact dopamine release relative to those on dorsostriatal axons (Brimblecombe et al., 2015). There is also evidence that levels of the dopamine transporter DAT, which is the primary mechanism for clearance of extracellular dopamine (Cass, Zahniser, Flach, & Gerhardt, 1993; Giros et al., 1996, 1996; Mundorf, Joseph, Austin, Caron, & Wightman, 2001; Rice et al., 2011; Vaughan & Foster, 2013), are higher in the DS than the VS (Ciliax et al., 1995; Nirenberg et al., 1997).

The existence of differences in local modulation would in turn suggest that the dynamics of dopamine release may differ across the striatum. Indeed, recent work has

found considerable variation in the characteristics of dopamine transients. For example, van Elzelingen et al. (2022) recorded phasic dopamine transients across several striatal regions using fast-scan cyclic voltammetry (FCV), evoked by the delivery of gustatory rewards. There was considerable regional heterogeneity in both the magnitude and timescale of the resulting reward-evoked dopamine transients, with transients in VS much larger and longer lasting than their counterparts in DMS and DLS.

While FCV has been the primary tool in dopamine research for measuring phasic dopamine release in striatum, the size of native transients in DS has made it a challenge to record physiological levels of dopamine transmission using FCV, as reading out these signals requires a very high signal-to-noise ratio. Furthermore, FCV is a challenging technique to employ, and especially so in behaving animals, as chronically implanted carbon-fibre microelectrodes are prone to fouling after prolonged exposure to brain tissue (Aguilar-Rivera, Gatica, Azócar, Buc, & Fuentealba-Evans, 2023). In recent years, researchers have developed genetically-encoded fluorescent sensors for dopamine that provide a powerful alternative to FCV for reading out dopamine signalling (Patriarchi et al., 2018; Sun et al., 2020). These sensors consist of a dopamine receptor conjugated with a circularly permuted green fluorescent protein (cpGFP). The binding of dopamine to this modified receptor induces a conformational change in the cpGFP, resulting in increased fluorescence when excited by blue light. As such, fluctuations in fluorescence, and thus in dopaminergic activity, can be read out optically, for instance using fibre-photometry (Howe et al., 2019; Howe & Dombeck, 2016; Mohebi et al., 2019). As discussed in Chapter 3 of this thesis, optical techniques are considerably easier to combine with electrophysiology than FCV. Fluorescent sensors for dopamine provide exciting new

avenues for conducting simultaneous recordings of dopaminergic firing and release, as well as providing a potentially easier way of measuring physiological dopamine release across the striata of awake and behaving animals.

Despite the enormous potential of these fluorescent sensors, their relative novelty means that their dynamics *in vivo* have not yet been fully characterised. In particular, no research has yet been published evaluating how the measurements obtained by these novel fluorescent sensors compare to FCV, a well-established technique (although this question has been addressed in unpublished work; Salinas et al., 2022). In this chapter, I made some initial steps to addressing this issue by measuring evoked dopamine transients with FCV and, in separate animals, with photometry in combination with dLight 1.1, the first of these fluorescent sensors to be made publicly available (Patriarchi et al., 2018). To evoke striatal dopamine release, I use a broad range of midbrain stimulation parameters, chosen to encompass the full range of phasic midbrain dopaminergic neuronal firing in response to salient external stimuli (e.g. reward) (Montague et al., 1996; Schultz et al., 1997; Watabe-Uchida et al., 2017). In addition, to assess whether dLight can be used to address questions about heterogeneity in dopamine release across the striatum, FCV and dLight recordings were made from both the VS and the DLS. Similarities and differences in the evoked transients measured in each striatal region and with each technique (FCV and dLight photometry) are reported.

4.2. Aims

- To assess whether dLight can reliably encode striatal dopamine dynamics across the physiological range of phasic dopaminergic neuronal activity.
- To examine the relationship between transients measured with FCV and with dLight photometry.
- To investigate regional differences in striatal dopamine release.

4.3. Methods

4.3.1. Recording electrically evoked dopamine transients

Electrically evoked dopamine was recorded from anaesthetised mice with two different techniques: FCV and dLight photometry. As one of the aims of this experiment was to compare these techniques, the experimental protocol was kept constant wherever practical. Dopamine release was evoked via electrical stimulation of the midbrain (*AP* = -3.3, *ML* = ±1.0, *DV* = +4.7-5.2). The stimulation parameters were conserved across modalities: stimulation at 6 different frequencies (5, 10, 20, 30, 40 and 50 Hz), each at one of three numbers of pulses (NP; 3, 6 and 12 pulses). FCV and dLight recordings were taken from the DLS (*AP* = +0.5, *ML* = ±2.3, *DV* = 2.5) and the VS (*AP* = +1.4, *ML* = ±0.8, *DV* = 3.8) in counterbalanced order.

The experimental setup for the measurement of electrically evoked FCV transients is shown in Figure 4.1A (see also section 2.3.3). On the day of recording, mice (n = 9, F = 5) were prepared for general anaesthesia and non-recovery surgery (section 2.2.2). A square window craniotomy was drilled in the skull above the midbrain for the placement of the

stimulation electrode, and two smaller craniotomies were drilled above the ipsilateral DLS and VS for the FCV working electrode. The FCV reference electrode was cemented in the brain at an anterior location in the hemisphere contralateral to midbrain stimulation and striatal recordings (section 2.3.2). The FCV working electrode was lowered into the first striatal recording site and cycled until the signal stabilised (section 2.3.2). A parallel stimulation electrode interfaced with a constant-current stimulus isolator (section 2.3.3) was lowered into ipsilateral midbrain. The positions of both the FCV working electrode and the stimulation electrode were optimised by measuring the evoked stimulation at different positions of both electrodes, after which FCV transients were recorded in response to the stimulation protocol at fixed sites (3-5 trials for each combination of stimulation parameters). After collecting data from one striatal region, the FCV working electrode was moved to the other striatal region and the process was repeated. Once all recordings had been made, a lesion was made at the final FCV recording site using the FCV working electrode (section 2.3.2) and the mouse was transcardially perfused with fixative for histological analysis (section 2.7.1).

The experimental setup for the measurement of electrically evoked dLight transients is shown in Figure 4.1B (see also section 2.5.3). Prior to recording, mice in the dLight photometry cohort (n = 11, F = 4) were prepared for general anaesthesia and recovery surgery (section 2.2.1) and intracranially injected with the dLight viral vector in DLS and VS (section 2.2.3). One injection was made in each hemisphere, and the hemisphere chosen for each striatal region was counterbalanced across animals. On the day of recording, mice were prepared for general anaesthesia and non-recovery surgery (section 2.2.2). Two square window craniotomies were drilled above the midbrain bilaterally for

the placement of the stimulation electrode. Two smaller craniotomies were drilled above the striatal injection sites, one in each hemisphere for either DLS or VS. A fibre-optic cannula interfaced with the photometric recording equipment (section 2.5.2) was stereotaxically lowered into the initial striatal recording site. A concentric stimulation electrode interfaced with a constant-current stimulus isolator (section 2.5.3) was stereotaxically lowered into the midbrain ipsilateral to the initial striatal recording site. The positions of both the working and the stimulation electrode were optimised by measuring the evoked stimulation at different positions of both electrodes, after which dLight transients were recorded in response to the stimulation protocol (10 trials for each combination of stimulation parameters). After collecting data from one region, the fibre-optic cannula was moved to the other (contralateral) striatal region and the stimulation electrode was moved to the contralateral midbrain so that the process could be repeated. Once all recordings had been made, the mouse was transcardially perfused with fixative for histological analysis (section 2.7.1)

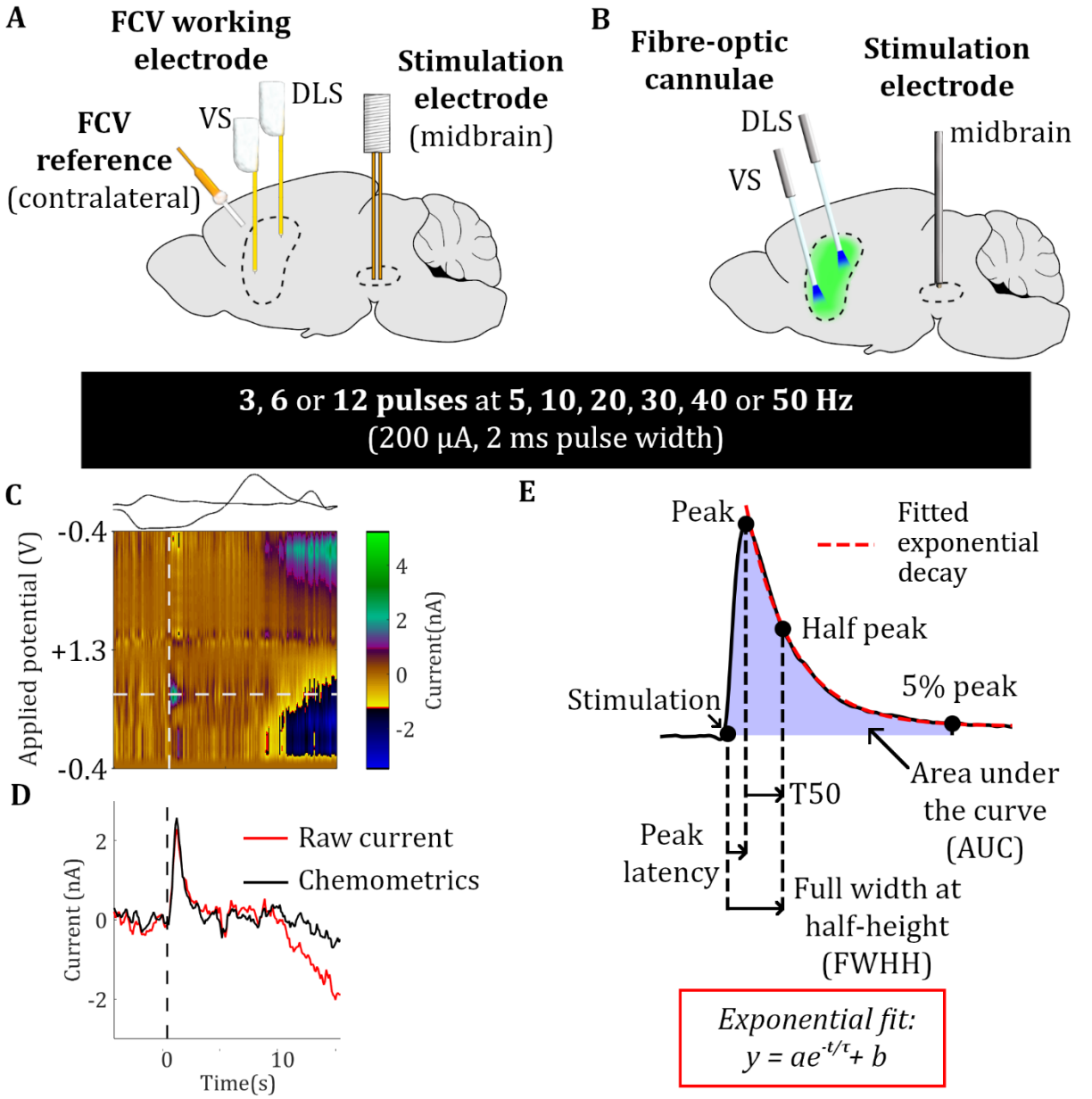


Figure 4.1: ***Experimental configuration for measuring electrically evoked FCV and dLight transients. A & B****, Schematics of the experimental configuration used to measure electrically evoked dopamine transients with FCV and dLight respectively, visualised on a parasagittal section of a mouse brain. The black dashed lines demarcate the striatum (left) and the midbrain (right). Midbrain stimulation parameters for both experiments are given below both subfigures.* ***C****, A single trial from the FCV dataset (30 Hz and 12 p) visualised as a colour plot. Peak dopamine after stimulation at timepoint 0 (white vertical dashed line) was at point 313 (white horizontal dashed line).* ***D****, The raw (0.664 V) and chemometrically extracted voltammetric dopamine signal from the same trial as C. Stimulation occurred at timepoint 0 (black dashed line). The cyclic voltammogram is shown above the colour plot.* ***E****, Schematic demonstrating how parameter estimates for characteristics of evoked dopamine transients were determined. T50 is the decay time from peak to half peak. The exponential decay function is given below.*

4.3.2. Data processing

FCV and dLight data were initially pre-processed separately as described in section 2.3.4 and section 2.5.4 respectively. FCV were put through a chemometrics analysis pipeline (section 2.3.4) prior to further analysis to ensure the dopamine signal was minimally affected by nuisance contaminants. Shown in Figure 4.1C is a data from a typical trial (30 Hz, 12 pulses) from the FCV dataset, expressed as a colour plot. Figure 4.1D shows the extracted dopamine signal overlaid with the raw current (extracted at point number 313). Note that chemometric pre-processing results in a cleaner transient, without the post-peak dip shown in the raw trace ~10 s after stimulation caused by pH changes resulting from stimulation. For data recorded in both voltammetric and photometric modalities, the signal from each trial was mean-normalised to the signal in a 1 second window before the onset of stimulation. Data were averaged across trials so that each animal had a single mean trace in each striatal region for each midbrain stimulation parameter.

In all plots shown in this chapter, striatal recording data were corrected such that the mean peak response was assigned a value of 1 for each region of each animal at 6 pulses of 30 Hz stimulation. This is because the absolute value of the signal is dependent on factors which are not of experimental interest (e.g. the placement of the stimulation and recording electrodes in relation to each other). Including this variation in the figures would obscure what is of interest to this chapter, namely the *relative* magnitude of signals evoked by stimulation with different parameters.

4.3.3. Defining parameters of interest

To operationalise the characteristics of evoked dopamine signals, several features were extracted from each transient. A full diagram of these characteristics is shown in Figure 4.1E. Two primary aspects of the evoked dopamine signal were of interest in this experiment: the magnitude and the timescale. Both can be measured in multiple ways, but each measure assesses a slightly different aspect of the signal. One of the traditional approaches to examining the clearance of FCV signals is Michaelis-Menten-based modelling, but this is specifically based on the dynamics of voltammetric signals and thus may not be appropriate for dLight transients. Instead, I used a variety of different approaches to characterise evoked dopamine transients adapted from those used by others in the field (e.g. Chen & Rice, 2001; Everett et al., 2022; Korn et al., 2021; Saddoris, 2016; Yavich, Forsberg, Karayiorgou, Gogos, & Männistö, 2007). These approaches are outlined and discussed in detail in this section.

Both peak amplitude and area under the curve (AUC) are measures of the magnitude of the dopamine response. The peak was identified as the maximum value between timepoints 0 (stimulation onset) and 3 s, which would be beyond the maximum stimulation duration of 2.1 s at 12 pulses of 5 Hz stimulation. Area under the curve (AUC) was calculated using trapezoidal integration between timepoint 0 and 5% peak (the first measured point after the peak to reach 5% of the peak signal). The peak and AUC are not necessarily equivalent measures. For example, two signals with the same peak but very different decay times might have a different AUC. AUC can also be considered a measure of the total relative quantity of dopamine; however, it can be hard to accurately determine

in data with poor signal-to-nose ratio, as one must accurately identify appropriate limits within which to integrate, and its estimation is biased when there is signal drift.

The timescale of an evoked transient can also be assessed in several ways. The duration of the signal was defined as the full width at half-height (FWHH) of the evoked transient, taken as the latency between the onset of stimulation (timepoint 0) and the half peak (the first measured point after the peak to reach 50% of the peak signal). As a measure of the timescale of an evoked transient, it conflates two separable components: peak latency (from timepoint 0) and 50% decay (T50; the latency between the peak and the half peak). With the stimulation parameters used in this experiment, the duration of each pulse train varies systematically with both frequency and number of pulses, which therefore means there may be systematic differences in the peak latency and therefore the FWHH. As such, it is important not to conflate the duration of a signal with its decay time.

T50 is the simplest measure of decay time. However, its estimation requires the pinpointing of two potentially noisy timepoints: the peak and the half peak. Another approach is to find an estimate of the exponential decay by curve fitting. A simple exponential decay curve was fitted to the signal in a 20 second window from the peak: $y = ae^{-t/\tau} + b$, wherein a is the slope, b is the intercept, t is the time from peak (in seconds) and τ is the time constant of exponential decay. Smaller values of τ represent steeper exponential decay. τ is a pure measure of decay and is therefore a very biologically relevant parameter; however, curve fitting can be prone to error, especially in data with poor signal-to-noise ratio.

In this chapter, the magnitude, duration and decay of evoked dopamine transients are operationalised and extracted. Subsets of these parameters will be examined in both FCV and dLight transients, chosen based on the considerations outlined above.

4.3.4. Linear mixed-effects modelling

To statistically investigate the role of stimulation frequency, number of pulses (NP) and region on evoked dopamine transients, linear mixed-effects models (LMM) were built using the lmer package in R (version 4.4.2), using each measure of interest as a dependent variable. To improve the accuracy of parameter estimation, each parameter was estimated from mean traces of the data for each animal, region and unique stimulation parameter (frequency and NP).

LMMs are statistical models containing both fixed effects and random effects, useful when the assumption of independence of observations is known to be violated, such as in a repeated-measures design (de Melo, Daldegan-Bueno, Menezes Oliveira, & de Souza, 2022). Here, I use a random-intercepts model. The full model for these data can be expressed as,

$$Y_i = (\beta_0|animal) + \beta_1 Freq + \beta_2 NP + \beta_3 Region + \beta_4 Freq{:}NP + \beta_5 Freq{:}Region + \beta_6 NP{:}Region + \beta_7 Freq{:}NP{:}Region + \varepsilon_i$$

where Y_i represents a single data point, $(\beta_0|animal)$ is the intercept for each animal, $\beta_1 \ldots \beta_n$ are the slope coefficients for each predictor (frequency, number of pulses, region and their interactions) and ε_i is the error term. Interactions between two or more predictors are given as X_1:X_2. Frequency and NP are both continuous repeated measures variables while region is a categorical variable. This model treats all three as fixed effects

while animal is treated as a random factor. To reduce multicollinearity when interaction terms were added, both continuous variables were z-scored (Irwin & McClelland, 2001).

Models were constructed systematically. First, each of the three fixed effects was compared against a null model, containing only the random effect and no other predictors. All significant main effects were added to the first-level model. Individual two-way interactions between pairs of significant fixed effects were individually added to the first-level model and retained when significant. The second-level model consisted of all main effects and significant two-way interactions. In the case that all interactions were significant, a three-way interaction was also added and was kept in the final model when significant. Only the final model will be shown in each section. All coefficients, standard errors (SE) and test statistics (with degrees of freedom (df) and *p*-values) are provided. The intercept is reported alongside the fixed effects, as it is a component of the final model, but its significance only represents whether the grand intercept is significantly higher than 0. As such, it is not meaningfully interpretable. Parameters of the random effects structure are also reported: the intra-class correlation (ICC) of the null model and the SD (SD_{animal}) of the random effect.

As a final note regarding the interpretation of the models' output, investigating differences between striatal regions is not always as not as straightforward as simply finding a significant main effect of region. The absolute value of any evoked transient is dependent on several factors which are not scientifically relevant to these experiments, e.g. the placement of the recording electrode in relation to the stimulation electrode. As such, finding a significant difference between the magnitude of the response in each region does not say anything interpretable about the magnitude of underlying biological signal

in each region. Throughout this chapter, whenever the magnitude of the signal is being evaluated, the data used in the model will be region-corrected (scaled such that the overall mean of the peak amplitude is 1 for each region), which will remove any main effect of region from these analyses. However, it is still possible to investigate regional differences in the magnitude of evoked transients with LMMs. For example, a significant interaction between striatal region and frequency would suggest that the measured dopamine activity in each region is affected differently by manipulations of stimulation frequency.

4.4. Results: Electrically evoked FCV transients

Full data from experiments measuring electrically evoked FCV transients in DLS and VS are shown in Figure 4.2A. Two general trends can be observed from this data. Firstly, that higher frequency stimulation results in a higher peak signal. Secondly, that the peak signal also increases with more pulses.

To statistically investigate these effects, LMM were constructed around parameters of interest. The peak and AUC of electrically evoked FCV transients were highly positively correlated (Figure 4.2B; Spearman's rank correlation; $rs(284) = .813$, $p < .001$), suggesting that either would be an appropriate measure. However, as the FCV data are noisy, peak amplitude was used as the measure of signal magnitude. The τ of evoked FCV transients was difficult to accurately determine due to the noisiness of the underlying data, so T50 was used as the measure of decay.

There was a significant positive correlation between the FWHH and the T50 of evoked FCV transients (Figure 4.2C; Spearman's rank correlation; $rs(284) = .325$, $p < .001$). The variation in the y-axis seems related to frequency: 5 Hz stimulation results in a longer

FWHH relative to T50, while the reverse is true at 50 Hz. However, this relationship is relatively weak, which may signify either a genuinely weak relationship between FWHH and T50 or perhaps noisiness in the estimation of these parameters.

The duration of each pulse train varies systematically with both frequency and number of pulses, and the resulting effect on peak latency might explain the observed pattern. To explore this, the duration of each stimulation was compared to the peak latency. Assuming the first stimulation pulse is located at timepoint 0, the stimulation duration can be expressed as (1/Hz)*(NP-1). For instance, 6 pulses at 50 Hz will have a stimulation duration of (1/50)*(6-1) = 0.1 s. Stimulation duration and peak latency were significantly positively correlated (Figure 4.2D; Spearman rank correlation; rs(284) =.429, $p < .001$). The rs value here was also relatively small, thus it is difficult to draw firm conclusions from this analysis. However, the trend shown here does support the idea that FWHH may be better interpreted as a measurement of signal duration than decay.

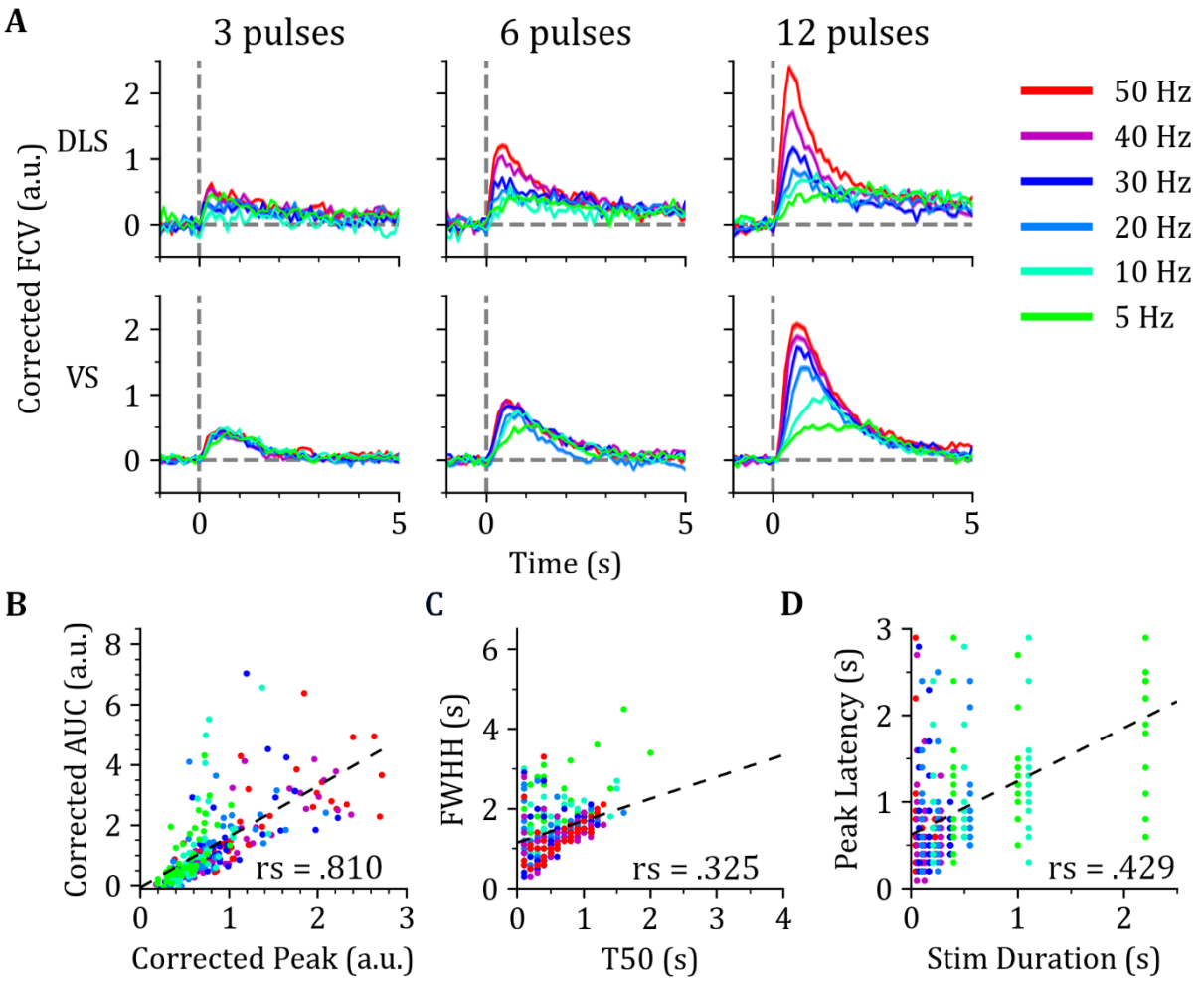


Figure 4.2: ***A****,* ***Electrically evoked dopamine transients measured with FCV. A****, Mean (SEM) of corrected FCV transients at each across animals, reported in arbitrary units (a.u.). Each row of plots shows data from a different striatal region. Columns of plots show data evoked with different numbers of stimulation pulses. The horizontal and vertical grey dashed respectively represent 0 on the y-axis (FCV baseline) and y-axis (timepoint 0, the onset of stimulation). The size of the evoked FCV response is greater with more stimulation pulses and higher frequency stimulation.* ***B-D,*** *Scatter plots showing the relationships between the corrected peak amplitude and the area under the curve (AUC) of corrected evoked FCV signals (****B****); the estimate of τ (exponential decay constant) and FWHH of evoked FCV signals (****C****); and between the duration of stimulation and the peak latency (****D****) of evoked FCV signals. These plots contain data from both the DLS and VS. Each data point represents a single trial; the colour represents the stimulation frequency. The Spearman's correlation is displayed on each plot along with a line of best fit (black dashed line).*

4.4.1. LMM for frequency, number of pulses and region on peak height

As is clear from Figure 4.3A, increasing the frequency of stimulation or the number of stimulation pulses results in higher amplitudes of peak release. Furthermore, the effect of frequency on peak amplitude appears to be greater with more stimulation pulses.

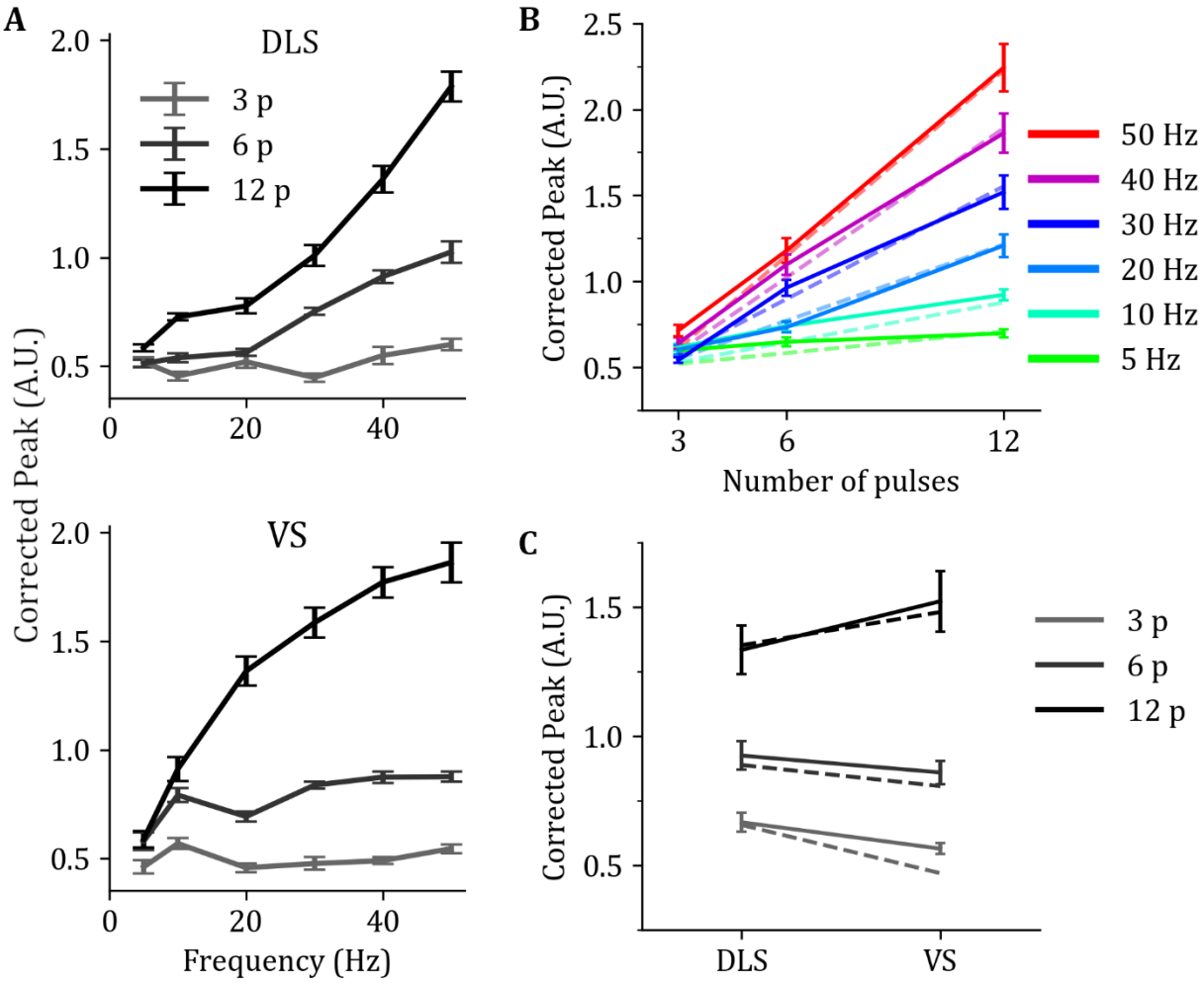


Figure 4.3: ***Plots showing the effect of frequency, NP and region on the peak amplitude of electrically evoked FCV transients in arbitrary units (A.U.). A****, Mean (SEM) amplitudes of electrically evoked FCV release. Data recorded from the DLS are shown in the upper plot and data recorded from VS are shown in the lower plot.* ***B****, Interaction plot for the frequency:NP interaction effect on the peak amplitude of FCV transients. The mean (SEM) of the real data is shown with solid lines; the model predictions are shown as dashed lines.* ***C****, Interaction plot for the NP:region interaction, again showing real data overlaying model predictions. In both* ***B*** *and* ***C****, the plotted data has been region-corrected.*

To assess the role of frequency, NP and region on the peak amplitude of evoked FCV transients, the data were entered into a LMM regression. Data from the VS of one animal was excluded as the mean peak height was 3 SD above the overall mean, but the DLS data from this animal was still included in the model. The final model explained significantly more of the variance in the data than the null model ($\chi^2(5) = 360$, $p < .001$). Full details of the final model are shown in Table 4.1. There was a highly significant main effect of frequency, suggesting that peak height increases with frequency. There was a highly significant main effect of NP, with more stimulation pulses also resulting in a higher peak. There was also a highly significant interaction between frequency and NP: while increasing the frequency of stimulation increases peak amplitude, this effect is greater with more stimulation pulses (Figure 4.3B). The model predictions for the peak amplitude at each frequency and number of pulses (shown by the dashed lines in Figure 4.3B) closely match the real data (solid lines).

Table 4.1: Fixed effects, estimates and statistics for peak amplitude of electrically evoked FCV transients.

β term	β-estimate	SE	df	*t*-statistic	*p*-value
Intercept	0.985	0.112	9.48	8.80	<.001
Frequency	0.271	0.0277	259	9.75	<.001
NP	0.288	0.0376	260	7.66	<.001
Region	-0.0379	0.0588	264	-0.646	.519
Freq:NP	0.209	0.0278	259	7.52	<.001
NP:Region	0.131	0.0563	260	2.32	.021

Animal: n = 9; 268 observations; $SD_{animal} = 0.317$; $ICC_{null} = .329$.
Region coding: DLS = 0; VS = 1.

As the data were mean-corrected by region, the main effect of region was not significant. However, there was a significant interaction between NP and region. The interaction plot for the significant NP:region interaction (Figure 4.3C) shows that increasing the number of pulses has a greater effect on the peak amplitude of transients measured in the VS than in the DLS.

The frequency response at 12 pulses differs between the striatal regions: there is a suggestion of superlinearity in the frequency response in the DLS, but sublinearity in the VS. To investigate whether this nonlinearity in each region was significant, two separate LMMs were constructed *post-hoc,* using the peak amplitude of FCV transients from each region evoked by each number of stimulation pulses. Each model contained only 2 predictors: frequency and its 2nd-order polynomial. Significance of the polynomial would suggest that the frequency response in that region is best described with a nonlinear fit. At 12 pulses in the DLS, both the main effect of frequency ($\beta = 3.92$, $t(45.0) = 9.38$, $p < .001$) and the polynomial ($\beta = 0.885$, $t(45.0) = 2.12$, $p = .0398$) were significant. In the VS, only the main effect of frequency was significant ($\beta = 3.54$, $t(34.0) = 6.53$, $p < .001$), while the polynomial was not ($\beta = -1.01$, $t(34.0) = 1.87$, $p = .071$). At 6 pulses in the DLS, the main effect of frequency was significant ($\beta = 1.92$, $t(45.0) = 6.74$, $p < .001$) but the polynomial was not ($\beta = 0.274$, $t(45.0) = .965$, $p = .340$). In the VS, again the main effect of frequency was significant ($\beta = .785$, $t(34.0) = 3.57$, $p = .001$) but the polynomial was not ($\beta = -0.254$, $t(34.0) = 1.16$, $p = .256$). At 3 pulses in the DLS, neither the main effect of frequency ($\beta = 0.236$, $t(35.0) = 1.32$, $p = .195$) nor the polynomial ($\beta = 0.300$, $t(35.0) = 1.68$, $p = .102$) were significant. The same pattern was true for VS, with no significant main effect of frequency ($\beta = 0.135$, $t(30) = 1.21$, $p = .235$) or the polynomial ($\beta = 0.122$, $t(30) = 1.10$, $p = .281$). In

summary, the frequency dependence of evoked FCV transients is only present at higher numbers of stimulation pulses (3 and 6), but this pattern is the same for both regions. Furthermore, there is evidence of superlinearity in the DLS signal at 12 pulses, but not sublinearity in the VS signal at 12 pulses.

4.4.2. LMM for frequency, NP and region on FCV FWHH

The FWHH of electrically evoked FCV transients across all frequencies, numbers of pulses and in both regions is shown in Figure 4.4. There is an overall trend that higher frequency stimulation results in a lower FWHH, but this is most apparent at 12 pulses; here, the relationship also seems non-linear, with greater differences between transients evoked by lower frequency stimulation (5-20 Hz) and greater similarity at higher frequency stimulation (20-50 Hz). There is no consistent difference between the FWHH of FCV transients in different striatal regions.

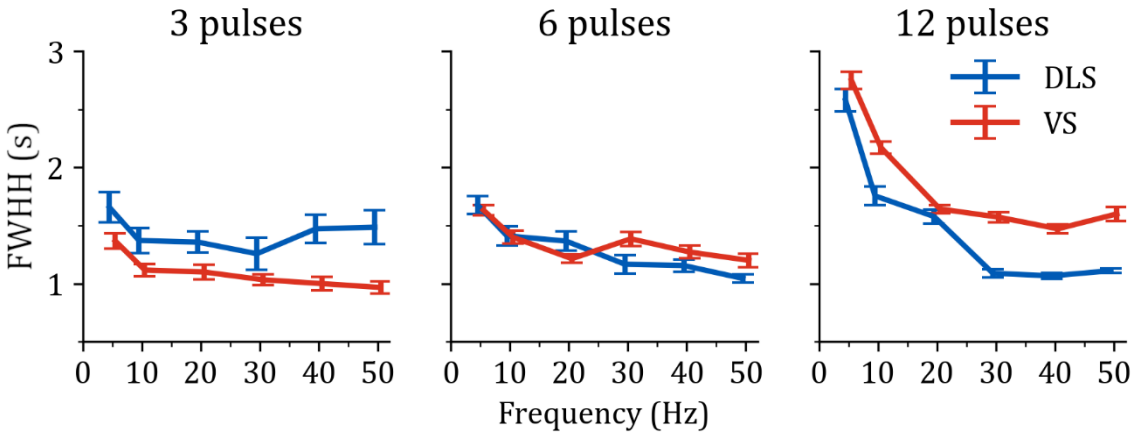


Figure 4.4: ***The mean (SEM) FWHH of electrically evoked FCV transients at all frequencies and numbers of pulses, separated by striatal region.***

Table 4.2: Fixed effects, estimates and statistics for FWHH of electrically evoked FCV transients.

β term	β-estimate	SE	df	*t*-statistic	*p*-value
Intercept	1.43	0.0877	11.0	16.3	<.001
Frequency	-0.226	0.0320	277	-7.06	<.001
NP	0.168	0.0321	277	5.24	<.001
Region	0.0330	0.0659	284	0.501	.617

Animal: n = 9; 286 observations; SD_{animal} = 0.167; ICC_{null} = .126.
Region coding: DLS = 0; VS = 1.

To assess the role of frequency, NP and region on FWHH in the FCV dataset, the data were entered in a LMM regression. The final model explained significantly more of the variance in the data than the null model ($\chi^2(3) = 68.1$, $p < .001$). Full details of the final model are shown in Table 4.2. There was a highly significant main effect of frequency, with higher frequency stimulation having a shorter duration. The main effect of NP was also highly significant, but in the opposite direction, with more pulses resulting in signals of longer duration. The main effect of region was not significant.

4.4.3. LMM frequency, NP and region on FCV T50

The effect of stimulation frequency on the T50 of evoked FCV transients is notably distinct from its effect on FWHH. Where the overall trend in Figure 4.4 shows a decrease in FWHH at higher frequencies overall, T50 instead shows an overall trend of increasing with stimulation frequency (Figure 4.5A). T50 is also highest with more stimulation pulses. There is a clear regional difference as well: in VS, FCV transients have consistently longer T50s, which indicates longer decay times than in DLS. However, these patterns are less clear at 3 pulses, where the evoked signals tend to be smallest and thus the signal-to-noise ratio poorer.

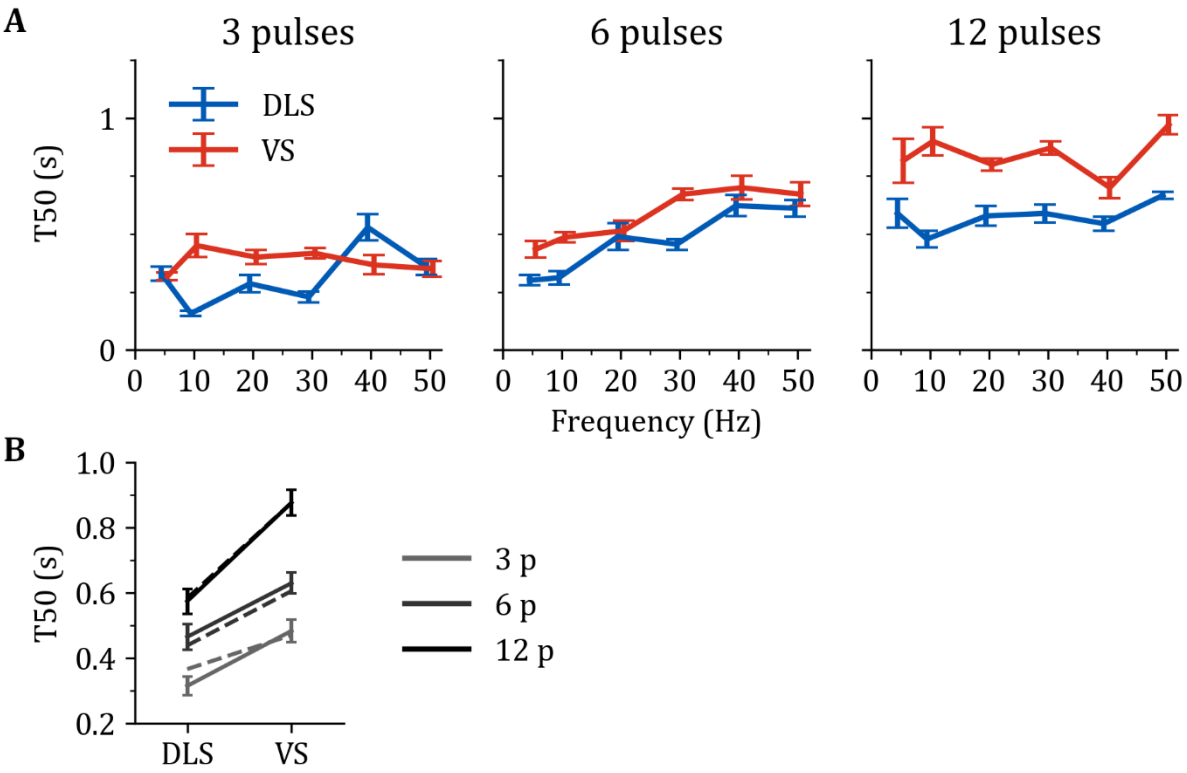


Figure 4.5: ***The T50 of electrically evoked FCV transients at all frequencies and numbers of pulses, separated by striatal region and interaction plot. A****, Mean (SEM) amplitudes of electrically evoked FCV release. Transients evoked by different numbers of pulses are shown on different plots, from 3 to 12 pulses left to right.* ***B****, Interaction plot for the NP:region interaction effect on the T50 of FCV transients. The mean (SEM) of the real data is shown with solid lines; the model predictions are shown as dashed lines.*

To assess the effects of frequency, NP and region on the T50 of evoked FCV transients, the data were entered into a LMM regression. The final model explained significantly more of the variance in the data than the null model ($\chi^2(4) = 79.8$, $p < .001$). Full details of the final model are shown in Table 4.3. Stimulation at lower frequencies resulted in significantly shorter decay times. The main effect of NP was highly significant, with more pulses also resulting in shorter decay times. The main effect of region was highly significant, with shorter decay times overall in DLS than VS. The interaction plot for the significant NP:region interaction (Figure 4.5B) shows that the model predictions closely

match the real data: more stimulation pulses results in a longer T50 of FCV transients, but this effect is stronger in the VS than the DLS.

To investigate whether the differences between the models for FWHH and T50 in the FCV dataset were due to systematic effects of stimulation parameters on peak latency, another LMM was constructed *post-hoc* with peak latency as a dependent variable, and frequency, NP and region as fixed effects. There was a main effect of region (β = -0.165, $t(282) = 2.64$, $p = .00870$), wherein the VS had shorter peak latencies than DLS. There was also a highly significant main effect of frequency (β = -0.276, $t(277) = 9.14$, $p < .001$): higher frequency stimulation resulted in a shorter peak latency. The main effect of NP was not significant.

Table 4.3: Fixed effects, estimates and statistics for T50 of electrically evoked FCV transients.

β term	β-estimate	SE	df	*t*-statistic	*p*-value
Intercept	0.468	0.0435	12.2	10.8	<.001
Frequency	0.0506	0.0176	277	2.87	.00442
NP	0.0900	0.0246	279	3.66	<.001
Region	0.193	0.0363	285	5.32	<.001
NP:Region	0.0210	0.00952	279	2.20	.0287

Animal: n = 9; 286 observations; $SD_{animal} = 0.108$; $ICC_{null} = .104$.
Region coding: DLS = 0; VS = 1.

4.5. Results: Electrically evoked dLight transients

Full data from these experiments are shown in Figure 4.6A. The same general trends can be observed from these data as in the FCV dataset: that higher frequency stimulation results in a higher peak signal, and that the peak amplitude increases with more stimulation pulses. To statistically investigate these effects, LMMs were constructed around parameters of interest.

As comparing FCV with dLight photometry is one of the aims of this experiment, all parameters of interest evaluated in the FCV dataset were also evaluated in the dLight dataset. Correlational analyses were performed to assess the relationship between parameters of interest for these. The overall pattern of these relationships was the same as in the FCV dataset. The two measures of signal magnitude, peak and AUC, were significantly positively correlated (Figure 4.6B; Spearman rank correlation; $rs(376) = .630$, $p < .001$). As in the FCV dataset, there was also a significant positive correlation between T50 and FWHH (Figure 4.6C; Spearman rank correlation; $rs(376) = .706$, $p < .001$). There was also a strong correlation between peak latency and stimulation duration (Figure 4.6D; Spearman's rank correlation; $rs(376) = .770$, $p < .001$). Unlike in the FCV dataset, τ could be determined with reasonable accuracy for all traces. This means signal decay could be estimated with either τ or T50. Both measures are evaluated in this section.

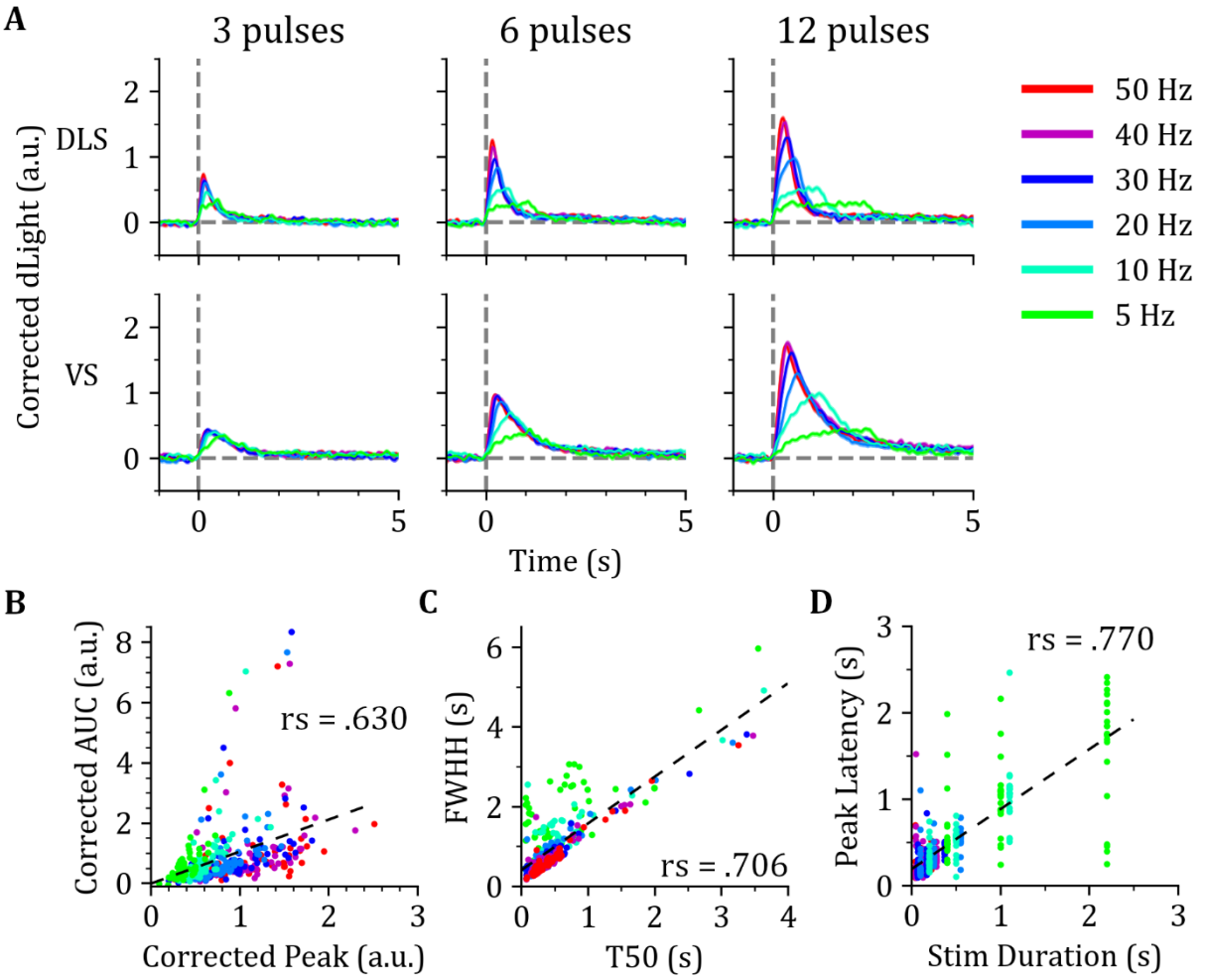


Figure 4.6: ***Electrically evoked dopamine transients measured with dLight photometry. A****, Mean (SEM) of corrected dLight transients at each across animals, reported in arbitrary units (a.u.). Each row of plots shows data from a different striatal region. Columns of plots show data evoked with different numbers of stimulation pulses. The horizontal and vertical grey dashed respectively represent 0 on the y-axis (dLight baseline) and y-axis (timepoint 0, the onset of stimulation). The size of the evoked dLight response is greater with more stimulation pulses and higher frequency stimulation.* ***B-D,*** *Scatter plots showing the relationships between the corrected peak amplitude and the area under the curve (AUC) of corrected evoked dLight signals (****B****); the estimate of τ (exponential decay constant) and FWHH of evoked dLight signals (****C****); and between the duration of stimulation and the peak latency (****D****) of evoked dLight signals. These plots contain data from both the DLS and VS. Each data point represents a single trial; the colour represents the stimulation frequency. The Spearman's correlation is displayed on each plot along with a line of best fit (black dashed line).*

4.5.1. LMM for frequency, NP and region on dLight peak

As is clear from Figure 4.7A, increasing the frequency of stimulation or the number of stimulation pulses results in higher amplitudes of peak release. Furthermore, the effect of frequency on peak amplitude appears to be greater with more stimulation pulses. This overall pattern is very similar to the pattern of evoked FCV transients in response to the same manipulations of stimulation frequency and number of stimulation pulses. However, while there was superlinearity in the frequency response of FCV transients at 12 pulses in the DLS but not the VS (Figure 4.3A), here there is a suggestion of sublinearity in both regions, especially between 40 and 50 Hz stimulation.

To assess the role of frequency, NP and region on the peak amplitude of dLight dopamine transients, the data were entered into a LMM regression. Data from the DLS of one animal was excluded as the mean peak amplitude was 3 SD above the overall mean, but the data recorded from the VS was included in the analysis. The final model explained significantly more of the variance in the data than the null model ($\chi^2(5) = 230$, $p < .001$). Full details of the final model are shown in Table 4.4. The final model for the peak amplitudes of dLight transients was very similar to that of FCV transients (Table 4.2). There was a highly significant positive main effect of frequency, which means that peak amplitude increased with stimulation frequency. There was also a highly significant main effect of NP, with more stimulation pulses resulting in higher peaks. There was also a highly significant interaction between frequency and NP: while increasing the frequency of stimulation increases peak amplitude regardless of the number of pulses, the effect is greater with more stimulation pulses (Figure 4.7B). The main effect of region was not significant, but there was a significant interaction between NP and region. From the

interaction plot (Figure 4.7C), the effect of increasing the number of pulses is greater in the VS than the DLS.

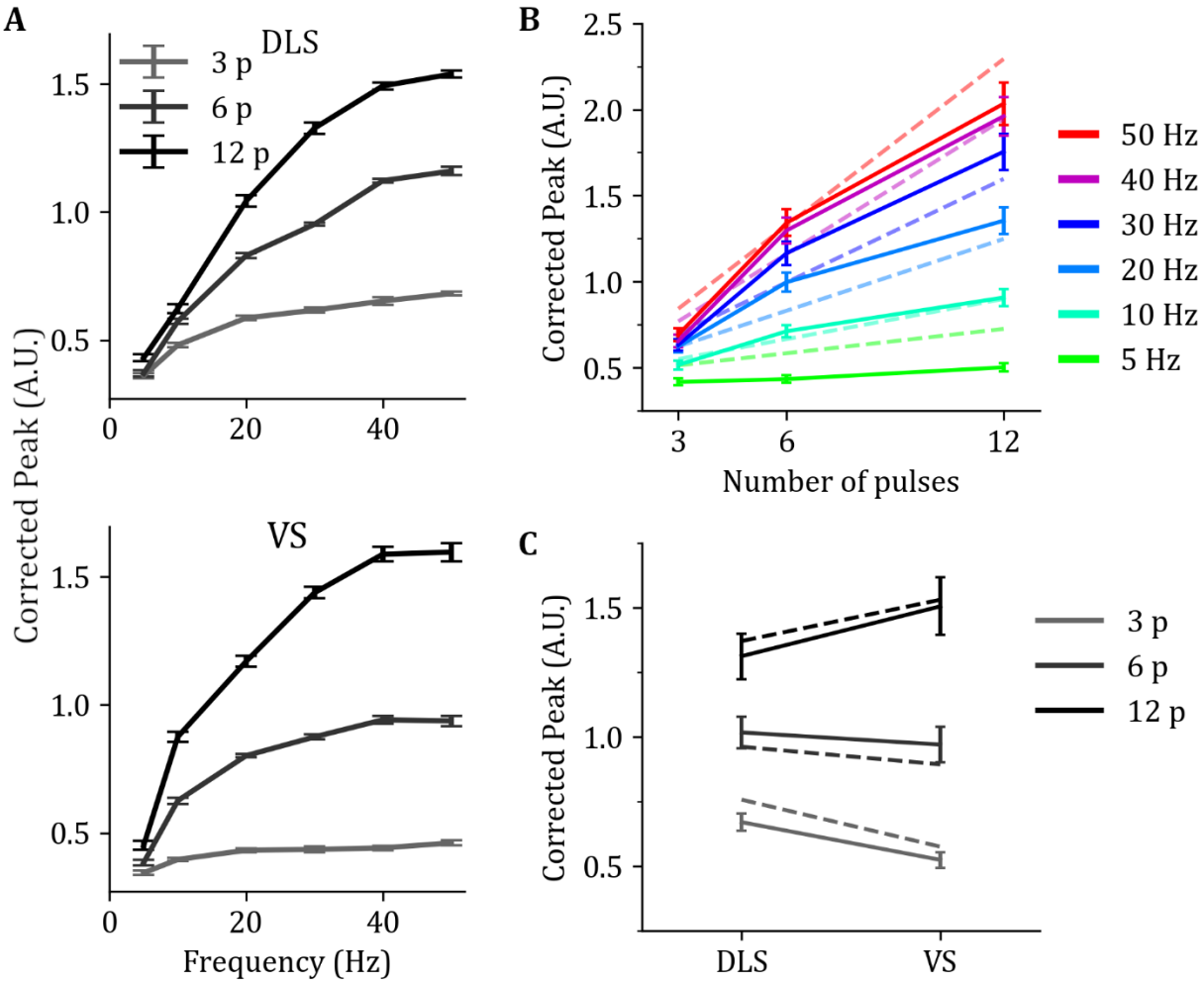


Figure 4.7: ***Plots showing the effect of frequency, NP and region on the peak amplitude of electrically evoked dLight transients in arbitrary units (A.U.). A****, Mean (SEM) amplitudes of electrically evoked dLight transients. Data recorded from the DLS are shown in the upper plot and data recorded from VS are shown in the lower plot.* ***B****, Interaction plot for the frequency:NP interaction effect on the peak amplitude of dLight transients. The mean (SEM) of the real data is shown with solid lines; the model predictions are shown as dashed lines.* ***C****, Interaction plot for the NP:region interaction, again showing real data overlaying model predictions. In both* ***B*** *and* ***C****, the plotted data has been region-corrected.*

Table 4.4: Fixed effects, estimates and statistics for peak amplitude of electrically evoked dLight transients.

β term	β-estimate	SE	df	*t*-statistic	*p*-value
Intercept	1.03	0.159	11.9	6.47	<.001
Frequency	0.312	0.0275	349	11.3	<.001
NP	0.256	0.0411	349	6.23	<.001
Region	-0.0301	0.0578	352	-0.521	.603
Freq:NP	0.183	0.0276	349	6.62	<.001
NP:Region	0.142	0.0554	349	2.57	.0105

Animal: n = 11; 360 observations; SD_{animal} = 0.507; ICC_{null} = .317.
Region coding: DLS = 0; VS = 1.

The frequency response at 12 pulses appears sublinear in both the DLS and VS data. To investigate whether this nonlinearity in both regions was significant, two separate LMMs were constructed *post-hoc* using the peak amplitude of dLight transients from each region evoked by each number of stimulation pulses. Each model contained only 2 predictors: frequency and its 2nd-order polynomial. Significance of the polynomial would suggest that the frequency response in that region is best described with a nonlinear fit. At 12 pulses in the DLS, both the main effect of frequency (β = 3.97, t(45.0) = 10.3, p < .001) and the polynomial (β = -0.916, t(45.0) = 2.37, p = .0222) were significant. Similarly, in the VS both the main effect of frequency (β = 4.37, t(55.0) = 8.16, p < .001) and of the polynomial were significant (β = -1.44, t(55.0) = 2.69, p = .00953). Again at 6 pulses in the DLS, the main effect of frequency (β = 2.70, t(45.0) = 11.0, p < .001) and the polynomial (β = -0.639, t(45.0) = 2.61, p = .0122) were both significant. The same was true in the VS, with a main effect of frequency (β = 2.13, t(55.0) = 6.92, p < .001) and the polynomial (β = -0.863, t(55.0) = 2.80, p = .00700). At 3 pulses in the DLS, the main effects of frequency (β = 0.927, t(45.0) = 8.09, p < .001) and the polynomial (β = -0.344, t(45.0) = 3.00, p = .00434) were again significant. However, in the VS, only the main effect of frequency was

significant (β = 0.420, $t(55.0) = 4.56$, $p < .001$) and not the polynomial (β = -0.163, $t(55.0) = 1.77$, $p = 0.820$). Here, there is frequency dependence for all numbers of stimulation pulses. Furthermore, there is evidence of biregional sublinearity at all numbers of pulses except at 3 pulses in the VS.

4.5.2. LMM for frequency, NP and region on dLight FWHH

The FWHH of electrically evoked dLight transients across all frequencies, numbers of pulses and in both regions is shown in Figure 4.8A. The FWHH of the dLight transients have a similar overall pattern in response to the experimental manipulations of frequency, NP and region compared to FCV (see Figure 4.4A): there is an overall trend that higher frequency stimulation results in a lower FWHH, but this is most apparent at 12 pulses. The frequency response at 12 pulses seems non-linear, with greater differences between transients evoked by lower frequency stimulation (5-20 Hz) and greater similarity at higher frequency stimulation (20-50 Hz). Unlike the FWHH of FCV transients, there does seem to be a consistent regional difference, with longer transients in VS than DLS. Additionally, the error bars are consistently smaller in DLS, which indicates that there is more consistency in the durations of dLight transients measured in the DLS than the VS.

To assess the role of the parameters of interest on FWHH in the dLight dataset, the data were entered in a LMM regression. The final model explained significantly more of the variance in the data than the null model ($\chi^2(5) = 292$, $p < .001$). Full details of the final model are shown in Table 4.5. There was a highly significant main effect of frequency, with higher frequency stimulation resulting in dLight transients with a shorter duration. The main effect of NP was also highly significant in the opposite direction, with more pulses

resulting in dLight transients with a longer duration. There was also a highly significant main effect of region, with shorter transients in DLS than in VS.

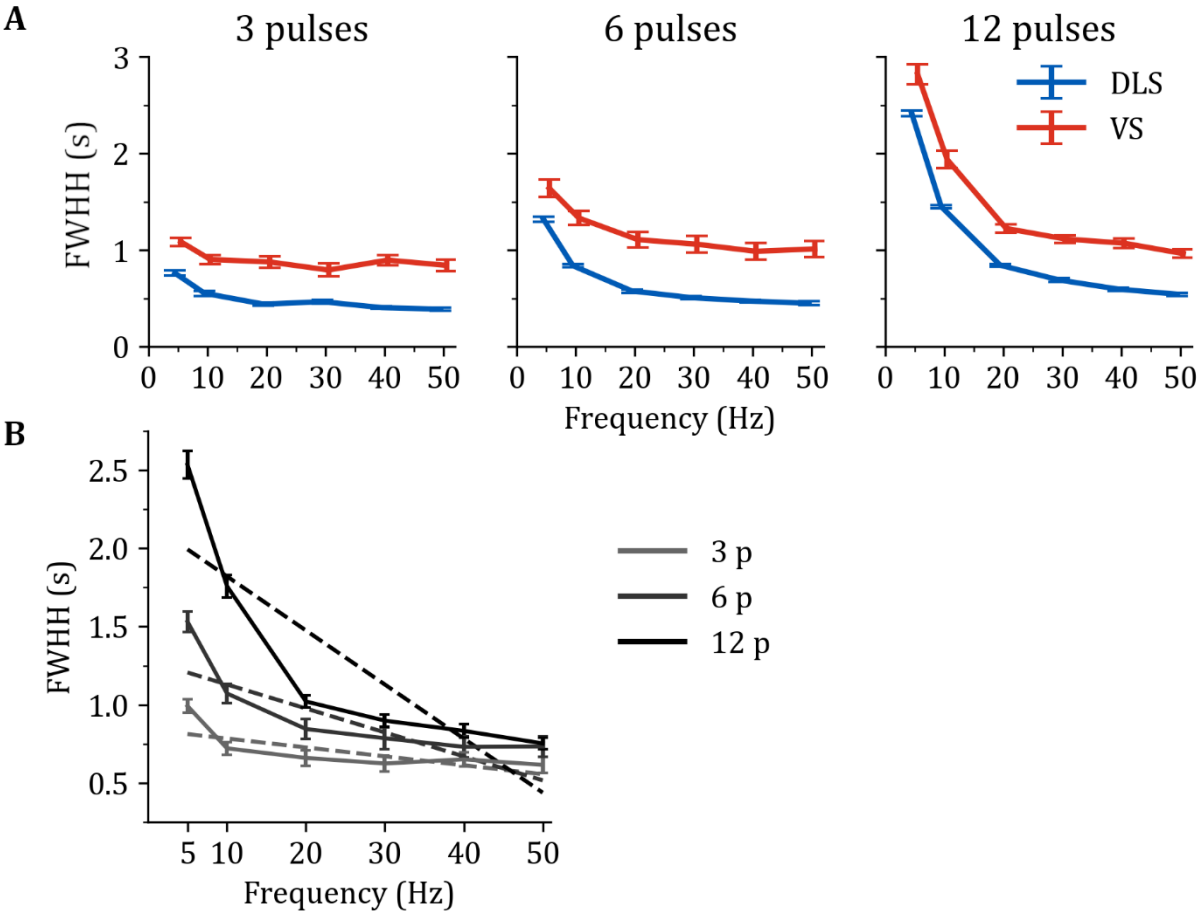


Figure 4.8: ***The FWHH of electrically evoked dLight transients at all frequencies and numbers of pulses, separated by striatal region and interaction plot. A****, Mean (SEM) amplitudes of electrically evoked dLight release. Transients evoked by different numbers of pulses are shown on different plots, from 3 to 12 pulses left to right.* ***B****, Interaction plot for the frequency:NP interaction effect on the FWHH of dLight transients. The mean (SEM) of the real data is shown with solid lines; the model predictions are shown as dashed lines.*

Table 4.5: Fixed effects, estimates and statistics for FWHH of electrically evoked dLight transients.

β term	β-estimate	SE	df	*t*-statistic	*p*-value
Intercept	0.700	0.126	11.9	5.56	<.001
Frequency	-0.295	0.0233	367	-12.7	<.001
NP	0.241	0.0233	367	10.4	<.001
Region	0.504	0.0475	370	10.6	<.001
Freq:NP	-0.191	0.0233	367	-8.22	<.001

Animal: n = 11; 378 observations; SD_{animal} = 0.401; ICC_{null} = .231.
Region coding: DLS = 0; VS = 1.

The interaction between frequency and NP was highly significant: lower stimulation frequencies resulted in longer dLight transients, but this effect was strongest when more stimulation pulses were delivered. However, the interaction plot suggests that, while this overall pattern is true of the actual data, the model's predictions are not a perfect fit (Figure 4.8B), as the relationship between frequency and FWHH in the real data appears noticeably non-linear.

4.5.3. LMM for frequency, NP and region on dLight T50

Plots showing the effects of frequency, NP and striatal region on the T50 of evoked dLight transients are shown in Figure 4.9A. Overall, stimulation with more pulses also results in a longer T50. The effect of stimulation frequency and number of pulses on the T50 of evoked dLight transients follows a similar pattern to the FWHH in the DLS (Figure 4.8), but this pattern is slightly different in the VS. In the DLS, there is a clear trend that lower stimulation frequencies will result in longer decay times, an effect that is more apparent with more stimulation pulses. In the VS, this relationship is less clear and consistent. At 3 and 6 pulses, T50 increases with stimulation frequency; at 12 pulses, the

reverse is true instead. Despite these differences in the pattern of frequency responses across regions, the T50 of evoked dLight transients in VS is consistently longer than in DLS, regardless of the stimulation parameters.

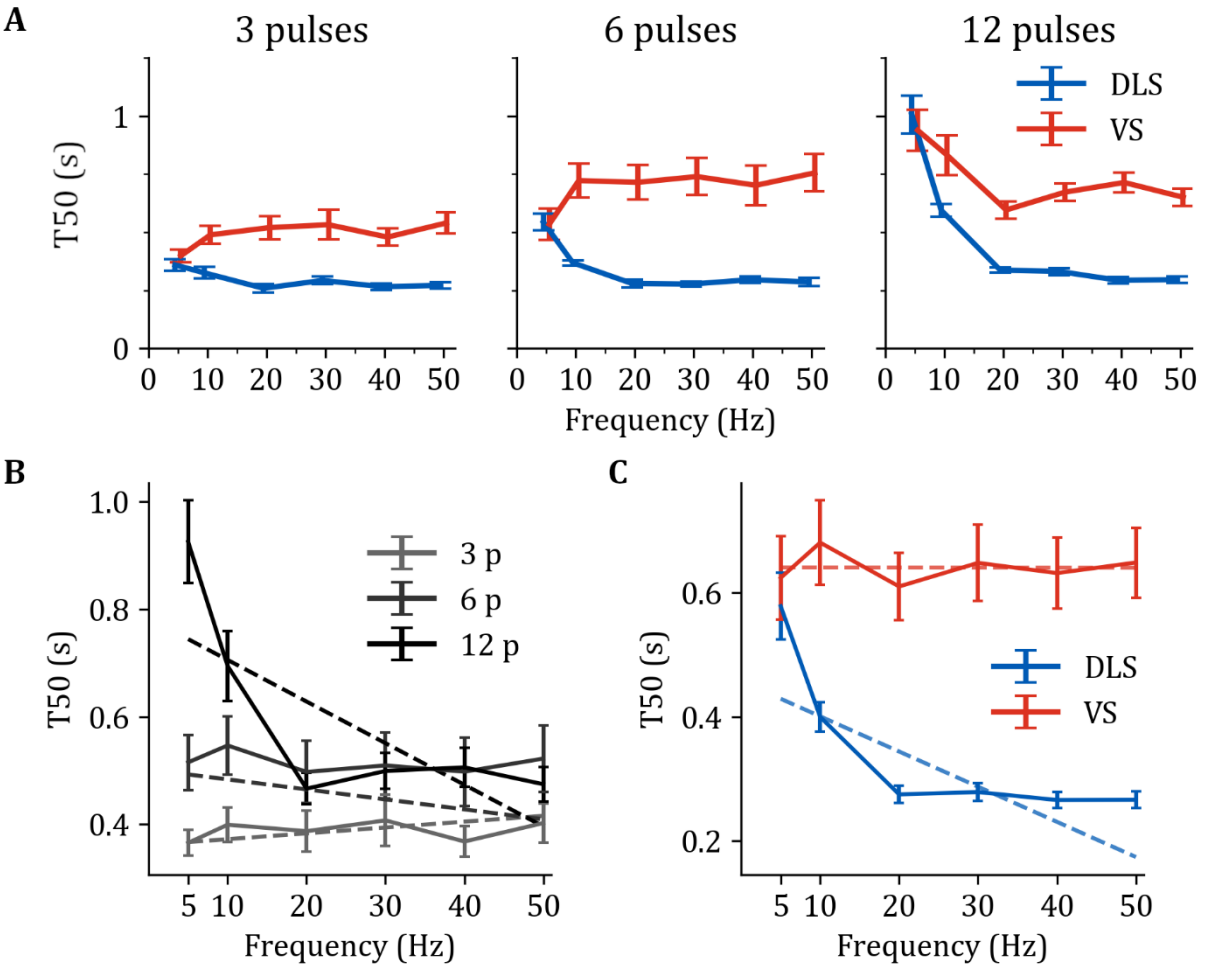


Figure 4.9: ***The T50 of electrically evoked dLight transients at all frequencies and numbers of pulses (separated by striatal region) and interaction plots. A****, Mean (SEM) T50s of electrically evoked dLight transients. Transients evoked by different numbers of pulses are shown on different plots, from 3 to 12 pulses left to right.* ***B****, Interaction plot for the frequency:NP interaction effect on the T50 of dLight transients. The mean (SEM) of the real data is shown with solid lines; the model predictions are shown as dashed lines.* ***C****, Interaction plot for the frequency:NP interaction effect on the T50 of dLight transients. As in* ***B****, both the real data and the model are shown.*

To assess the role of frequency, NP and region on T50 in the dLight dataset, the data were entered into a LMM regression. The final model explained significantly more of the variance in the data than the null model ($\chi^2(4) = 79.8$, $p < .001$). Full details of the final model are shown in Table 4.6. There was a significant main effect of frequency, suggesting that stimulation at lower frequencies results in longer decay times. The main effect of NP was highly significant, with more stimulation pulses also resulting in longer decay times. The main effect of region was highly significant, with shorter decay times overall in DLS than VS.

There was a significant interaction between frequency and NP: stimulation at lower frequencies resulted in longer decay times, but this effect was stronger with more stimulation pulses. However, as shown in the interaction plot (Figure 4.9B), the model predictions are not a perfect fit for the actual data, as the relationship between the stimulation frequency and the T50 of evoked dLight transients does not appear to be linear. At higher frequencies (20-50 Hz), increasing the frequency of stimulation does not seem to affect T50.

Table 4.6: Fixed effects, estimates and statistics for T50 of electrically evoked dLight transients.

β term	β-estimate	SE	df	*t*-statistic	*p*-value
Intercept	0.311	0.105	12.0	2.96	.0120
Frequency	-0.0903	0.0281	367	-3.22	.00141
NP	0.0806	0.0194	367	4.16	<.001
Region	0.329	0.0396	370	8.32	<.001
Frequency:NP	-0.0586	0.0194	367	-3.02	.00270
Frequency:Region	0.0902	0.0388	367	2.33	.0206

Animal: n = 11; 378 observations; $SD_{animal} = 0.335$; $ICC_{null} = .362$.
Region coding: DLS = 0; VS = 1.

There was also a significant interaction between stimulation frequency and region. The interaction plot (Figure 4.9C) shows that the model fits well for the VS data, with no clear effect of stimulation frequency on the T50 of evoked dLight transients when averaging across different numbers of pulses; by contrast, the DLS shows the negative relationship described above, with shorter decay times at higher frequencies. Again, the relationship between the stimulation frequency and the T50 of evoked DLS dLight transients appears to be flat and linear between 20 and 50 Hz, with only 5 and 10 Hz stimulation resulting in longer decay times.

In both interaction plots (Figure 4.9B, C), the T50 at 5 and 10 Hz did not fit the pattern seen in the rest of the data, which seemed to be driving the interaction effects found by the model. As the signal evoked by low frequency stimulation can have a less defined peak, some of the model effects could be due to inaccurate estimates of T50 rather than meaningful underlying biological difference. The LMM was repeated excluding trials of 5 and 10 Hz stimulation. In this model, the main effects of NP and frequency were no longer significant, but T50 was still significantly longer in the VS than the DLS ($\beta = 0.399$, $t(242) = 9.60$, $p < .001$).

To investigate the differences between the models for FWHH and T50 in the dLight dataset, another LMM was constructed *post-hoc* with peak latency as a dependent variable, and frequency, NP and region as fixed effects. There was a highly significant main effect of region ($\beta = 0.168$, $t(376) = -2.61$, $p < .001$): the VS had longer peak latencies than DLS. There was also a highly significant main effect of frequency ($\beta = -0.0158$, $t(366) = 16.6$, $p < .001$), with higher frequency stimulation resulting in a shorter peak latency, and a highly significant main effect of NP ($\beta = 0.0428$, $t(366) = 10.6$, $p < .001$), with more pulses

resulting in longer peak latency. Finally, the interaction between frequency and NP was highly significant (β = -0.00222, $t(366) = -8.74$, $p < .001$), with the strongest of effect of NP at low frequencies of stimulation.

4.5.4. LMM for frequency, NP and region on dLight τ

Unlike in the FCV dataset, τ could be calculated as an estimate of signal decay for the majority of the dLight transients. The DLS of one animal was excluded from analysis as τ could not be accurately estimated for most parameters, but τ calculated from transients in the VS of that animal were still included in the analysis. These data are displayed in Figure 4.10. Overall, there is no strong evidence that the number of stimulation pulses consistently affects τ. Frequency has little effect either, except at 5 and 10 Hz stimulation where τ is slightly larger in DLS. Most noticeable is the difference between regions: there is consistently steeper exponential decay (smaller values of τ) in the DLS compared to the VS. The data are also more variable in the VS than DLS, with larger error bars overall but especially in dLight transients evoked by 3 pulse stimulation.

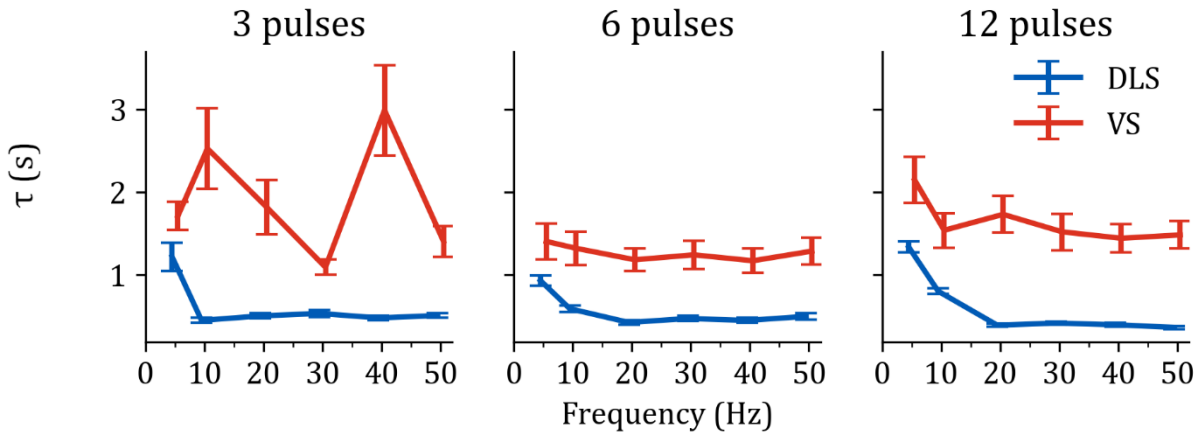


Figure 4.10: ***The mean (SEM) τ of electrically evoked dLight transients at all frequencies and numbers of pulses, separated by striatal region.***

Table 4.7: Fixed effects, estimates and statistics for τ for electrically evoked dLight transients.

Fixed effect	β-estimate	SE	df	*t*-statistic	*p*-value
Intercept	0.000470	0.000312	14.9	1.51	.153
Frequency	-0.000131	0.0000976	347	-1.34	.182
NP	-0.0000391	0.0000978	347	-0.400	.689
Region	0.00115	0.000204	356	5.63	<.001

Animal: n = 11; 358 observations; SD_{animal} = 0.000895; ICC_{null} = .159.
Region coding: DLS = 0; VS = 1.

To assess the role of frequency, NP and region on τ in the dLight dataset, the data were entered into a LMM regression. The final model explained significantly more of the variance in the data than the null model ($\chi^2(3) = 22.2$, $p < .001$). Full details of the final model are shown in Table 4.7. There was no significant main effect for either frequency or NP. However, there was a significant main effect of region, with smaller values of τ, meaning steeper decay, in DLS (Figure 4.10).

4.6. Results: Comparing dopamine transients measured with FCV and dLight photometry

The LMMs built for peak height are very similar between the FCV and dLight datasets, with the same main effects (frequency and NP) and interactions (frequency:NP and NP:region) present in both models. However, there is a marked difference between the LMMs for FWHH between the two techniques. In the FCV dataset, there was a main effect of frequency and NP, but not of region. Conversely, in the dLight dataset, there were main effects of frequency, NP and region as well as a significant interaction between frequency and NP. To evaluate this difference between techniques, a LMM for FWHH was built from

the combined FCV and dLight datasets. There were four predictors in this model: frequency, NP, region and technique, this last predictor being whether the data were collected using FCV or dLight photometry.

The final model explained significantly more of the variance in the data than the null model (χ^2 (7) = 389, p < .001). Full details of the final model are shown in Table 4.8. As in the model for FWHH constructed on the dLight dataset, there was a highly significant main effect of frequency, with higher frequency stimulation evoking transients of a shorter duration. The main effect of NP was also highly significant in the opposite direction, with more pulses resulting in transients of longer duration. The interaction between frequency and NP was highly significant, with the effect of frequency in decreasing FWHH greater with more pulses. There was also a highly significant main effect of region, with shorter transients in DLS than in VS. In these data, the interaction between NP and region was also highly significant.

Table 4.8: Fixed effects, estimates and statistics on FWHH of combined FCV and dLight data.

β term	β-estimate	SE	df	*t*-statistic	*p*-value
Intercept	0.705	0.108	22.5	6.52	<.001
Frequency	-0.265	0.0187	644	-14.2	<.001
NP	0.145	0.0266	645	5.47	<.001
Region	0.505	0.0505	650	10.0	<.001
Technique	0.721	0.161	22.3	4.49	<.001
Freq:NP	-0.172	0.0187	644	-9.21	<.001
NP:Region	0.126	0.0374	644	3.37	<.001
Region: Technique	-0.481	0.0777	651	-6.19	<.001

Animal: n = 20; 664 observations; SD_{animal} = 0.336; ICC_{null} = .269.
Region coding: DLS = 0; VS = 1. Technique coding: dLight = 0; FCV = 1.

The most important effect in this analysis is the main effect of technique and its potential interactions with other fixed effects: these interactions indicate differences between FCV and dLight photometry in how they are reading out the evoked release in different regions or in response to different stimulation parameters. There was a highly significant main effect of technique, with FWHH overall being shorter when measured using dLight than FCV. There was also a significant interaction between region and technique. Both these effects are clearly visible in Figure 4.11. The mean duration of transients recorded from both regions is longer when recorded with FCV than with dLight photometry. Furthermore, the regional difference in FWHH between DLS and VS is much greater when measured with dLight photometry than with FCV.

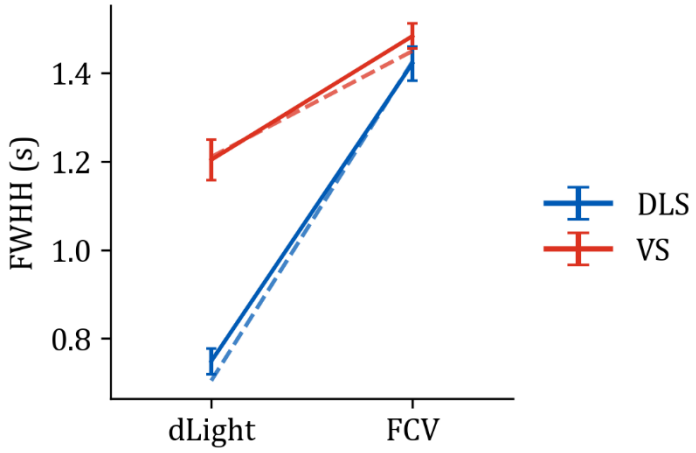


Figure 4.11: ***Interaction plot showing the FWHH of electrically evoked dLight and FCV transients in each region.*** *The plot demonstrates the model's predictions for the Region:Technique interaction (dashed lines) and overlays the mean (SEM) real data (solid lines).*

4.7. Discussion

dLight photometry is a relatively novel method of measuring dopamine transients, the dynamics of which have yet to be comprehensively explored *in vivo*. Here, I measured electrically evoked dopamine transients with both dLight and FCV in response to three variables of interest: number of pulses, frequency and region (DLS and VS). Both techniques were able to read out the expected increase in the magnitude of the striatal dopamine signal with higher frequency stimulation and more stimulation pulses directed to midbrain. It was also demonstrated that the timescale of measured dopamine transients differed between regions, with faster decay in the DLS than the VS. However, this regional difference was stronger in the dLight dataset, with photometric transients also consistently faster than voltammetric transients.

4.7.1. Increasing frequency and NP resulted in larger dopamine transients.

It has been demonstrated extensively in many stimulation experiments that increasing either the frequency or the number of pulses used to stimulate the midbrain results in a higher amplitude of dopamine release (e.g. Beckstead et al., 2004; Bunin et al., 1998; Iravani & Kruk, 1997; John et al., 2006; Melchior et al., 2015; Rice et al., 1997). When the inter-pulse interval is shorter than the decay time of single transients, the evoked release will summate with each additional pulse, thereby increasing the peak amplitude of the signal in striatum. Similarly, the frequency dependence of evoked dopamine release arises because at higher frequencies of stimulation, less time is available between individual pulses for uptake, thereby increasing the maximal peak amplitude. As a natural consequence of this relationship, these two factors will interact on dopamine release, with

the effect of frequency greatest with a high number of pulses. Both the FCV and dLight datasets follow this trend: both frequency and number of pulses increased the magnitude of the evoked dopamine signal. The expected interaction between these factors was also found. Increasing the frequency of stimulation with 3 pulses has relatively small effect; the same change in frequency at 12 pulses has a much greater effect on the peak amplitude.

However, it is important to note is that this frequency dependence is also normally controlled by acetylcholine, which affects the short-term plasticity of release probability at the level of the striatum (Cragg, 2003; Exley & Cragg, 2008; Rice & Cragg, 2004). The action of acetylcholine in these anaesthetised experiments is not known, but it is important to consider that this frequency dependence may not merely be a consequence of summating individual pulses. In the awake brain, this frequency dependence may be dynamically modulated by environmental stimuli affecting ChI activity.

For this experiment, the stimulation parameters were chosen to encompass the range of physiological firing of midbrain dopaminergic neurons, with the typical dopamine neuron 'burst' in response to salient external or internal stimuli (e.g. rewards or reward-predicting cues) consisting of roughly 6 action potentials occurring between 15-50 Hz (Montague et al., 1996; Schultz et al., 1997; Watabe-Uchida et al., 2017). It is of particular interest to the aims of this study that the measured dLight signals were sensitive to manipulations both of stimulation frequency and the number of stimulation pulses, as this suggests that dLight photometry can read out dopamine transients across the physiological range of dopamine neuronal activity. Notably, while 30-50 Hz bursts of 12 action potentials are unlikely to occur naturally, the signal measured by both FCV and dLight photometry is still frequency dependent in this supraphysiological range.

The magnitude of the evoked dopamine response measured with either technique varies considerably and somewhat reliably across the range of stimulation parameters. Stimulation reflecting small bursts of 3 spikes at 5-10 Hz produces relatively small transients, small enough that they may be difficult to read out with either dLight or FCV; stimulation at higher frequencies and/or with more pulses produce larger transients. The parameter-dependence of the striatal release dynamics suggests that native dopamine release would also be strongly dependent on the degree of the midbrain neuronal response. This is especially important as the magnitude of dopaminergic neuronal activity and dopamine release is known to encode subjective value, e.g. the size, latency and likelihood of rewards (Bayer & Glimcher, 2005; Eshel et al., 2016; Lak et al., 2014; Roesch, Calu, Burke, & Schoenbaum, 2007; Takahashi, Langdon, Niv, & Schoenbaum, 2016; van Elzelingen et al., 2022).

There was evidence of non-linearity in the frequency response of dopamine transients measured by both techniques, which were also regionally distinct. The peak amplitude of FCV transients increased in a superlinear manner in the DLS. In the VS, the data appeared sublinear, but this trend was not strong enough to be found as significant. As the associated *p*-value was close to significance, it's possible there was insufficient statistical power to detect this nonlinearity with the sample size used for these FCV experiments. Power calculations carried out in R (Green & MacLeod, 2016) estimated a type II error rate of <60% for all of these nonlinearity tests on FCV dopamine transients (range: 15.3-55.9%). As such it is difficult to make any firm claims about the linearity or otherwise of this relationship.

The superlinearity of the frequency response in DLS at 12 pulses (and only 12 pulses) is surprising, especially given that the dLight data paints a different picture: the frequency responses of dLight transients in both striatal regions were consistently sublinear at most numbers of stimulation pulses. This could reflect a genuine difference between regions and techniques, but it is difficult to tell from these data how best to interpret these conflicting findings. From the FCV data alone, one could argue that dopamine release in DLS is selectively boosted at higher frequencies of stimulation. Conversely, the sublinearity of the frequency response in the dLight dataset could represent an inability of the dopaminergic system to respond consistently to stimulation with maximal parameters (high frequency and many pulses). Alternatively, the sublinearity in dLight data may reflect the kinetics of dLight 1.1, which are themselves sublinear at high concentrations of dopamine (Patriarchi et al., 2018). Which interpretation is the correct one is impossible to deduce from these data alone.

4.7.2. Evaluating the timescale of FCV transients with different stimulation parameters.

In this experiment, FCV transients were longer in response to stimulation at lower frequencies and with more stimulation pulses as measured by FWHH. This fits well with a model of analysis in which peak latency has a strong effect on the overall duration of the signal. The duration of a transient can be separated into two components: rise time, or peak latency; and fall time, or signal decay. The rate of decay of striatal dopamine transients is primarily governed by diffusion but also DAT, which is thought to mediate a largely activity-independent mechanism for the clearance of extracellular dopamine (Cass et al., 1993; Giros et al., 1996, 1996; Mundorf et al., 2001; Rice et al., 2011; Vaughan &

Foster, 2013). Michaelis-Menten kinetics suggest that the rate of decay of voltammetric dopamine transients is dependent on the concentration of extracellular dopamine – higher concentrations generally mean faster clearance. In line with these assumptions, the T50 of evoked FCV transients was greater at higher stimulation frequencies and with more stimulation pulses. Furthermore, the total decay time will be longer for transients of greater amplitude.

The change in the FWHH (signal duration) of evoked FCV transients in response to different stimulation parameters was not the same as for T50: FWHH increased with more stimulation pulses but decreased with frequency. This finding is predictable considering that FWHH is the sum of T50 and peak latency. This pattern of response is in line with how changing the frequency and number of pulses would affect the duration of stimulation, and therefore the peak latency. This highlights the importance of evaluating different components of the signal's timescale when trying to characterise the temporal dynamics of a signal.

4.7.3. Evaluating the timescale of dLight transients with different stimulation parameters.

As in the FCV data, the duration of dLight transients (measured as FWHH) were longer in response to stimulation at lower frequencies and with more pulses. One might therefore conclude, as with the FCV data, that the overall duration of dLight transients is dependent on the peak latency. However, while increasing the number of pulses had the expected effect of extending decay time, dLight transients instead had shorter decay time (measured as T50) at higher frequencies. Furthermore, this effect was greater with more stimulation pulses.

One would assume that transients evoked by higher frequency stimulation would take longer to decay to the half peak; therefore, these findings might suggest that the rate of decay of evoked dLight transients was dependent on the frequency of stimulation. However, neither frequency nor number of pulses had a significant effect on τ. A *post-hoc* test confirmed that T50 was no longer frequency- or NP-dependent between 20 and 50 Hz of stimulation. It is likely that this negative frequency-dependence of T50 across the entire range of stimulation is due to inaccurate location of the peaks of transients evoked by low frequency stimulation at 5 or 10 Hz. When signal amplitude is not dependent on the number of pulses, this indicates that that the pulses are not spaced close enough together for them to 'stack' on top of one another. In this scenario, the result would either be a series of individual peaks or, as is likely in this case, a plateau response, visible in these data during 5-10 Hz stimulation. The closer one gets to a signal plateau (rather than a sharp peak), the more prone peak location is to error; at a true plateau, the peak's precise location holds no useful biological meaning and thus T50 is a poor estimate of decay time. With this interpretation, the data show that the decay time of dLight transients is most likely also independent of frequency and NP.

4.7.4. Regional differences in evoked transients in both modalities

Both the duration and the decay time of the recorded FCV transients were longer in the VS than the DLS. As discussed in the previous section, decay time can be longer for transients with a greater peak amplitude; however, as the data were normalised by region, the overall amplitude for both regions is equal. In this case, the observed difference in

decay time in both modalities (FCV and dLight photometry) is best explained as a real biological difference between regions.

A regional difference in the decay time may also explain why the magnitude of FCV transients is affected more strongly by the number of stimulation pulses in the VS than DLS. At a fixed frequency in which pulses are close enough together to 'stack', adding more pulses will increase the amplitude linearly (within the biological limits of the system). At the same frequency but with slower decay, the amount of dopamine already extant in the extracellular space will be higher at the time of each pulse, thus the overall magnitude of the signal will increase. Therefore, some interaction between region and stimulation intensity is predictable from an additive model. Contrary to this explanation, there was no significant interaction between region and frequency, another manipulation of stimulation intensity. However, this may simply be due to a lack of power in the model to detect this interaction.

The regional difference in the timescale of photometric dLight transients matched well with the pattern observed in the FCV data, in that dLight transients overall had a longer duration in the VS than the DLS. Furthermore, both measures of signal decay, T50 and τ, suggested that decay occurred faster in the DLS than the VS. One likely mechanism for this is a different rate of dopamine uptake in both regions. It is known that levels of DAT are higher in the dorsal striatum than in the VS (Ciliax et al., 1995; Nirenberg et al., 1997), which would result in faster uptake and therefore more rapid transients in DLS compared to VS. If this is the case, dopamine release arising from a fixed pattern of action potentials firing would have longer-lasting effects on dopamine-mediated striatal neurons

in VS than in DLS, assuming these neurons express similar levels of the same types of dopamine receptors.

4.7.5. Comparing dLight photometry with FCV

As described in the previous sections, there is a great deal of agreement between the dynamics of dopamine measured with dLight and FCV: both techniques show the expected dynamics in response to changing the stimulation parameters, but also show the same regional difference: that the duration of ventrostriatal dopamine transients measured in these experiments is longer than those measured in the DLS. However, while both techniques can read out this difference in this data, dLight photometry and FCV show different temporal dynamics, in that the regional difference measured with dLight photometry is much greater than that measured by FCV. When considering why this might be, it is important to remember the intrinsic differences between these techniques. FCV requires the adsorption of dopamine molecules to the carbon fibre electrode to read out the signal. Dopamine does not immediately desorb from the carbon fibre, which may prolong the timescale of the actual transients, especially those with faster kinetics. By contrast, as an optical reporter tied to the dynamics of dopamine binding to the modified D1 dopamine receptor, dLight theoretically has a similar temporal resolution to the native dopamine receptor itself (~10 ms on time; ~100 ms off time; Patriarchi et al., 2018). With its faster kinetics, dLight may therefore be a better technique for reading out the finer timescale of dopamine signals in the brain. This may explain why FCV is in general slower than dLight (see Figure 4.11).

Another significant advantage that dLight has over FCV is its signal-to-noise ratio. While it is certainly possible to record very large evoked transients with FCV, the signal to noise ratio at physiological levels of stimulation can be poor, making detection of transients a challenge, especially in the dorsal striatum (van Elzelingen et al., 2022). In my experiments, FCV transients had poorer signal-to-noise ratio than the equivalent evoked dLight transients, so much so that τ could not be accurately estimated from the mean traces across multiple trials in the FCV dataset, only in the dLight dataset. To characterise the striatal dopamine signal at physiological levels of dopamine release, FCV users may need to collect more data than dLight users to make clean averages of evoked transients.

The main advantage of FCV as a technique is that one can calculate the absolute concentration of the dopamine release; by contrast, the absolute value of the dLight signal says little about the actual quantity of dopamine, instead reflecting the degree of dLight expression in the local area, the placement of the fibre with respect to dLight-expressing tissue and the intensity of light transmitted through the photometric equipment. However, while some authors have attempted to calculate the concentration of dopamine measured with FCV in a chronic *in vivo* preparation (Clark et al., 2010; van Elzelingen et al., 2022), this is not trivial, as the sensitivity of the electrode is affected over time by the electrochemical environment of the brain. As such, this advantage of FCV mostly holds true for *ex-vivo* experiments.

Nonetheless, FCV does have one key advantage of fluorescent sensors in that that the dynamic range is linear unlike dLight (Patriarchi et al., 2018). As a result, we can interpret non-linearity in of the frequency response of FCV transients as reflecting a meaningful biological effect; with dLight, we cannot be sure whether the same non-linearity reflects

differences in the actual concentration of dopamine or the position of each response along the dynamic range of the sensor.

4.7.6. Limitations of the present study

In these experiments, electrically evoked dopamine transients were recorded from urethane-anaesthetised animals, an approach which has several advantages and disadvantages for addressing the aims of this chapter. As mice were anaesthetised, there was less native fluctuation of activity in the dopaminergic system as compared to awake mice, aware of an immediate environment which may contain biologically relevant (e.g., rewarding) stimuli. There are also practical considerations for choosing anaesthetised animals. FCV is easier in anaesthetised preparations as recordings can be conducted acutely, which circumvents many of the pitfalls of chronically implanting FCV electrodes, such as the necessity of daily cycling and degradation of the measured signal over time. However, the dynamics of signals measured in anaesthetised animals cannot necessarily be transposed to activity in awake animals, as the effects of urethane on electrically evoked dopamine release are unknown.

Measuring evoked rather than native dopamine transients was very useful for addressing the aims of these experiments, as it allowed for precise control over the dopaminergic system with a wide range of stimulation parameters. However, one of the aims of this study is to assess whether dLight can read out physiological levels of dopamine activity. To this end, the stimulation parameters in this study were selected to encompass the range of physiological dopamine 'burst' firing in response to biologically relevant stimuli such as rewards (Montague et al., 1996; Schultz et al., 1997; Watabe-

Uchida et al., 2017). Nonetheless, phasic increases in dopaminergic activity evoked by stimulation may not reflect native phasic dopaminergic activity patterns: the population of dopamine neurons activated by external electrical stimulation will be hyper-synchronised to an extent that is physiologically implausible in a native setting. This could explain why stimulation at 5 Hz consistently resulted in an elevation of the dopaminergic signal above the baseline, despite 5 Hz being comfortably within the range of tonic dopaminergic neuronal firing in the absence of stimulation (Brown et al., 2009; Dai & Tepper, 1998; Dodson et al., 2016; Grace & Bunney, 1983). In this study, electrical stimulation may result in dopamine release which is elevated relative to the equivalent rate of firing of dopaminergic neurons that are not highly synchronised.

The decision to measure electrically rather than optically evoked transients may also have impacted on the results obtained. Electrical stimulation was chosen primarily because it is easier to combine with dLight. Expressing opsin in midbrain neurons would mean that opsin is also expressed in the striatal axons of those neurons. This means that the LED used for photometric recordings in striatum could potentially activate the axonally expressed opsin, causing a photometric recording artifact. However, electrical stimulation has a major limitation: unlike optical stimulation, it cannot be targeted to specific cell types (e.g. via Cre-dependent expression of opsin in dopaminergic cells). This means that additional circuits may be activated alongside the neurons of interest, resulting in evoked firing that is both antidromic on top of the desired evoked orthodromic firing.

4.7.7. Conclusions and future work

The conclusions drawn about the differences between the two recording techniques rely on the assumption that the transients are evoked by stimulation of equivalent intensity in each dataset. However, there are some differences in the setup which may challenge this assumption, chiefly that in FCV experiments a parallel bipolar stimulation electrode was used to evoke dopamine release while a concentric stimulation electrode was used in dLight experiments. The choice of stimulation electrodes was made according to the available resources at the time of the experiments, but this may have affected the evoked dopamine transients. In the midbrain, the parallel bipolar electrode stimulates an area between the two prongs, while a concentric electrode stimulates a discrete area around the electrode's tip. This means that, depending on the stimulation electrode, different populations of dopamine neurons will be stimulated. Considering that parallel bipolar electrodes can span a wide area of tissue depending on the distance between the prongs, the absolute magnitude of the evoked response may differ as well.

Transients from different animals within each cohort were themselves not perfectly matched. One cause may have been differences in the dLight expression between different mice, affecting the absolute value of the signal. However, this also may have been caused by within-region heterogeneity. As the data were collected in different animals, the precise recording sites within the striatum were not constant. This experiment aimed to evaluate heterogeneity in the striatum in a broad scale, specifically comparing dopamine release in the DLS with the VS (specifically, the NAc), but the existence of striosome and matrix subdivisions (Brimblecombe & Cragg, 2017; Graybiel, Flaherty, & Giménez-Amaya, 1991) mean that there might be significant variation in the shape and size of transients

even within a relatively small area. One way to address this would be through histology. Unfortunately, the fibre-optic cannulae used acutely on the dLight cohort caused too little lasting damage, such that the tips of the fibres were not possible to accurately locate in the fixed tissue. The FCV cohort was lesioned in the final recording location, but the brains of FCV mice have not yet been processed due to time constraints. And even so, one would still not be able to determine from this the location of the initial striatal recording site.

It is important to note that, as the only fluorescence sensor used in these experiments was dLight 1.1, the results detailed here might not be generalisable to other dopamine sensors. Several versions of dLight exist which have different affinities and dynamic ranges (Patriarchi et al., 2018), and these differences may affect the signal evoked by these stimulation parameters. $GRAB_{DA}$ (Sun et al., 2020) may be even more distinct from dLight as it is constructed from a modified D2 receptor, which is known to have a far higher affinity for dopamine than the D1 receptor (Martel & Gatti McArthur, 2020). More research is necessary to fully understand the dynamics of different fluorescence sensors for dopamine *in vivo*.

One of the limitations of the present work is the use of electrical stimulation to evoke dopamine transients. Electrical stimulation is straightforward to implement, but optogenetic stimulation allows for purely orthodromic and cell-type selective stimulation. While optogenetic stimulation would be potentially difficult to combine with dLight as the LED used for photometric recording could interact with the opsin, there are several ways around this. One option would be to use an opsin and fluorescent sensor conjugated to different fluorophores, e.g. by using a red-shifted opsin or RdLight1 (Patriarchi et al., 2020), the latter of which was not available at the time of these experiments. However,

there is still some overlap in the excitation ranges of most red and green fluorophores, so there is still a potential for a confounding opsin/sensor interaction. A more refined approach would be to use a soma-targeted opsin, therefore ensuring that opsin would not be expressed in parts of the brain from which dLight is being recorded. This is an intriguing possibility for future work, as it would allow for precise control over dopaminergic neurons and could easily be transposed into awake animals, so that evoked dopamine transients could be recorded in conjunction with evoked changes in the mouse's behaviour.

Another intriguing avenue for future work would be see how these data compare to an *in silico* model. An additive model would be one in which transients evoked by trains of stimuli (as used here) can be described as the sum of equally sized single pulses at a given number of pules and at a given frequency. Many of the assumptions of an additive model were met with these data, but these assumptions were evaluated on a binary classification, by the presence or absence of a significant effect. There is also the possibility that the data could show the same broad pattern but still not match perfectly with the additive model. For instance, if the population of stimulated neurons cannot fire action potentials in a reliable manner at each pulse during high frequency stimulation (see also Figure 3.6), the actual data might be below the predictions of the additive model. Such modelling would help to characterise the precise nature of the relationships between the stimulation parameters and the evoked transients for each technique.

Finally, the biological underpinnings of the observed regional difference cannot be assumed from this study. While differences in DAT levels between regions is a plausible explanation for this difference, this would have to be verified with pharmacological

intervention, for instance using DAT-blockers in slice preparations in each region. Doing this with both dLight and FCV would also build confidence that the regional difference in dLight data is meaningful.

In conclusion. dLight photometry is a powerful tool for measuring dopamine activity in the brain. Overall, the pattern of evoked dLight responses matches well with FCV, a very well-studied technique for measuring dopamine dynamics. Furthermore, both techniques found that VS signals were slower than DLS, but this difference was more apparent when measured with dLight. Striatal dLight recordings are less noisy than FCV at physiological levels of midbrain activity and may be more sensitive to the fine temporal dynamics of striatal dopamine transients. Given the advantages of dLight and the fact that it can precisely read out dopamine transients across the physiological range of dopaminergic neuronal firing, I use dLight as my tool of choice for recording striatal dopamine transients in awake, behaving mice (see chapter 5).

Chapter 5. RESULTS III: LOCOMOTION- AND REWARD-RELATED DOPAMINE SIGNALLING IN DORSOLATERAL AND VENTRAL STRIATUM

5.1. Introduction

Striatal release of dopamine has a powerful modulatory effect on basal ganglia circuits. Research into the function of this modulation has historically fallen into two broad categories. The reward prediction error (RPE) hypothesis, originally developed by Read Montague and Peter Dayan, working with Wolfram Schultz, posits that phasic dopamine acts as a learning signal (Montague et al., 1996; Schultz et al., 1997). Unexpected rewards represent a positive prediction error and are accompanied by phasic increases in dopamine. After learning a stimulus that strongly predicts a reward, the classical RPE hypothesis suggests that this positive prediction error shifts to the stimulus itself rather than occurring at reward delivery; meanwhile, omission of an expected reward would result in a negative prediction error, reflected as a phasic decrease in dopamine, at the time of expected reward delivery. The RPE-like characteristics of dopamine signalling have been reported across a range of paradigms (Chang et al., 2016; Keiflin et al., 2019; Lak et al., 2014; Stauffer et al., 2016; Steinberg et al., 2013; Watabe-Uchida et al., 2017; Witten et al., 2011).

However, dopaminergic signalling is also well-established to be crucial for movement and locomotion. The progressive dysfunction of dopaminergic neurons in the substantia nigra pars compacta (SNc), and the subsequent malfunction of dopaminergic modulation in the projection targets of these neurons, are responsible for the movement-related

pathology of Parkinson's Disease (Kalia & Lang, 2015). There is a compelling body of research which posits a role of phasic dopamine activity in encoding action initiation and the vigour of movements (Klaus et al., 2019). From single-unit recordings of head-fixed behaving mice, Dodson et al. (2016) found a population of neurons in the SNc which transiently decreased their firing at the initiation of movement and increased their firing following termination. Furthermore, the population activity was also dependent on the duration of movement. Those VTA neurons that encoded movement have conversely been shown to increase their firing at the onset of movements (Dodson et al., 2016). Other authors have also reported encoding of movement and vigour in the phasic activity of dopaminergic neurons (Avvisati et al., 2022; Coddington & Dudman, 2018; da Silva et al., 2018; Hamid et al., 2016; Howe & Dombeck, 2016; Jin & Costa, 2010; Panigrahi et al., 2015). Importantly, this action encoding is not uniform across the midbrain. The majority of dopaminergic neurons showing movement-related firing have been recorded from the SNc (da Silva et al., 2018; Dodson et al., 2016; Howe & Dombeck, 2016). Although movement correlates have been reported in VTA neurons (Dodson et al., 2016; Hughes et al., 2020), several studies have reported that the majority of VTA neurons show more RPE-like activity (Saunders et al., 2018; Schultz et al., 1997).

Considering the spatial organisation of midbrain-striatal projections, this heterogeneity in neuronal firing likely reflects a corresponding modulation of different striatal circuits. The striatal projection targets of midbrain dopaminergic neurons span a medial-lateral to ventral-dorsal gradient with VTA dopaminergic neurons preferentially innervating the ventral striatum (VS) and SNc dopaminergic neurons preferentially innervating the dorsal striatum (DS) (Björklund & Dunnett, 2007; Ungerstedt, 1971).

Within this broad classification, different subregions of striatum are also preferentially innervated by distinct subpopulations of dopaminergic neurons (Poulin et al., 2018). Dorsolateral striatum (DLS) receives input from dopamine neuron subtypes mostly located in the SNc, while those projecting to the core of the nucleus accumbens (NAcc) are located in the VTA and express different molecular markers. Projections to the dorsomedial striatum (DMS) are less binary, receiving innervation from a mixture of different subtypes of dopamine neurons, but these neurons are mostly located in the medial aspect of SNc (Avvisati et al., 2022; Poulin et al., 2018). Assuming a broad division of reward-/movement-related function in VTA and SNc, it is reasonable to assume that the VS (especially NAcc) and the DLS in particular might be receiving differential dopaminergic modulation during behaviour.

Although much of the literature on midbrain dopamine function has separately explored the neural encoding of reward and movement, the story may be more complex in more naturalistic situations where movements are carried out to gain rewards. Indeed, some researchers have reported a multiplexing of function, in which movement is required in order to measure RPE-like activity (Hamid et al., 2016; Howe & Dombeck, 2016). When trying to investigate separable encoding of movement and reward in brain signals, an elegant approach is to use a task in which these aspects can be dissociated. One such approach is a Go/No-Go (GNG) task, a dual-condition paradigm in which an animal can receive a reward either for performing an action (the Go condition) or abstaining from that action (e.g. remaining still; the No-Go condition). Syed et al. (2016) recorded FCV transients from the NAcc of freely-moving rats trained in a GNG task, in which reward was contingent on pressing a lever in the Go condition and remaining in a central reward port

in the No-Go condition. The authors found an RPE-like response to the Go cue, but *not* to the No-Go cue – in other words, RPE-like responses only arose when obtaining reward was contingent on movement. A GNG paradigm is an excellent tool to pick apart the functional role of brain signals relating to different aspects of behaviour.

In work described in this chapter, I investigated the role of reward- and movement-related dopaminergic signalling in different striatal regions. Following on from work in Chapter 4, I used dLight photometry to record striatal dopamine simultaneously from DLS and VS in head-fixed, behaving mice situated on a treadmill. dLight transients were recorded from mice performing both spontaneous and reward-contingent movements, using both an instrumental paradigm and a GNG task modified for head-fixed behaviour. The functional role of DLS and VS dopamine signals and their similarities and differences are reported in detail.

5.2. Aims

- To investigate dopaminergic signalling of RPE and movement in the striatum.
- To explore striatal regional differences in these signals.

5.3. Methods

5.3.1. Surgery

All mice undergoing head-fixed behavioural training alongside striatal dopamine recordings underwent recovery surgery prior to training. After general anaesthesia was induced (section 2.2.1), viral vectors expressing dLight or tdTomato were injected into DLS (*AP* = +0.5, *ML* = ±2.3, *DV* = 2.5) and VS (*AP* = +1.4, *ML* = ±0.8, *DV* = 3.8; section 2.2.3) of the same hemisphere (Figure 5.1). The injected hemisphere was counterbalanced across animals. Two fibre-optic cannulae were lowered into the DLS and VS craniotomies to the depth of each injection (section 2.2.5). The cannulae were then cemented in place alongside the headplate (section 2.2.4).

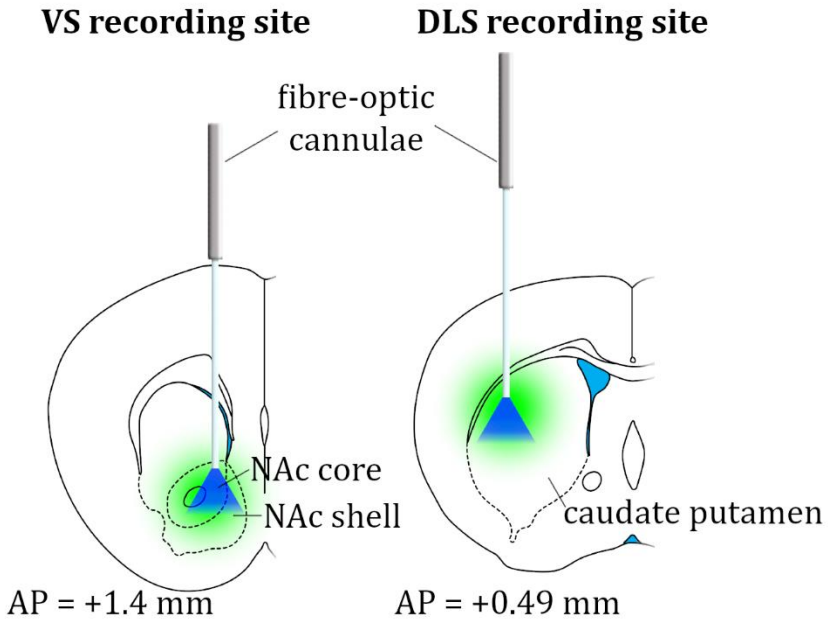


Figure 5.1: ***Schematic of the surgical protocol for behavioural animals represented on coronal sections.*** *dLight was expressed in both DLS and VS and optic fibre cannulae were implanted chronically. The area of targeted dLight expression is shown in green.*

5.3.2. Water restriction

All mice used for behavioural experiments were under a water restriction protocol, to enable the use of water as a behavioural incentive. Water restriction began no sooner than a week after surgical procedure. On the first day of water restriction, baseline body weight was taken. Baseline weight and percentages thereof were calculated by subtracting 1 g from the real value to account for the weight of the headplate and cement. Animals were weighed and individually given at least 1 ml of water each day to maintain a weight of no less than 85% of baseline body weight. Mice new to the protocol were considered ready to begin behavioural testing when their weights were between 85% and 90% of baseline for two consecutive days.

5.3.3. Behavioural training: Apparatus

All behavioural training was conducted in custom-built behavioural apparatuses, each consisting of a head-fixation device, water delivery spout (controlled by an external solenoid valve), a lickometer, a speaker, an IR light and two IR cameras (front and side view; section 2.6.2), all contained within a sound-attenuating box. Also included in each box was a custom-built treadmill attached to a rotary encoder, allowing for online readout and recording of treadmill activity (section 2.6.1). Distance and velocity on the treadmill are reported in encoder counts (rotations of the rotary encoder) and encoder counts/s respectively. Each box was fitted with a pyControl board to control and/or record from all task-related hardware (Akam et al., 2022; section 2.6.3). Each box was also interfaced with two pyPhotometry kits (Akam & Walton, 2019; section 2.5.2) for the simultaneous

recording of photometric dLight signals via the implanted fibre-optic cannulae in DLS and VS.

5.3.4. Behavioural training: Habituation

Before any training was performed, mice were first habituated to head-fixation. This involved putting each mouse in the head-fixed apparatus on the treadmill for a set duration with no behavioural expectations. The initial duration of a session of habituation was 5 minutes, and the duration increased by 5 minutes each day, up to a maximum of 30 minutes of habituation after 6 days. All mice were successfully habituated, running freely during head-fixation by the end of the habituation protocol.

Treadmill and dLight data were recorded from mice undergoing habituation (n = 9, F = 4). As there was no reward available at this stage of training, all locomotion was considered to be 'spontaneous', without any instrumental value or expectation of reward.

5.3.5. Behavioural training: Run-for-reward (RFR) task

Habituated animals were first trained in a simple head-fixed instrumental task on the treadmill, referred to in this chapter as the Run-for-Reward (RFR) task. This was a self-paced task without any external cues. In this task, mice would receive a water drop reward (8 μl, delivered by a spout next to the animal's mouth) immediately after reaching a specified distance threshold on the treadmill within 2 s. The distance travelled in the preceding 2 s was evaluated every 250 ms. The task continued either until the mouse had obtained 125 rewards (1 ml of water) or a time limit of 30 minutes was reached. The distance threshold was initially set at 4 counts (e.g., 4 revolutions of the rotary encoder).

Once a mouse had succeeded in obtaining all rewards within one session for two consecutive days, this threshold was incrementally raised by 2 counts (based on the animal's performance) up to a maximum of 8 counts. After a mouse performed two consecutive fully rewarded sessions of this task at this 'maximum difficulty', the mouse was moved on to the GNG task (see section 5.3.6 below).

Treadmill and dLight data were recorded from mice training in the RFR task (n = 17, F = 8). In the RFR task, reward was contingent on locomotion. Therefore, locomotion in the RFR task had an instrumental value, unlike movements during habituation.

5.3.6. Behavioural training: Go/No-go (GNG) task

The basic premise of a Go/No-Go (GNG) task is that the appropriate action of the animal is contingent on the task condition: in a Go trial, the animal must perform some action to receive a reward, but in a No-Go trial the animal must refrain from that action to receive the reward. In either case, failure results in no reward being delivered.

The GNG task used in this chapter follows the same basic structure as the version described above. Mice performed the task while head-fixed on a treadmill. All rewards were 8 µl water droplets delivered directly to the animal via a spout next to their mouth. After a random ITI (6-14 seconds), mice heard one of two distinct auditory cues (sine wave tones): a Go cue or a No-Go cue. In the GO condition, mice had to reach a distance threshold on the treadmill (set by training stage and the animal's performance, see section 5.3.7 below) to obtain reward. The initial pitch of the Go cue was 10 kHz. As the animal moved forward on the treadmill, the pitch would increase up to 12kHz at the distance threshold, contingent on their movement. The Go cue played continuously until either this threshold

was met or the time-limit was reached (2-10s, titrated for each animal's performance). If the threshold was met, the animal had succeeded and a reward was delivered after a delay of 300 ms; if not, no reward was delivered. Following this was another ITI. In the No-Go condition, mice had to instead avoid reaching a distance threshold on the treadmill (again, set by training stage and the animal's performance, see section 5.3.7 below) to obtain reward. The initial pitch of the No-Go cue was 4 kHz and rose over time towards 6 kHz as the animal stayed below the threshold. Any movement would result in a freeze in the pitch. The No-Go cue played continuously until either this threshold was met or the time-limit was reached (1-2 s, titrated for each animal's performance). Here the contingency is reversed from the Go trials: if the animal exceeded the threshold, no reward was delivered; if not, they received a reward. A schematic of the full task structure is shown in Figure 5.2A.

All outcome states (reward vs non-reward) occurred after a 300 ms delay to allow for separation between potential cue-termination-related dopamine fluctuation and outcome-related fluctuation. When a reward was delivered, a brief click was played. When no reward was delivered, the animal instead heard a 200 ms burst of white noise.

At the start of each GNG training session, mice received an initial uncued reward. Go and No-Go trials were arranged in a block design: 17 Go trials followed by 8 No-Go trials, repeated 5 times for a total of 125 trials per daily session. A block design was chosen as it was assumed it would make it easier for the mice to learn the desired behaviour for each condition.

Treadmill and dLight data were recorded from mice training in the GNG task (n = 16, F = 8). In Go trials, movement had instrumental value, just as it did in the RFR task.

However, in No-Go trials, where success was contingent on refraining from excessive locomotion, *avoiding* movement had instrumental value.

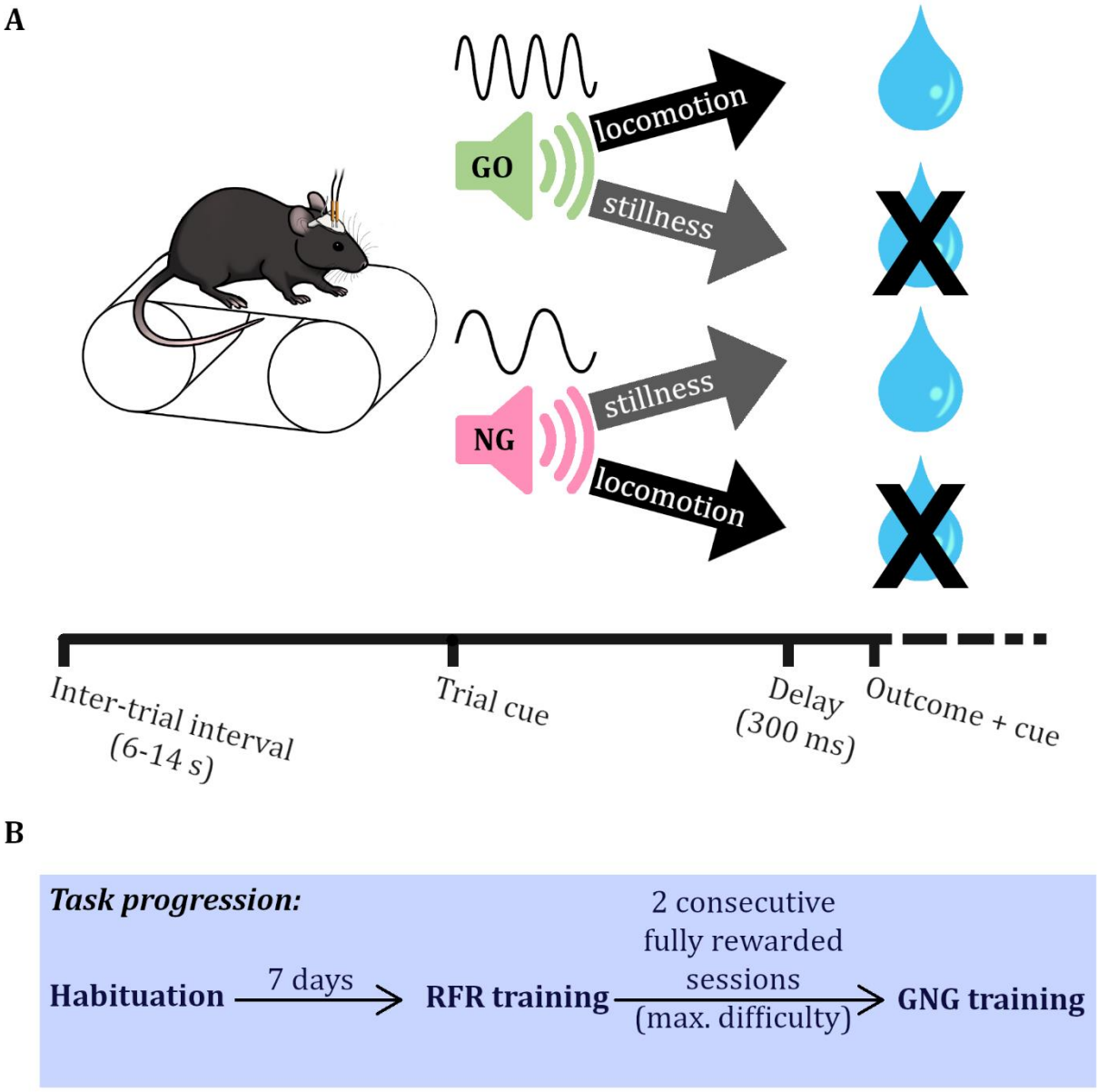


Figure 5.2: ***Structure of the full GNG task. A****, A head-fixed mouse is placed on a treadmill. If the Go cue is played (high frequency sine wave), the mouse can run to obtain a reward; if the No-Go (NG) cue is played (low frequency sine wave), the mouse must remain under a movement threshold to obtain a reward. Failure to meet these conditions in either case results in no reward.* ***B****, A schematic of the training progression across the three behavioural paradigms.*

5.3.7. Behaviour training: Training progression for the GNG task

A timeline of the typical training progression for mice prior to GNG training is shown in Figure 5.2B. Due to the complexity of the GNG task, training was separated into different phases, with parameters adjusted based on individual animal performance. Initially, mice were trained on a simplified version of the GNG task containing only of Go cues (125 Go trials). As in the RFR task, the distance threshold was initially set at 4 counts and the duration of the Go cue was set to 10 s. As the animal's performance improved (achieving a consistent reward rate of 70% or higher), the distance threshold was first incrementally raised by 2 counts at a time to a maximum of 8 encoder counts. After this, the duration of the Go cue was reduced, also incrementally, to a minimum of 2 s. Mice were progressed to the next phase of training when they achieved a consistent reward rate of 70% or higher at these 'maximum difficulty' parameters. Some animals were also moved to the next phase earlier when there was high confidence that they were attending to the Go cue (e.g., clear presence of cue-related dLight signals). Some animals showed a strategy of constantly running without paying attention to the cue. To combat this, a stillness threshold (distance below 4 encoder counts for 2 seconds) was introduced in these cases. The next trial would only be triggered when the animal met this condition.

In the final phase of training, No-Go tones were added. The parameters for Go trials were kept the same. The initial maximum distance threshold for No-Go trials was set to 8 encoder counts. Note that while this may seem high for a 'No-Go' threshold, most mice at this phase exceeded that threshold on most trials; on a subset (the equivalent of a 'failed Go' trial), they may run below this threshold and gain a reward. Once the mouse was

performing above chance in No-Go trials, this threshold was incrementally lowered to a minimum of 2 encoder counts.

5.3.8. Isolating locomotive bouts

One of the aims of this experiment was to identify the movement-related fluctuations in dLight activity, especially related to locomotion. To this end, the treadmill data were processed to identify the initiation and termination of running bouts, along with the duration (ms) and average speed (mean encoder counts/s) across each bout. While others in the literature operationalised 'movement' as a postural adjustments and jerks as well as locomotion (e.g. Coddington & Dudman, 2018; Dodson et al., 2016), I specifically chose to look at locomotion alone, thus my approach here aimed to segregate locomotion from other types of movement.

These analyses used a custom script I wrote in Python. The script works by taking the treadmill velocity (converted to a moving sum, and then made absolute to remove negative treadmill values) and comparing it to a given threshold (2.5 counts/s). The resulting Boolean vector (true = above-threshold movement, false = below threshold movement; see Figure 5.3) required further processing. To separate brief postural changes of mice from 'true' locomotion, bouts of movement shorter than 50 ms were not considered locomotion and removed. In Figure 5.3, the small and short-lived increases in treadmill velocity between 30 and 45 seconds are not counted as locomotion. As single bouts can contain below-threshold values, pauses in locomotion of less than 2 s were assumed to be part of the same bout of movement. Again in Figure 5.3, the treadmill data within the first bout shown (~15-25 s) returns to 0 at several points, but this is still

counted as a single running bout as these returns to 0 are < 2 s. To reduce the interference of previous and subsequent bouts, bouts were only counted when the initiation of a bout was ≥ 2 s after the termination of a preceding bout.

It is important to note that treadmill activity may sometimes be an indirect measure of locomotion onset. For instance, if the treadmill is stiff, mice may initiate their movement before the rotary encoder registers movement on the treadmill. At the time of data collection, the movements of mice on the treadmill were monitored and compared online with simultaneously acquired video feed, and therefore a large discrepancy (e.g. ~1 s) would have been clearly noticeable. Furthermore, the treadills were checked regularly to ensure they turned smoothly. However, any such discrepancy has not been quantified (for example, by comparison with video tracking) so the potential of a mismatch between locomotion onset and its readout in the treadmill data should be kept in mind when interpreting these data.

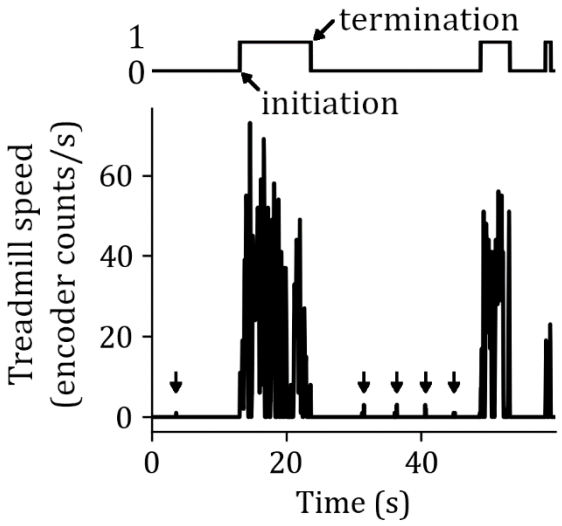


Figure 5.3: ***Transformation of raw treadmill data into discrete bouts of locomotion.*** *An excerpt of the raw treadmill data is shown below a Boolean trace of identified locomotion: 1 (up) is running, 0 (down) is still. The initiation of locomotion is the transition from 0 to 1; termination is the transition from 1 to 0. The downwards arrows represent small, short-lived movements that are not counted as incidents of locomotion.*

5.3.9. Isolating rewarded and non-rewarded locomotive bouts during RFR

Treadmill data from all mice were processed to identify the initiation, termination, speed and duration of each bout as outlined in the section above (5.3.8). However, the addition of a rewarding component in the RFR task (unlike in habituation) meant that the expected brain signal would necessarily differ between rewarded and unrewarded running bouts.

In the case that multiple running bouts have been identified by the script as a single bout, the estimated duration will not reflect reality. To isolate locomotive bouts that promptly resulted in reward, rewarded trials were identified as those in which the mouse achieved a reward within 2 s of bout initiation ***and*** in which the recorded duration of the bout was also under 2 s. While this may exclude trials in which the animal ran continuously for more than 2 seconds but did obtain a reward, it prevented contamination

of the analyses with individual bouts that were not cleanly isolated. Non-rewarded bouts were defined as those in which the initiation of movement did not result in delivery of a reward.

5.3.10. Processing dLight data

dLight data were preprocessed as outlined in section 2.5.4, including motion correction (section 2.5.5). As the absolute magnitude of the dLight signal recorded from each fibre is arbitrary, dependent on factors like the degree of viral expression and optic fibre placement rather than factors which are relevant to the aims of this experiment, all striatal recording data were corrected such that the mean of the modulus of the dLight signal around all events of interest (e.g. initiation, termination or reward delivery) was assigned a value of 1 for each region of each animal. This approach was taken rather than z-scoring the data to keep the analyses consistent with those performed in Chapter 4. When corrected dLight data is shown in plots, the y-axis will be marked with a.u. (arbitrary units).

5.3.11. Time-based linear regression

To disentangle the unique effects of various predictors on the dLight signal across time, I extracted the uncorrected dLight signal in a window around a timepoint of interest (e.g. movement initiation) and performed a separate linear regression at each timepoint (c.f. Blanco-Pozo et al., 2021). This can be expressed as:

$$y(i,t) = \sum_{p} \beta_0(t) + \beta_p(t)X_p(i) + \varepsilon(i,t)$$

where $y(i,t)$ is the ΔF/F dLight activity on trial i at timepoint t, $\beta_0(t)$ is the intercept at timepoint t, $\beta_p(t)$ is the coefficient for predictor p at timepoint t, $X_p(i)$ is the value of predictor p at trial i and $\varepsilon(i,t)$ is the residual unexplained variance. This time-based approach was applied separately to each subject to obtain the coefficient timecourses $\beta_p(t)$. All continuous regressors were z-scored; categorical regressors were dummy coded. For each predictor, the mean and standard error across subjects is shown.

To test for significant deviation across the coefficient timecourse of a single predictor, a 1-sample t-test was performed at each 25th timepoint (0.192 s) against a population mean of 0 (df = n_{animal} – 1). The resulting p-values were corrected for multiple comparisons across different timepoints using the Benjamini-Hochberg correction (Benjamini & Hochberg, 1995). The same method was applied to test differences between regions, but instead using an independent-measures t-test.

5.3.12. Using time-based linear regression across data from different tasks

Across the habituation and RFR datasets, dLight transients accompanying running bouts were recorded with 3 different reward contingencies: no reward contingency for

spontaneous movements (habituation dataset), failed reward contingency (non-rewarded running bouts in RFR) and successful reward contingency (rewarded running bouts in RFR). For these analyses, the regressor of interest, reward contingency, was defined as pairs of groups, coded as follows:

1. non-rewarded (+0.5) vs. spontaneous (-0.5)
2. rewarded (+0.5) vs. spontaneous (-0.5)
3. rewarded (+0.5) vs non-rewarded (-0.5)

Each regression was performed separately for dLight signals from each pair of groups, and for each movement event (initiation or termination). Each regression used only data from mice in both datasets and with meaningful striatal dLight recordings from both regions (see section 5.3.14). Although reward contingency was the regressor of interest, three other regressors were included in each model: bout speed, bout duration and inter-bout interval (pre-bout interval for dLight data around initiation; post-bout interval for dLight data around termination). These regressors took the form of quartiles (Q1 = 0; Q2 = 1; Q3 = 2; Q4 = 3).

5.3.13. Identifying cue-learning in mice trained in the GNG task

In Go trials in the GNG task, mice were trained to run at the presentation of an instrumental cue. Theoretically, mice can reach a 70% threshold for the number of successful trials without actually learning the cue association: if the mouse runs in short, frequent bouts or continuously with no regard for external stimuli, it may still obtain many of the available rewards. However, mice who had learned the importance of the cue would change their behaviour when the cue is presented to maximise their chance of obtaining

a reward. Therefore, to separate cue-learners from non-leaners, the treadmill velocity in the 1 s preceding and following cue onset were statistically compared. A mean velocity within these pre- and post-cue windows was extracted for each trial. A within-subjects *t*-test was used to compare pre- and post-cue velocity within a single session. A significant increase in velocity immediately after the onset of the cue was taken as evidence of cue learning. Mice with ≥ 10 consecutive sessions over the course of their training in which their velocity increased significantly at the onset of the cue were considered 'cue-learners'. All remaining mice were considered 'non-learners'.

Even within mice identified as 'cue-learners', the performance of cue-related locomotion in these animals was dependent on the stage of training. As one of the aims of this chapter is to investigate how learned cues are represented in the dopamine signal, it was necessary to exclude from all analyses the sessions in which the mouse's performance did not exceed this criterion of increased velocity at cue onset.

5.3.14. Exclusion criteria for analyses

Not all recorded striatal dopamine transients reflected meaningful biological changes in dopamine, for instance, if fibres are placed incorrectly or dLight is poorly expressed in the local tissue. In the habituation dataset, dLight signals from a striatal region that had an SD of < 0.01 were excluded, as this reflected a lack of biological fluctuation in the dLight signal. In the RFR and GNG tasks, this was assessed by checking for a measurable dLight signal in response to the delivery a reward (8 μl). If the identified peak in the dLight signal was not more than 3 SD away from the baseline, the data from that striatal region of the animal was not used in further analyses.

In all analyses which required comparison of dLight data between regions in the same animal (e.g., within-subjects t-tests or trial-by-trial comparisons between data in each region), animals with meaningful signals in only one region were excluded. Animals were also excluded from analyses when the averaged signal consisted of < 20 transients, as the resulting averaged signal would be too noisy to pinpoint any pertinent characteristics.

Finally, in analyses requiring the identification of a specific characteristic of the dLight signal, animals were excluded when this characteristic could not be isolated. For example if, when trying to locate an event-related signal peak, the dLight signal from an individual region did not display this characteristic, then the identified value and latency of the peak would not be meaningful. In this example, an animal would be excluded from the analysis if the identified 'peak' within the time window for identification was less than 3 SD away from the dLight baseline. For each analysis in which animals are excluded for this reason, the number of animals excluded will be reported.

5.4. Results: dLight activity in DLS and VS during spontaneous movement

My first aim was to examine treadmill and dLight data from mice undergoing habituation to identify how the initiation and termination of spontaneous locomotion is reflected by changes in dopamine levels in the DLS and VS.

5.4.1. Treadmill and dLight data during initiation and termination of spontaneous locomotion

Treadmill and dLight data were extracted in a time window around the initiation and termination of locomotion. Figure 5.4 shows the full data from these mice ($n_{animals}$ = 9, F = 4) averaged across all bouts (n_{bouts} = 1,956). As is shown in Figure 5.4A and B, the averaged treadmill activity in the 2 s just prior to initiation and just after termination is close to 0, but then changes sharply at the onset of the critical event (vertical grey dashed line). At initiation, the average movement speed on the treadmill increases sharply (Figure 5.4A); at termination, the average movement speed drops sharply (Figure 5.4B). This shows that initiation and termination events were cleanly isolated.

Dopaminergic signals (shown as corrected dLight data) were also modulated at both initiation and termination of bouts in both DLS and VS. The initiation of each running bout is preceded by a decrease in the dLight signal in both regions, followed by a subsequent increase in the signal soon after. This pattern of activity shall henceforth be referred to as the 'peri-initiation trough'. After the termination of a running bout, the dLight signal in both regions increases transiently, which will henceforth be referred to as the 'post-termination peak'.

There were clear differences in the dynamics of the dopamine signals in each region around initiation and termination. While activity in the VS smoothly increased after the peri-initiation peak and reaches above baseline within roughly 1 second of initiation, the DLS signal fluctuates more sharply, with a small, sub-baseline post-initiation peak and then a more gradual increase to baseline within one or two seconds (Figure 5.4C). Just preceding the termination of running bouts, there is a smaller peak in the VS but not the DLS (Figure 5.4D).

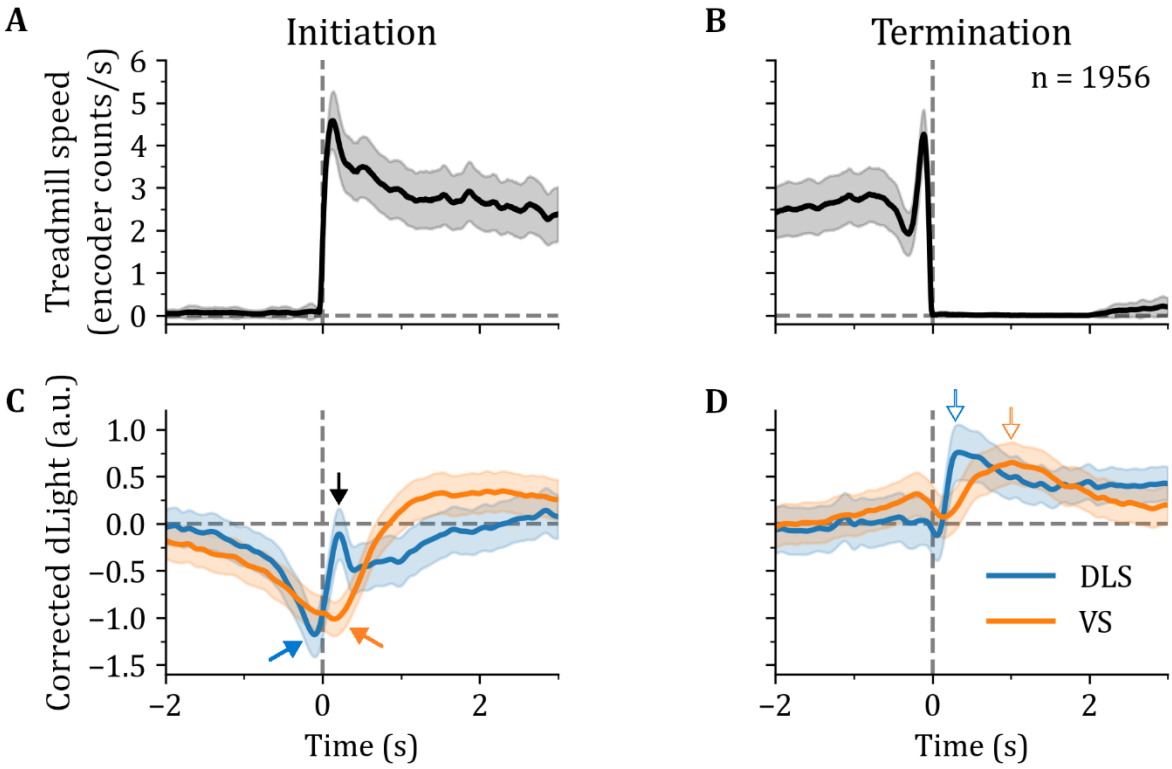


Figure 5.4: ***Mean (SEM) treadmill and dLight data across all locomotive bouts.*** *0 on the x axis represents the initiation (**A** and **C**) or the termination (**B** and **D**) of running bouts, demarcated by the vertical grey dashed line. The horizontal dashed line represents 0 on the y axis: stillness on the treadmill or the baseline of the dLight signal. The dLight data shown is the corrected signal (a.u.). Arrows in **C** and **D** highlight features of the signal for each region. Solid arrows indicate the peri-initiation trough. White arrows indicate the post-termination peak. The black arrow in **C** indicates the post-initiation peak. DLS: n = 8; VS: n = 9.*

Although both the peri-initiation trough and post-termination peak are present in both the DLS and VS, the timing of these events appears slower or delayed in the VS. To investigate this further, the timing of the trough in the dLight signal relative to bout initiation was compared between regions. Trough timings were extracted by separately averaging the dLight data from the DLS and VS of each mouse and finding the location of the minimum value relative to initiation in a -1.5 to 1.5 s window around initiation. One mouse was excluded from this analysis as the minimum of the peri-initiation trough in the VS could not be extracted. Overall, the data showed that the minimum of the average trough occurred *before* movement onset in the DLS (M = -127 ms, SD = 0.0435) but *after* movement onset in the VS (M = 78.0 ms, SD = 0.133; Figure 5.5A). A within subjects t-test showed a significant difference between regions ($t(6) = 3.22$, $p = .0182$).

To investigate whether the timing of the post-termination peak was significantly later in VS, the timing between bout termination and the signal peak were extracted as described above in a 3 s window after termination. One mouse was excluded from this analysis as the maximum of the post-termination peak in the DLS could not be extracted. Overall, the data showed that the average maximum of the post-termination peak with respect to bout termination was later in VS (M = 1.08 s, SD = 0.202) than in DLS (M = 0.518 s, SD = 0.168; Figure 5.5A). A within subjects t-test showed a significant difference between regions ($t(6) = 3.932$, $p = .008$).

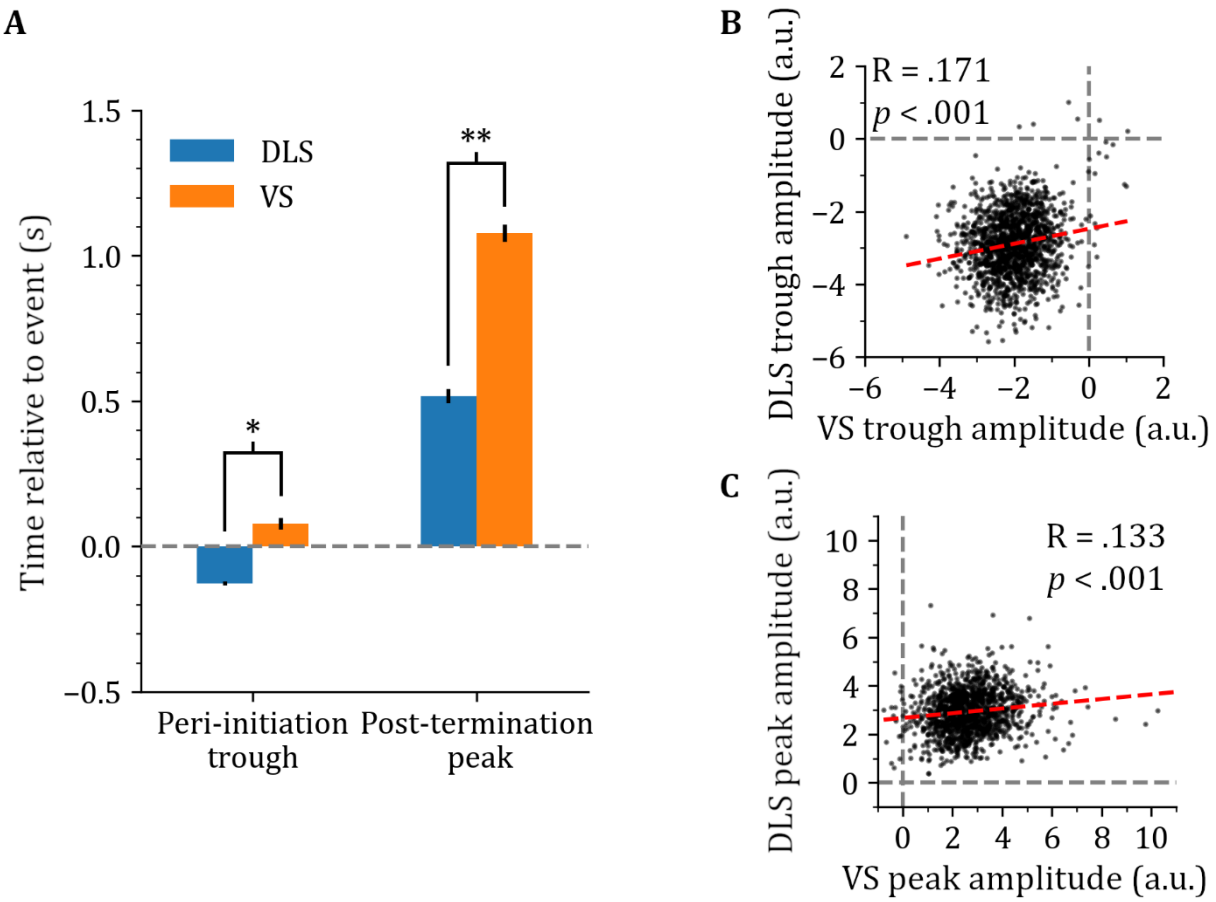


Figure 5.5: ***Comparisons and trial-by-trial correlations of peri-initiation troughs and post-termination peaks in DLS and VS. A****, Bar plot comparing the mean (SEM) timing of the peri-initiation trough and the post-termination peak compared to bout initiation and termination respectively. The time of the event (0) is demarcated with the grey dashed line. On average, the peri-initiation trough occurs prior to bout initiation in the DLS but after initiation in the VS. The post-termination peak occurs later in the VS than the DLS. The single asterisk indicates a significant difference between groups (repeated-measures t-test, n = 7) at p < .05; double asterisk is p < .001.* ***B & C****, Trial-by-trial correlations between the amplitudes of the peri-initiation trough (**B**) and the post-termination peak (**C**) in the DLS and VS. Pearson R ($n_{animals}$ = 7, n_{bouts} = 1477) and associated p-value are shown on each plot. The vertical and horizontal grey dashed lines demarcate 0 on the x and y axes respectively for each plot.*

Despite the average consistency in patterns of dopamine signals in the two regions, there was also a considerable amount of trial-by-trial variation. While some of this may be due to variance within the dLight signal itself, this could also reflect some trial-by-trial differences in the movement-associated dopamine activity. If this were the case, one might expect to see trial-by-trial correlation of the dLight signals collected from each region. To investigate this, the amplitude of the peri-initiation trough and the post-termination peak from each trial were extracted, again taking data from a -1.5 to 1.5 s window around initiation and a 3 s window after termination. To minimise the effect of differences in the signal-to-noise ratio between animals, the corrected dLight data were used for this analysis. The correlation between the amplitudes of the peri-initiation trough in DLS and VS are shown in Figure 5.5B. There was a significant positive correlation between the amplitudes of DLS signal and the VS signal at the peri-initiation trough (Pearson's Correlation; $R(1476) = .171$, $p < .001$). Similarly, there was a significant positive correlation between the amplitudes of DLS signal and the VS signal at the post-termination peak (Pearson's Correlation; $R(1323) = .133$, $p < .001$; Figure 5.5C). However, these correlation coefficients are both small, which suggests that any trial-by-trial correlations is these data would be fairly weak.

Taken together, the data show that dLight signals around the initiation and termination of spontaneous locomotion have dissociable dynamics between striatal regions. Although a trough around initiation (peri-initiation trough) and a peak after termination (post-termination peak) are present in dLight signals recorded from both regions, the timings of these events are later in VS dopamine signals. Furthermore, the

dLight signal in DLS shows rapid fluctuation after initiation (post-initiation peak) which is not present in VS.

5.4.2. The effect of bout speed and duration on striatal dopamine signals around the initiation of spontaneous locomotion

Spontaneous running bouts varied across several parameters which might plausibly affect the recorded dopamine signal in either region. Bouts occurred at a range of different average speeds (Figure 5.6A), which might reflect a varying vigour of movement. Duration of movement could be considered another aspect of vigour. These data are strongly skewed, with most bouts lasting no longer than 1 s (Figure 5.6B).

The inter-bout interval could also affect the dLight signals, not only because briefer gaps might reflect a generally heightened state of activity or motivation but also because dopamine levels may not yet have returned to baseline (as fluctuations in the dLight signal around initiation and termination can last several seconds). Again, the distribution of inter-bout intervals is strongly skewed but there is a great deal of variation in the data, with some gaps lasting minutes while others last seconds (Figure 5.6C).

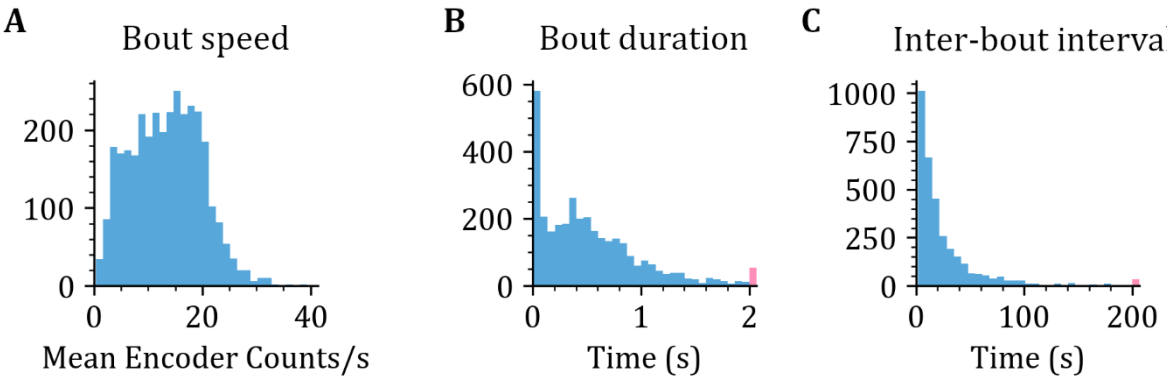


Figure 5.6: ***Histograms of the parameters for each spontaneous locomotive bout across all animals.*** *Pink bars on the far right of the plot represent all outliers for each plot (B and C; Duration > 2 s; Time between bouts > 200).*

To determine the effect of a bout's speed and duration on the accompanying dopamine signal around initiation, a separate time-based linear regression was performed on the dLight data measured from each striatal region at the onset of spontaneous movements. Four regressors were used in these models: bout speed, bout duration, pre-bout interval (time since termination of a previous bout) and bout number (chronological). A summary of this regression is shown in Figure 5.7. To break down the effect of each regressor on the dopamine signals, the real data (both treadmill data and dLight data for each region) were divided into quartiles for each regressor and plotted alongside the betas (see Table 5.1 for the quantiles used to divide each predictor).

The speed of each bout had minimal impact on the DLS data but predicted a significant increase in the VS signal ~2 s after initiation (Figure 5.7A). The difference between regions was not significant. The treadmill data from each quartile are cleanly separated without a major difference in the duration of subsequent bouts (Figure 5.7B). The data recorded in DLS looks nearly identical in each quartile (Figure 5.7C); by contrast, the increase in the VS signal seconds after initiation is lowest in Q1 (slowest bouts) and highest in Q4 (fastest bouts; Figure 5.7D), which follows the pattern predicted by the regression.

Table 5.1: Quantiles for each predictor of dLight signal around the initiation and termination of locomotive bouts.

Predictor	q25%	q50%	q75%	max
Speed (mean encoder counts/s)	7.42	12.7	17.9	39.4
Duration (s)	0.104	0.373	0.734	6.00
Inter-bout interval (s)	6.23	14.6	32.4	319

These quantiles were used to divide the data in quartiles in Figure 5.7 and Figure 5.8 (Q1 = 0-q25; Q2 = q25-q50; Q3 = q50-q75; Q4 = q75-max).

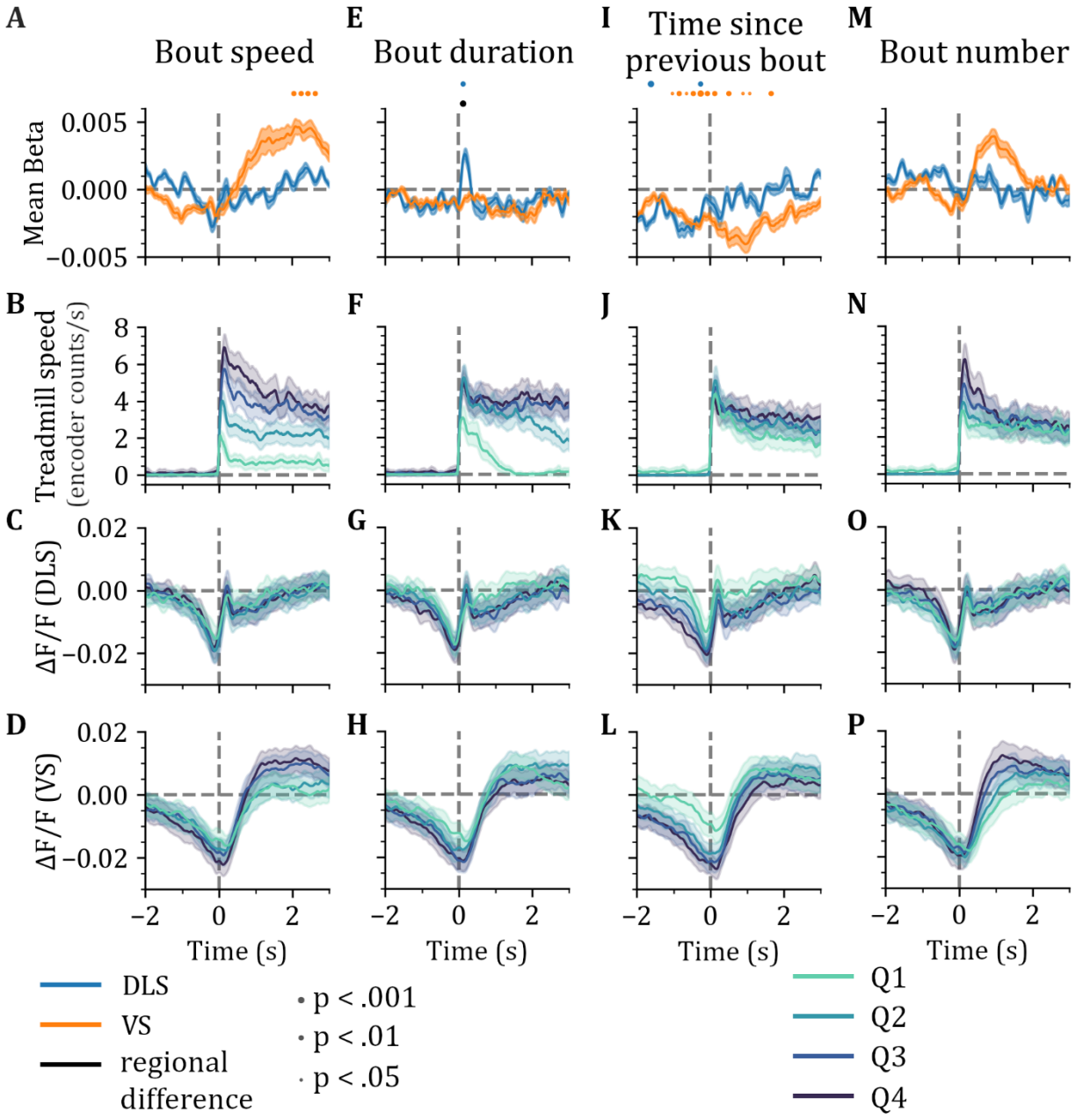


Figure 5.7: ***Breakdown of the timepoint-based regression by each of the four predictors (bout speed, bout duration, pre-bout interval and bout number) around bout initiation.*** *Each column of plots represents a single predictor:* ***A-D*** *speed;* ***E-H*** *duration;* ***I-L*** *pre-bout interval; and* ***M-P*** *bout number. At the top of each column, the timecourse of beta-values around bout initiation (time = 0) is shown in each region. Orange dots above the trace represent timepoints of significant deviation from 0 in the VS data; blue dots are the same but in the DLS data. Black dots indicate significant difference between regions. The size of the dot represents the degree of significance. Below each plot of beta values, the real data around initiation are shown, with treadmill data in the second row, DLS dLight signals in the third row and VS dLight signals in the fourth. These data are separated into quartiles for each predictor (Q1-Q4).*

Conversely, the duration of each bout had minimal impact on the VS data but predicted a change in the size of the post-initiation peak in the DLS. This was significant in the DLS, as well as significantly different between regions (Figure 5.7E). The shortest treadmill bouts (Q1) return to baseline within 2 s and have a slightly lower movement speed than other quartiles. Mean treadmill data in the second quartile is longer lasting and decreases before treadmill activity in the third or fourth quartiles (Figure 5.7F). Notably, the post-initiation peak in the DLS data is present in Q2-Q4 but not clearly distinct in Q1: the signal increases almost to baseline in Q2-Q4 but in Q1 alone does not descend afterwards (Figure 5.7G). Considering the brevity of the treadmill data in Q1 for duration (Figure 5.7G), it is possible that this is due to the post-termination peak (see Figure 5.4D) overlapping with this post-initiation peak, making the latter functionally undetectable during very short bouts. Data in VS, which does not have a post-initiation peak (Figure 5.4C), shows a similar shape of activity across all quartiles (Figure 5.7H).

Pre-bout interval was a significant predictor of decreased DLS signal prior to initiation, but only marginally at isolated timepoints (Figure 5.7I). The effect in VS was stronger, with a depression in the dopamine signal both preceding and following initiation. There was no significant difference between regions. Treadmill data was broadly very similar across quartiles, although tending slightly towards shorter durations at shorter pre-bout intervals (Figure 5.7J). The shape of the dLight signal in the DLS following initiation is broadly the same across quartiles, although the post-initiation peak in DLS is less distinct in Q1 specifically. There are, however, notable differences prior to initiation. In Q1, the dLight signal is elevated above baseline before it starts to decrease roughly 1 s before initiation. In Q2, the signal is at baseline 2 s before initiation and begins

to decrease then. In Q3 and Q4, the signal is already below baseline at 2 s pre-initiation (Figure 5.7K). Overall, this follows the pattern predicted by the regression for DLS. The VS shows a similar pattern pre-initiation, with the dLight signal in Q1 at baseline 2 s pre-initiation while Q2-Q4 are already below baseline at that point in time. The peri-initiation trough for Q1 VS dLight data is notably smaller than for the other three quartiles (Figure 5.7L).

Bout number was not found to be a significant predictor in either region, although the predicted beta values for VS tend to be elevated following initiation (Figure 5.7M). From the treadmill data, mice seemed to have a greater initial speed and/or run for longer later on in a session (Figure 5.7N). The overall shape of the dLight data around initiation in DLS is highly conserved across quartiles (Figure 5.7O). However, in VS there is a suggestion of a difference between quartiles in the amplitude and timing of the post-initiation peak, with higher and earlier peaks in later trials within a session (Figure 5.7P).

Taken together, the data show that the speed of an ensuing locomotive bout can to some extent be read out from the dopamine transients in the VS but not the DLS, with a higher VS signal after the initiation of faster bouts. At the shortest bouts, the post-initiation peak in DLS is not present, but the duration of an ensuing bout is otherwise not reflected by differences in the dLight signal.

5.4.3. The effect of bout speed and duration on striatal dopamine signals around termination of spontaneous locomotion

To determine the effect of a bout's speed and duration on the evoked dLight signal locomotive bout around termination, a time-based linear regression was performed on the dLight data measured from each striatal region at the conclusion of spontaneous movements. Four regressors were used in these models: bout speed, bout duration, post-bout interval (time until initiation of another bout) and bout number (chronological). Bout speed and duration were the primary regressors of interest. Post-bout interval and bout number were included as control variables. A summary of this regression is shown in Figure 5.8. As with the data in the previous section (section 5.4.2), the real data is shown in the plots below, divided into quartiles for each regressor.

The speed of each bout did not significantly impact the dLight signal around bout termination in either region, but there are still trends present in the beta timecourses. Specifically, the betas are higher at higher speeds, pre-termination for the DLS signal and peri-termination for the VS signal (Figure 5.8A). The treadmill data from each quartile are cleanly separated without a major difference in the duration of preceding bouts (Figure 5.8B). The dLight signal in DLS does vary slightly across quartiles just prior to termination: in Q3 and Q4, there is a slight elevation, while Q2 is at baseline and Q1 is below baseline (Figure 5.8C). Post-termination, the data looks consistent across quartiles, although Q1 has a lower post-termination peak (Figure 5.8C). In VS, the difference between Q1 and the other quartiles pre-termination is starker but follows the same trend as DLS: Q3 and Q4 have a clear pre-termination peak which is smaller in Q2 and below baseline in Q1 (Figure 5.8D).

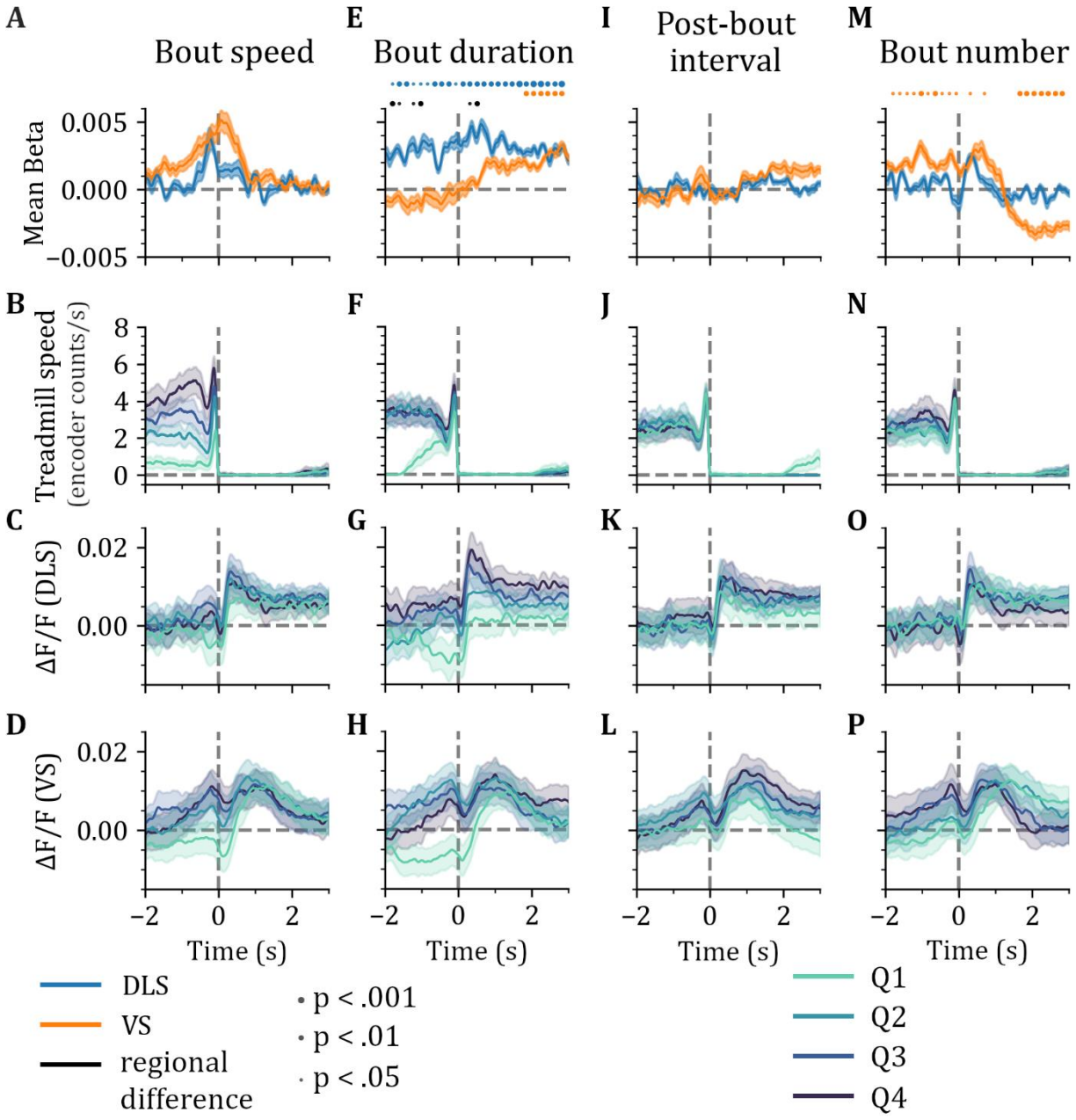


Figure 5.8: ***Breakdown of the timepoint-based regression by each of the four predictors (bout speed, bout duration, pre-bout interval and bout number) around bout termination.*** *Each column of plots represents a single predictor:* ***A-D*** *speed;* ***E-H*** *duration;* ***I-L*** *pre-bout interval; and* ***M-P*** *bout number. At the top of each column, the timecourse of beta-values around bout termination (time = 0) is shown in each region. Orange dots above the trace represent timepoints of significant deviation from 0 in the VS data; blue dots are the same but in the DLS data. Black dots indicate significant difference between regions. The size of the dot represents the degree of significance. Below each plot of beta values, the real data around initiation are shown, with treadmill data in the second row, DLS dLight signals in the third row and VS dLight signals in the fourth. These data are separated into quartiles for each predictor (Q1-Q4)***.**

Longer bouts were associated with significant elevation of the dLight signal across the whole timecourse in DLS and 2-3 s after termination in the VS (Figure 5.8E). There was a significant difference between regions prior to termination and immediately post-termination (Figure 5.8E). The shortest treadmill bouts (Q1) begin < 2 s prior to termination, return to baseline within 2 s and have a lower movement speed than other quartiles, which are all highly consistent within time window shown here (Figure 5.8F). As suggested by the timecourse of betas for duration of bouts (Figure 5.8E), longer bouts are associated with general elevation in the dLight signal in the DLS. While the shape of the signal around bout termination is well-conserved across all quartiles, in higher quartiles the signal is above baseline prior to termination and the post-termination peak is also higher; the reverse is true for Q1, with the post-termination peak only reaching baseline (Figure 5.8G). In the VS, the pattern is slightly more complex. Data from Q1 show the greatest divergence from the overall trend, with an absence of the pre-termination peak seen in the other quartiles and the overall signal staying below baseline until after termination. However, the pattern is reversed within Q2-Q4, with Q2 having a higher pre-termination peak than Q4. The post-termination peak is slightly lower in Q1 relative to other quartiles, while from 2 s after termination Q4 is slightly elevated relative to other quartiles (Figure 5.8H).

There was minimal deviation from 0 across the timecourse of betas for post-bout interval, with only a suggestion of a slight elevation in the VS dLight signal beginning 1 s after termination (Figure 5.8I). The treadmill data show that the pre-termination activity was highly consistent across quartiles. The earliest next bouts begin from 2 s after termination in Q1 (Figure 5.8J). The dLight data in DLS are also highly consistent across

quartiles (Figure 5.8K). In the VS, the post-termination activity seems to be slightly elevated in higher quartiles relative to lower ones, with Q1 dipping below baseline within 3 s of termination (Figure 5.8L).

Bout number was a significant predictor of VS signal, positively so before and just after termination and negatively so from 2 s after termination (Figure 5.8M). The treadmill data suggests there was a great deal of consistency between quartiles, with minimal differences in speed or duration within the time window shown (Figure 5.8N). DLS data look consistent across quartiles prior to termination (Figure 5.8O). In the VS, there does seem to be a trend wherein higher post-bout intervals are associated with elevation in the dLight signal prior to termination and slightly more extended signals after termination (Figure 5.8P).

Taken together, the data show that the duration of the preceding bout predicted an increase in the DLS dLight signal around termination and after termination in the VS, with a higher dLight signal around the around the termination of longer bouts . Bout speed was not a significant predictor of the dLight signals recorded from either striatal region.

5.5. Results: dLight activity in DLS and VS during reward contingent movement

Treadmill and dLight data from mice training in the RFR task were used to identify how the initiation and termination of reward-contingent locomotion is represented in the DLS and VS. In this results subsection, data from rewarded and non-rewarded trials are evaluated individually and then compared. I first discuss the dLight transients recorded during non-rewarded locomotive bouts and relate them to the dLight data from mice

initiating spontaneous locomotion during habituation, in which there is no potential expectation of a reward. I then discuss the dLight transients recorded during rewarded bouts and how they differ from non-rewarded bouts. Finally, I shall present the dLight response in both regions to reward delivery.

5.5.1. dLight transients during initiation and termination of non-rewarded bouts during RFR

Treadmill and dLight data for non-rewarded trials were extracted in a time window around initiation and termination of locomotion. Figure 5.9 shows the full data from these mice averaged across all bouts (n_{bouts} = 2775). As is shown in Figure 5.9A and B, the averaged treadmill activity in the 2 s just prior to initiation and just after termination is close to 0 and changes sharply at the onset of the critical event (vertical grey dashed line). At initiation, the average movement speed on the treadmill increases sharply (Figure 5.9A); at termination, the average movement speed drops sharply (Figure 5.9B). This shows that initiation and termination events were cleanly isolated.

Non-rewarded running bouts occurred at a diverse range of speeds (Figure 5.10A) and were generally brief, with the vast majority lasting under 1 s in duration (Figure 5.10B). On average, the speed of non-rewarded bouts appeared to be lower than that of spontaneous bouts during habituation (Figure 5.6A) and were of shorter duration (Figure 5.6B). This is not unexpected, as non-rewarded bouts in the RFR task are specifically those in which mice were not moving fast enough or for long enough to obtain a reward. The inter-bout intervals were wide-ranging, but the distribution was highly skewed towards intervals of less than 100 s (Figure 5.10C).

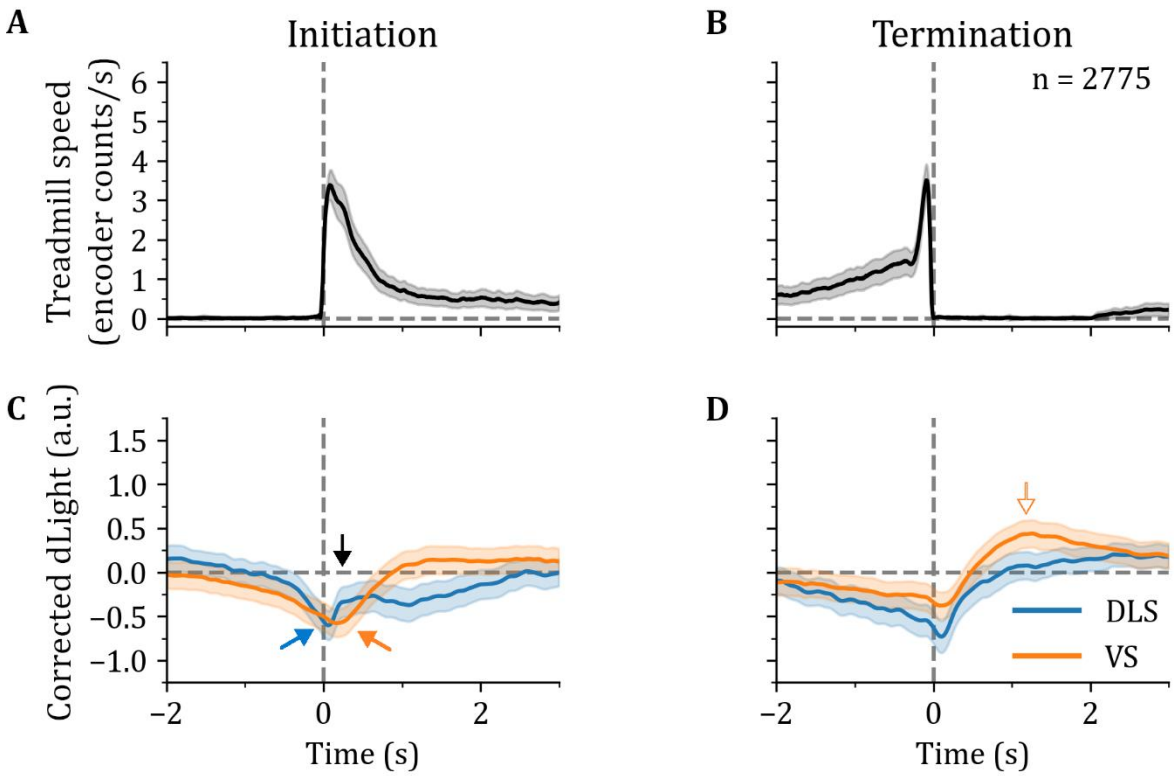


Figure 5.9: ***Mean (SEM) treadmill and dLight data across all non-rewarded running bouts in the run-for-reward (RFR) task.*** *0 on the x axis represents the initiation (**A** and **C**) or the termination (**B** and **D**) of running bouts, demarcated by the grey dashed line. The horizontal dashed line represents 0 on the y axis: stillness on the treadmill or the dLight baseline. The dLight data shown is the corrected signal (a.u.). Arrows in **C** and **D** highlight features of the signal for each region. Solid arrows indicate the peri-initiation trough. The white arrow indicates the post-termination peak in VS (the post-termination peak for DLS is not identifiable). The black arrow in **C** indicates the post-initiation peak. DLS: n = 15; VS: n = 15.*

The striatal dLight signals accompanying this treadmill activity look very similar to dLight signals during spontaneous movement (Figure 5.9C and D). The peri-initiation trough present in the habituation dataset (Figure 5.4C) are also present in non-rewarded trials during RFR (Figure 5.9C). However, the post-initiation peak in DLS during spontaneous movements (Figure 5.4C) is much less clearly defined in non-rewarded trials (Figure 5.9C), which notably was also true of the shortest spontaneous running bouts (Figure 5.7E).

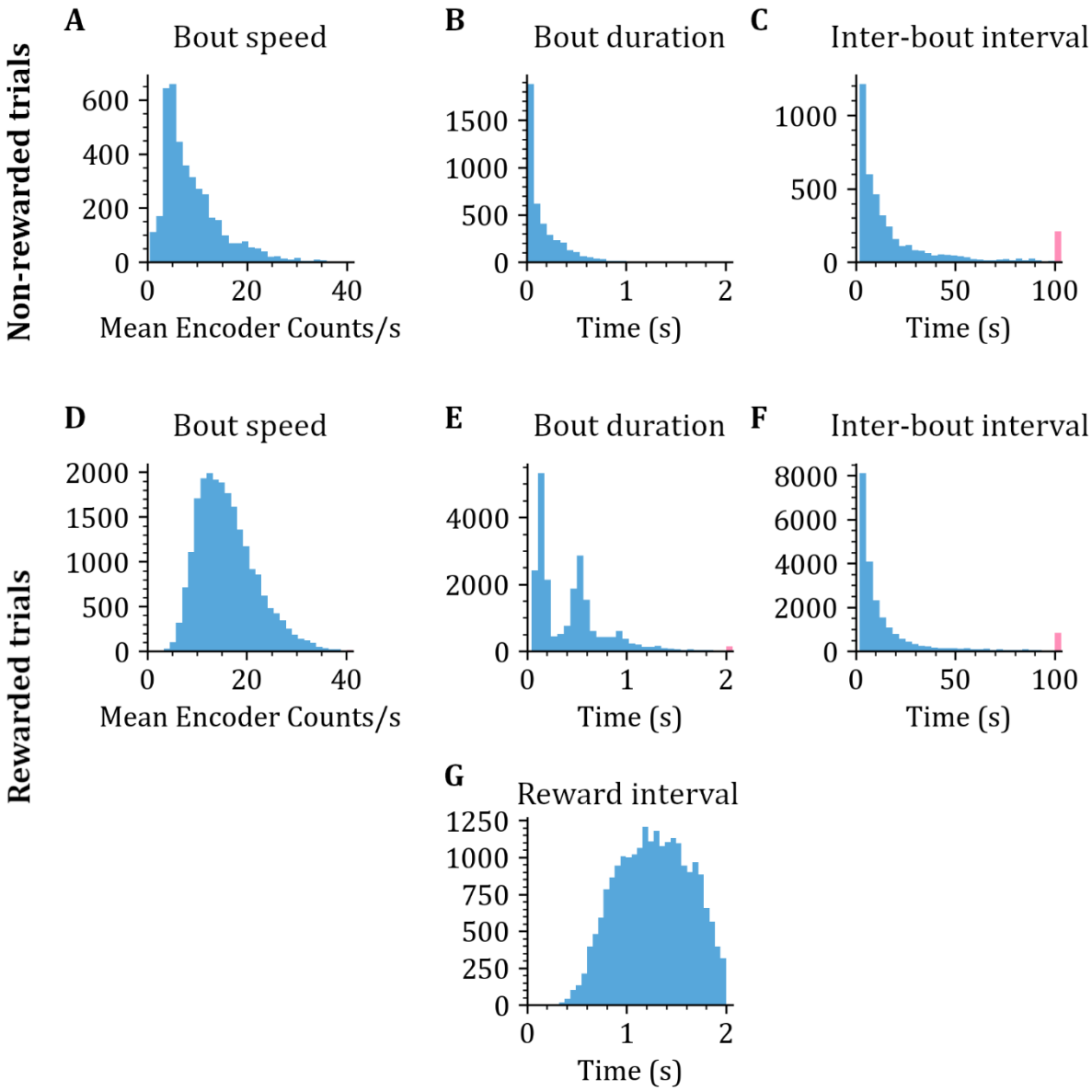


Figure 5.10: ***Histograms showing the distribution of running bout parameters (speed, duration, inter-bout interval and time to reward) for non-rewarded and rewarded bouts during RFR. A-C*** *show locomotive parameters from non-rewarded trials;* ***D-G*** *from rewarded trials. Pink bars on the far right of the plot represent all outliers for each plot (C, E and F; Duration > 2 s; Inter-bout interval > 200).*

However, the dLight signals around non-rewarded bout termination in the RFR task look noticeably distinct from dLight signals accompanying the termination of spontaneous locomotion, with the averaged dLight signal decreasing prior to termination (Figure 5.9D) rather than staying at or above baseline, as they do in the habituation data (Figure 5.4D).

Furthermore, there is a clear post-termination peak in both striatal regions during spontaneous movements, but here the post-termination peak is only clear in the VS, not in the DLS. This may be an effect of the reward contingency. In these trials, mice initiate a movement expecting a reward; however, when no reward is delivered this may result in a negative prediction error or encoding of movement value.

5.5.2. dLight transients during initiation and termination of rewarded bouts during RFR

Treadmill and dLight data for rewarded trials were extracted in a time window around bout initiation and termination. Figure 5.11 shows the full data from these mice averaged across all bouts (n_{bouts} = 13,024). The averaged treadmill data shown in Figure 5.11A and B show that bout initiation and termination events were cleanly isolated. Predictably, rewarded bouts were generally at higher speeds (Figure 5.10D; Figure 5.11A) than non-rewarded bouts (Figure 5.10A; to be expected, since speed is criterion to obtaining a reward in this task) and at similar speeds to spontaneous bouts (Figure 5.6A). All bout durations were under 2 s, again due to the selection criteria of what is considered a 'rewarded bout' (see section 5.3.9). Interestingly, the distribution of rewarded bout durations is bimodal, with a peak at just under 0.25 s and a second, smaller peak at ~0.5 s (Figure 5.10E). The distribution of inter-bout-intervals, as with both non-rewarded bouts (Figure 5.10C) and spontaneous bouts (Figure 5.6C), was diverse but highly skewed. For rewarded bouts, the reward interval could also be calculated. All reward intervals (time between bout initiation and reward delivery) were below 2 s and were distributed roughly symmetrically (Figure 5.10G). Of note is that the shape of the distribution of

reward intervals does not match the shape of the distribution of bout durations, suggesting that there is variance in the intervals been termination and reward.

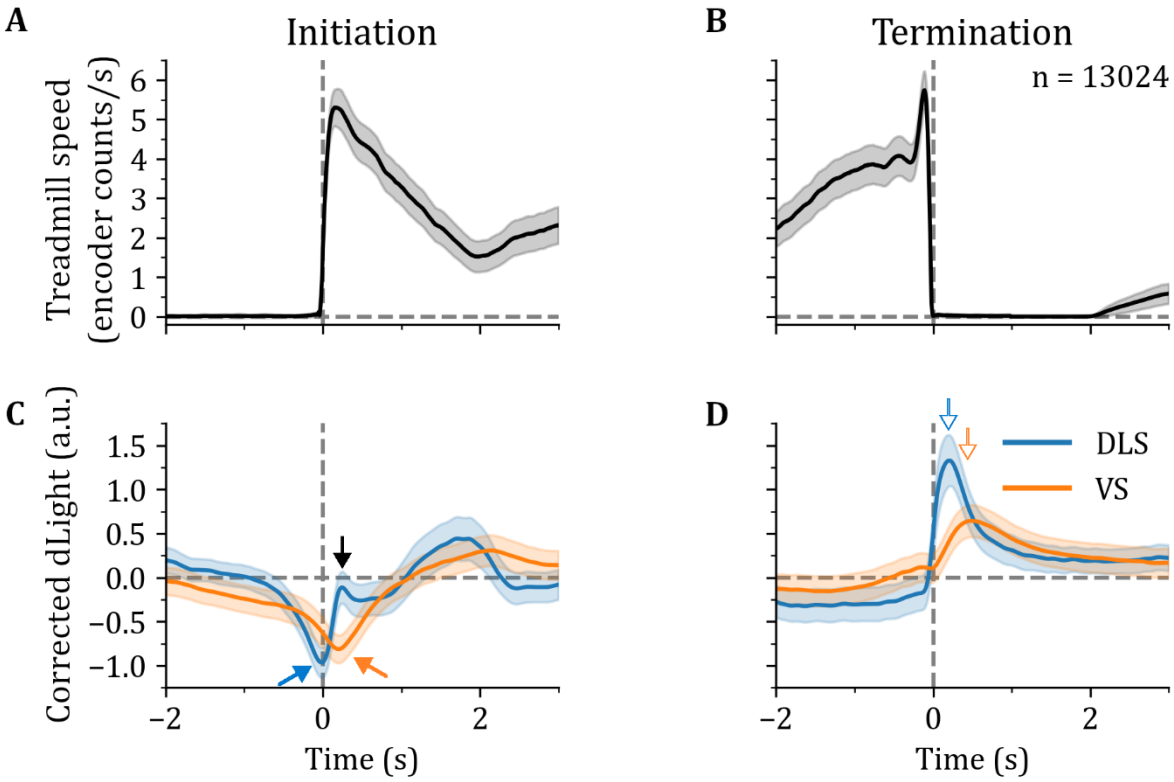


Figure 5.11: ***Mean (SEM) treadmill and dLight data across all rewarded running bouts in the run-for-reward (RFR) task.*** *0 on the x axis represents the initiation (**A** and **C**) or the termination (**B** and **D**) of running bouts, demarcated by the grey dashed line. The horizontal dashed line represents 0 on the y axis: stillness on the treadmill or the dLight baseline. The dLight data shown is the corrected signal (a.u.). Arrows in **C** and **D** highlight features of the signal for each region. Solid arrows indicate the peri-initiation trough. White arrows indicate the post-termination peak/reward peak. The black arrow in **C** indicates the post-initiation peak. DLS: n = 15; VS: n = 15.*

The striatal dLight signals around the initiation of rewarded running bouts looks very similar to dLight signals during spontaneous movement (Figure 5.9C and D), with a clear peri-initiation trough and post-initiation peak in the DLS (Figure 5.11C; c.f. Figure 5.9C); however, there is a transient increase in the dLight signal of both striatal regions ~1-2 s after bout initiation. The dLight signal following bout termination (Figure 5.11D) also appears much higher than the post-termination peak seen at the termination of spontaneous locomotive bouts (Figure 5.4D). Given that most rewards are delivered between 1 and 2 s after the initiation of movement (Figure 5.10G), the post-initiation elevation of the dLight signal and the higher 'post-termination peak' likely represent the consumption of a reward. As such, the dopamine signal following termination is most likely a conflation of the post-termination peak and a 'reward peak'. The depression of the dLight signal prior to termination (Figure 5.11D) may reflect the decrease in the dopamine signal around the initiation of locomotion (e.g., Figure 5.11C).

5.5.3. Regional differences in the latencies of peri-initiation troughs during RFR

As was previously shown (Figure 5.5A), the latency of the peri-initiation trough during spontaneous movements differs between striatal regions, with the trough occurring before bout initiation in the DLS but after initiation in the VS. To test whether this was also true of running bouts during the RFR task, the latencies of the trough to initiation was compared between regions for both non-rewarded and rewarded bouts. Latencies were extracted by separately averaging the dLight signals from the DLS and VS of each mouse and finding the location of the minima relative in a -1.5 to 1.5 s window

around initiation. 3 mice were excluded from this analysis as the location of the trough could not be accurately identified.

Within-subjects *t*-tests were used to compare the latency of the peri-initiation trough between regions, separately for rewarded and non-rewarded bouts. For non-rewarded bouts, the minimum of the average trough preceded bout initiation in the DLS (M = -70.3 ms, SD = 0.0866) but followed bout initiation in the VS (M = 185 ms, SD = 0.0642; Figure 5.12A). The regional difference in the timing of the peri-initiation trough in dLight signals was significant ($t(6) = 5.46$, $p = .001$). In rewarded trials, the same patten of pre-initiation DLS troughs (M = -52.3 ms, SD = 0.0594) and post-initiation VS troughs (M = 182 ms, SD = 0.0751) was again observed (Figure 5.12B) and was also found to be significant ($t(9) = 8.52$, $p < .001$). Overall, the latencies of the peri-initiation trough in both regions are extremely similar across movements with different reward contingencies.

The same analyses were not performed on the post-termination peak. In dLight signals recorded during non-rewarded trials in RFR, the post-termination peak was not identifiable in DLS (Figure 5.9D). As discussed above, the 'post-termination peak' in dLight signals recorded during rewarded trials in RFR was most likely a superposition of the post-termination peak and a reward peak, potentially confounding analyses of the timings of this event.

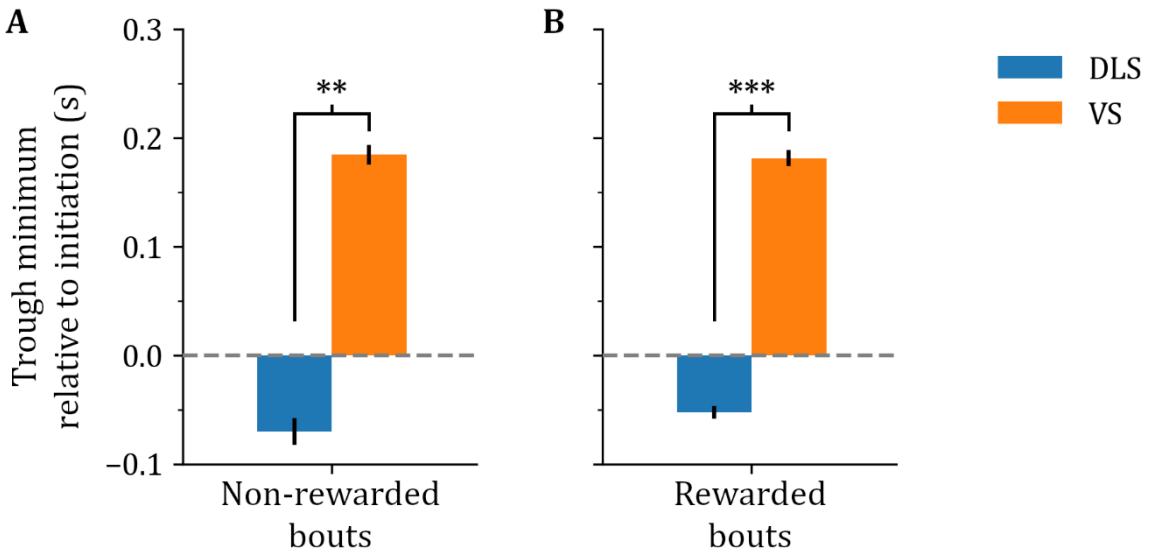


Figure 5.12: ***Comparisons of the latencies of peri-initiation troughs between DLS and VS.*** *Bar plots comparing the mean (SEM) timing of the peri-initiation trough relative to the initiation of non-rewarded and rewarded bouts. The time of the event (0) is demarcated with the grey dashed line. For both rewarded and non-rewarded trials, the peri-initiation trough occurs prior to bout initiation in the DLS but after bout initiation in the VS. ** p < .01; *** p < .001 (within-subjects t-test, non-rewarded bouts: n = 7; rewarded bouts: n = 10).*

5.5.4. The effect of reward contingency on dLight signals in DLS and VS around initiation and termination of running bouts

dLight transients were recorded accompanying running bouts with 3 different reward contingencies: no reward contingency for spontaneous movements (habituation dataset), failed reward contingency (non-rewarded running bouts in RFR) and successful reward contingency (rewarded running bouts in RFR). The effect of reward contingency on the dLight signals around movement initiation and termination was evaluated using a series of timepoint-based regressions (see section 5.3.12 for full details). Each regression was performed separately for dLight signals from each pair of groups (3 pairs: rewarded vs. non-rewarded; rewarded vs. spontaneous; non-rewarded vs. spontaneous), and for each locomotion event (initiation or termination). Each regression used only data from mice in both the habituation and RFR datasets and with meaningful striatal dLight recordings

from both regions. Although reward contingency was the regressor of interest, three other regressors were included in each model, expressed as quartiles: bout speed, bout duration and inter-bout interval (pre-bout interval for dLight data around initiation; post-bout interval for dLight data around termination).

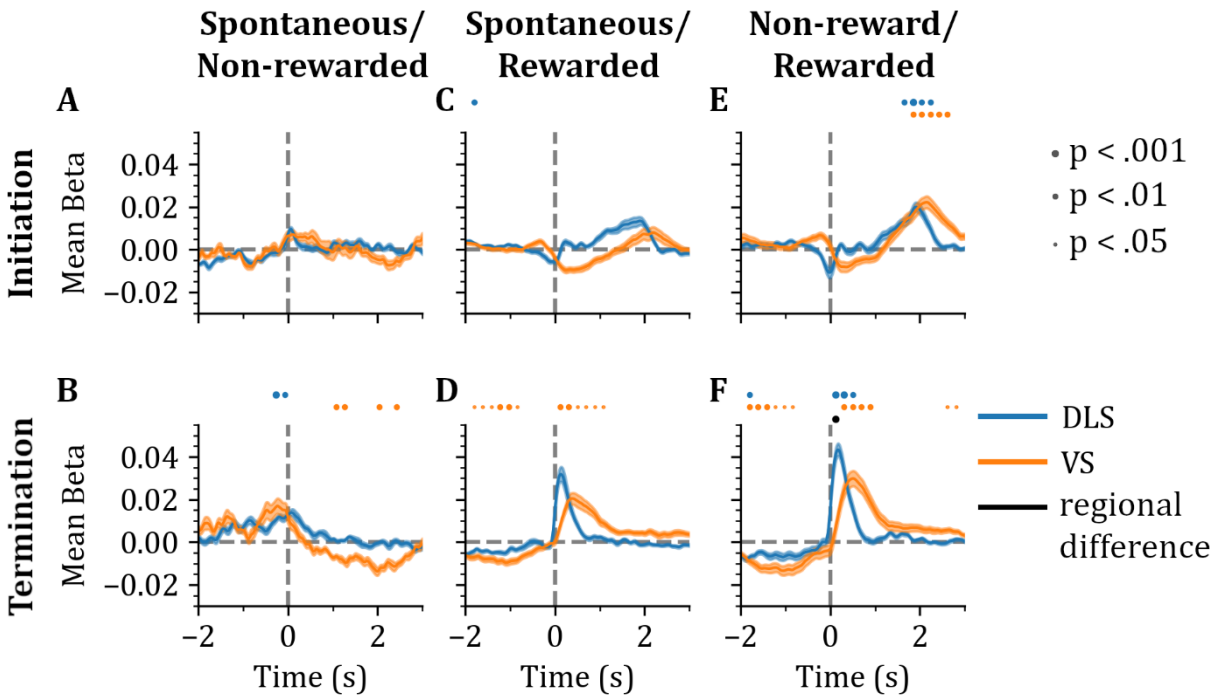


Figure 5.13: ***The effect of reward contingency on dLight signals recorded from the DLS and VS around the initiation and termination of locomotion.*** *Timepoint-based regressions were performed on dLight data around spontaneous, rewarded, and non-rewarded locomotive bouts. Three separate regressions were performed around on dLight signals around both initiation and termination using pairs of dLight data from each of these groups: spontaneous bouts and non-rewarded bouts (**A** and **B**), spontaneous and rewarded bouts (**C** and **D**) and non-rewarded and rewarded bouts (**E** and **F**). Each regression model also contained four other predictors: bout speed, bout duration, inter-bout interval (pre-bout interval for initiation; post-bout interval for termination) not shown here. The results for the regressions performed on the dLight signals around initiation are shown on the top row (**A**, **C** & **E**); termination on the bottom row (**B**, **D** &**F**). For each regression, the mean (SEM) timecourse of beta values is shown for each region. Orange dots above the trace represent timepoints of significant deviation from 0 in the VS data; blue dots are the same but in the DLS data. Black dots indicate significant difference between regions. The size of the dot represents the degree of significance.*

For the pair of non-rewarded vs. spontaneous bouts, positive betas represent a higher dLight signal during spontaneous compared to non-rewarded RFR locomotion. Both the decrease in dopamine signal around bout initiation and a transient increase following termination were present in both cohorts, but the dopamine signal in both regions appeared lower prior to termination during non-rewarded bouts (Figure 5.9C, D) compared to spontaneous bouts (Figure 5.4C, D). Reward contingency did not significantly affect dLight signals around bout initiation (Figure 5.13A). In the DLS, the regression predicted a higher dLight signal prior to termination of spontaneous movements relative to non-rewarded movements; additionally, the model predicted a briefly higher dLight signal in the DLS prior to the initiation of spontaneous as opposed to non-rewarded locomotion and a lower dLight signal in the VS following the termination of spontaneous movements compared to non-rewarded movements (Figure 5.13B).

For the pair of rewarded vs. spontaneous bouts, positive betas represent a higher dLight signal during rewarded compared to spontaneous bouts. dLight activity from both regions preceding initiation and termination of rewarded bouts is again broadly similar to that seen during spontaneous bouts (see also Figure 5.4C, D; Figure 5.11C, D). Indeed, reward contingency did not significantly affect dLight signals around initiation (Figure 5.13C), except for a slightly elevated signal in the DLS ~2 s prior to initiation of rewarded movements. At termination of rewarded movements, the model predicted rapid transient elevation of the dLight signal in the VS, which likely represents the added effect of reward delivery. While this pattern was present in the DLS signal, it was not found to be significant. The model also predicted a significant depression in the dLight signal prior to termination of rewarded locomotion in the VS (Figure 5.13D).

For the pair of rewarded vs. non-rewarded movements, positive betas represent a higher dLight signal during rewarded compared to non-rewarded bouts. Again, the broad pattern of the dLight signal around bout initiation was similar, but the post-termination peak was noticeably larger in rewarded trials (see also Figure 5.9C, D; Figure 5.11C, D). Reward outcome (rewarded or non-rewarded) was not a significant predictor of dLight activity around initiation except for ~2 s after initiation in both regions, which likely represents reward delivery (Figure 5.13E). At termination, the same pattern of activity can be observed: a sharp increase in the dLight signal after termination of rewarded bouts is apparent in both regions (again likely representing reward delivery), preceded by a pre-termination depression which is stronger in the VS (Figure 5.13F), possibly representing the initiation of bouts.

5.5.5. Representation of reward in DLS and VS dLight signals

To evaluate the representation of reward delivery in the DLS and VS during the RFR task, dLight transients were extracted around the timepoint of reward delivery ($n_{animals}$ = 17; $n_{rewards}$ = 25,227). These data are shown in Figure 5.14A and B. The treadmill activity is highest just prior to reward delivery and decreases sharply at reward delivery, suggesting that mice are reducing their movement when a reward is delivered (in order to drink). Notably, the signal does not reduce to 0, meaning that sometimes mice are running continually (albeit slowly) throughout this period (Figure 5.14A).

In the accompanying dopamine signal (Figure 5.14B), there is a clear reward peak in both regions just after reward delivery. The signal prior to reward delivery is depressed slightly below baseline throughout the 2 s pre-reward time window shown here. Judging

from the ramping up of treadmill activity during this period, this may reflect the depression in the dopamine signal around the initiation of running bouts. Strikingly, the amplitude of the reward peak is greater in the DLS by a factor of ~5 despite the data shown here being corrected such that the mean absolute dLight signal in each region is 1 across all initiation, termination, and reward events.

The reward peak in the DLS dLight signal is considerably sharper than in the VS signal and appears to occur sooner after reward. To test whether this difference between regions in the latency of the reward peak was significant, DLS and VS dLight signals were extracted in a 3 s window after reward delivery and averaged for each mouse. The reward peak for each animal was defined as the maximum of this averaged signal in each striatal region within this 3 s window. As is shown in Figure 5.14C, the latency to DLS (M = 262 ms, SD = 0.161) reward peak is consistently shorter than in the VS (M = 677 ms, SD = 0.293). A repeated measures t-test found a significant difference between striatal regions ($n_{animals}$ = 13; $t(12) = 5.44$, $p < .001$).

If reward-associated dLight activity across striatal regions is related, one might expect to see trial-by-trial correlations between the amplitudes of the reward peaks in DLS and VS in response to the same reward. To evaluate this, the amplitude of the reward peak at each reward delivery was extracted from the corrected dLight signal in each striatal region. The data are shown in the scatter plot in Figure 5.14D. There was considerable variation in the amplitude of reward peaks, including some 'peaks' which were below 0 (potentially due to fluctuation in the baseline), although the majority of data points are above baseline. A Pearson's correlation found a significant positive correlation between the amplitudes of reward peaks in both DLS and VS ($n_{animals}$ = 13; R(17,201) = .376, $p <$

.001). However, R value is relatively small, and thus this relationship should be interpreted with caution, as significance may merely reflect the large sample.

Taken together, these data suggest that reward contingency does not necessarily affect the dLight signals around the initiation of locomotion: the dLight signals of mice initiating rewarded locomotion were not significantly different to those of mice initiating spontaneous locomotion, except for presence of a reward peak in rewarded trials. Around the termination of bouts, there was some suggestion that non-rewarded locomotion results in different dLight signals when compared to spontaneous locomotion is associated with differences in the dLight signal (briefly lower DLS signals prior to termination and elevated VS signals after termination). Prior to the termination of rewarded bouts, the dLight signal is below baseline in both DLS and VS, which may represent the initiation of locomotion.

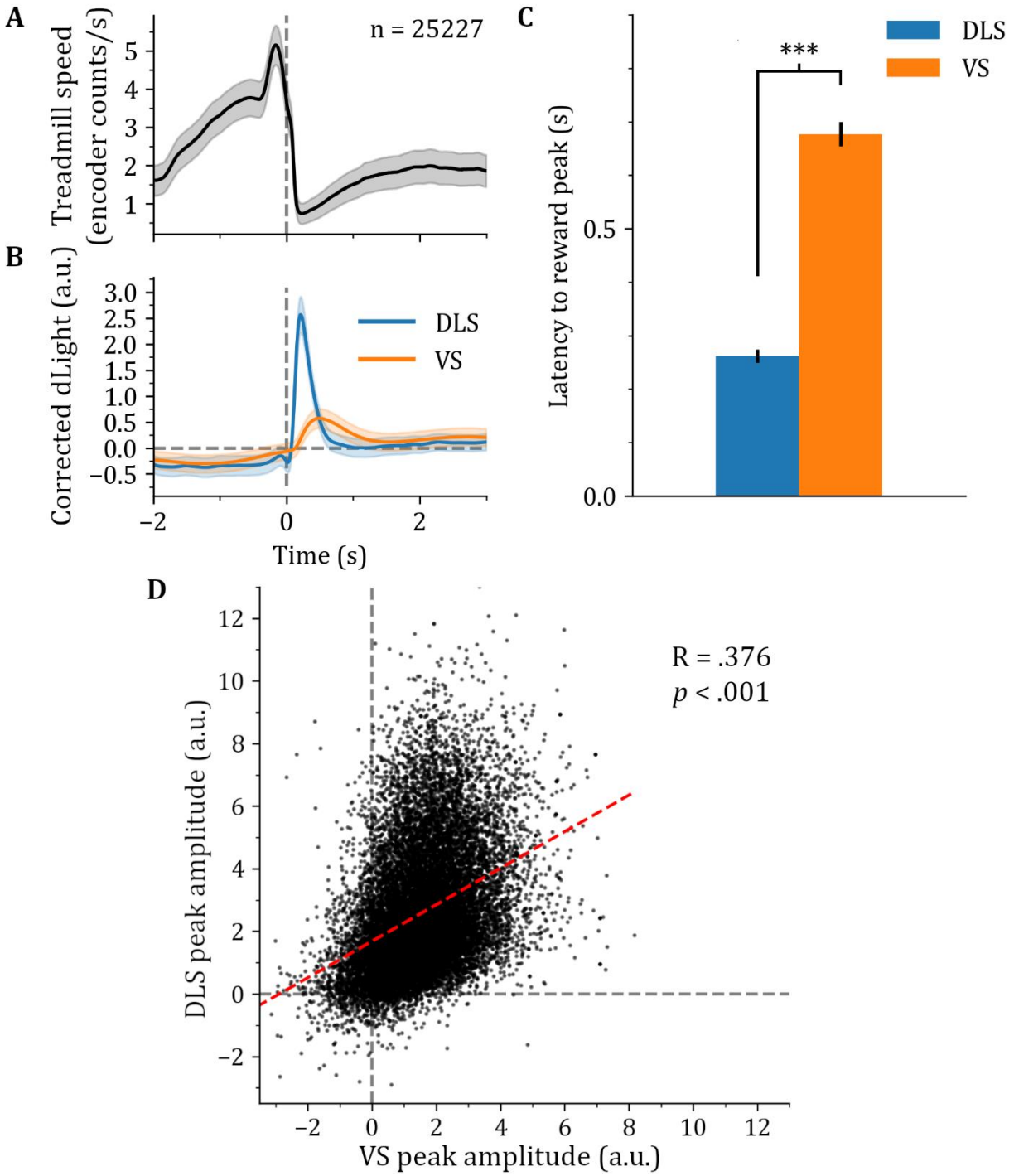


Figure 5.14: ***Evaluating reward peaks after delivery of rewards in the RFR task. A****, Mean (SEM) treadmill data around reward delivery (timepoint 0).* ***B****, Mean (SEM) corrected dLight transients collected from the DLS and VS around reward delivery (timepoint 0). The reward peak in DLS is sharper and at shorter latency than in VS.* ***C****, Bar plot showing the mean (SEM) latency of the reward peak in each striatal region. *** p < .001 (repeated-measures t-test).* ***D****, Trial-by-trial correlations of amplitude of reward peaks in the DLS and VS ($n_{animals}$ = 13; n_{bouts} = 18,299). The red dashed line is the line of best fit. For A, B and D, grey dashed vertical and horizontal lines represent 0 on the x and y axes respectively.*

5.6. Results: Response to instrumental cues in DLS and VS

Treadmill and dLight data from mice training in the GNG task were used to identify how instrumental reward cues are represented in the DLS and VS. Unfortunately, due to time constraints and poor training outcomes, only 3 mice reached the early stages of training involving the No-Go cue. Because of this, only data related to the Go cue will be presented in this section.

Using the criteria outlined in section 5.3.13, 7/16 mice that began training on the GNG task were identified as non-learners. The remaining cohort of 9 mice all showed evidence of cue-learning over the course of training. Data from the VS of two mice were excluded as they did not show a clear reward response (see section 5.3.14), but dLight data recorded from the DLS of these mice were still included in the analysis.

Even within this cohort of cue-learner mice, there was considerable variation in both their behaviour and the accompanying dLight signals. Treadmill and dLight data from 2 mice are shown in Figure 5.15. While both animals showed a clear increase in movement speed at the onset of the cue, the behaviour of animal 1 was less stereotyped than animal 2. movement speed was relatively slow on average, and the latency between cue and reward in animal 1 was highly variable (Figure 5.15A). By contrast, animal 2 had relatively high movement speed after cue onset and consistently short latency between cue and reward (Figure 5.15B). Strikingly, the dLight data from these two mice also shows a very different pattern of activity. The dopamine signal recorded from both regions of animal 1 shows a clear decrease in activity at cue onset (Figure 5.15C). The dopamine signal recorded from animal 2 shows the opposite pattern: a biregional increase in the dLight signal at cue onset (Figure 5.15D).

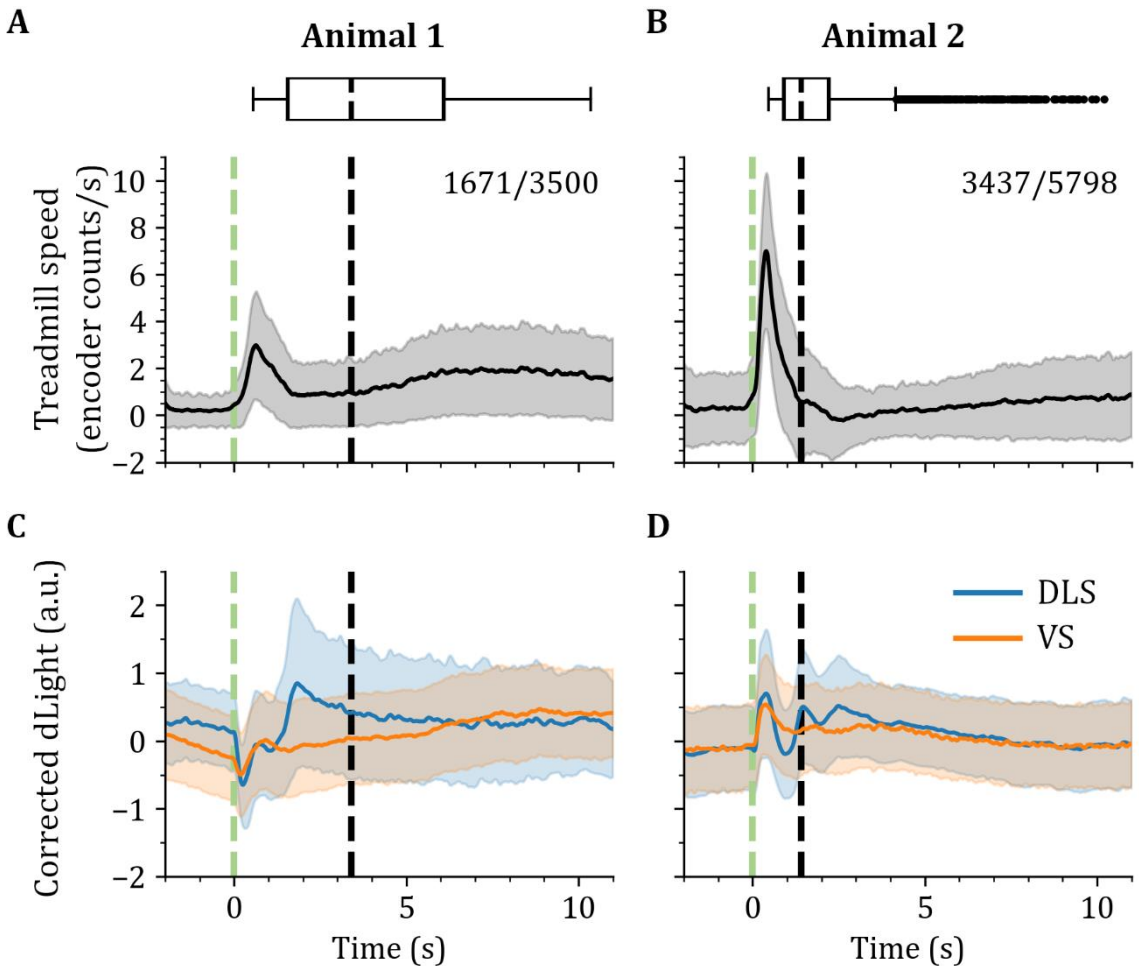


Figure 5.15: ***Mean (SD) treadmill and dLight data from rewarded GO trials of individual animals performing the GNG task****. **A** and **B** are treadmill data from an individual animal; **C** and **D** are the accompanying dopamine signals. The onset of the GO cue (timepoint 0) is marked with a vertical green dashed line. The median timepoint of reward delivery (for rewarded trials only) is shown with the black dashed line. Above both the treadmill and dLight data is a box plot showing the distribution of reward delivery times. The success rate (proportion of rewarded trials) is also reported for each animal.*

Variability in the dopaminergic cue response could reflect corresponding variability in the animals' behaviour. To investigate this, animals were divided based on their performance in the GNG task. Strong learners (n = 5) were mice with a success rate on Go trials across all sessions of > 50%; weak learners (n = 3) were those with a success rate of < 50%. While the treadmill activity on correct trials in both groups was similar (Figure 5.16A, B), the dLight signal at cue onset was clearly distinct: dLight signals in weak

learners decreased after cue onset (a 'negative cue response'; Figure 5.16C) while dLight signals in strong learners increased after cue onset (a 'positive cue response'; Figure 5.16D). To evaluate this statistically, the minima or maxima of the cue-related trough or peak were located for each animal, calculated as the change in value from a 1s pre-cue baseline. These data are shown in Figure 5.17A. For weak learners, the average cue response was negative in both DLS (*Mdn* = -0.839) and VS (*Mdn* = -0.453). For strong learners, the average cue response was instead positive in both DLS (*Mdn* = 0.670) and VS (*Mdn* = 0.416). For dLight data collected from each striatal region, a Mann-Whitney *U* test was performed comparing the value of the cue response between groups. There was a significant difference between groups in the DLS ($U = 0$, $p = .0184$), but in the VS the difference between groups was not significant ($U = 1$, $p = 0.124$).

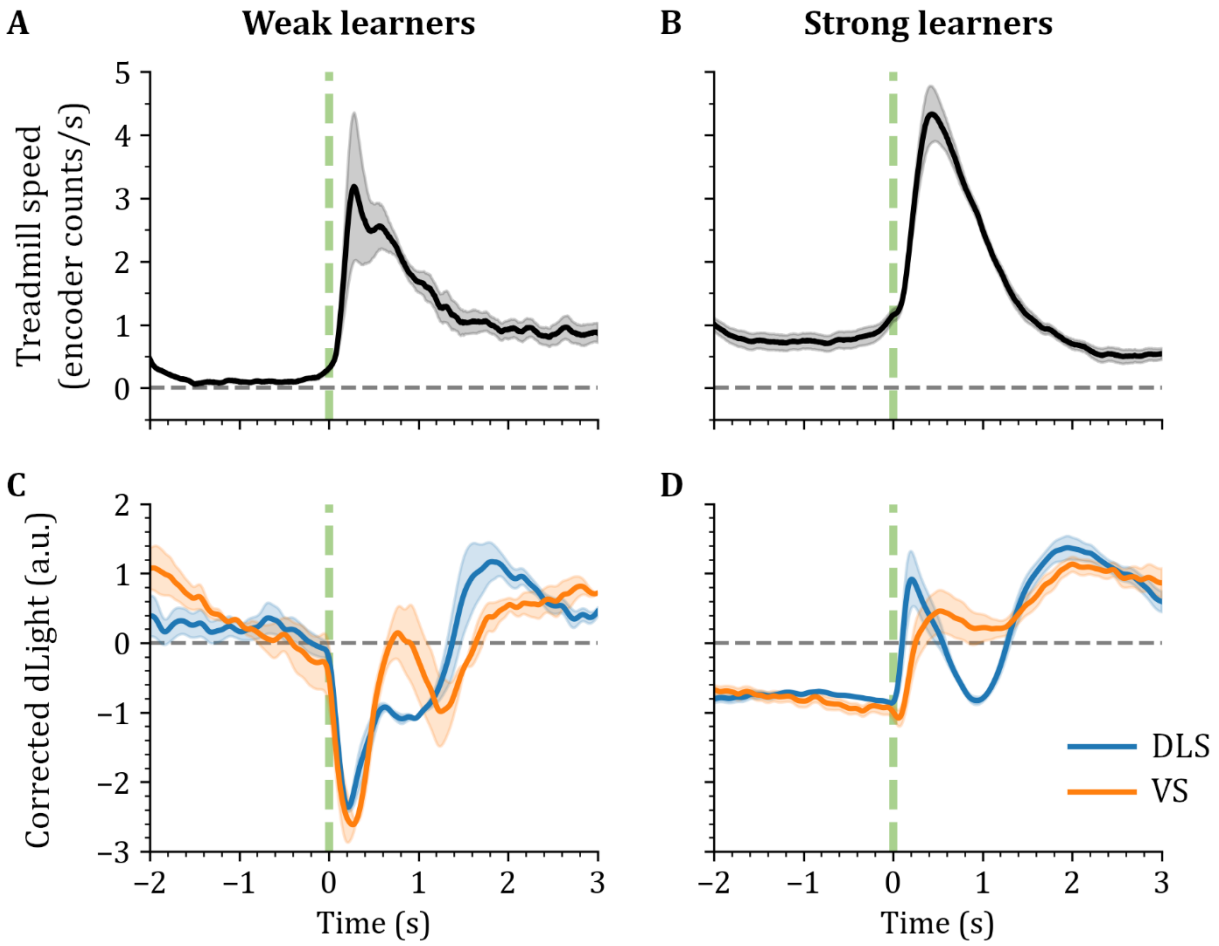


Figure 5.16: ***Mean (SEM) treadmill and dLight data from rewarded GO trials of weak and strong learners performing the GNG task****.* ***A*** *and* ***B*** *are the average treadmill data from each group;* ***C*** *and* ***D*** *are the accompanying dLight signals. The onset of the GO cue (timepoint 0) is marked with a vertical green dashed line. 0 on the y-axis (stillness on the treadmill or baseline dLight) is marked with the horizontal grey dashed line.*

If the valency of the cue response in the dLight signal reflects performance, one might also expect that sessions in which mice were more successful would have higher cue responses. To test this, the minima/maxima of the cue response was again calculated, this time for each session, and compared against the success rate within that same session. These data are shown in Figure 5.17B. Pearson's correlations for each region did not find a significant relationship between cue response and success rate in either the DLS ($R(235) = .0982$, $p = .132$) or the VS ($R(198) = .130$, $p = .0665$).

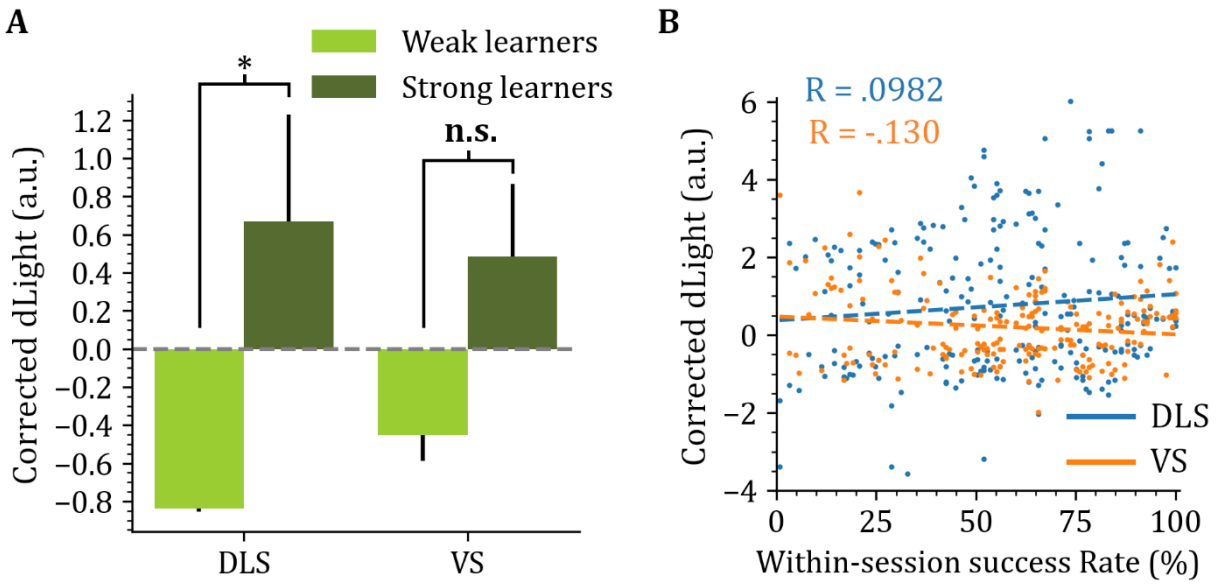


Figure 5.17: ***Cue response across cue-learner animals in rewarded GNG trials****.* ***A****, Bar plot showing the median (IQR) value of the cue response in each region. Mann-Whitney U-tests were performed to compare cue response between weak learners and strong learners (* p < .05). The horizontal grey dashed line demarcates the baseline dLight signal.* ***B****, Scatter plot comparing the value of the cue response within a session with the success rate for that session. The line of best fit for each region is shown with the coloured dashed lines. Pearson R values for each striatal region are also reported.*

Mice show a sharp decrease in movement speed just after reward delivery (Figure 5.18A), which likely reflects the mice stopping to drink. There is a clear reward peak in both striatal regions immediately after reward delivery (Figure 5.18B). The reward peak in the DLS dLight signal during RFR occurs at a shorter latency than in the VS (see Figure 5.14C). To test whether this was also true of cue learners in the GNG task, DLS and VS dLight signals were extracted in a 3 s window after reward delivery and averaged for each mouse. The reward peak for each animal was defined as the maximum of this averaged signal in each striatal region. As is shown in Figure 5.18C, the latency to the DLS reward peak (M = 231 ms, SD = 0.0492) is consistently shorter than in the VS (M = 679 ms, SD = 0.587). A repeated measures t-test found a significant difference between striatal regions ($t(5) = 11.1$, $p < .001$).

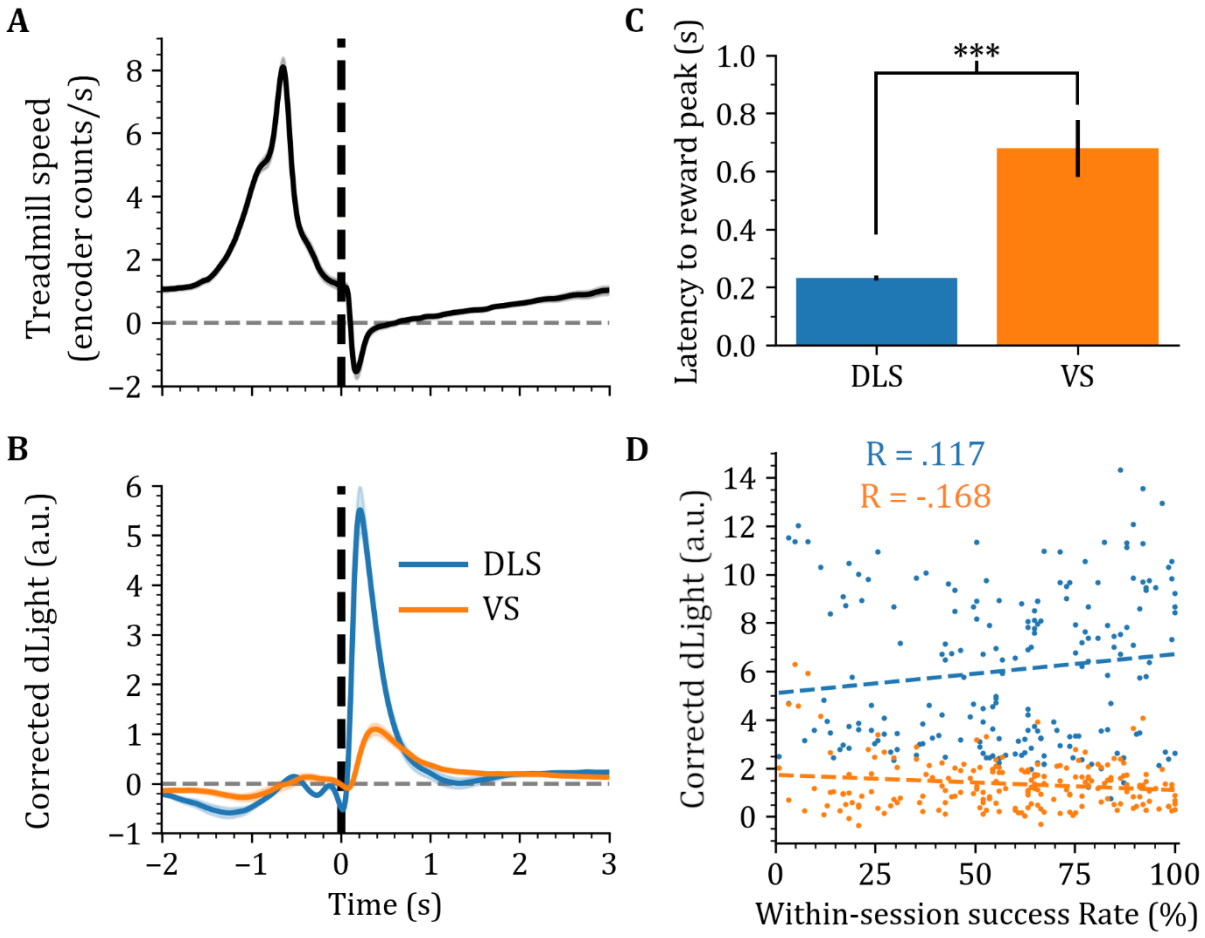


Figure 5.18: ***Reward peak of cue-learner animals in rewarded GNG trials. A****, Mean (SEM) treadmill data around reward delivery (timepoint 0). The grey dashed horizontal line represent 0 on the x axis (stillness on the treadmill or the dLight baseline). The black vertical dashed line represents reward delivery.* ***B****, Mean (SEM) corrected dLight transients collected from the DLS and VS around reward delivery (timepoint 0).* ***C****, Bar plot showing the mean (SEM) latency of the reward peak in each striatal region. *** p < .001 (repeated-measures t-test).* ***D****, Scatter plot comparing the ampitude of the reward peak within a session with the success rate for that session. The line of best fit for each region is shown with the coloured dashed lines. Pearson R values for each striatal region are also reported.*

Cue-learner mice also showed a sharp, biregional increase in the striatal dLight signal just after reward delivery (Figure 5.18B). According to RPE, the reward signal in better learners may be more likely to transfer to the cue and thus the reward peak would be smaller (Montague et al., 1996; Schultz et al., 1997; Watabe-Uchida et al., 2017). The amplitude of the reward peak for each session was identified in a 3 s window after reward

delivery and compared against the success rate within that same session. These data are shown in Figure 5.18C. Pearson's correlations found a significant negative relationship between reward peak amplitude and success rate in VS ($R(198) = -.168$, p .0177) but no significant relationship in DLS ($R(235) = .117$, $p = .0715$). However, even the significant relationship found is weak, and thus may not reflect a meaningful relationship in the data.

5.7. Discussion

Here, I show that the initiation and termination of spontaneous locomotion is characterised by specific patterns of dopaminergic activity in both the DLS and the VS. The dLight signal recorded from both striatal regions decreases around initiation and peaks following termination. Dopamine signals from both regions also clearly report delivery of instrumentally acquired rewards with large, transient peaks, and there is a positive relationship between the amplitude of the reward peak in each region on a trial-by-trial basis in the RFR task. At the onset of a cue signalling an instrumental reward contingency, the response in the dLight signal is positive for strong learners and negative for weak learners, although this pattern is stronger for dLight transients in the DLS than VS.

While these trends were present in dLight signals recorded from both regions, there are also number of differences between regions. In the DLS alone, there is a sub-baseline post-initiation peak during self-paced locomotion (e.g. from the habituation and RFR datasets). The most consistent regional difference is the timing of the signals: the peri-initiation trough occurs before bout initiation in the DLS but after bout initiation in the VS, and the latencies of both the post-termination peak and reward peaks are consistently longer in the VS than the DLS. Additionally, while the characteristics of each running bout

do seem to impact on the characteristics of the accompanying dLight signal, the nature of this impact differs between striatal regions. The speed of bouts had no effect on the dLight activity around bout termination in either striatal region, but longer bouts were associated with elevation in the dLight signals, pre- and post-termination in DLS and post-termination in VS (Figure 5.8E). The VS signal 2 s after the initiation of faster bouts was higher than during slower bouts, while the DLS was unaffected. Conversely, the duration of running bouts had no effect on the VS signal, but the DLS post-initiation peak was not present during the shortest bouts.

5.7.1. Encoding of self-paced movement initiation and termination in both DLS and VS

In data collected during habituation and RFR, both DLS and VS dopamine transients, reflecting striatal dopamine release, showed an initial decrease in activity around initiation and a phasic elevation following termination of locomotion. These findings are broadly in line with patterns of SNc dopaminergic neuronal firing reported around movement (Coddington & Dudman, 2018; Dodson et al., 2016), which found that most SNc neurons decrease their firing at movement onset and increase their firing following termination. However, there is an important difference between these previous electrophysiological findings and my photometric data: this decrease in SNc neuronal firing has been reported to occur just *after* initiation (Coddington & Dudman, 2018; Dodson et al., 2016), but in my experiments the decrease in dopamine began seconds before movement initiation. Furthermore, the minima of this peri-initiation trough actually preceded the initiation of locomotion in the DLS. This disconnect is especially surprising given that the majority of dopaminergic afferents to the DLS originate in SNc,

thus one might expect the striatal dopamine signal to closely reflect this pattern of firing in midbrain neurons.

This contradiction could be explained in a number of ways. One possibility is that this represents a genuine dissociation between dopaminergic neuronal firing and striatal release; this transient decrease in striatal dopamine could be mediated by local striatal modulation of dopamine release rather than by changes in the midbrain population firing patterns. However, perhaps a more likely interpretation is that different types of movement are encoded differently. Dodson et al. (2016) identified movement as a heterogeneous set of behaviours, including limb movements, postural adjustments, and locomotion. I have strictly defined 'movement' as 'locomotion' alone, which may be represented differently from non-locomotive movements by the dopamine system. This caveat extends more generally to the interpretation of my findings in regards to other, similar findings in the literature which may operationalise 'movement' according to different criteria than my treadmill-based approach.

Another surprising finding was that VS dopamine also decreased around movement in a pattern that was very similar to that observed in the DLS. This is despite a relative scarcity of reports of activity in VTA dopaminergic neurons being related to the initiation of spontaneous movements, from which the VS preferentially receives afferents (Dodson et al., 2016; Howe & Dombeck, 2016). This could again reflect locomotion-specific firing of VTA neurons not recorded in other paradigms or reflect movement-related local modulation of VS striatal dopamine release.

5.7.2. Dopaminergic encoding of movement vigour in DLS and VS

A number of researchers have argued that dopaminergic neurons encode aspects of movement vigour, such as the speed and duration of movements (da Silva et al., 2018; Klaus et al., 2019; Saunders et al., 2018). In this chapter, I showed some tentative evidence that the speed or duration of locomotion might affect dopamine signals at the initiation and termination of movement, but my results were neither clear nor consistent across striatal regions. This is in part because fluctuations in the dopamine signals around initiation and termination can last for several seconds. For example, the post-initiation peak in DLS was absent during the shortest bouts of spontaneous locomotion (see Figure 5.7G) and also in dLight responses during non-rewarded bouts in RFR (see Figure 5.9B). While this could signify that the post-initiation peak encodes some aspect of the vigour of ensuing locomotion, this could also merely reflect a superposition of the post-initiation peak (Figure 5.4C) and the transient increase in dLight following termination (Figure 5.4D): the slight dip following the post-initiation peak would be obscured or 'flattened' by this increase. In a similar vein, elevation in the dopamine signal following the termination of longer bouts may simply reflect a superposition of the signals around termination and initiation. The dopamine signal decreases around initiation and does not return to baseline for ~2 s (Figure 5.4C), meaning that the same absolute elevation in the dopamine signal would be lower relative to baseline after a bout of 1 s than a bout of 3 s. To address this, one would have to perform the same analysis on bouts long enough for this superposition to be unlikely; however, the vast majority of bouts in this experiment were < 2 s long, which makes it difficult to investigate this issue in this dataset.

However, there is some evidence for the dopaminergic encoding of speed, as the VS signal following initiation was elevated during faster bouts. A regional difference in this direction is interesting, as neurons encoding the vigour of movement are more often found in the SNc (da Silva et al., 2018; Klaus et al., 2019), but the DLS did not show the same speed-related modulation of activity post-initiation.

5.7.3. Dopaminergic encoding of reward contingency in DLS and VS

DLS and VS signals were recorded from mice during the initiation of both spontaneous and reward-contingent movements. The same broad features of the initiation- and termination-related dopamine signals were preserved, but there were specific differences between cohorts depending on the motivation (spontaneous vs. reward-contingent) and the outcome (rewarded vs. non-rewarded) of locomotion.

In the RFR task, mice dramatically reduced their movement at reward delivery (Figure 5.14A), which means that the majority of rewards were delivered at the termination of locomotive bouts. This then means that the post-termination elevation of the dopamine signal was the result of encoding both the termination of movement and reward delivery, but comparing dopamine signals from different cohorts helps to distinguish between these different elements. Comparing dLight signals around the termination of rewarded locomotion during RFR to the post-termination peak following spontaneous locomotion revealed a clear phasic elevation in the dopamine signal just after termination that was not movement-related, which strongly suggests that this is a 'reward peak'. The presence of a reward peak also explains the transient increase in the dopamine

signal several seconds after the initiation of rewarded trials. The dLight signal around bout initiation was not otherwise affected by the reward contingency of locomotion.

The identified reward peak following the termination of locomotion was greater when comparing the rewarded with the non-rewarded bouts than when comparing the rewarded with spontaneous bouts. Additionally, the dLight signal around termination of non-rewarded bouts is lower before termination relative to spontaneous movements in the DLS, and higher after termination in the VS. While this could reflect differences in the movement parameters, as non-rewarded bouts were typically shorter and slower than rewarded movements, this seems unlikely as the shortest bouts during spontaneous movement did not show this pattern in the dLight signals. Another interpretation is that this pattern reflects the encoding of a negative value for movement as the mouse doesn't receive a potentially expected reward, although the data are insufficient to fully support this claim.

Despite these trends being present in the signals recorded from both striatal regions, most of these trends was only found to be significant in the VS and not the DLS. However, this does not necessarily reflect a true regional difference, and may simply correspond to a lack of statistical power in these analyses. The dynamics of DLS transients are on the whole more rapid than those measured in VS, which is important as the strategy of detecting significance only at certain timepoints naturally makes it easier to find significant periods of deviation in more extended signals. As such, I cannot conclusively argue for or against a regional difference in the encoding of value across these tasks.

5.7.4. Cue and reward responses in DLS and VS dopamine signals

Both DLS and VS dopamine signals showed a clear reward peak during both the RFR and GNG tasks. Despite much of the literature on striatal dopaminergic correlates for reward focusing on the VS, reward responses have also been found in the DLS (Avvisati et al., 2022; Burton, Nakamura, & Roesch, 2015). A reward peak in DLS and VS signals was present during both RFR and GNG paradigms and the size of the reward peak was not strongly dependent on performance. This suggests that the reward response does not diminish with cue learning as predicted by classical RPE (Schultz et al., 1997; Watabe-Uchida et al., 2017), although this may be because mice were not sufficiently well-trained for this to occur (Coddington & Dudman, 2018).

There was also tentative evidence for dLight signals in both DLS and VS representing cues. The valence of the cue responses seemed tied to learning, as strong learners had an RPE-like positive cue response while weak learners had a negative response. Crucially, this trend was the same across regions. Avvisati et al. (2022) found with a Pavlovian paradigm that VS-projecting neurons selectively increased their firing at cue presentation, but DLS-projecting neurons did not. However, this could reflect the difference in experimental paradigms: the cue here represented an instrumental contingency, and the DS in general has been associated with instrumental (but less so Pavlovian) learning (Balleine et al., 2009; Wendler et al., 2014).

The negative cue response in weak learners was more difficult to interpret. This decrease is unlikely to reflect the initiation of locomotion, as the pattern of activity does not match that seen in other work in this chapter; however, it could reflect some aspect of movement, e.g. reflecting the previously reported post-initiation decrease in SNc neuronal

firing following the onset of movement (Dodson et al., 2016). It is perhaps also worth noting that there was no clear decrease in dopamine prior to the cue despite the initiation of locomotion being closely timelocked to cue-presentation. It is possible that a pre-movement decrease in dopamine signals only occurs prior to the initiation of self-paced movements, not to those triggered by an external cue. Although there is insufficient evidence to make a firm claim to this effect from these data, this would dovetail with the literature showing that external cues help Parkinsonian patients to initiate movements (Rubinstein et al., 2002; Snijders et al., 2012).

5.7.5. VS signals occur with different timing

The most consistent finding across all behavioural paradigms was the difference in timing between DLS and VS dopamine signals. The peri-initiation trough in DLS occurs prior to bout initiation in DLS but after bout initiation in VS. Additionally, both the post-termination and reward peaks have a consistently longer latency in the VS. Given this consistency, it is reasonable to assume that this difference in timing is mostly action-independent.

This regional difference could be interpreted in two ways. Firstly, this could reflect differences in the timescales of the signals, for instance that the dynamics of VS signalling are simply slower than those in DLS, most likely due to differences in local striatal modulation of dopamine release (e.g. DAT levels; Ciliax et al., 1995; Nirenberg et al., 1997). This would be in line with findings from Chapter 4 that evoked VS transients were consistently longer than DLS transients evoked by the same stimulation parameters. Alternatively, this could reflect a relative delay in VS dopamine signalling, for instance that

the signals occur at the same timescale but happen later in VS than DLS. If this were the case, this could reflect differences in the latencies of SNc and VTA neuronal firing. Alternatively, this could reflect a 'wave-like' spread of dopamine signalling from DLS to VS, as has been recently reported from DLS to DMS in a decision-making paradigm (Hamid et al., 2016). There is insufficient data in these experiments to come to a conclusion as to the nature of this regional difference in the timing of signals.

5.7.6. Strengths and limitations of the present study

As has already been mentioned throughout this discussion, there are a number of limitations in these experiments that make it challenging to draw firm conclusions about the functional relevance of the dopamine signals measured in this chapter. Especially in the GNG task, the majority of mice did not show clear evidence of robust learning and as a result the sample size of these experiments is small. Furthermore, not all mice used in these analyses were at the same stage of training (e.g., using the same task parameters) which could create further heterogeneity in their behaviour and the accompanying dopamine signals.

Behaviour in the GNG task itself may also be challenging to interpret. In this task, it was possible for mice to achieve a high number of rewards without learning the cue, for instance if they adopted a behavioural strategy of making brief but frequent bouts of locomotion. Accordingly, 'cue-learners' were identified based on their treadmill activity, but this is only a proxy measure of learning. Within this group, 'strong' and 'weak' cue learners were identified based on their reward rate, but again this may not accurately reflect whether the mouse has learned the cue-action-outcome association. Furthermore,

the GNG task was specifically chosen to distinguish reward- from movement-related neural activity, but animals did not progress far enough in training to record a meaningful cohort of No-Go learners. The potentially separable contributions of reward and movement to the recorded dopamine signals are difficult to disentangle with Go trials alone.

Due to time constraints, viral expression and the locations of the tips of implanted fibre-optic cannulae were not histologically verified. Therefore, one must exercise caution when using these data to make assumptions about the function and dynamics of DLS and VS signals measured in this study. There is significant variation in the dynamics of dopamine signals across the striatum, including temporally (van Elzelingen et al., 2022). Furthermore, there is considerable heterogeneity across the striatum itself, both in its innervation from different dopaminergic neurons (Poulin et al., 2018) and its role in learning and movement (Balleine et al., 2009; Burton et al., 2015). Confirming the locations of striatal recordings is a crucial step towards interpreting the findings shown here.

From a more general perspective, one must consider the external validity of measuring movement when animals are head-fixed. Locomotion while the head is held in a fixed-position, and while the animal is on a treadmill, is not necessarily a natural movement for an animal. It is possible that equivalent locomotion in freely-moving mice would have a different neural representation in the dopamine signals than was recorded in these experiments.

However, one major strength of this experiment is that dopamine signals were recorded simultaneously from both striatal regions. As a result, I can be sure that neural

signals recorded from each region reflect dopamine activity for the same behaviour, which allows me to draw firmer conclusions about the relationship between the dopaminergic signalling in these regions, including finding evidence of trial-by-trial correlations of specific characteristics of the dopamine signal.

5.7.7. Future work

Further work on the current dataset would greatly aid in interpretation of these findings, particularly those aspects which were not thoroughly investigated due to time constraints on the project. As mentioned above, histological verification of recording locations would provide confidence that the dopamine signals measured are reflective of signalling in the DLS and VS respectively. Furthermore, the poor learning outcomes (and resulting small sample size) of the GNG behavioural cohort hinder interpretation of the data. Training additional cohorts of mice to completion in the GNG task, which may require adjusting the training protocol to aid cue learning, would be of considerable benefit to the present work.

Additionally, further analyses could be carried out on data already collected to characterise the behaviour of mice more fully. Video data of the mice were collected throughout training. Sophisticated video analyses, for instance using DeepLabCut (Mathis et al., 2018), would allow me to identify dopamine signalling associated with other forms of movement, such as whisking, postural adjustment, limb movements or anticipatory licking. This could also be used to build confidence that mice are collecting the delivered rewards, as the lickometer data did not always reliably report licking behaviour. Furthermore, treadmill data can be a crude measure of movement, from which the

isolation of individual running bouts is not trivial. Video tracking of locomotion could provide a more refined approach to identifying and characterising locomotive bouts.

The data shown in this chapter also highlight some exciting new avenues for research. One such avenue is comparing locomotion evoked by internal vs. external factors. As discussed above, the decrease in dopamine release prior to the initiation of self-paced locomotion does not appear to be in evidence preceding presentation of a cue that leads to movement initiation. This is only logical, as the animal would not be aware that it would need to run until hearing this cue, but it does imply that this pre-initiation decrease in the dopamine signal is not necessary for cue-evoked locomotion. The question remains as to whether this pre-initiation decrease is necessary or sufficient for self-paced movement, a question which might be addressed by optogenetic activation or inactivation of dopaminergic neurons transfected with a soma-targeted opsin in concert with dLight photometry in the striatum. This work is currently being carried out in our research group, using dLight photometry in conjunction with soma-targeted opsin in the midbrain.

Another intriguing possibility is directly comparing dopaminergic neuronal firing to dopamine release during locomotion. Here, I report patterns of striatal release around movement onset and termination that are not fully consistent with published electrophysiological data recorded from SNc neurons. In Chapter 3, I demonstrated a method of simultaneously recording neuronal firing and striatal release in the same animal. With the potential of optotagging DLS- or VS-projecting dopaminergic neuronal subpopulations (Avvisati et al., 2022; Poulin et al., 2018) and the advent of dLight (Patriarchi et al., 2018), this kind of simultaneous recording in awake animals is all the more feasible. Recording midbrain neuronal firing with an optrode during online

photometric readout of dopamine dynamics in different striatal regions, for example, would allow me to replicate these findings while verifying the functional relationship between neuronal firing and striatal release.

In conclusion, dopamine signals in both DLS and VS encode the initiation and termination of self-paced locomotion and the receipt of reward. There is tentative evidence to suggest some encoding of vigour in VS dopamine signals and the biregional encoding of instrumental cues, but the evidence from these data alone is not strong enough to draw firm conclusions. However, the finding that VS signals occurred with different timing to those recorded in DLS is consistent, regardless of the motivation for movement. Further research is needed to pick apart the heterogeneity in function of DLS and VS striatal dopamine release.

Chapter 6. General Discussion

6.1. Summary

The overarching aim of this thesis was to explore the heterogeneity of midbrain and striatal dopamine signalling *in vivo*, as well as to evaluate different tools used to measure this signalling. Said heterogeneity was explored in several ways throughout this thesis, comparing the firing of dopaminergic neurons to striatal dopamine release as well as the dynamics and function of dopaminergic signalling in different striatal subregions. Methodological approaches to measuring this signalling were also explored, including a novel approach which combines single-unit electrophysiology with fast-scan cyclic voltammetry (FCV) for reading out dopaminergic neuron firing and dopamine release, respectively. I have demonstrated the feasibility of combining these techniques in individual anaesthetised mice and described a linear relationship between optogenetically evoked dopaminergic neuronal firing and striatal dopamine release. I also explored the use of *in vivo* photometry for assessing the signalling dynamics of dLight, a novel genetically encoded fluorescent sensor for dopamine (Patriarchi et al., 2018), as an alternative approach to reading out striatal dopamine release. Through electrical stimulation of the midbrain, I found that dLight transients responded to a range of stimulation parameters in a manner similar to transients measured by FCV, but that those measured by dLight were consistently shorter than those measured by voltammetry. Exploring the differences in dopamine signalling between the dorsolateral striatum (DLS) and ventral striatum (VS) in anaesthetised mice revealed striking regional differences in the timescales of signals, as VS signals were consistently longer than those in DLS. In head-

fixed behaving mice, dopamine signalling correlates for the initiation and termination of locomotion, reward delivery, and presentation of an instrumental cue were found in both striatal regions but with some key differences. This work paves the road for further investigations into the heterogeneity and function of dopaminergic signalling in the midbrain and striatum.

6.1.1. Chapter 3 - Combining optically evoked single-unit electrophysiology with fast-scan cyclic voltammetry

Several studies have found functional dissociations between the firing of midbrain dopaminergic neurons and the release of dopamine in the striatum (Cachope & Cheer, 2014; Mohebi et al., 2019; Sulzer et al., 2016), but not by simultaneously recording both aspects of signalling within individual animals. In chapter 3, I took some initial steps to developing a method of recording single-unit activity in midbrain in parallel with FCV in striatum. Using anaesthetised mice, the optogenetically evoked firing of midbrain dopaminergic neurons was recorded in concert with striatal dopamine release.

Both dopamine neuron action potential firing and dopamine release were positively modulated by the frequency of optical stimulation. However, the frequency dependence of neuronal firing was not linear, as neurons did not fire consistently to single pulses of stimulation at high frequencies. At these high frequencies, neurons typically showed a decrease in their firing after the end of the stimulation train, something which has often been observed *in vitro* (Nedergaard, 2004; Shepard & Bunney, 1991), but is not often observed in behaving animals (Dodson et al., 2016; Eshel et al., 2016; Schultz et al., 1997; Starkweather et al., 2017). From this, it was assumed that this non-linearity was due to

the supraphysiological parameters of some of the optical stimulation trains, as a 'burst' of 10 action potentials at 30-50 Hz would be unlikely to occur naturally (Grace & Bunney, 1983). Crucially, however, the same pattern of non-linearity in frequency dependence was found in both the firing of midbrain dopaminergic neurons and the simultaneously recorded striatal dopamine release, suggesting that the relationship between both measures of dopamine signalling was itself linear. Thus, it would be reasonable to assume that striatal dopamine release is closely related to midbrain dopamine neuronal firing under these conditions.

These experiments were conducted, at least in part, to demonstrate the feasibility of simultaneous electrophysiological recordings and FCV, which could potentially be extrapolated to awake and behaving animals. However, combining these techniques came with several unique challenges. FCV 'scans' caused a sizeable and frequent artifact in the electrophysiological recording channel, which presented challenges for spike-sorting single-unit data. Furthermore, grounding both the electrophysiological recording equipment and the voltameter caused a ground loop, which meant the collected data was also noisier. The issues are in addition to the existing difficulties of using either of these techniques in isolation: single-unit recordings are low yield, especially when coupled with cell labelling, while FCV is highly sensitive to electrical noise. Both of these techniques are especially difficult to translate to awake preparations, as single-unit recording and labelling requires a high degree of stability, which can be a problem when animals are moving; furthermore, FCV electrodes are prone to fouling when exposed to brain tissue for long periods and therefore require careful maintenance in chronic preparations. In Chapter 4, I explored the use of photometry for assessing the activity of the genetically

encoded fluorescent sensor dLight (Patriarchi et al., 2018) as an alternative to FCV for measuring striatal dopamine release.

6.1.2. Chapter 4 - Measuring electrically evoked dopamine transients with FCV and dLight photometry

I made first steps towards characterising the *in vivo* dynamics of the novel fluorescent sensor dLight in comparison with FCV, a technique which has been extensively used for decades to study dopamine release. Additionally, to assess whether dLight can be used to address questions about heterogeneity in dopamine release across the striatum, FCV and dLight photometry were recorded from both the dorsolateral striatum (DLS) and ventral striatum (VS). Both these regions are heterogeneous in their local striatal microcircuitry in ways that might affect the dynamics of dopamine release and uptake (Brimblecombe et al., 2015; Ciliax et al., 1995; Nirenberg et al., 1997; Threlfell et al., 2010; Threlfell & Cragg, 2011). FCV and dLight transients were recorded from both striatal regions in anaesthetised mice; the transients were electrically evoked by midbrain stimulation across a broad range of stimulation parameters (at different frequencies and with different numbers of pulses), encompassing and surpassing the physiological range of dopaminergic neuronal burst firing *in vivo* (Brown et al., 2009; Dai & Tepper, 1998; Dodson et al., 2016; Grace & Bunney, 1983).

The magnitude of evoked transients recorded with both techniques and from both regions followed similar patterns, increasing in amplitude when stimulation was at higher frequencies and consisted of more stimulation pulses. Additionally, the timescales of all signals were modulated in a manner that was parameter-dependent, often reflecting the

duration of stimulation: more pulses resulted in longer transients and higher frequencies in shorter transients, whereas the decay time of the signal was mostly parameter-independent. However, there was consistent regional heterogeneity in the timescales of both signals, with longer transients recorded in the VS compared to the DLS, both in terms of their duration and decay time.

I also observed some striking differences in the transients recorded by both techniques. Evoked transients recorded with dLight photometry were biregionally shorter than those recorded with FCV. Furthermore, the observed differences in the timescales of DLS and VS transients were significantly more apparent when measured with dLight photometry. If indeed dLight is capable of reporting phasic dopaminergic activity with greater temporal resolution than FCV, and given the differences in timescale found in these experiments, it is an especially useful tool for investigating regional heterogeneity in striatal dopaminergic signalling. The utility of dLight photometry should also extend to investigations of dopaminergic signalling accompanying behaviour. In Chapter 5, I used dLight photometry to explore the dopaminergic signalling during locomotion, reward delivery and instrumental learning, recording from the same striatal subregions as in Chapter 4 (DLS and VS).

6.1.3. Chapter 5: Locomotion- and reward-related dopamine signalling in dorsolateral and ventral striatum

Beyond the aforementioned heterogeneity of local striatal microcircuitry modulating dopamine signalling, the striatum is also heterogeneous in its assumed function (Balleine et al., 2007) and receives projections from molecularly distinct populations of midbrain

dopaminergic neurons (Poulin et al., 2018). These neurons are reported to encode different aspects of behaviour. A broad (and perhaps crude) distinction can be made between dopaminergic neurons in the ventral tegmental area (VTA), which preferentially project to the VS and are said to encode reward prediction error (RPE; Montague et al., 1996; Schultz et al., 1997; Watabe-Uchida et al., 2017); and those in the substantia nigra *pars compacta* (SNc), said to encode action initiation and movement vigour (da Silva et al., 2018; Dodson et al., 2016; Howe & Dombeck, 2016; Panigrahi et al., 2015). To investigate striatal heterogeneity in the function and dynamics of dopamine signalling in behaving animals, I simultaneously recorded photometric dLight transients from the DLS and VS of awake, head-fixed mice situated on a treadmill. Mice performed locomotion spontaneously but were also trained in instrumental tasks in which reward was contingent on their movement, both self-paced and evoked by an external instrumental cue.

Dopamine signalling correlates were found in both striatal regions for locomotion, reward delivery and instrumental cues. Self-paced locomotion was preceded by a dip in the dopamine signal beginning ~ 2 s prior to movement initiation, reaching a minimum around initiation ('peri-initiation trough'). The dopamine signal transiently increased following the termination of locomotion ('post-termination peak'). These characteristics were broadly independent of the instrumental motivation for movement, present around both spontaneous and reward-contingent self-paced locomotion. However, there was a depression in the signal preceding the termination of non-rewarded running bouts, potentially reflecting a declining value of movement. Both striatal regions also reported positive dopamine transients in response to delivery of rewards ('reward peak').

Findings were more mixed on the dopaminergic representation of the instrumental cue, potentially as these findings are more preliminary. Mice that had learned the instrumental cue typically showed a cue response in striatal dopamine, but this cue was positive in some animals and negative in others. Dividing the cohort into the mice that showed strong evidence of cue learning and those that did not suggests that the valence of the cue response reflects learning, as an RPE-like positive cue response was specifically found in strong learners. Interestingly, cue-provoked locomotion in these mice was not preceded by a decrease in the dopamine signal, as was reported prior to the initiation of self-paced movements.

While these overall patterns in the dopamine signals were found in both regions, there were also clear differences in the dynamics of these signals between regions. In line with the findings of Chapter 4, VS signals were consistently delayed compared to those recorded in the DLS, with longer latencies to the reward and post-termination peaks; furthermore, the peri-initiation trough occurred just *before* the initiation of locomotion in the DLS but just *after* in the VS. The DLS signal after movement initiation also showed more phasic fluctuation, reaching a small 'post-initiation peak' that was not observed in the VS signal. While these experiments found minimal functional differences in dopaminergic signalling in different striatal regions, the temporal dynamics of signals in the DLS and VS of behaving animals are nevertheless clearly distinct from one another. These results suggest that the crude functional segregation of the mesolimbic and nigrostriatal pathways is oversimplistic, as both DLS and VS robustly encode both movement and reward.

6.2. Theoretical and technical considerations

6.2.1. Measurement of evoked potentials in anaesthetised preparations

The dynamics of the dLight signal were characterised in anaesthetised animals by electrically evoked stimulation of the midbrain. This allowed for precise experimental control over the dopaminergic system. This precision allowed me to confirm that striatal dopamine release recorded with dLight photometry could read out fine-scale differences in the intensity of the stimulation (e.g. frequency and number of pulses), which is important given that the magnitude of the dopaminergic response is said to encode important aspects of behaviour such as movement vigour (da Silva et al., 2018). Furthermore, this allowed me to explore the dynamics of dLight outside of this physiological range, testing the limits of this novel fluorescent sensor.

However, the dynamics of the dLight signal in response to evoked stimulation may not map to native dopaminergic signals. In particular, the population of dopamine neurons will be hypersynchronised during stimulation, which does not reflect native population activity. This explains why even low levels of stimulation within the range of tonic firing (Brown et al., 2009; Dai & Tepper, 1998; Dodson et al., 2016; Grace & Bunney, 1983) resulted in clear elevation of the dopamine signal. Furthermore, I also demonstrated in Chapter 3 that dopaminergic neurons will not be reliably entrained to stimulation above what might be considered the physiological range, and the same may also be true of dopamine release. As such, the dLight dynamics shown here would not necessarily reflect the readout of *in vivo* dopamine signalling during physiological levels of dopamine activity.

6.2.2. Characterising the neural correlates of movement and reward

In Chapter 5, I recorded dopamine transients around both movement- and reward-related behaviour, e.g. locomotion and collection of an instrumentally acquired reward. Although the literature suggests that DLS and VS receive projections from functionally distinct dopaminergic neurons (Dodson et al., 2016; Howe & Dombeck, 2016; Poulin et al., 2018; Schultz et al., 1997), I did not find a clear regional difference within the striatum in the encoding of either movement or reward, only in the temporal dynamics of the signalling.

Despite this, one must be circumspect when interpreting these results. Firstly, the attempt made here to characterise functional dopaminergic signalling is only preliminary; the behaviours and stimuli examined in these experiments were only a small subset of those which might feasibly be represented in striatal dopamine signals. For instance, striatal dopamine release may be differentially modulated for a Pavlovian cue versus and instrumental cue (Avvisati et al., 2022); alternatively, non-locomotive movements may manifest in entirely different patterns of signalling (Hughes et al., 2020). Furthermore, functional heterogeneity may appear when one examines different aspects of reward signalling, such as cue value (West & Carelli, 2016). Additionally, while I aimed to separate out movement- vs reward-related neural signals with the use of a Go/No-Go task, mice did not reach a stage of training where this was possible. More work is needed to characterise the functional heterogeneity of striatal dopamine signalling.

6.3. Future directions

6.3.1. The (potentially separable) dopaminergic signalling accompanying movement and reward

The Go/No-Go task used in Chapter 5 was chosen as a behavioural paradigm because it can be used to disentangle dopaminergic signalling related to reward from that related to movement. However, due to time constraints and poor learning outcomes, the mice in my experiments did not progress far enough in their behavioural training to learn the No-Go reward contingency. This hinders interpretation of the responses in the dopamine signals to the Go cue, as cue onset frequently coincides temporally with the initiation of locomotion. This means that I cannot be confident that the striatal dopamine signals I recorded truly represent an RPE-like cue response rather than a correlate of movement. Therefore, the natural next step for these experiments is to train a fresh cohort of mice in the No-Go reward contingency. These data would shine light on the function of dopaminergic signalling in the DLS and VS.

6.3.2. FCV and dLight: What do they measure?

In Chapter 4, electrically evoked FCV and dLight signals were recorded and compared. Crucially, there was a marked difference in the temporal dynamics of the dopamine transients recorded with each technique. Not only were FCV transients slower overall, but dLight reported a much larger difference in the duration of signals measured in the two striatal regions.

Some differences between these techniques are expected, as they measure fundamentally different aspects of dopamine signalling: FCV represents extracellular

dopamine, while dLight reflects the kinetics of engagement of its modified dopamine receptor. However, it is not yet clear what about these different techniques would result in the temporal differences seen in my data. Do these differences reflect differences between the dynamics of dopamine receptors as opposed to extracellular dopamine? This question could be addressed by comparing the dynamics of dLight to those of fluorescent sensors conjugated to different dopamine receptors, such as D2-conjugated $GRAB_{DA}$ (Sun et al., 2020). *Ex vivo* work could also be used to comprehensively explore the temporal heterogeneity in evoked DLS and VS transients, for instance by pharmacologically manipulating the levels of the dopamine transporter DAT to test whether differing levels of DAT can explain the timescale differences in DLS and VS dopamine transients. Answering these kinds of questions is especially important as genetically encoded fluorescent dopamine sensors become more and more widely used as a measure of dopamine release and will be used to draw conclusions about dopaminergic signalling.

6.3.3. Closing the loop: What is the relationship between dopamine neuron firing and striatal release?

Chapter 3 of this thesis highlighted the importance of understanding the relationship between dopaminergic neuronal firing and striatal release, and presented a potential approach to recording both aspects of dopaminergic signalling simultaneously in the same animal. Subsequently, I have demonstrated that dLight is a powerful alternative to FCV, allowing for read out of dopamine release at high temporal resolution in anaesthetised and awake animals without some of the pitfalls of FCV recordings, especially chronic FCV. As such, a logical next step would be to record dopaminergic neuronal firing in concert

with dLight photometry. The development of this methodology would allow for further exploration of some of the findings from Chapter 5. The initiation and termination of self-paced locomotion were accompanied by distinct patterns of striatal dopamine. Recording the activity of a population of dopamine neurons during locomotion would allow us for investigation of whether these distinct striatal dopamine patterns emerge from changes in the firing rate pattern of dopaminergic neurons or are unique to release, thereby also shedding light on whether fluctuations in the striatal signal are instead caused by local modulation at the level of the striatum. Combined midbrain electrophysiology and striatal dLight may also help to explain region-specific characteristics of dopamine release such as the post-initiation peak found in DLS but not VS transients: is this phasic fluctuation also represented in the firing of a population of midbrain dopamine neurons? Simultaneous recordings of neuronal activity and release from within the same animal would be especially advantageous to looking at complex aspects of behaviour and movement, as it would allow for trial-by-trial comparisons of these two distinct modes of dopaminergic signalling.

6.4. Concluding statement

I have demonstrated an approach for simultaneous recordings of dopaminergic midbrain neuronal firing and striatal dopamine release. Additionally, I have demonstrated the enormous potential of dLight as an alternative to FCV for measuring striatal dopamine release. I report consistent heterogeneity in the dynamics of dopamine signals between DLS and VS, but that dopaminergic correlates for both self-paced locomotion and reward

are represented in both regions. I conclude that future explorations of dopaminergic signalling should take this heterogeneity into consideration.

REFERENCES

Afonso-Oramas, D., Cruz-Muros, I., de la Rosa, D. Á., Abreu, P., Giráldez, T., Castro-Hernández, J., … González-Hernández, T. (2009). Dopamine transporter glycosylation correlates with the vulnerability of midbrain dopaminergic cells in Parkinson's disease. *Neurobiology of Disease*, *36*, 494–508.

Aguilar-Rivera, M., Gatica, R. I., Azócar, V., Buc, D., & Fuentealba-Evans, J. A. (2023). Electrophysiological Characterization of Dopaminergic Neurons of the Rat Substantia Nigra Compacta. In J. A. Fuentealba-Evans & P. Henny (Eds.), *Dopaminergic System Function and Dysfunction: Experimental Approaches* (pp. 121–146). New York, NY: Springer US.

Akam, T., Lustig, A., Rowland, J. M., Kapanaiah, S. K., Esteve-Agraz, J., Panniello, M., … Walton, M. E. (2022). Open-source, Python-based, hardware and software for controlling behavioural neuroscience experiments. *ELife*, *11*, e67846.

Akam, T., & Walton, M. E. (2019). pyPhotometry: Open source Python based hardware and software for fiber photometry data acquisition. *Scientific Reports*, *9*, 1–11.

Albin, R. L., Young, A. B., & Penney, J. B. (1989). The functional anatomy of basal ganglia disorders. *Trends in Neurosciences*, *12*, 366–375.

Alcantara, A. A., Mrzljak, L., Jakab, R. L., Levey, A. I., Hersch, S. M., & Goldman-Rakic, P. S. (2001). Muscarinic m1 and m2 receptor proteins in local circuit and projection neurons of the primate striatum: Anatomical evidence for cholinergic modulation of glutamatergic prefronto-striatal pathways. *Journal of Comparative Neurology*, *434*, 445–460.

Al-Hasani, R., McCall, J. G., Shin, G., Gomez, A. M., Schmitz, G. P., Bernardi, J. M., … Bruchas, M. R. (2015). Distinct subpopulations of nucleus accumbens dynorphin neurons drive aversion and reward. *Neuron*, *87*, 1063–1077.

Anderegg, A., Poulin, J.-F., & Awatramani, R. (2015). Molecular Heterogeneity of Midbrain Dopaminergic Neurons – Moving Toward Single Cell Resolution. *FEBS Letters*, *589*, 3714–3726.

Aoki, S., Smith, J. B., Li, H., Yan, X., Igarashi, M., Coulon, P., … Jin, X. (2019). An open cortico-basal ganglia loop allows limbic control over motor output via the nigrothalamic pathway. *ELife*, *8*, e49995.

Aransay, A., Rodríguez-López, C., García-Amado, M., Clascá, F., & Prensa, L. (2015). Long-range projection neurons of the mouse ventral tegmental area: A single-cell axon tracing analysis. *Frontiers in Neuroanatomy*, *9*, 59.

Attwell, D., & Laughlin, S. B. (2001). An Energy Budget for Signaling in the Grey Matter of the Brain. *Journal of Cerebral Blood Flow & Metabolism*, *21*, 1133–1145.

Avshalumov, M. V., & Rice, M. E. (2003). Activation of ATP-sensitive K+ (KATP) channels by H_2O_2 underlies glutamate-dependent inhibition of striatal dopamine release. *Proceedings of the National Academy of Sciences*, *100*, 11729–11734.

Avvisati, R., Kaufmann, A.-K., Young, C. J., Portlock, G. E., Cancemi, S., Costa, R. P., … Dodson, P. D. (2022, July 19). *Distributional coding of associative learning within projection-defined populations of midbrain dopamine neurons* (p. 2022.07.18.500429). p. 2022.07.18.500429. bioRxiv.

Azcorra, M., Gaertner, Z., Davidson, C., Hayes, C. K., Ramakrishnan, C., Fenno, L., … Dombeck, D. A. (2022, December 19). *Unique functional responses differentially map onto genetic subtypes of dopamine neurons* (p. 2022.12.19.521076). p. 2022.12.19.521076. bioRxiv.

Bäckman, C. M., Malik, N., Zhang, Y., Shan, L., Grinberg, A., Hoffer, B. J., … Tomac, A. C. (2006). Characterization of a mouse strain expressing Cre recombinase from the 3′ untranslated region of the dopamine transporter locus. *Genesis*, *44*, 383–390.

Bailey, K. R., & Mair, R. G. (2006). The Role of Striatum in Initiation and Execution of Learned Action Sequences in Rats. *Journal of Neuroscience*, *26*, 1016–1025.

Balleine, B. W., Delgado, M. R., & Hikosaka, O. (2007). The role of the dorsal striatum in reward and decision-making. *Journal of Neuroscience*, *27*, 8161–8165.

Balleine, B. W., Liljeholm, M., & Ostlund, S. B. (2009). The integrative function of the basal ganglia in instrumental conditioning. *Behavioural Brain Research*, *199*, 43–52.

Bannon, M. J., & Whitty, C. J. (1997). Age-related and regional differences in dopamine transporter mRNA expression in human midbrain. *Neurology*, *48*, 969–977.

Bao, L., Avshalumov, M. V., Patel, J. C., Lee, C. R., Miller, E. W., Chang, C. J., & Rice, M. E. (2009). Mitochondria are the source of hydrogen peroxide for dynamic brain-cell signaling. *Journal of Neuroscience*, *29*, 9002–9010.

Barbera, G., Liang, B., Zhang, L., Gerfen, C. R., Culurciello, E., Chen, R., … Lin, D.-T. (2016). Spatially compact neural clusters in the dorsal striatum encode locomotion relevant information. *Neuron*, *92*, 202–213.

Barnett, M. W., & Larkman, P. M. (2007). The action potential. *Practical Neurology*, *7*, 192–197.

Barrot, M., Sesack, S. R., Georges, F., Pistis, M., Hong, S., & Jhou, T. C. (2012). Braking dopamine systems: A new GABA master structure for mesolimbic and nigrostriatal functions. *Journal of Neuroscience*, *32*, 14094–14101.

Bassareo, V., & Di Chiara, G. (1999). Differential responsiveness of dopamine transmission to food-stimuli in nucleus accumbens shell/core compartments. *Neuroscience*, *89*, 637–641.

Bath, B. D., Michael, D. J., Trafton, B. J., Joseph, J. D., Runnels, P. L., & Wightman, R. M. (2000). Subsecond adsorption and desorption of dopamine at carbon-fiber microelectrodes. *Analytical Chemistry*, *72*, 5994–6002.

Bayer, H. M., & Glimcher, P. W. (2005). Midbrain dopamine neurons encode a quantitative reward prediction error signal. *Neuron*, *47*, 129–141.

Beckstead, M. J., Grandy, D. K., Wickman, K., & Williams, J. T. (2004). Vesicular dopamine release elicits an inhibitory postsynaptic current in midbrain dopamine neurons. *Neuron*, *42*, 939–946.

Beier, K. T., Steinberg, E. E., DeLoach, K. E., Xie, S., Miyamichi, K., Schwarz, L., … Luo, L. (2015). Circuit architecture of VTA dopamine neurons revealed by systematic input-output mapping. *Cell*, *162*, 622–634.

Benjamini, Y., & Hochberg, Y. (1995). Controlling the false discovery rate: A practical and powerful approach to multiple testing. *Journal of the Royal Statistical Society. Series B. Methodological*, *57*, 289–300.

Bernard, V., & Bolam, J. P. (1998). Subcellular and subsynaptic distribution of the NR1 subunit of the NMDA receptor in the neostriatum and globus pallidus of the rat: Co-localization at synapses with the GluR2/3 subunit of the AMPA receptor. *European Journal of Neuroscience*, *10*, 3721–3736.

Björklund, A., & Dunnett, S. B. (2007). Dopamine neuron systems in the brain: An update. *Trends in Neurosciences*, *30*, 194–202.

Blanco-Pozo, M., Akam, T., & Walton, M. (2021, August 3). *Dopamine reports reward prediction errors, but does not update policy, during inference-guided choice* (p. 2021.06.25.449995). p. 2021.06.25.449995. bioRxiv.

Bolam, J. P., Wainer, B. H., & Smith, A. D. (1984). Characterization of cholinergic neurons in the rat neostriatum. A combination of choline acetyltransferase immunocytochemistry, Golgi-impregnation and electron microscopy. *Neuroscience*, *12*, 711–718.

Brimblecombe, K. R., & Cragg, S. J. (2017). The striosome and matrix compartments of the striatum: A path through the labyrinth from neurochemistry toward function. *ACS Chemical Neuroscience*, *8*, 235–242.

Brimblecombe, K. R., Gracie, C. J., Platt, N. J., & Cragg, S. J. (2015). Gating of dopamine transmission by calcium and axonal N-, Q-, T- and L-type voltage-gated calcium channels differs between striatal domains. *The Journal of Physiology*, *593*, 929–946.

Britt, J. P., & McGehee, D. S. (2008). Presynaptic opioid and nicotinic receptor modulation of dopamine overflow in the nucleus accumbens. *Journal of Neuroscience*, *28*, 1672–1681.

Brown, H. D., McCutcheon, J. E., Cone, J. J., Ragozzino, M. E., & Roitman, M. F. (2011). Primary food reward and reward-predictive stimuli evoke different patterns of phasic dopamine signaling throughout the striatum. *European Journal of Neuroscience*, *34*, 1997–2006.

Brown, M. T. C., Henny, P., Bolam, J. P., & Magill, P. J. (2009). Activity of neurochemically heterogeneous dopaminergic neurons in the substantia nigra during spontaneous and driven changes in brain state. *Journal of Neuroscience*, *29*, 2915–2925.

Bunin, M. A., Prioleau, C., Mailman, R. B., & Wightman, R. M. (1998). Release and uptake rates of 5-hydroxytryptamine in the dorsal raphe and substantia nigra reticulata of the rat brain. *Journal of Neurochemistry*, *70*, 1077–1087.

Burton, A. C., Nakamura, K., & Roesch, M. R. (2015). From ventral-medial to dorsal-lateral striatum: Neural correlates of reward-guided decision-making. *Neurobiology of Learning and Memory*, *117*, 51–59.

Cachope, R., & Cheer, J. F. (2014). Local control of striatal dopamine release. *Frontiers in Behavioral Neuroscience*, *8*. Retrieved from https://www.frontiersin.org/articles/10.3389/fnbeh.2014.00188

Cachope, R., Mateo, Y., Mathur, B. N., Irving, J., Wang, H.-L., Morales, M., … Cheer, J. F. (2012). Selective activation of cholinergic interneurons enhances accumbal phasic dopamine release: Setting the tone for reward processing. *Cell Reports*, *2*, 33–41.

Calabresi, P., Centonze, D., Gubellini, P., Pisani, A., & Bernardi, G. (2000). Acetylcholine-mediated modulation of striatal function. *Trends in Neurosciences*, *23*, 120–126.

Calipari, E. S., Huggins, K. N., Mathews, T. A., & Jones, S. R. (2012). Conserved dorsal–ventral gradient of dopamine release and uptake rate in mice, rats and rhesus macaques. *Neurochemistry International*, *61*, 986–991.

Carter, M., & Shieh, J. C. (2010). Chapter 3—Stereotaxic Surgeries and In Vivo Techniques. In M. Carter & J. C. Shieh (Eds.), *Guide to Research Techniques in Neuroscience* (pp. 73–90). New York: Academic Press.

Cass, W. A., Zahniser, N. R., Flach, K. A., & Gerhardt, G. A. (1993). Clearance of exogenous dopamine in rat dorsal striatum and nucleus accumbens: Role of metabolism and effects of locally applied uptake inhibitors. *Journal of Neurochemistry*, *61*, 2269–2278.

Castro, D. C., & Berridge, K. C. (2014). Opioid hedonic hotspot in nucleus accumbens shell: Mu, delta, and kappa maps for enhancement of sweetness "liking" and "wanting". *Journal of Neuroscience*, *34*, 4239–4250.

Cazorla, M., de Carvalho, F. D., Chohan, M. O., Shegda, M., Chuhma, N., Rayport, S., … Kellendonk, C. (2014). Dopamine D2 receptors regulate the anatomical and functional balance of basal ganglia circuitry. *Neuron*, *81*, 153–164.

Chang, C. Y., Esber, G. R., Marrero-Garcia, Y., Yau, H.-J., Bonci, A., & Schoenbaum, G. (2016). Brief optogenetic inhibition of dopamine neurons mimics endogenous negative reward prediction errors. *Nature Neuroscience*, *19*, 111–116.

Chen, B. T., & Rice, M. E. (2001). Novel Ca^{2+} dependence and time course of somatodendritic dopamine release: Substantia nigra versus striatum. *Journal of Neuroscience*, *21*, 7841–7847.

Chen, Q., Veenman, L., Knopp, K., Yan, Z., Medina, L., Song, W.-J., … Reiner, A. (1998). Evidence for the preferential localization of Glutamate Receptor-1 subunits of AMPA receptors to the dendritic spines of medium spiny neurons in rat striatum. *Neuroscience*, *83*, 749–761.

Ciliax, B. J., Heilman, C., Demchyshyn, L. L., Pristupa, Z. B., Ince, E., Hersch, S. M., … Levey, A. I. (1995). The dopamine transporter: Immunochemical characterization and localization in brain. *Journal of Neuroscience*, *15*, 1714–1723.

Clark, J. J., Sandberg, S. G., Wanat, M. J., Gan, J. O., Horne, E. A., Hart, A. S., … Martinez, V. (2010). Chronic microsensors for longitudinal, subsecond dopamine detection in behaving animals. *Nature Methods*, *7*, 126.

Clark, P. J., & España, R. A. (2023). Fast Scan Cyclic Voltammetry to Assess Dopamine Function: From Circuits to Behavior. In J. A. Fuentealba-Evans & P. Henny (Eds.), *Dopaminergic System Function and Dysfunction: Experimental Approaches* (pp. 249–281). New York, NY: Springer US.

Coddington, L. T., & Dudman, J. T. (2018). The timing of action determines reward prediction signals in identified midbrain dopamine neurons. *Nature Neuroscience*, *21*, 1563–1573.

Cohen, J. Y., Haesler, S., Vong, L., Lowell, B. B., & Uchida, N. (2012). Neuron-type-specific signals for reward and punishment in the ventral tegmental area. *Nature*, *482*, 85–88.

Comoli, E., Coizet, V., Boyes, J., Bolam, J. P., Canteras, N. S., Quirk, R. H., … Redgrave, P. (2003). A direct projection from superior colliculus to substantia nigra for detecting salient visual events. *Nature Neuroscience*, *6*, 974–980.

Condon, M. D., Platt, N. J., Zhang, Y.-F., Roberts, B. M., Clements, M. A., Vietti-Michelina, S., … Cragg, S. J. (2019). Plasticity in striatal dopamine release is governed by release-independent depression and the dopamine transporter. *Nature Communications*, *10*, 4263.

Corbett, D., & Wise, R. A. (1980). Intracranial self-stimulation in relation to the ascending dopaminergic systems of the midbrain: A moveable electrode mapping study. *Brain Research*, *185*, 1–15.

Corbit, L. H. (2018). Understanding the balance between goal-directed and habitual behavioral control. *Current Opinion in Behavioral Sciences*, *20*, 161–168.

Corbit, L. H., Nie, H., & Janak, P. H. (2012). Habitual alcohol seeking: Time course and the contribution of subregions of the dorsal striatum. *Biological Psychiatry*, *72*, 389–395.

Costa, R. M. (2007). Plastic Corticostriatal Circuits for Action Learning. *Annals of the New York Academy of Sciences*, *1104*, 172–191.

Cragg, S. J. (2003). Variable dopamine release probability and short-term plasticity between functional domains of the primate striatum. *Journal of Neuroscience*, *23*, 4378–4385.

Cragg, S. J. (2006). Meaningful silences: How dopamine listens to the ACh pause. *Trends in Neurosciences*, *29*, 125–131.

Cragg, S. J., Hille, C. J., & Greenfield, S. A. (2000). Dopamine release and uptake dynamics within nonhuman primate striatum in vitro. *Journal of Neuroscience*, *20*, 8209–8217.

Cragg, S. J., & Rice, M. E. (2004). DAncing past the DAT at a DA synapse. *Trends in Neurosciences*, *27*, 270–277.

Cui, G., Jun, S. B., Jin, X., Pham, M. D., Vogel, S. S., Lovinger, D. M., & Costa, R. M. (2013). Concurrent activation of striatal direct and indirect pathways during action initiation. *Nature*, *494*, 238–242.

da Silva, J. A., Tecuapetla, F., Paixão, V., & Costa, R. M. (2018). Dopamine neuron activity before action initiation gates and invigorates future movements. *Nature*, *554*, 244–248.

Dahlström, A., & Fuxe, K. (1964). Localization of monoamines in the lower brain stem. *Experientia*, *20*, 398–399.

Dai, M., & Tepper, J. M. (1998). Do silent dopaminergic neurons exist in rat substantia nigra in vivo? *Neuroscience*, *85*, 1089–1099.

Davidson, C., & Stamford, J. A. (1993). Neurochemical evidence of functional A10 dopamine terminals innervating the ventromedial axis of the neostriatum: In vitro voltammetric data in rat brain slices. *Brain Research*, *615*, 229–239.

Day, J. J., & Carelli, R. M. (2007). The nucleus accumbens and pavlovian reward learning. *The Neuroscientist*, *13*, 148–159.

Day, J. J., Roitman, M. F., Wightman, R. M., & Carelli, R. M. (2007). Associative learning mediates dynamic shifts in dopamine signaling in the nucleus accumbens. *Nature Neuroscience*, *10*, 1020–1028.

de Melo, M. B., Daldegan-Bueno, D., Menezes Oliveira, M. G., & de Souza, A. L. (2022). Beyond ANOVA and MANOVA for repeated measures: Advantages of generalized estimated equations and generalized linear mixed models and its use in neuroscience research. *European Journal of Neuroscience*, *56*, 6089–6098.

Debanne, D. (2004). Information processing in the axon. *Nature Reviews Neuroscience*, *5*, 304–316.

DeLong, M. R. (1990). Primate models of movement disorders of basal ganglia origin. *Trends in Neurosciences*, *13*, 281–285.

Descarries, L., & Mechawar, N. (2000). Ultrastructural evidence for diffuse transmission by monoamine and acetylcholine neurons of the central nervous system. In *Volume Transmission Revisited*: *Vol. 125*. *Progress in Brain Research* (pp. 27–47). Elsevier.

Descarries, L., Watkins, K. C., Garcia, S., Bosler, O., & Doucet, G. (1996). Dual character, asynaptic and synaptic, of the dopamine innervation in adult rat neostriatum: A quantitative autoradiographic and immunocytochemical analysis. *Journal of Comparative Neurology*, *375*, 167–186.

Di Chiara, G. (1995). The role of dopamine in drug abuse viewed from the perspective of its role in motivation. *Drug and Alcohol Dependence*, *38*, 95–137.

Dickinson, A. (1994). Instrumental conditioning. In *Handbook of Perception and Cognition Series (2nd Ed.) 3. Animal learning and cognition* (pp. 45–79). San Diego, CA, US: Academic Press.

Dodson, P. D., Dreyer, J. K., Jennings, K. A., Syed, E. C. J., Wade-Martins, R., Cragg, S. J., … Magill, P. J. (2016). Representation of spontaneous movement by dopaminergic neurons is cell-type selective and disrupted in parkinsonism. *Proceedings of the National Academy of Sciences*, *113*, E2180–E2188.

Eshel, N., Tian, J., Bukwich, M., & Uchida, N. (2016). Dopamine neurons share common response function for reward prediction error. *Nature Neuroscience*, *19*, 479–486.

Everett, A. C., Graul, B. E., Ronström, J. W., Robinson, J. K., Watts, D. B., España, R. A., … Yorgason, J. T. (2022). Effectiveness and relationship between biased and unbiased measures of dopamine release and clearance. *ACS Chemical Neuroscience*, *13*, 1534–1548.

Exley, R., Clements, M. A., Hartung, H., McIntosh, J. M., & Cragg, S. J. (2008). A6-containing nicotinic acetylcholine receptors dominate the nicotine control of dopamine neurotransmission in nucleus accumbens. *Neuropsychopharmacology*, *33*, 2158–2166.

Exley, R., & Cragg, S. J. (2008). Presynaptic nicotinic receptors: A dynamic and diverse cholinergic filter of striatal dopamine neurotransmission. *British Journal of Pharmacology*, *153 Suppl 1*, S283-297.

Farassat, N., Costa, K. M., Stojanovic, S., Albert, S., Kovacheva, L., Shin, J., … Roeper, J. (2019). In vivo functional diversity of midbrain dopamine neurons within identified axonal projections. *ELife*, *8*, e48408.

Fields, H. L., Hjelmstad, G. O., Margolis, E. B., & Nicola, S. M. (2007). Ventral tegmental area neurons in learned appetitive behavior and positive reinforcement. *Annual Review of Neuroscience*, *30*, 289–316.

Figueredo-Cardenas, G., Morello, M., Sancesario, G., Bernardi, G., & Reiner, A. (1996). Colocalization of somatostatin, neuropeptide Y, neuronal nitric oxide synthase and NADPH-diaphorase in striatal interneurons in rats. *Brain Research*, *735*, 317–324.

Floresco, S. B., West, A. R., Ash, B., Moore, H., & Grace, A. A. (2003). Afferent modulation of dopamine neuron firing differentially regulates tonic and phasic dopamine transmission. *Nature Neuroscience*, *6*, 968–973.

Freed, C., Revay, R., Vaughan, R. A., Kriek, E., Grant, S., Uhl, G. R., & Kuhar, M. J. (1995). Dopamine transporter immunoreactivity in rat brain. *Journal of Comparative Neurology*, *359*, 340–349.

Fujiyama, F., Fritschy, J.-M., Stephenson, F. A., & Bolam, J. P. (2000). Synaptic localization of $GABA_A$ receptor subunits in the striatum of the rat. *Journal of Comparative Neurology*, *416*, 158–172.

Garris, P. A., Ciolkowski, E. L., Pastore, P., & Wightman, R. M. (1994). Efflux of dopamine from the synaptic cleft in the nucleus accumbens of the rat brain. *Journal of Neuroscience*, *14*, 6084–6093.

Garris, P. A., & Wightman, R. M. (1994). Different kinetics govern dopaminergic transmission in the amygdala, prefrontal cortex, and striatum: An in vivo voltammetric study. *Journal of Neuroscience*, *14*, 442–450.

Gerfen, C. R. (1992). The neostriatal mosaic: Multiple levels of compartmental organization. In A. H. Tuma, E. M. Stricker, & S. Gershon (Eds.), *Advances in Neuroscience and Schizophrenia* (pp. 43–59). Vienna: Springer.

Gerfen, C. R., Engber, T. M., Mahan, L. C., Susel, Z., Chase, T. N., Monsma, F. J., & Sibley, D. R. (1990). D1 and D2 dopamine receptor-regulated gene expression of striatonigral and striatopallidal neurons. *Science*, *250*, 1429–1432.

Gerfen, C. R., & Surmeier, D. J. (2011). Modulation of striatal projection systems by dopamine. *Annual Review of Neuroscience*, *34*, 441–466.

Giros, B., Jaber, M., Jones, S. R., Wightman, R. M., & Caron, M. G. (1996). Hyperlocomotion and indifference to cocaine and amphetamine in mice lacking the dopamine transporter. *Nature*, *379*, 606–612.

Gonon, F. G. (1988). Nonlinear relationship between impulse flow and dopamine released by rat midbrain dopaminergic neurons as studied by in vivo electrochemistry. *Neuroscience*, *24*, 19–28.

Gonon, F. G., & Buda, M. J. (1985). Regulation of dopamine release by impulse flow and by autoreceptors as studied by in vivo voltammetry in the rat striatum. *Neuroscience*, *14*, 765–774.

González-Hernández, T., Barroso-Chinea, P., de la Cruz Muros, I., del Mar Pérez-Delgado, M., & Rodríguez, M. (2004). Expression of dopamine and vesicular monoamine

transporters and differential vulnerability of mesostriatal dopaminergic neurons. *Journal of Comparative Neurology*, *479*, 198–215.

Grace, A. A. (1991). Phasic versus tonic dopamine release and the modulation of dopamine system responsivity: A hypothesis for the etiology of schizophrenia. *Neuroscience*, *41*, 1–24.

Grace, A. A. (1993). Cortical regulation of subcortical dopamine systems and its possible relevance to schizophrenia. *Journal of Neural Transmission / General Section JNT*, *91*, 111–134.

Grace, A. A., & Bunney, B. S. (1983). Intracellular and extracellular electrophysiology of nigral dopaminergic neurons—1. Identification and characterization. *Neuroscience*, *10*, 301–315.

Graybiel, A. M. (1998). The basal ganglia and chunking of action repertoires. *Neurobiology of Learning and Memory*, *70*, 119–136.

Graybiel, A. M., Flaherty, A. W., & Giménez-Amaya, J.-M. (1991). Striosomes and Matrisomes. In G. Bernardi, M. B. Carpenter, G. Di Chiara, M. Morelli, & P. Stanzione (Eds.), *The Basal Ganglia III* (pp. 3–12). Boston, MA: Springer New York.

Green, P., & MacLeod, C. J. (2016). SIMR: An R package for power analysis of generalized linear mixed models by simulation. *Methods in Ecology and Evolution*, *7*, 493–498.

Gremel, C. M., & Costa, R. M. (2013). Orbitofrontal and striatal circuits dynamically encode the shift between goal-directed and habitual actions. *Nature Communications*, *4*, 2264.

Haber, S. N., Fudge, J. L., & McFarland, N. R. (2000). Striatonigrostriatal pathways in primates form an ascending spiral from the shell to the dorsolateral striatum. *Journal of Neuroscience*, *20*, 2369–2382.

Haber, S. N., & Knutson, B. (2010). The reward circuit: Linking primate anatomy and human imaging. *Neuropsychopharmacology*, *35*, 4–26.

Hamid, A. A., Pettibone, J. R., Mabrouk, O. S., Hetrick, V. L., Schmidt, R., Vander Weele, C. M., … Berke, J. D. (2016). Mesolimbic dopamine signals the value of work. *Nature Neuroscience*, *19*, 117–126.

Hartung, H., Threlfell, S., & Cragg, S. J. (2011). Nitric oxide donors enhance the frequency dependence of dopamine release in nucleus accumbens. *Neuropsychopharmacology*, *36*, 1811–1822.

Herkenham, M., & Nauta, W. J. H. (1979). Efferent connections of the habenular nuclei in the rat. *Journal of Comparative Neurology*, *187*, 19–47.

Hersch, S. M., Ciliax, B. J., Gutekunst, C. A., Rees, H. D., Heilman, C. J., Yung, K. K., … Levey, A. I. (1995). Electron microscopic analysis of D1 and D2 dopamine receptor proteins in the dorsal striatum and their synaptic relationships with motor corticostriatal afferents. *Journal of Neuroscience*, *15*, 5222–5237.

Hidaka, S., & Totterdell, S. (2001). Ultrastructural features of the nitric oxide synthase-containing interneurons in the nucleus accumbens and their relationship with tyrosine hydroxylase-containing terminals. *Journal of Comparative Neurology*, *431*, 139–154.

Hikosaka, O., Miyashita, K., Miyachi, S., Sakai, K., & Lu, X. (1998). Differential roles of the frontal cortex, basal ganglia, and cerebellum in visuomotor sequence learning. *Neurobiology of Learning and Memory*, *70*, 137–149.

Hikosaka, O., Nakahara, H., Rand, M. K., Sakai, K., Lu, X., Nakamura, K., … Doya, K. (1999). Parallel neural networks for learning sequential procedures. *Trends in Neurosciences*, *22*, 464–471.

Hilario, M., Holloway, T., Jin, X., & Costa, R. M. (2012). Different dorsal striatum circuits mediate action discrimination and action generalization. *European Journal of Neuroscience*, *35*, 1105–1114.

Howard, C. D., Li, H., Geddes, C. E., & Jin, X. (2017). Dynamic nigrostriatal dopamine biases action selection. *Neuron*, *93*, 1436-1450.e8.

Howe, M. W., & Dombeck, D. A. (2016). Rapid signalling in distinct dopaminergic axons during locomotion and reward. *Nature*, *535*, 505–510.

Howe, M. W., Ridouh, I., Allegra Mascaro, A. L., Larios, A., Azcorra, M., & Dombeck, D. A. (2019). Coordination of rapid cholinergic and dopaminergic signaling in striatum during spontaneous movement. *ELife*, *8*, e44903.

Hughes, R. N., Bakhurin, K. I., Petter, E. A., Watson, G. D. R., Kim, N., Friedman, A. D., & Yin, H. H. (2020). Ventral tegmental dopamine neurons control the impulse vector during motivated behavior. *Current Biology: CB*, *30*, 2681-2694.e5.

Ikemoto, S. (2007). Dopamine reward circuitry: Two projection systems from the ventral midbrain to the nucleus accumbens–olfactory tubercle complex. *Brain Research Reviews*, *56*, 27–78.

Iravani, M. M., & Kruk, Z. L. (1997). Real-time measurement of stimulated 5-hydroxytryptamine release in rat substantia nigra pars reticulata brain slices. *Synapse*, *25*, 93–102.

Irwin, J. R., & McClelland, G. H. (2001). Misleading heuristics and moderated multiple regression models. *Journal of Marketing Research*, *38*, 100–109.

Isomura, Y., Takekawa, T., Harukuni, R., Handa, T., Aizawa, H., Takada, M., & Fukai, T. (2013). Reward-modulated motor information in identified striatum neurons. *Journal of Neuroscience*, *33*, 10209–10220.

Jin, X., & Costa, R. M. (2010). Start/stop signals emerge in nigrostriatal circuits during sequence learning. *Nature*, *466*, 457–462.

Jin, X., Tecuapetla, F., & Costa, R. M. (2014). Basal ganglia subcircuits distinctively encode the parsing and concatenation of action sequences. *Nature Neuroscience*, *17*, 423–430.

John, C. E., Budygin, E. A., Mateo, Y., & Jones, S. R. (2006). Neurochemical characterization of the release and uptake of dopamine in ventral tegmental area and serotonin in substantia nigra of the mouse. *Journal of Neurochemistry*, *96*, 267–282.

Jones, S. R., Gainetdinov, R. R., Hu, X.-T., Cooper, D. C., Wightman, R. M., White, F. J., & Caron, M. G. (1999). Loss of autoreceptor functions in mice lacking the dopamine transporter. *Nature Neuroscience*, *2*, 649–655.

Jones, S. R., Gainetdinov, R. R., Jaber, M., Giros, B., Wightman, R. M., & Caron, M. G. (1998). Profound neuronal plasticity in response to inactivation of the dopamine transporter. *Proceedings of the National Academy of Sciences*, *95*, 4029–4034.

Jones, S. R., Garris, P. A., Kilts, C. D., & Wightman, R. M. (1995). Comparison of dopamine uptake in the basolateral amygdaloid nucleus, caudate-putamen, and nucleus accumbens of the rat. *Journal of Neurochemistry*, *64*, 2581–2589.

Jones, S. R., O'Dell, S. J., Marshall, J. F., & Wightman, R. M. (1996). Functional and anatomical evidence for different dopamine dynamics in the core and shell of the nucleus accumbens in slices of rat brain. *Synapse*, *23*, 224–231.

Joshua, M., Adler, A., & Bergman, H. (2009). The dynamics of dopamine in control of motor behavior. *Current Opinion in Neurobiology*, *19*, 615–620.

Kalia, L. V., & Lang, A. E. (2015). Parkinson's disease. *The Lancet*, *386*, 896–912.

Kawaguchi, Y., Wilson, C. J., Augood, S. J., & Emson, P. C. (1995). Striatal interneurones: Chemical, physiological and morphological characterization. *Trends in Neurosciences*, *18*, 527–535.

Keiflin, R., Pribut, H. J., Shah, N. B., & Janak, P. H. (2019). Ventral tegmental dopamine neurons participate in reward identity predictions. *Current Biology*, *29*, 93-103.e3.

Kelley, A. E., & Delfs, J. M. (1991). Dopamine and conditioned reinforcement. *Psychopharmacology*, *103*, 187–196.

Khan, Z. U., Mrzljak, L., Gutierrez, A., de la Calle, A., & Goldman-Rakic, P. S. (1998). Prominence of the dopamine D2 short isoform in dopaminergic pathways. *Proceedings of the National Academy of Sciences*, *95*, 7731–7736.

Kiyatkin, E. A. (1994). Behavioral significance of phasic changes in mesolimbic dopamine-dependent electrochemical signal associated with heroin self-injections. *Journal of Neural Transmission / General Section JNT*, *96*, 197–214.

Klaus, A., Alves da Silva, J., & Costa, R. M. (2019). What, if, and when to move: Basal ganglia circuits and self-paced action initiation. *Annual Review of Neuroscience*, *42*, 459–483.

Klaus, A., Martins, G. J., Paixao, V. B., Zhou, P., Paninski, L., & Costa, R. M. (2017). The spatiotemporal organization of the striatum encodes action space. *Neuron*, *95*, 1171-1180.e7.

Koob, G. F. (1992). Drugs of abuse: Anatomy, pharmacology and function of reward pathways. *Trends in Pharmacological Sciences*, *13*, 177–184.

Korn, C., Akam, T., Jensen, K. H. R., Vagnoni, C., Huber, A., Tunbridge, E. M., & Walton, M. E. (2021). Distinct roles for dopamine clearance mechanisms in regulating behavioral flexibility. *Molecular Psychiatry*, *26*, 7188–7199.

Kramer, P. F., Brill-Weil, S. G., Cummins, A. C., Zhang, R., Camacho-Hernandez, G. A., Newman, A. H., … Khaliq, Z. M. (2022). Synaptic-like axo-axonal transmission from striatal cholinergic interneurons onto dopaminergic fibers. *Neuron*, *110*, 2949-2960.e4.

Kraus, M. M., & Prast, H. (2001). The nitric oxide system modulates the in vivo release of acetylcholine in the nucleus accumbens induced by stimulation of the hippocampal fornix/fimbria-projection. *European Journal of Neuroscience*, *14*, 1105–1112.

Kravitz, A. V., Freeze, B. S., Parker, P. R. L., Kay, K., Thwin, M. T., Deisseroth, K., & Kreitzer, A. C. (2010). Regulation of parkinsonian motor behaviours by optogenetic control of basal ganglia circuitry. *Nature*, *466*, 622–626.

Kremers, G.-J., Hazelwood, K. L., Murphy, C. S., Davidson, M. W., & Piston, D. W. (2009). Photoconversion in orange and red fluorescent proteins. *Nature Methods*, *6*, 355–358.

Lak, A., Stauffer, W. R., & Schultz, W. (2014). Dopamine prediction error responses integrate subjective value from different reward dimensions. *Proceedings of the National Academy of Sciences*, *111*, 2343–2348.

Lammel, S., Hetzel, A., Häckel, O., Jones, I., Liss, B., & Roeper, J. (2008). Unique properties of mesoprefrontal neurons within a dual mesocorticolimbic dopamine system. *Neuron*, *57*, 760–773.

Lammel, S., Lim, B. K., Ran, C., Huang, K. W., Betley, M. J., Tye, K. M., … Malenka, R. C. (2012). Input-specific control of reward and aversion in the ventral tegmental area. *Nature*, *491*, 212–217.

Lerner, T. N., Shilyansky, C., Davidson, T. J., Evans, K. E., Beier, K. T., Zalocusky, K. A., … Deisseroth, K. (2015). Intact-brain analyses reveal distinct information carried by SNc dopamine subcircuits. *Cell*, *162*, 635–647.

Liang, C.-L., Nelson, O., Yazdani, U., Pasbakhsh, P., & German, D. C. (2004). Inverse relationship between the contents of neuromelanin pigment and the vesicular monoamine transporter-2: Human midbrain dopamine neurons. *Journal of Comparative Neurology*, *473*, 97–106.

Lima, S. Q., Hromádka, T., Znamenskiy, P., & Zador, A. M. (2009). PINP: A new method of tagging neuronal populations for identification during in vivo electrophysiological recording. *PLOS ONE*, *4*, e6099.

Liu, C., Cai, X., Ritzau-Jost, A., Kramer, P. F., Li, Y., Khaliq, Z. M., … Kaeser, P. S. (2022). An action potential initiation mechanism in distal axons for the control of dopamine release. *Science*, *375*, 1378–1385.

Liu, C., Kershberg, L., Wang, J., Schneeberger, S., & Kaeser, P. S. (2018). Dopamine secretion is mediated by sparse active zone-like release sites. *Cell*, *172*, 706-718.e15.

Mailly, P., Charpier, S., Menetrey, A., & Deniau, J.-M. (2003). Three-dimensional organization of the recurrent axon collateral network of the substantia nigra pars reticulata neurons in the rat. *Journal of Neuroscience*, *23*, 5247–5257.

Malvaez, M., & Wassum, K. M. (2018). Regulation of habit formation in the dorsal striatum. *Current Opinion in Behavioral Sciences*, *20*, 67–74.

Markowitz, J. E., Gillis, W. F., Beron, C. C., Neufeld, S. Q., Robertson, K., Bhagat, N. D., … Datta, S. R. (2018). The striatum organizes 3D behavior via moment-to-moment action selection. *Cell*, *174*, 44-58.e17.

Marshall, J. F., O'Dell, S. J., Navarrete, R., & Rosenstein, A. J. (1990). Dopamine high-affinity transport site topography in rat brain: Major differences between dorsal and ventral striatum. *Neuroscience*, *37*, 11–21.

Martel, J. C., & Gatti McArthur, S. (2020). Dopamine receptor subtypes, physiology and pharmacology: New ligands and concepts in schizophrenia. *Frontiers in*

Pharmacology, *11*. Retrieved from https://www.frontiersin.org/articles/10.3389/fphar.2020.01003

Mathis, A., Mamidanna, P., Cury, K. M., Abe, T., Murthy, V. N., Mathis, M. W., & Bethge, M. (2018). DeepLabCut: Markerless pose estimation of user-defined body parts with deep learning. *Nature Neuroscience*, *21*, 1281–1289.

Matsuda, W., Furuta, T., Nakamura, K. C., Hioki, H., Fujiyama, F., Arai, R., & Kaneko, T. (2009). Single nigrostriatal dopaminergic neurons form widely spread and highly dense axonal arborizations in the neostriatum. *The Journal of Neuroscience*, *29*, 444–453.

May, L. J., & Wightman, R. M. (1989). Heterogeneity of stimulated dopamine overflow within rat striatum as observed with in vivo voltammetry. *Brain Research*, *487*, 311–320.

Melchior, J. R., Ferris, M. J., Stuber, G. D., Riddle, D. R., & Jones, S. R. (2015). Optogenetic versus electrical stimulation of dopamine terminals in the nucleus accumbens reveals local modulation of presynaptic release. *Journal of Neurochemistry*, *134*, 833–844.

Mohebi, A., Pettibone, J. R., Hamid, A. A., Wong, J.-M. T., Vinson, L. T., Patriarchi, T., … Berke, J. D. (2019). Dissociable dopamine dynamics for learning and motivation. *Nature*, *570*, 65–70.

Molinoff, P. B., & Axelrod, J. (1971). Biochemistry of catecholamines. *Annual Review of Biochemistry*, *40*, 465–500.

Montague, P. R., Dayan, P., & Sejnowski, T. J. (1996). A framework for mesencephalic dopamine systems based on predictive Hebbian learning. *Journal of Neuroscience*, *16*, 1936–1947.

Morales, M., & Margolis, E. B. (2017). Ventral tegmental area: Cellular heterogeneity, connectivity and behaviour. *Nature Reviews Neuroscience*, *18*, 73–85.

Morris, G., Arkadir, D., Nevet, A., Vaadia, E., & Bergman, H. (2004). Coincident but distinct messages of midbrain dopamine and striatal tonically active neurons. *Neuron*, *43*, 133–143.

Mundorf, M. L., Joseph, J. D., Austin, C. M., Caron, M. G., & Wightman, R. M. (2001). Catecholamine release and uptake in the mouse prefrontal cortex. *Journal of Neurochemistry*, *79*, 130–142.

Nedergaard, S. (2004). A Ca^{2+}-independent slow afterhyperpolarization in substantia nigra compacta neurons. *Neuroscience*, *125*, 841–852.

Neve, K. A., Seamans, J. K., & Trantham-Davidson, H. (2004). Dopamine receptor signaling. *Journal of Receptors and Signal Transduction*, *24*, 165–205.

Nirenberg, M. J., Chan, J., Pohorille, A., Vaughan, R. A., Uhl, G. R., Kuhar, M. J., & Pickel, V. M. (1997). The dopamine transporter: Comparative ultrastructure of dopaminergic axons in limbic and motor compartments of the nucleus accumbens. *Journal of Neuroscience*, *17*, 6899–6907.

Oorschot, D. E. (1996). Total number of neurons in the neostriatal, pallidal, subthalamic, and substantia nigral nuclei of the rat basal ganglia: A stereological study using the

cavalieri and optical disector methods. *Journal of Comparative Neurology*, *366*, 580–599.

Panayi, M. C., Boerner, T., Jahans-Price, T., Huber, A., Sprengel, R., Gilmour, G., … Bannerman, D. M. (2023). Glutamatergic dysfunction leads to a hyper-dopaminergic phenotype through deficits in short-term habituation: A mechanism for aberrant salience. *Molecular Psychiatry*, *28*, 579–587.

Panigrahi, B., Martin, K. A., Li, Y., Graves, A. R., Vollmer, A., Olson, L., … Dudman, J. T. (2015). Dopamine is required for the neural representation and control of movement vigor. *Cell*, *162*, 1418–1430.

Parker, J. G., Marshall, J. D., Ahanonu, B., Wu, Y.-W., Kim, T. H., Grewe, B. F., … Schnitzer, M. J. (2018). Diametric neural ensemble dynamics in parkinsonian and dyskinetic states. *Nature*, *557*, 177–182.

Patel, J., Trout, S. J., & Kruk, Z. L. (1992). Regional differences in evoked dopamine efflux in brain slices of rat anterior and posterior caudate putamen. *Naunyn-Schmiedeberg's Archives of Pharmacology*, *346*, 267–276.

Patriarchi, T., Cho, J. R., Merten, K., Howe, M. W., Marley, A., Xiong, W.-H., … Jang, M. J. (2018). Ultrafast neuronal imaging of dopamine dynamics with designed genetically encoded sensors. *Science*, *360*, eaat4422.

Patriarchi, T., Mohebi, A., Sun, J., Marley, A., Liang, R., Dong, C., … Tian, L. (2020). An expanded palette of dopamine sensors for multiplex imaging in vivo. *Nature Methods*, *17*, 1147–1155.

Phillips, P. E. M., Stuber, G. D., Heien, M. L. A. V., Wightman, R. M., & Carelli, R. M. (2003). Subsecond dopamine release promotes cocaine seeking. *Nature*, *422*, 614–618.

Pinault, D. (1996). A novel single-cell staining procedure performed in vivo under electrophysiological control: Morpho-functional features of juxtacellularly labeled thalamic cells and other central neurons with biocytin or Neurobiotin. *Journal of Neuroscience Methods*, *65*, 113–136.

Pisani, A., Bernardi, G., Ding, J., & Surmeier, D. J. (2007). Re-emergence of striatal cholinergic interneurons in movement disorders. *Trends in Neurosciences*, *30*, 545–553.

Pisani, A., Centonze, D., Bernardi, G., & Calabresi, P. (2005). Striatal synaptic plasticity: Implications for motor learning and Parkinson's disease. *Movement Disorders*, *20*, 395–402.

Pissadaki, E., & Bolam, J. P. (2013). The energy cost of action potential propagation in dopamine neurons: Clues to susceptibility in Parkinson's disease. *Frontiers in Computational Neuroscience*, *7*. Retrieved from https://www.frontiersin.org/articles/10.3389/fncom.2013.00013

Poulin, J.-F., Caronia, G., Hofer, C., Cui, Q., Helm, B., Ramakrishnan, C., … Awatramani, R. (2018). Mapping projections of molecularly defined dopamine neuron subtypes using intersectional genetic approaches. *Nature Neuroscience*, *21*, 1260–1271.

Povlock, S. L., & Schenk, J. O. (1997). A multisubstrate kinetic mechanism of dopamine transport in the nucleus accumbens and its inhibition by cocaine. *Journal of Neurochemistry*, *69*, 1093–1105.

Prasad, B. M., & Amara, S. G. (2001). The dopamine transporter in mesencephalic cultures is refractory to physiological changes in membrane voltage. *Journal of Neuroscience*, *21*, 7561–7567.

Reyes, S., Cottam, V., Kirik, D., Double, K. L., & Halliday, G. M. (2013). Variability in neuronal expression of dopamine receptors and transporters in the substantia nigra. *Movement Disorders*, *28*, 1351–1359.

Rice, M. E., & Cragg, S. J. (2004). Nicotine amplifies reward-related dopamine signals in striatum. *Nature Neuroscience*, *7*, 583–584.

Rice, M. E., & Cragg, S. J. (2008). Dopamine spillover after quantal release: Rethinking dopamine transmission in the nigrostriatal pathway. *Brain Research Reviews*, *58*, 303–313.

Rice, M. E., Cragg, S. J., & Greenfield, S. A. (1997). Characteristics of electrically evoked somatodendritic dopamine release in substantia nigra and ventral tegmental area in vitro. *Journal of Neurophysiology*, *77*, 853–862.

Rice, M. E., Patel, J. C., & Cragg, S. J. (2011). Dopamine release in the basal ganglia. *Neuroscience*, *198*, 112–137.

Richard, J. M., & Berridge, K. C. (2011). Nucleus accumbens dopamine/glutamate interaction switches modes to generate desire versus dread: D1 alone for appetitive eating but D1 and D2 together for fear. *Journal of Neuroscience*, *31*, 12866–12879.

Rizzi, G., & Tan, K. R. (2019). Synergistic nigral output pathways shape movement. *Cell Reports*, *27*, 2184-2198.e4.

Rodeberg, N. T., Sandberg, S. G., Johnson, J. A., Phillips, P. E. M., & Wightman, R. M. (2017). Hitchhiker's guide to voltammetry: Acute and chronic electrodes for in vivo fast-scan cyclic voltammetry. *ACS Chemical Neuroscience*, *8*, 221–234.

Roesch, M. R., Calu, D. J., Burke, K. A., & Schoenbaum, G. (2007). Should I stay or should I go? *Annals of the New York Academy of Sciences*, *1104*, 21–34.

Roitman, M. F., Stuber, G. D., Phillips, P. E. M., Wightman, R. M., & Carelli, R. M. (2004). Dopamine operates as a subsecond modulator of food seeking. *Journal of Neuroscience*, *24*, 1265–1271.

Roitman, M. F., Wheeler, R. A., Wightman, R. M., & Carelli, R. M. (2008). Real-time chemical responses in the nucleus accumbens differentiate rewarding and aversive stimuli. *Nature Neuroscience*, *11*, 1376–1377.

Rubinstein, T. C., Giladi, N., & Hausdorff, J. M. (2002). The power of cueing to circumvent dopamine deficits: A review of physical therapy treatment of gait disturbances in Parkinson's disease. *Movement Disorders*, *17*, 1148–1160.

Saddoris, M. P. (2016). Terminal dopamine release kinetics in the accumbens core and shell are distinctly altered after withdrawal from cocaine self-administration. *ENeuro*, *3*, ENEURO.0274-16.2016.

Saddoris, M. P., Cacciapaglia, F., Wightman, R. M., & Carelli, R. M. (2015). Differential dopamine release dynamics in the nucleus accumbens core and shell reveal complementary signals for error prediction and incentive motivation. *Journal of Neuroscience*, *35*, 11572–11582.

Salinas, A. G., Lee, J. O., Augustin, S. M., Zhang, S., Patriarchi, T., Tian, L., … Lovinger, D. M. (2022, January 11). *Sub-second striatal dopamine dynamics assessed by simultaneous fast-scan cyclic voltammetry and fluorescence biosensor* (p. 2022.01.09.475513). p. 2022.01.09.475513. bioRxiv.

Sanghera, M. K., Manaye, K. F., Liang, C. L., Lacopino, A. M., Bannon, M. J., & German, D. C. (1994). Low dopamine transporter mRNA levels in midbrain regions containing calbindin. *Neuroreport*, *5*, 1641–1644.

Santiago, M., & Westerink, B. H. C. (1991). Characterization and pharmacological responsiveness of dopamine release recorded by microdialysis in the substantia nigra of conscious rats. *Journal of Neurochemistry*, *57*, 738–747.

Saunders, B. T., Richard, J. M., Margolis, E. B., & Janak, P. H. (2018). Dopamine neurons create Pavlovian conditioned stimuli with circuit-defined motivational properties. *Nature Neuroscience*, *21*, 1072–1083.

Schreiner, D. C., Renteria, R., & Gremel, C. M. (2020). Fractionating the all-or-nothing definition of goal-directed and habitual decision-making. *Journal of Neuroscience Research*, *98*, 998–1006.

Schultz, W., Apicella, P., & Ljungberg, T. (1993). Responses of monkey dopamine neurons to reward and conditioned stimuli during successive steps of learning a delayed response task. *Journal of Neuroscience*, *13*, 900–913.

Schultz, W., Dayan, P., & Montague, P. R. (1997). A neural substrate of prediction and reward. *Science*, *275*, 1593–1599.

Sesack, S. R., Aoki, C., & Pickel, V. M. (1994). Ultrastructural localization of D2 receptor-like immunoreactivity in midbrain dopamine neurons and their striatal targets. *Journal of Neuroscience*, *14*, 88–106.

Shepard, P. D., & Bunney, B. S. (1991). Repetitive firing properties of putative dopamine-containing neurons in vitro: Regulation by an apamin-sensitive Ca^{2+}-activated K+ conductance. *Experimental Brain Research*, *86*, 141–150.

Snijders, A. H., Kesteren, M. van, & Bloem, B. R. (2012). Cycling is less affected than walking in freezers of gait. *Journal of Neurology, Neurosurgery & Psychiatry*, *83*, 575–576.

Sombers, L. A., Beyene, M., Carelli, R. M., & Wightman, R. M. (2009). Synaptic overflow of dopamine in the nucleus accumbens arises from neuronal activity in the ventral tegmental area. *Journal of Neuroscience*, *29*, 1735–1742.

Stamford, J. A., Kruk, Z. L., Palij, P., & Millar, J. (1988). Diffusion and uptake of dopamine in rat caudate and nucleus accumbens compared using fast cyclic voltammetry. *Brain Research*, *448*, 381–385.

Starkweather, C. K., Babayan, B. M., Uchida, N., & Gershman, S. J. (2017). Dopamine reward prediction errors reflect hidden-state inference across time. *Nature Neuroscience*, *20*, 581–589.

Stauffer, W. R., Lak, A., Yang, A., Borel, M., Paulsen, O., Boyden, E. S., & Schultz, W. (2016). Dopamine neuron-specific optogenetic stimulation in rhesus macaques. *Cell*, *166*, 1564-1571.e6.

Steinberg, E. E., Keiflin, R., Boivin, J. R., Witten, I. B., Deisseroth, K., & Janak, P. H. (2013). A causal link between prediction errors, dopamine neurons and learning. *Nature Neuroscience*, *16*, 966–973.

Stopper, C. M., Tse, M. T. L., Montes, D. R., Wiedman, C. R., & Floresco, S. B. (2014). Overriding phasic dopamine signals redirects action selection during risk/reward decision making. *Neuron*, *84*, 177–189.

Stuber, G. D., Roitman, M. F., Phillips, P. E. M., Carelli, R. M., & Wightman, R. M. (2005). Rapid dopamine signaling in the nucleus accumbens during contingent and noncontingent cocaine administration. *Neuropsychopharmacology*, *30*, 853–863.

Sulzer, D., Cragg, S. J., & Rice, M. E. (2016). Striatal dopamine neurotransmission: Regulation of release and uptake. *Basal Ganglia*, *6*, 123–148.

Sun, F., Zhou, J., Dai, B., Qian, T., Zeng, J., Li, X., … Li, Y. (2020). Next-generation GRAB sensors for monitoring dopaminergic activity in vivo. *Nature Methods*, *17*, 1156–1166.

Surmeier, D. J., Ding, J., Day, M., Wang, Z., & Shen, W. (2007). D1 and D2 dopamine-receptor modulation of striatal glutamatergic signaling in striatal medium spiny neurons. *Trends in Neurosciences*, *30*, 228–235.

Surmeier, D. J., Plotkin, J., & Shen, W. (2009). Dopamine and synaptic plasticity in dorsal striatal circuits controlling action selection. *Current Opinion in Neurobiology*, *19*, 621–628.

Surmeier, D. J., Song, W.-J., & Yan, Z. (1996). Coordinated expression of dopamine receptors in neostriatal medium spiny neurons. *Journal of Neuroscience*, *16*, 6579–6591.

Sutton, R. S. (1988). Learning to predict by the methods of temporal differences. *Machine Learning*, *3*, 9–44.

Sutton, R. S., & Barto, A. G. (2018). *Reinforcement Learning, second edition: An Introduction*. MIT Press.

Swanson, L. W. (1982). The projections of the ventral tegmental area and adjacent regions: A combined fluorescent retrograde tracer and immunofluorescence study in the rat. *Brain Research Bulletin*, *9*, 321–353.

Syed, E. C. J., Grima, L. L., Magill, P. J., Bogacz, R., Brown, P., & Walton, M. E. (2016). Action initiation shapes mesolimbic dopamine encoding of future rewards. *Nature Neuroscience*, *19*, 34–36.

Takahashi, Y. K., Langdon, A. J., Niv, Y., & Schoenbaum, G. (2016). Temporal specificity of reward prediction errors signaled by putative dopamine neurons in rat VTA depends on ventral striatum. *Neuron*, *91*, 182–193.

Tecuapetla, F., Matias, S., Dugue, G. P., Mainen, Z. F., & Costa, R. M. (2014). Balanced activity in basal ganglia projection pathways is critical for contraversive movements. *Nature Communications*, *5*, 4315.

Tepper, J. M., Koós, T., Ibanez-Sandoval, O., Tecuapetla, F., Faust, T. W., & Assous, M. (2018). Heterogeneity and diversity of striatal GABAergic interneurons: Update 2018. *Frontiers in Neuroanatomy*, *12*, 91.

Tepper, J. M., Sawyer, S. F., & Groves, P. M. (1987). Electrophysiologically identified nigral dopaminergic neurons intracellularly labeled with HRP: Light-microscopic analysis. *Journal of Neuroscience*, *7*, 2794–2806.

Threlfell, S., Clements, M. A., Khodai, T., Pienaar, I. S., Exley, R., Wess, J., & Cragg, S. J. (2010). Striatal muscarinic receptors promote activity dependence of dopamine transmission via distinct receptor subtypes on cholinergic interneurons in ventral versus dorsal striatum. *Journal of Neuroscience*, *30*, 3398–3408.

Threlfell, S., & Cragg, S. (2011). Dopamine signaling in dorsal versus ventral striatum: The dynamic role of cholinergic interneurons. *Frontiers in Systems Neuroscience*, *5*. Retrieved from https://www.frontiersin.org/articles/10.3389/fnsys.2011.00011

Threlfell, S., Lalic, T., Platt, N. J., Jennings, K. A., Deisseroth, K., & Cragg, S. J. (2012). Striatal dopamine release is triggered by synchronized activity in cholinergic interneurons. *Neuron*, *75*, 58–64.

Tian, J., Uchida, N., & Eshel, N. (2017). Chapter 5 - Reward and Decision Encoding in Basal Ganglia: Insights From Optogenetics and Viral Tracing Studies in Rodents. In J.-C. Dreher & L. Tremblay (Eds.), *Decision Neuroscience* (pp. 59–69). San Diego: Academic Press.

Tritsch, N. X., Ding, J. B., & Sabatini, B. L. (2012). Dopaminergic neurons inhibit striatal output through non-canonical release of GABA. *Nature*, *490*, 262–266.

Tritsch, N. X., Oh, W.-J., Gu, C., & Sabatini, B. L. (2014). Midbrain dopamine neurons sustain inhibitory transmission using plasma membrane uptake of GABA, not synthesis. *ELife*, *3*, e01936.

Trout, S. J., & Kruk, Z. L. (1992). Differences in evoked dopamine efflux in rat caudate putamen, nucleus accumbens and tuberculum olfactorium in the absence of uptake inhibition: Influence of autoreceptors. *British Journal of Pharmacology*, *106*, 452–458.

Trudeau, L.-E., Hnasko, T. S., Wallén-Mackenzie, Å., Morales, M., Rayport, S., & Sulzer, D. (2014). Chapter 6—The multilingual nature of dopamine neurons. In M. Diana, G. Di Chiara, & P. Spano (Eds.), *Progress in Brain Research* (pp. 141–164). Elsevier.

Ungerstedt, U. (1971). Stereotaxic mapping of the monoamine pathways in the rat brain. *Acta Physiologica Scandinavica*, *82*, 1–48.

Ungless, M. A., & Grace, A. A. (2012). Are you or aren't you? Challenges associated with physiologically identifying dopamine neurons. *Trends in Neurosciences*, *35*, 422–430.

Ungless, M. A., Magill, P. J., & Bolam, J. P. (2004). Uniform inhibition of dopamine neurons in the ventral tegmental area by aversive stimuli. *Science*, *303*, 2040–2042.

van Elzelingen, W., Goedhoop, J., Warnaar, P., Denys, D., Arbab, T., & Willuhn, I. (2022). A unidirectional but not uniform striatal landscape of dopamine signaling for motivational stimuli. *Proceedings of the National Academy of Sciences of the United States of America*, *119*, e2117270119.

Vandaele, Y., & Janak, P. H. (2018). Defining the place of habit in substance use disorders. *Progress in Neuro-Psychopharmacology & Biological Psychiatry*, *87*, 22–32.

Vaughan, R. A., & Foster, J. D. (2013). Mechanisms of dopamine transporter regulation in normal and disease states. *Trends in Pharmacological Sciences*, *34*, 489–496.

Watabe-Uchida, M., Eshel, N., & Uchida, N. (2017). Neural circuitry of reward prediction error. *Annual Review of Neuroscience*, *40*, 373–394.

Watabe-Uchida, M., Zhu, L., Ogawa, S. K., Vamanrao, A., & Uchida, N. (2012). Whole-brain mapping of direct inputs to midbrain dopamine neurons. *Neuron*, *74*, 858–873.

Weiss, F., Paulus, M. P., Lorang, M. T., & Koob, G. F. (1992). Increases in extracellular dopamine in the nucleus accumbens by cocaine are inversely related to basal levels: Effects of acute and repeated administration. *Journal of Neuroscience*, *12*, 4372–4380.

Wendler, E., Gaspar, J. C. C., Ferreira, T. L., Barbiero, J. K., Andreatini, R., Vital, M. A. B. F., … Da Cunha, C. (2014). The roles of the nucleus accumbens core, dorsomedial striatum, and dorsolateral striatum in learning: Performance and extinction of Pavlovian fear-conditioned responses and instrumental avoidance responses. *Neurobiology of Learning and Memory*, *109*, 27–36.

West, E. A., & Carelli, R. M. (2016). Nucleus accumbens core and shell differentially encode reward-associated cues after reinforcer devaluation. *Journal of Neuroscience*, *36*, 1128–1139.

Wieczorek, W., & Kruk, Z. L. (1995). Influences of neuronal uptake and D2 autoreceptors on regulation of extracellular dopamine in the core, shell and rostral pole of the rat nucleus accumbens. *Brain Research*, *699*, 171–182.

Wightman, R. M., Heien, M. L. A. V., Wassum, K. M., Sombers, L. A., Aragona, B. J., Khan, A. S., … Carelli, R. M. (2007). Dopamine release is heterogeneous within

microenvironments of the rat nucleus accumbens. *European Journal of Neuroscience*, *26*, 2046–2054.

Wise, R. A. (2004). Dopamine, learning and motivation. *Nature Reviews Neuroscience*, *5*, 483–494.

Witten, I. B., Steinberg, E. E., Lee, S. Y., Davidson, T. J., Zalocusky, K. A., Brodsky, M., … Deisseroth, K. (2011). Recombinase-driver rat lines: Tools, techniques, and optogenetic application to dopamine-mediated reinforcement. *Neuron*, *72*, 721–733.

Wyvell, C. L., & Berridge, K. C. (2000). Intra-accumbens amphetamine increases the conditioned incentive salience of sucrose reward: Enhancement of reward "wanting" without enhanced "liking" or response reinforcement. *Journal of Neuroscience*, *20*, 8122–8130.

Xiao, L., Priest, M. F., Nasenbeny, J., Lu, T., & Kozorovitskiy, Y. (2017). Biased oxytocinergic modulation of midbrain dopamine systems. *Neuron*, *95*, 368-384.e5.

Yan, Z., & Surmeier, D. J. (1996). Muscarinic (m2/m4) receptors reduce N- and P-type Ca^{2+} currents in rat neostriatal cholinergic interneurons through a fast, membrane-delimited, G-protein pathway. *Journal of Neuroscience*, *16*, 2592–2604.

Yavich, L., Forsberg, M. M., Karayiorgou, M., Gogos, J. A., & Männistö, P. T. (2007). Site-specific role of catechol-o-methyltransferase in dopamine overflow within prefrontal cortex and dorsal striatum. *Journal of Neuroscience*, *27*, 10196–10209.

Yin, H. H., & Knowlton, B. J. (2006). The role of the basal ganglia in habit formation. *Nature Reviews Neuroscience*, *7*, 464–476.

Yin, H. H., Knowlton, B. J., & Balleine, B. W. (2005). Blockade of NMDA receptors in the dorsomedial striatum prevents action–outcome learning in instrumental conditioning. *European Journal of Neuroscience*, *22*, 505–512.

Yin, H. H., Mulcare, S. P., Hilário, M. R. F., Clouse, E., Holloway, T., Davis, M. I., … Costa, R. M. (2009). Dynamic reorganization of striatal circuits during the acquisition and consolidation of a skill. *Nature Neuroscience*, *12*, 333–341.

Yin, H. H., Ostlund, S. B., Knowlton, B. J., & Balleine, B. W. (2005). The role of the dorsomedial striatum in instrumental conditioning. *European Journal of Neuroscience*, *22*, 513–523.

Yttri, E. A., & Dudman, J. T. (2016). Opponent and bidirectional control of movement velocity in the basal ganglia. *Nature*, *533*, 402–406.

Yung, K. K. L., Bolam, J. P., Smith, A. D., Hersch, S. M., Ciliax, B. J., & Levey, A. I. (1995). Immunocytochemical localization of D1 and D2 dopamine receptors in the basal ganglia of the rat: Light and electron microscopy. *Neuroscience*, *65*, 709–730.

Zhang, H., & Sulzer, D. (2004). Frequency-dependent modulation of dopamine release by nicotine. *Nature Neuroscience*, *7*, 581–582.

Zhou, F.-M., Liang, Y., & Dani, J. A. (2001). Endogenous nicotinic cholinergic activity regulates dopamine release in the striatum. *Nature Neuroscience*, *4*, 1224–1229.

Zhou, F.-M., Wilson, C. J., & Dani, J. A. (2002). Cholinergic interneuron characteristics and nicotinic properties in the striatum. *Journal of Neurobiology*, *53*, 590–605.